

Dissertation zur Erlangung des Doktorgrades
der Fakultät für Chemie und Pharmazie
der Ludwig-Maximilians-Universität München

Auxiliary factors regulating ribosome function:
Roles in biogenesis, antibiotic resistance and ribosome recycling



Alexandra Dönhöfer

aus München

2012

Erklärung

Diese Dissertation wurde im Sinne von § 7 der Promotionsordnung vom 28. November 2011 von Herrn Prof. Dr. Roland Beckmann betreut.

Eidesstattliche Versicherung

Diese Dissertation wurde eigenständig und ohne unerlaubte Hilfe erarbeitet.

München,.....

.....

Alexandra Dönhöfer

Dissertation eingereicht am:	09.02.2012
1. Gutachter:	Herr Prof. Dr. Roland Beckmann
2. Gutachter:	Herr Dr. Daniel N. Wilson
Mündliche Prüfung am:	29.03.2012

Table of Contents

LIST OF PUBLICATIONS	7
CONTRIBUTION REPORT	8
ABBREVIATIONS	10
1 INTRODUCTION	13
1.1 The Flow of Genetic Information	13
1.2 The Ribosome	13
1.3 Ribosome Biogenesis in Eubacteria	14
1.3.1 Processing of ribosomal RNA	15
1.3.2 Modification of ribosomal RNA	16
1.3.3 Modification of ribosomal Proteins	19
1.3.4 Non-ribosomal Factors involved in Ribosome Assembly.....	20
1.4 Ribosomal Proteins	23
1.4.1 Ribosomal Proteins in Eubacteria	23
1.4.2 Ribosomal Proteins in Eukaryotes and Archaea	24
1.4.3 Specific Ribosomal Proteins in Organelles.....	25
1.4.3.1 Chloroplasts.....	25
1.4.3.2 Mitochondria	26
1.5 Translation Mechanism in Eubacteria.....	27
1.5.1 Initiation Phase.....	27
1.5.2 Elongation Phase: Decoding, Peptide-Bond Formation and Translocation	29
1.5.3 Termination & Recycling	31
1.6 Inhibition of Translation: Antibiotics	33
1.6.1 Stages of Inhibition during Translation	35
1.6.2 Mechanisms of Antibiotic Resistance and Strategies to overcome this Problem	37

2 OBJECTIVES AND AIMS OF THE THESIS	40
3 CUMULATIVE THESIS: SUMMARY OF PUBLISHED RESULTS	42
3.1 Paper I.....	42
3.2 Paper II.....	43
3.3 Paper III.....	44
3.4 Paper IV	45
3.5 Paper V	46
4 EXTRA-RIBOSOMAL FACTORS IN RIBOSOME BIOGENESIS.....	48
4.1 Project Aims.....	48
4.2 Introduction.....	48
4.2.1 Post-transcriptional Modification by Methyltransferases.....	49
4.2.2 Guanine 966 specific Methyltransferase YhhF (RsmD).....	50
4.2.3 Ψ 1915 specific Methyltransferase RlmH (YbeA).....	51
4.2.4 Ribosome maturation factor M (RimM).....	52
4.3 Results.....	54
4.3.1 Purification of <i>E. coli</i> YhhF protein	54
4.3.2 <i>In vitro</i> binding assay: <i>Eco30S</i> Δ <i>yhhF</i> + YhhF + sinefungin	55
4.3.3 3D-reconstruction of the [<i>Eco30S</i> Δ <i>yhhF</i> -YhhF] complex	56
4.3.4 <i>In vitro</i> binding assay: <i>Eco70S</i> Δ <i>rluD/rlmH</i> + RlmH + sinefungin	57
4.3.5 3D-reconstruction of the [<i>Eco70S</i> Δ <i>rluD/rlmH</i> -RlmH] complex.....	59
4.3.6 Ribosome profiles and purification of <i>E. coli</i> RimM	61
4.3.7 <i>In vitro</i> binding assay: <i>Eco30S</i> / <i>Eco30S</i> Δ <i>rimM</i> + RimM	62
4.3.8 3D-reconstruction of the [<i>Eco30S</i> Δ <i>rimM</i> -RimM] complex.....	63
4.4 Conclusions and Outlook	65
5 ORGANELLAR-SPECIFIC RIBOSOMAL PROTEINS.....	67

5.1 Project Aims	67
5.2 Introduction	67
5.2.1 Mitochondrion-specific ribosomal proteins (MSRPs)	67
5.3 Results	68
5.3.1 Expression and purification of yeast MSRPs	68
5.3.2 <i>In vivo</i> association of individual MSRPs with <i>E. coli</i> ribosomes	70
5.3.3 Purification of [<i>Eco</i> 70S·MRPL3] complexes	72
5.3.4 3D-reconstruction of [<i>Eco</i> 70S·MRPL3] complexes	73
5.4 Conclusions and Outlook	74
6 ANTIBIOTIC RESISTANCE PROTEINS	76
6.1 Project Aims	76
6.2 Introduction	76
6.2.1 Ribosome protection protein Tet(M)	76
6.3 Results	78
6.3.1 Purification of <i>E. faecalis</i> Tet(M)	78
6.3.2 <i>In vitro</i> binding assay: <i>Eco</i> 70S + Tet(M) + GDPNP +/- Tgc	79
6.3.3 3D-reconstruction of [<i>Eco</i> 70S·Tet(M)·GDPNP·Tgc] complex	81
6.4 Conclusions and Outlook	101
7 MATERIAL AND METHODS	106
7.1 Methods in Molecular Biology	106
7.1.1 Media and Supplements	106
7.1.2 Strains	106
7.1.3 Polymerase Chain Reaction (PCR)	106
7.1.4 Agarose Gel Electrophoresis	108
7.1.5 Cloning	108
7.2 Methods in Biochemistry	109

7.2.1 Isolation of <i>E. coli</i> 70S ribosomes and ribosomal subunits.....	109
7.2.2 Protein purification: Ni ²⁺ -NTA-Agarose.....	110
7.2.3 Protein purification: TALON®.....	111
7.2.4 SDS-PAGE.....	112
7.2.5 Western blot Analysis.....	112
7.2.6 <i>In vitro</i> binding assay.....	113
7.2.7 <i>In vivo</i> association of individual MSRPs with <i>E. coli</i> ribosomes	113
7.3 Electron microscopy (EM).....	114
7.3.1 Negative-Stain Electron Microscopy.....	114
7.3.2 Cryo-Electron Microscopy (Cryo-EM).....	114
7.3.3 Image Processing and 3D-reconstruction	115
7.3.4 Structural Modeling and Preparation of Figures	116
8 REFERENCES	117
9 ACKNOWLEDGEMENTS	144
10 PUBLICATIONS.....	146
CURRICULUM VITAE ALEXANDRA DÖNHÖFER.....	216

List of Publications

This dissertation is partially based on the following publications. The respective Roman numerals refer to publications in the text and to the reprints attached at the end of the thesis:

Paper I

Dönhöfer A, Sharma MR, Datta PP, Nierhaus KH, Agrawal RK, Wilson DN. *Factor-mediated ribosome assembly in bacteria*. Encyclopedia of Life Sciences (ELS), 2009. Review.

Paper II

Siibak T, Peil L, **Dönhöfer A**, Tats A, Remm M, Wilson DN, Tenson T, Remme J. *Antibiotic-induced ribosomal assembly defects result from changes in the synthesis of ribosomal proteins*. Mol. Microbiol. 2011 Apr; 80(1): 54-67.

Paper III

Márquez V, Fröhlich T, Armache JP, Sohmen D, **Dönhöfer A**, Mikolajka A, Berninghausen O, Thomm M, Beckmann R, Arnold GJ, Wilson DN. *Proteomic characterization of archaeal ribosomes reveals the presence of novel archaeal specific ribosomal proteins*. J Mol Biol. 2011 Feb 4; 405(5): 1215-32.

Paper VI

Sharma MR*, **Dönhöfer A***, Barat C, Márquez V, Datta PP, Fucini P, Wilson DN, Agrawal RK. *PSRP1 is not a ribosomal protein, but a ribosome-binding factor that is recycled by the ribosome-recycling factor (RRF) and elongation factor G (EF-G)*. J Biol Chem. 2010 Feb 5; 285(6): 4006-14.

*Both authors contributed equally to this work.

Paper V

Ratje AH, Loerke J, Mikolajka A, Brünner M, Hildebrand PW, Starosta AL, **Dönhöfer A**, Connell SR, Fucini P, Mielke T, Whitford PC, Onuchic JN, Yu Y, Sanbonmatsu KY, Hartmann RK, Penczek PA, Wilson DN, Spahn CM. *Head swivel on the ribosome facilitates translocation by means of intra-subunit tRNA hybrid sites*. Nature 2010 Dec 2; 468(7324): 713-6.

Contribution Report

This dissertation is based on work which was conducted during my PhD from September 2007 to December 2011. Parts of my work are already published in cooperation with the laboratories of Professor R.K. Agrawal (Albany, USA), Professor J. Remme (Tartu, Estonia) and Professor C.M. Spahn (Berlin, Germany).

Paper I (Dönhöfer, Sharma et al., 2009)

The review summarizes the insights which were known about non-ribosomal factors being involved in bacterial ribosome biogenesis in 2009. I designed and produced Figure 1 illustrating the processing of ribosomal RNA in bacteria and contributed to the writing of the review.

Paper II (Siibak, Peil et al., 2011)

This publication deals with ribosome assembly defects caused by antibiotic treatment based on alterations in the synthesis of ribosomal proteins. I performed negative-stain EM on mature *E. coli* 30S and 50S ribosomal subunits and 70S ribosomes in comparison to intermediate particles from the small (25S) and the large (35S and 45S) ribosomal subunit derived from cam- and ery-treated cells summarized in Figure 2 of this publication. Moreover, I contributed to the design and production of Figure 3, 5 and 6 as well as to the writing of the publication.

Paper III (Márquez, Fröhlich et al., 2011)

This paper focuses on the characterization of archaeal ribosomes. I performed negative-stain EM to characterize archaeal ribosomal subunits purified from two different archaeal species, *Sulfolobus acidocaldarius* and *Pyrobaculum aerophilum*, in comparison to *Escherichia coli* ribosomes (Figure 4) and contributed to write the manuscript.

Paper IV (Sharma, Dönhöfer et al., 2010)

This publication summarizes the functional role of the protein factor PSRP1, present in chloroplast ribosomes. I performed the biochemical experiments for this study, characterizing the behavior of PSRP1 in the presence of factors involved in ribosome recycling visualized by *in vitro* binding experiments and sucrose density gradient centrifugation under various conditions (Figure 6 and 7). The insights, which were achieved here, are summarized in a

model illustrating the action of PSRP1 and *E. coli* pY on the ribosome under conditions of stress resulting in Figure 8. Moreover, I designed Figure 3c and participated in writing the manuscript.

Paper V (Ratje, Loerke *et al.*, 2010)

This paper deals with the translocation event during translation, in particular showing two different sub-steps of this process visualized by cryo-EM. I performed the *in vitro* binding assay, prepared the complex that was used for further cryo-EM analysis consisting of purified *Thermus thermophilus* 70S ribosomes, EF-G, GDP and the compound fusidic acid and contributed in finishing the manuscript.

Abbreviations

30S-IC	30S initiation complex
70S-IC	70S initiation complex
A-site	acceptor site for tRNA on the ribosome
aa-tRNA	aminoacyl-tRNA
ATP	adenosine triphosphate
cam	chloramphenicol
C-terminal	carboxy terminal
CTD	C-terminal domain
CTF	contrast transfer function
cryo-EM	cryo-electron microscopy
Da	Dalton (kDa: kilo Dalton, MDa: mega Dalton)
DNA	deoxyribonucleic acid
DTT	dithiothreitol
<i>E. coli</i>	<i>Escherichia coli</i>
EDTA	ethylenediaminetetraacetic acid
<i>E. faecalis</i>	<i>Enterococcus faecalis</i>
EF	elongation factor
e.g.	<i>exempli gratia</i> / for example
EM	electron microscopy
ery	erythromycin
E-site	exit site for tRNA on the ribosome
FRET	fluorescence resonance energy transfer
FSC	fourier shell correlation
GDP	guanosine diphosphate
GDPNP	non-hydrolyzable analogue of GTP
GTPase	guanosine triphosphate hydrolase
GTP	guanosine triphosphate
GuHCl	guanidine hydrochloride
H ⁺	proton
h	hour

h44	helix 44 (of the small ribosomal subunit)
H69	Helix 69 (of the large ribosomal subunit)
Hepes	4-(2-hydroxyethyl)-1-piperazineethanesulfonic acid
i.e.	id est
IF	initiation factor
IPTG	isopropyl- β -D-thiogalactoside
LB	Luria Broth medium
min	minute
mitoribosomes	mitochondrial ribosomes
mRNA	messenger RNA
MSRPs	mitochondrion-specific ribosomal proteins
NADH	nicotinamide adenine dinucleotide
<i>N. crassa</i>	<i>Neurospora crassa</i>
NS	negative-stain
N-terminal	amino terminal
NTD	N-terminal domain
nt(s)	nucleotide(s)
OD	optical density
<i>P. aeruginosa</i>	<i>Pseudomonas aeruginosa</i>
pI	isoelectric point
P _i	inorganic phosphate
PAGE	polyacrylamide gelelectrophoresis
PCR	polymerase chain reaction
pmol	pico mole
PMSF	phenylmethylsulfonyl fluoride
P-site	peptidyl site for tRNA on the ribosome
P/I state	peptidyl/initiation hybrid state
PSRPs	plastid-specific ribosomal proteins
PTC	peptidyl transferase center
RF	release factor
RNA	ribonucleic acid
RNCs	ribosome-nascent chain complexes
rpm	revolutions per minute

RPP	ribosome protection protein
r-proteins	ribosomal proteins
rRNA	ribosomal RNA
RT	room temperature
RuBisCo	ribulose-1,5-bisphosphate carboxylase oxygenase
S	sedimentation coefficient (Svedberg)
<i>S. cerevisiae</i>	<i>Saccharomyces cerevisiae</i>
<i>S. rimosus</i>	<i>Streptomyces rimosus</i>
SD	Shine-Dalgarno
SDS	sodium dodecyl sulfate
smFRET	single molecule FRET
SPOUT	SpoU-TrmD (family)
SRL	sarcin-ricin-loop
TAE	Tris-acetate-EDTA buffer
TB	Terrific Broth medium
TCA	trichloro acetic acid
Tet	tetracycline
Tet1/2	primary/ secondary binding site of tetracycline on the ribosome
Tgc	tigecycline
<i>T. thermophilus</i>	<i>Thermus thermophilus</i>
tRNA	transfer RNA
WT	wild-type
&	and
Ψ	pseudouridine

1 Introduction

1.1 The Flow of Genetic Information

In bacteria, as well as in all other living organisms, genetic information is stored in a deoxyribonucleic acid (DNA) sequence. To utilize this information, the message encoded in DNA has to be converted first into messenger RNA (mRNA) and then translated into a protein sequence. These processes are known as transcription and translation, respectively, and describe the central dogma of molecular biology.

The organization and utilization of genetic information differ in the three domains of life namely eubacteria, eukaryotes and archaea. In eubacteria, both transcription and translation take place in one compartment, the cytoplasm, and are therefore coupled. During transcription, the genetic information that is encoded in the DNA is converted into mRNA, due to the action of an intensively studied enzyme, the RNA polymerase, followed by protein synthesis.

One of the key components in translation is the ribosome, which is responsible for converting the information that is encoded in the mRNA into a polypeptide chain. The mRNA is organized in a triplet code, i.e. 3 nucleotides in the mRNA sequence encode for one specific amino acid in a protein sequence. A universal genetic code consisting of 64 codons translate the nucleic acid sequence into the appropriate protein sequence.

1.2 The Ribosome

In eubacteria, ribosomes are large ribonucleoprotein particles consisting of two unequally sized subunits, the small (30S) and the large (50S) subunit. Both subunits are composed of ribosomal RNA (rRNA) as well as a specific number of ribosomal proteins (r-proteins) and assemble together to form an active 70S ribosome. The 30S subunit contains one rRNA molecule (16S rRNA consisting of 1542 nucleotides (nts)) and 21 r-proteins, in contrast to the large subunit that is more complex, consisting of 2 rRNAs (23S and 5S rRNAs of 2904 and 120 nts, respectively) and 33 r-proteins (Wilson and Nierhaus 2005; Kaczanowska and Ryden-Aulin 2007). The functional roles of the ribosomal subunits are very well studied: The small subunit is responsible to ensure decoding and therefore the fidelity of translation, by monitoring the cognate mRNA-tRNA codon-anticodon interaction. In contrast,

the large ribosomal subunit contains a highly conserved region, the peptidyl transferase center (PTC), where the amino acids are consecutively linked together by peptide bonds to form a polypeptide chain (Schmeing and Ramakrishnan 2009). So far, a number of high-resolution structures of the prokaryotic ribosome and the ribosomal subunits are available (Ban, Nissen *et al.* 2000; Wimberly, Brodersen *et al.* 2000; Yusupov, Yusupova *et al.* 2001).

In contrast to bacterial ribosomes, 80S ribosomes in higher eukaryotes have a more complicated architecture and mechanism of regulation, but the translational process itself is well conserved. The eukaryotic ribosome, for example of *Saccharomyces cerevisiae* (baker's yeast), also consists of two subunits of unequal size, but there is an increase in both rRNA and r-protein content. The small ribosomal subunit (40S) consists of one rRNA molecule (18S rRNA) and 33 r-proteins and the large ribosomal subunit (60S) contains 3 rRNAs (25S, 5.8S and 5S rRNA) and 46 r-proteins. The increase in size in comparison to the prokaryotic ribosome is due to expansion segments in rRNAs as well as additional r-proteins and extensions of the r-proteins. This may reflect the higher complexity in mechanism and regulation of eukaryotic translation. During the last years, several structures from eukaryotic ribosomes as well as ribosomal subunits determined by both cryo-electron microscopy (cryo-EM) and crystallography became available. This includes cryo-EM reconstructions from the human (Spahn, Jan *et al.* 2004) and canine (Chandramouli, Topf *et al.* 2008) 80S ribosome as well as a recent structure from *Triticum aestivum* (Armache, Jarasch *et al.* 2010). In addition, high-resolution crystal structures from the yeast 80S ribosome (Ben-Shem, Garreau de Loubresse *et al.* 2011) and 40S and 60S crystals determined from *Tetrahymena thermophila* were determined recently (Rabl, Leibundgut *et al.* 2010; Klinge, Voigts-Hoffmann *et al.* 2011).

1.3 Ribosome Biogenesis in Eubacteria

Assembly of functional ribosomes is a complex and highly regulated process in the cell that is initiated already during rRNA transcription (Lewicki, Margus *et al.* 1993). The assembly process itself includes processing, modification and proper folding of the two main components, rRNA and r-proteins, which will be discussed in detail below.

1.3.1 Processing of ribosomal RNA

In total, *Escherichia coli* contain 7 *rrn* operons and each operon is generally transcribed as a primary transcript containing 16S, 23S and 5S rRNAs separated by spacer sequences or tRNAs (Deutscher 2009). The primary transcript is further processed by nucleases, principally through the action of RNase III (**Figure 1**). This enzyme specifically recognizes double stranded RNA sequences for its activity and the cleavage already takes place during the transcription process (Robertson, Webster *et al.* 1968). Pre-16S and pre-23S rRNA still possess additional nucleotides at both the 3' and 5' end: specifically, immature 16S rRNA (17S) contains 115 and 33 extra nucleotides at the 5' and 3' ends, respectively (Young and Steitz 1978), whereas pre-23S rRNA contain 3-7 and 8 additional nucleotides at the 5' and 3' ends (King, Sirdeshmukh *et al.* 1984; Sirdeshmukh and Schlessinger 1985) and therefore have to undergo further processing steps.

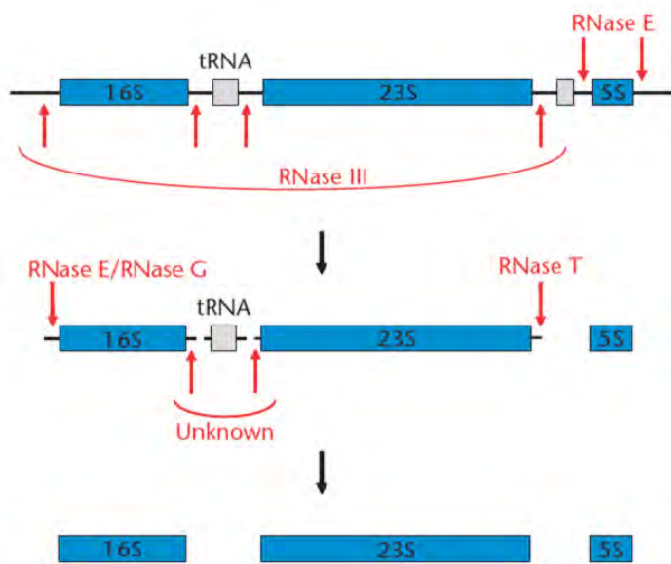


Figure 1: Processing of ribosomal RNA in eubacteria. The primary transcripts of premature 16S, 23S and 5S rRNA are further processed by individual RNases (RNase E, G and T) as highlighted in red. The enzymes responsible for the maturation of the 3' end of 16S rRNA as well as the 5' end of 23S rRNA are so far not identified (marked as unknown). The figure was taken from (Dönhöfer, Sharma *et al.* 2009).

For 17S rRNA, the precursor of the mature 16S rRNA, the action of at least two other RNases, RNase E and G, is involved. These enzymes are generally responsible for processing of the 5' end of the 17S rRNA precursor (Li, Pandit *et al.* 1999b). The maturation of the 3' end is still not clearly understood and the enzymes involved in this pathway have so far not been confirmed (Hayes and Vasseur 1976).

After initial cleavage by RNase III, pre-23S rRNA is processed on both the 5' and 3' ends, however the enzyme(s) responsible for the maturation of the 5' end are still unknown.

RNase T is the enzyme mainly involved in final 3' end processing of the pre-23S rRNA (Li, Pandit *et al.* 1999a).

The maturation of the 5S rRNA molecule is not understood in detail, but it is known that complete processing is not essential for cell growth (Li and Deutscher 1995). The pre-5S rRNA gets cleaved by RNase E resulting in an immature 5S rRNA with 3 additional nucleotides at both ends (Roy, Singh *et al.* 1983). The final maturation step of the 5S rRNA molecule happens late, during protein synthesis (Feunteun, Jordan *et al.* 1972). Exonuclease RNase T is mainly involved in 3' end maturation of the 5S rRNA, in contrast to the 5' end where the enzyme is again not determined (Li and Deutscher 1995).

Additional enzymes are involved in rRNA processing including ribonucleases like PNPase and RNase PH (Zhou and Deutscher 1997) and extra-ribosomal factors or RNA chaperones which will be discussed in detail below.

1.3.2 Modification of ribosomal RNA

After being processed, several nucleotides in both the 16S and 23S rRNA are modified (as well as a set of r-proteins, see section 1.3.3). To date, 10 methylations and one pseudouridylation are known to take place in the *E. coli* 16S rRNA molecule, whereas 25 modifications have been identified in the 23S rRNA, specifically 14 methylations, 9 pseudouridylations, one methylated pseudouridine and one unknown modification, all of which are summarized in **Table 1** and **2** (Kaczanowska and Ryden-Aulin 2007; Wilson and Nierhaus 2007).

Table 1: 16S rRNA modifications in *Escherichia coli*. In summary, the 16S rRNA molecule contains 10 methylations and one pseudouridylation, which are mainly carried out after transcription. $^a m^x_y N$ refers to methylation (m) of rRNA nucleotide N at the x position (with y number of methylation) of the base, whereas Nm indicates methylation of the sugar at the 2' position of nucleotide N.

Location	Enzyme	Substrate	Modification
516	RsuA (YejD)		Ψ
527	RsmG (GidB)		m^7G
966	RsmD (YhhF)	30S	m^2G

967	RsmB (RrmB)	16S	m ⁵ C
1207	RsmC (YjjT)	30S	m ² G
1402	RsmH (MraW)	30S	m ⁴ Cm
	RsmI (YraL)		
1407	RsmF (YebU)	30S	m ⁵ C
1498	RsmE (YggJ)	30S	m ³ U
1516	RsmJ (YhiQ)	30S	m ² G
1518	RsmA (KsgA)	30S	m ⁶ ₂ A
1519	RsmA (KsgA)	30S	m ⁶ ₂ A

Table 2: 23S rRNA modifications in *Escherichia coli*. In total, the 23S rRNA molecule contains 14 methylations, 10 pseudouridylations, 1 further methylation of a pseudouridine and one unknown modification. ^am^x_yN refers to methylation (m) of rRNA nucleotide N at the x position (with y number of methylation) of the base, whereas Nm indicates methylation of the sugar at the 2' position of nucleotide N. Enzymes written in *italic* are hypothetical.

Location	Enzyme	Modification
745	RlmA ^I (RrmA, YebH)	m ¹ G
746	RluA (YabO)	Ψ
747	RlmC (RumB, YbjF)	m ⁵ U (T)
748	RlmA ^{II} (TlrB)	m ¹ G
955	RluC (YceC)	Ψ
1618	RlmF (YbiN)	m ⁶ A
1835	RlmG (YgjO)	m ² G
1911	RluD (YfiL)	Ψ
1915	RluD (YfiL)	m ³ Ψ

1917	RluD (YfiL)	Ψ
1939	RlmD(RumA, YgcA)	m ⁵ U (T)
1962	RlmI (YccW)	m ⁵ C
2030	<i>RlmJ</i>	m ⁶ A
2069	<i>RlmK</i>	m ⁷ G
2251	RlmB (YjfH)	Gm
2445	RlmL (YcbY)	m ² G
2449	<i>RldA</i>	D
2457	RluE (YmfC)	Ψ
2498	RlmM (YgdE)	Cm
2503	RlmN (YfgB)	m ² A
2504	RluC (YceC)	Ψ
2552	RlmE (RrmJ, FtsJ)	Um
2580	RluC (YceC)	Ψ
2604	RluF (YjbC)	Ψ
2605	RluB (YciL)	Ψ

Additionally, there are many known modifications found in rRNA that confer resistance to specific antibiotics, for example, the dimethylation of A2058 for macrolides (reviewed by (Weisblum 1995)) or the methylation of G1408 in 16S rRNA for aminoglycosides (Skeggs, Thompson *et al.* 1985).

What is surprising is that the exact role of the modifications is still not clearly understood. Most of the modifications are not essential for cell viability and their absence has little or no effect on cell growth and translational efficiency, with a few exceptions, for example the deletion of the pseudouridine synthase RluD, which causes defects in cell growth and ribosome assembly (Gutgsell, Deutscher *et al.* 2005). Nevertheless, the majority of the modifications are located in significantly important regions on the ribosome, including the

tRNA-mRNA binding sites on the small ribosomal subunit as well as the PTC on the 50S subunit. Due to this clustering of modified nucleosides in functionally important regions of the ribosome, the post-transcriptional modifications are thought to be essential for the folding and assembly process of the ribosome, as well as the stability of the ribosome in the cell (Noller and Woese 1981; Brimacombe, Mitchell *et al.* 1993; Decatur and Fournier 2002; Xu, O'Farrell *et al.* 2008).

1.3.3 Modification of ribosomal Proteins

In total, 11 r-proteins are modified post-translationally in eubacteria (**Table 3**). According to current knowledge, these consist mainly of methylations and acetylations, as determined by mass spectrometry (Arnold and Reilly 1999; Kaczanowska and Ryden-Aulin 2007). Some of the r-protein modifications have already been well studied. For example, the number of glutamic acid residues at the C-terminal end of S6 varies and is mostly dependent on pH, reaching a maximum number at pH 9.5. The protein responsible for the addition of glutamic acid residues at the C-terminus of S6 was identified as RimK in *Escherichia coli* (Reeh and Pedersen 1979; Kang, Icho *et al.* 1989; Kino, Arai *et al.* 2011). Similar to the rRNA modification, the functional role of most of the post-translational r-protein modifications is also unclear, as exemplified by r-protein L11: L11 methylation is highly conserved and the protein responsible for this modification was identified in *E. coli* as the methyltransferase PrmA (Vanet, Plumbridge *et al.* 1994). Deletion of the *prmA* gene, and the therefore resulting absence of the L11 methylation, however, does not show any effect on the phenotype - which is in agreement to studies of rRNA modifications.

Table 3: Post-translational modifications of r-proteins in *Escherichia coli*. The table shows the specific protein of either the small (S) or the large (L) ribosomal subunit with the kind of modification (e.g. acetylation) and known position of the modification on the specific r-protein (e.g. N-terminus).

Protein	Modification	Position
S5	acetylation	N-terminus
S6	glutamic acid residues	C-terminus

S11	monomethylation	N-terminus
S12	methylthio-aspartate	D88
S18	acetylation	N-terminus
L3	monomethylation	Q150
L7/L12	monomethylation	K81
L12	acetylation	N-terminus
L11	3 trimethylations	N-terminus, K3, K39
L16	monomethylation	N-terminus
L33	monomethylation	N-terminus

1.3.4 Non-ribosomal Factors involved in Ribosome Assembly

There is experimental evidence that bacterial ribosomal subunits can be reconstituted *in vitro* from purified rRNA and r-protein components, but the conditions that are required for this are highly non-physiological (Nomura, Gourse *et al.* 1984; Nierhaus 1991). *In vivo*, the assembly process is supported by a multitude of extra-ribosomal factors. This is in particular well-characterized for *S. cerevisiae* where over 200 supporting factors have been identified to date (Hage and Tollervey 2004). In eubacteria, an ever-increasing number of proteins are found to be involved in ribosome biogenesis. These factors can be classified into different groups according to their specific functions during the assembly process, including RNA modification enzymes that were already mentioned above, RNA helicases, heat shock proteins, ribosome-dependent GTPases and RNA chaperones. These enzymes are summarized in **Table 4** and will be discussed in detail below (Kaczanowska and Ryden-Aulin 2007; Wilson and Nierhaus 2007).

Table 4: Summary of non-ribosomal factors involved in ribosome biogenesis in eubacteria. The table is divided into different sections consisting of the name (and maybe differing name in other species than *Escherichia coli*) of the protein factor, the appropriate class of the factor and the possible function of the protein during ribosome assembly.

Factor	Class	Function
CsdA (DeaD)	RNA helicase	Cold shock DeaD A ATP-dependent RNA helicase that binds to 50S to mediate unwinding of 23S rRNA during assembly
DbpA	RNA helicase	DEAD box protein A ATP-dependent RNA helicase that binds to 50S to mediate unwinding of 23S rRNA during assembly
EngA (Der/ YfgK)	ribosome-dependent GTPase	involved in 50S subunit assembly
EngB (YihA)	ribosome-dependent GTPase	involved in 50S subunit assembly
Era	ribosome-dependent GTPase	<i>E. coli</i> Ras-like protein facilitates processing of the 3' end of the 16S rRNA precursor molecule
Obg (CgtA)	ribosome-dependent GTPase	SpoOB-associated GTP-binding protein binds to the 50S subunit
RbfA	RNA chaperone	Ribosome binding factor A facilitates 30S subunit assembly suppresses cold sensitive phenotype of C23U mutation in 16S rRNA
RbgA (YlqF)	ribosome-dependent GTPase	ribosome biogenesis GTPase A involved in late 50S subunit assembly not present in <i>Escherichia coli</i>
RimM (21K, YfjA)	RNA chaperone	ribosome maturation factor M involved in the maturation of the 30S head region

RimN (YrdC)	RNA chaperone	ribosome maturation factor N
		binds to 16S rRNA to facilitate correct processing
RsgA (YjeQ)	ribosome-dependent GTPase	ribosome small subunit dependent GTPase A
		involved in small ribosomal subunit assembly
SrmB	RNA helicase	suppressor of temperature-sensitive mutation in r-protein L24
		involved in ribosome biogenesis

RNA helicases are needed during ribosome assembly to unwind double stranded RNA and therefore promote proper folding of secondary structures. These enzymes can be divided into different classes according to conserved sequence motifs (Cordin, Banroques *et al.* 2006). The largest family of this group is the DEAD-box family that harbors conserved motifs for ATPase and helicase activities as well as variable N- and C-termini that are involved in substrate specificity. So far, 5 DEAD box helicases are known in *E. coli* (DeaD, SrmB, DbpA, RhlB and RhlE), of which the first three are involved in ribosome biogenesis (Iost and Dreyfus 2006).

Ribosome-dependent GTPases are needed for inducing conformational changes of structural RNA components. In the case of *E. coli*, five enzymes have been determined to date to be involved in ribosome biogenesis, two of them are associated with the small subunit (Era and RsgA) and three with the large subunit (Der, YihA and Obg). The majority of these factors are well conserved and therefore essential for the cell (Caldon and March 2003). A direct involvement in ribosome assembly could be shown for these small GTPases (Karbstein 2007) and in addition, overexpression of some of the GTPases is able to rescue single gene deletion strains of other assembly factors (Tan, Jakob *et al.* 2002; Inoue, Chen *et al.* 2006; Campbell and Brown 2008), which is exemplified by the GTPase Era that is able to rescue a cold-sensitive *rbfA* deletion strain (Inoue, Alsina *et al.* 2003).

In addition, RNA chaperones and heat-shock proteins promote favorable conformations of the RNA during assembly to ensure fast and correct maturation of the ribosome. Two of the most prominent heat-shock proteins known to be involved in ribosome biogenesis are DnaK and DnaJ, which were studied in detail, as well as GroEL (Alix and

Guerin 1993; El Hage, Sbai *et al.* 2001; Al Refaii and Alix 2009). Deletion of *dnaK* leads to severe assembly defects, mainly affecting the maturation of the 50S subunit. Both proteins, DnaK and DnaJ, are mostly needed at moderate temperatures, whereas at higher temperatures (42°C), other sigma-32 dependent heat-shock proteins are involved. Moreover, it could be shown that overexpression of GroEL/GroES can compensate partially for the deletion of DnaK protein (El Hage, Sbai *et al.* 2001). Some years later, it was confirmed that ribosomal particles isolated from a temperature-sensitive *dnaK* strain were found as precursor forms of the mature subunits which were able to assemble together, but at much slower rates (El Hage and Alix 2004). Both precursor particles (21S and 45S particles as precursor of mature 30S and 50S subunits, respectively) lacked some late assembly r-proteins, suggesting that the assembly factors discussed here are involved in a late stage of ribosome maturation (Maki, Schnobrich *et al.* 2002; Maki, Southworth *et al.* 2003).

Some non-ribosomal factors involved in ribosome biogenesis will be discussed in more detail below since they were part of a project in this thesis: these are the methyltransferases YhhF and RlmH, and the RNA chaperone protein RimM (see section 4).

1.4 Ribosomal Proteins

As mentioned before, rRNA is the key component of the ribosome being crucial in all essential steps of translation. However, r-proteins also have important functional roles within the ribosome. It is clear that the r-proteins are essential for correct ribosome assembly and function. In the next sections, r-proteins and their functional roles will be discussed in detail, focusing also on differences within the kingdoms as well as on specific r-proteins exclusively present in organelles, such as chloroplasts and mitochondria.

1.4.1 Ribosomal Proteins in Eubacteria

In total, the bacterial 70S ribosome consists of 54 r-proteins and thus corresponds to one third of the total mass of a ribosome; 21 of them are associated with the small ribosomal subunit and 33 r-proteins with the large ribosomal subunit. Ribosomal proteins were originally assigned due to their behavior on a two-dimensional polyacrylamide gel resulting in large acidic proteins with small numbers and small basic proteins with large numbers (Kaltschmidt

and Wittmann 1970). R-proteins are usually basic proteins with an average isoelectric point (pI) of ~10 due to their interactions with negatively charged rRNA. Some r-proteins have specific functions on the ribosome including ribosome assembly, however, most often it is very complicated to assign a specific function to an individual r-protein. The ribosome could be better envisaged as a huge network, with the two main components, rRNA and r-proteins, interacting with each other in a cooperative way. To illustrate this phenomenon with an example, mutations in r-protein L4 and L22 can confer resistance to the antibiotic erythromycin. However, the drug does not contact these r-proteins directly, instead the mutations in r-protein L4 and L22 cause conformational alterations within the surrounding 23S rRNA which then leads to resistance indirectly (Gregory and Dahlberg 1999). Interestingly, there is a significant number of bacterial r-proteins that have orthologues in both eukaryotes and archaea (Lecompte, Ripp *et al.* 2002). In contrast, prokaryotes do not share any r-proteins exclusively with the domains of eukaryotes and archaea, but the latter two do have r-proteins in common that are not present in eubacteria. R-proteins are uniformly distributed over the ribosome but mainly over the solvent side leaving the interface region protein-free. For the small ribosomal subunit, S12 is the notable exception, being found on the interface side near the decoding region. Some functional important regions are particularly rich in r-proteins, namely the mRNA entry and exit sites on the 30S subunit, the region surrounding the L7/L12 stalk and the ribosomal tunnel exit of the large subunit. Most r-proteins possess a globular domain that is located on the surface structure of the ribosome together with a long extension at either the N- or the C-termini that interacts with regions located deeper inside the ribosome (see also review (Wilson and Nierhaus 2005)).

1.4.2 Ribosomal Proteins in Eukaryotes and Archaea

The proteome of eukaryotic ribosomes was already under intensive investigation and the r-protein composition for several different species ranging from *Saccharomyces cerevisiae* (Link, Eng *et al.* 1999; Lee, Berger *et al.* 2002) and *Drosophila melanogaster* (Alonso and Santaren 2006) to *Arabidopsis thaliana* (Giavalisco, Wilson *et al.* 2005) and humans (Vladimirov, Ivanov *et al.* 1996; Odintsova, Muller *et al.* 2003) has been characterized. For example, the ribosome of the lower eukaryote *S. cerevisiae* possesses 79 r-proteins, 34 of which have bacterial counterparts (Lecompte, Ripp *et al.* 2002).

Although the r-protein content of both bacterial and eukaryotic ribosomes has been studied in detail, a systematic analysis of archaeal ribosomes and their r-protein content has not been addressed. It seems that in comparison to the r-protein content of *E. coli*, the number of archaeal r-proteins increased but does not reach the r-protein content of eukaryotic ribosomes resulting in an intermediate version between the bacterial and the eukaryotic ribosome. In addition, archaea have evolved domain-specific ribosomal proteins, exemplified by r-protein LX (Ramirez, Louie *et al.* 1991), which has neither an equivalent in eubacteria nor in eukaryotes.

1.4.3 Specific Ribosomal Proteins in Organelles

1.4.3.1 Chloroplasts

Chloroplasts are intracellular organelles that are found predominantly in plants and other eukaryotes carrying out the important function of photosynthesis. This organelle originated from an early endosymbiotic event, most probably with a cyanobacterium as an ancestor. In particular, this process implies the absorption of a photosynthetic prokaryote by a eukaryotic host cell. During evolution, the majority of genes derived from the engulfed prokaryote were transferred to the host genome (Huang, Ayliffe *et al.* 2003; Timmis, Ayliffe *et al.* 2004). The genes which are still transcribed and translated by the chloroplast are targeted to the thylakoid membranes (including components of the ATP synthase, cytochrome B/F, photosystem I and II complexes) and encode for NADH dehydrogenase, the large subunit of RuBisCo, RNA polymerase subunits and a distinct subset of ribosomal proteins: 12 from the 30S subunit and 8 from the 50S subunit. The additional r-proteins are nuclear-encoded and imported into the organelle.

In general, chloroplast ribosomal proteins have homologues to all *E. coli* r-proteins (with the exception of L25 and L30, which are absent) and have extensions at both the N- and C-termini (Yamaguchi and Subramanian 2000). In addition, the chloroplast ribosome possesses six plastid-specific ribosomal proteins called PSRPs (Somanchi and Mayfield 1999). Four of them are associated with the small ribosomal subunit and two of them bind to the large ribosomal subunit (Yamaguchi and Subramanian 2000; Yamaguchi, von Knoblauch *et al.* 2000). All PSRPs are encoded by genes located in the nucleus and are synthesized as precursor proteins in the cytoplasm before being imported into the chloroplast. With the

exception of PSRP1 (Sharma, Wilson *et al.* 2007), the functional roles of these chloroplast-specific factors have not been identified to date. PSRP1 associates with the small ribosomal subunit and binds in particular to a functionally important region of the 30S subunit overlapping with the binding sites of A- and P-site tRNAs (Sharma, Wilson *et al.* 2007).

1.4.3.2 Mitochondria

Similar to chloroplasts, mitochondria are also derived from an early endosymbiotic event, most probably originating from proteobacteria, in particular *Rickettsiales* (Emelyanov 2001). The organelle still possesses a translation system that closely resembles the one from eubacteria, with the main function of the organelle associated with oxidative phosphorylation and the production of ATP (Allen 2003). As already mentioned above, the genomes of chloroplasts as well as mitochondria are highly reduced due to the superfluousness of the majority of proteins or the transfer of indispensable proteins to the nucleus (Martin and Herrmann 1998; Berg and Kurland 2000; Blanchard and Lynch 2000; Adams and Palmer 2003). However, mitochondrial ribosomes exhibit several features that distinguish them from the eubacterial translation system. On the one hand, the architecture of mitochondrial ribosomes (mitoribosomes) differs significantly at both the primary and secondary structural level resulting in a notably divergent evolution of the rRNA that is often accompanied by a length reduction in rRNA sequences (in higher eukaryotes) (Cedergren, Gray *et al.* 1988; De Rijk, Van de Peer *et al.* 1995). In general, a large variation exists between mitochondria from different eukaryotes (Pel and Grivell 1994) exemplified by the *S. cerevisiae* mitoribosome which is both rRNA- and protein-rich and the mammalian mitoribosome which is rRNA-poor and protein-rich. On the other hand, mitoribosomes contain a great variety of mitochondrion-specific ribosomal proteins (MSRPs) and this number differs significantly between eukaryotic species. A distinct set of 15 MSRPs are found in all mitochondrial genomes analyzed to date, however, both yeast and human mitoribosomes contain a multitude of lineage-specific MSRPs (Smits, Smeitink *et al.* 2007). For example, 81 r-proteins could be identified in the human 55S mitoribosome by proteomics, 33 and 48 r-proteins associated with the 30S and 50S ribosomal subunit, respectively (Koc, Burkhart *et al.* 2001a; Koc, Burkhart *et al.* 2001b). In addition, r-proteins in the organelle that have a bacterial counterpart are often significantly longer. A striking feature of mitoribosomes is the great variation in their sedimentation

coefficient, ranging from 50S in parasites (Maslov, Sharma *et al.* 2006) up to 80S in plants (Borst and Grivell 1971; Cury 1985; Kitakawa and Isono 1991).

Not surprisingly, only a few cryo-EM structures from mitochondrial ribosomes have been determined, revealing significant differences in comparison to eubacterial ribosome structures (Sharma, Koc *et al.* 2003; Sharma, Booth *et al.* 2009). The mammalian mitoribosome has an inverse r-protein:rRNA ratio (2:1) compared to prokaryotic ribosomes (r-protein:rRNA ratio 1:2), but many of the r-proteins have novel positions on the ribosome and are not found at sites which were originally occupied by rRNA (Sharma, Koc *et al.* 2003).

1.5 Translation Mechanism in Eubacteria

The ribosome facilitates translation by converting the information that is encoded in mRNA into the corresponding protein sequence. The mRNA binds on the small ribosomal subunit, in particular between the head and the body region of the 30S subunit. This is the place where the codons of mRNA interact with the anticodons of transfer RNA (tRNA). The ribosome offers three binding sites for tRNAs: the A-site where the incoming aminoacyl tRNA is binding to, the P-site which harbors the peptidyl tRNA with the growing nascent polypeptide chain attached to it and the E-site (exit site) where the empty, deacetylated tRNA is located after peptide-bond formation and before release from the ribosome. While “reading” the mRNA, tRNAs have to fulfill the function to deliver the correct amino acid which is attached to their 3' CCA end. The proper amino acid must then be connected to the already existing polypeptide chain via peptide-bond formation. Protein synthesis or the mechanism of translation is an intensively studied process that is still under investigation, especially in a structural point of view. The translation mechanism itself can be divided into three major parts – initiation, elongation and termination & recycling – and will be discussed in detail below (for review see (Schmeing and Ramakrishnan 2009), for schematic illustration, see **Figure 2**).

1.5.1 Initiation Phase

To initiate one round of translation, the start codon on the mRNA (usually AUG in eubacteria) has to be located in the P-site together with the initiator fMet-tRNA^{fMet}. One possible option to find the correct start position on the mRNA is that the ribosome recognizes

a specific sequence (AGGAGG) which is known as the Shine-Dalgarno (SD) sequence of the mRNA (Shine and Dalgarno 1974) and located upstream (5') of the initiator methionine codon. The SD sequence interacts with the anti-SD sequence on the 3' terminus of 16S rRNA resulting in the correct positioning of the start codon (Kaminishi, Wilson *et al.* 2007). However, there are other possibilities in eubacteria to start translation since the SD sequence was shown to be non-obligatory. A distinct secondary structure conformation of the mRNA can exist instead, which allows access to the AUG start codon and therefore prevents translation initiation at neighboring AUG codons (for review see (Nakamoto 2009)). Moreover, three initiation factors, IF1, IF2 and IF3, are required for this essential process. It was shown that the ability of the ribosome to screen for fidelity of a correct codon-anticodon interaction is strongly dependent on IF3 (Milon, Konevega *et al.* 2008). IF3 binds to the small ribosomal subunit and by doing so prevents the early binding of the 50S subunit (Karimi, Pavlov *et al.* 1999). IF3 binding occurs already during the termination & recycling step of the previous round of translation (see section 1.5.3, (Karimi, Pavlov *et al.* 1999; Peske, Rodnina *et al.* 2005)). The formation of the 30S initiation complex (30S-IC) requires the additional binding of mRNA, IF1 and IF2 as well as the initiator tRNA, which is recruited by the GTPase IF2 (Milon, Carotti *et al.* 2010). Recently, a cryo-EM structure of the complete 30S-IC became available showing IF2 interaction with IF1, the shoulder region of the 30S subunit and the CCA end of the initiator tRNA, which was found in a novel P/I site (peptidyl/ initiation site). The interaction of the IFs and the tRNA with the 30S subunit induces a 30S head movement relative to the body whereas the back-rotation takes place after 50S subunit joining, IF2-dependent GTP hydrolysis and IF2 release (Julian, Milon *et al.* 2011). IF1 binding blocks the ribosomal A-site (Carter, Clemons *et al.* 2001) and together with IF2, which is located in the intersubunit region of the 70S ribosome (Allen, Zavialov *et al.* 2005), facilitates the formation of the 70S initiation complex (70S-IC) by promoting the joining of the 50S subunit and therefore release of IF3 (Antoun, Pavlov *et al.* 2006; Grigoriadou, Marzi *et al.* 2007b; Milon, Konevega *et al.* 2008). IF2 is also responsible for holding the initiator tRNA in a distinct conformation to promote a stable complex formation (Simonetti, Marzi *et al.* 2008). After GTP hydrolysis and P_i release (Tomsic, Vitali *et al.* 2000; Grigoriadou, Marzi *et al.* 2007a), IF2 and the ribosome undergo substantial conformational changes (Myasnikov, Marzi *et al.* 2005). The initiator tRNA is then positioned in the PTC, the IFs are released from the ribosome and the ribosome is ready to enter the elongation phase of translation.

1.5.2 Elongation Phase: Decoding, Peptide-Bond Formation and Translocation

The elongation phase of translation is responsible for the synthesis of the nascent polypeptide chain. The initial step involves delivery of first tRNA to the vacant A-site by elongation factor Tu (EF-Tu) in the form of a so-called ternary complex together with GTP (Schmeing, Voorhees *et al.* 2009; Schuetz, Murphy *et al.* 2009). Firstly, the tRNA binds to the ribosome in a distinct conformation, with the A/T position, in which the anticodon stem-loop interacts with the A-site of the 30S subunit and the acceptor region carrying the amino acid still bound to EF-Tu. After initial binding of the ternary complex, the tRNA in the A-site is subject to a proof reading mechanism (Blanchard, Gonzalez *et al.* 2004). In this conformation, the tRNA directly contacts the decoding center of the small ribosomal subunit to verify the correct codon-anticodon interaction, thus discriminating against near-cognate or non-cognate ternary complexes. If the anticodon of the tRNA matches the codon of the mRNA, significant conformational changes within the ribosome, aa-tRNA and EF-Tu ensue (Rodnina, Fricke *et al.* 1994), leading to GTP hydrolysis by EF-Tu and its release from the ribosome. In particular, cognate tRNA binding involves the universally conserved bases A1492, A1493 (both are located in h44) and G530 of *E. coli* 16S rRNA by screening the Watson-Crick base-pairing between the first two codon-anticodon base pairs (Moazed and Noller 1990). The third, so-called “wobble” position of the codon is less strict, being able to accept different base-pair conformations (Ogle, Brodersen *et al.* 2001). Upon correct base-pairing, the 30S subunit converts from an open to a closed conformation that is unfavorable for near-cognate tRNAs but stimulates the GTPase activity of EF-Tu (Ogle, Murphy *et al.* 2002). This activation involves a catalytic histidine residue of EF-Tu (His84) that coordinates the attack of nucleophilic water on the γ -phosphate of GTP by interacting with A2662 of the sarcin-ricin loop of *E. coli* 23S rRNA (Voorhees, Schmeing *et al.* 2010). After dissociation of EF-Tu from the ribosome, the A-site tRNA converts from the initial A/T position to an A/A position (the tRNA is now bound to the A-site on both ribosomal subunits) and becomes accommodated into the PTC (Jenner, Demeshkina *et al.* 2010).

A still open question remains how the signal from the correct codon-anticodon interaction leads to stimulation of GTPase activity by EF-Tu. Recently, the group of M. Rodnina revealed that the A-site tRNA undergoes a large conformational rearrangement during the decoding process resulting in an open conformation of the tRNA that is retained until EF-Tu is released upon GTP hydrolysis (Mittelstaet, Konevega *et al.* 2011). In addition, the group of R. Green showed that miscoding tRNAs have an overall perturbed tertiary

structure and therefore an altered interaction with H69 of the large ribosomal subunit, which in turn represents an important signal for GTP activation (Ortiz-Meoz and Green 2010). Structures, determined by both cryo-EM and crystallography have visualized EF-Tu bound on the ribosome (Schmeing, Voorhees *et al.* 2009; Schuette, Murphy *et al.* 2009; Villa, Sengupta *et al.* 2009).

After tRNA accommodation, one important process of the elongation step takes place on the large ribosomal subunit, namely peptide-bond formation. The peptidyl-transferase reaction forms an ester bond, namely, the α -amino group of the aminoacyl tRNA on the A-site reacts with the carbonyl group of peptidyl-tRNA on the P-site. Therefore, the nascent polypeptide bound to the tRNA on the P-site is transferred to the tRNA located on the A-site. The mechanism behind this essential reaction is highly complicated and still under intensive investigation. One of the most recent hypotheses implies an important role for the 2'-OH group on the 3' terminal adenosine of the P-site tRNA (A76) suggesting an involvement of this group in a huge proton shuttle network. The ester bond is therefore accomplished by the stepwise formation of intermediate and transition states (Erlacher and Polacek 2008; Schmeing, Voorhees *et al.* 2009; Hiller, Singh *et al.* 2011). It was shown that replacement of this 2' OH by 2' H or 2' F leads to a dramatic decrease of peptide-bond formation (Weinger, Parnell *et al.* 2004). This step of translation was investigated using crystallography of the 70S ribosome in complex with A- and P-site tRNAs in pre- and post-peptidyl-transfer states (Voorhees, Weixlbaumer *et al.* 2009) and revealing interactions with r-protein L16 and L27 and the tRNA substrates (Moore, Atchison *et al.* 1975; Maguire, Beniaminov *et al.* 2005; Trobro and Aqvist 2008; Voorhees, Weixlbaumer *et al.* 2009).

After peptide-bond formation, the polypeptide chain is connected to the A-site bound tRNA, whereas the peptidyl tRNA becomes deacetylated. Elongation factor G (EF-G), a well-studied and conserved GTPase, moves the mRNA and tRNAs through the ribosome by one codon, a process which is called translocation. In summary, tRNAs have to move from their A- and P-site position to P- and E-sites, respectively. However, this process is highly dynamic since both tRNAs are oscillating after peptide-bond formation between classical states (A/A and P/P sites on 30S/50S) and hybrid states (A/P and P/E sites on 30S/50S) (Blanchard, Kim *et al.* 2004). Two independent groups have examined the hybrid states of both A/P and P/E tRNAs on the ribosome by cryo-EM and could show a correlation of the ratcheting movement with hybrid state formation (Agirrezabala, Lei *et al.* 2008; Julian, Konevega *et al.* 2008; Ratje, Loeke *et al.* 2010).

EF-G stabilizes the intermediate hybrid state and facilitates translocation on the 30S subunit in a GTP-dependent manner resulting in a post-translocational state ribosome with both tRNAs positioned at the P- and E-sites, respectively (Moazed and Noller 1989; Rodnina, Savelsbergh *et al.* 1997). R-protein L7/L12 is essential for EF-G function by the interaction with the G' sub-domain of EF-G (Mohr, Wintermeyer *et al.* 2002; Diaconu, Kothe *et al.* 2005; Nechifor, Murataliev *et al.* 2007). Mutational analyses of specific residues in the CTD of this protein (V66, I69, K70 and R73) affect EF-G binding, resulting in the inhibition of P_i release from the ribosome-EF-G-GDP- P_i complex. This seems to be important for the coordination of translocational rearrangements of EF-G and the ribosome as well as for EF-G dissociation (Savelsbergh, Mohr *et al.* 2005). The crystal structure of *Thermus thermophilus* EF-G in solution was solved in a nucleotide-free and GDP-bound state, visualizing a five-domain protein with a well-conserved G domain (Aevvarsson, Brazhnikov *et al.* 1994; Czworkowski, Wang *et al.* 1994). Domain VI of EF-G is essential for tRNA translocation on the ribosome, since the replacement of a highly conserved histidine residue in domain VI (His583) decreases the translocation rate dramatically (Savelsbergh, Matassova *et al.* 2000). Moreover, it could be shown that the switch I and II regions of the G domain interact with the sarcin-ricin loop of 23S rRNA (Connell, Takemoto *et al.* 2007). In addition, a structure of EF-G stalled on the ribosome in a post-translocational state by the antibiotic fusidic acid (FA) was investigated by crystallography showing factor-ribosome interactions via the L10-L12 stalk and the L11 region as well as domain IV of EF-G contacting P-site bound tRNA and mRNA (Gao, Selmer *et al.* 2009).

1.5.3 Termination & Recycling

Translation stops when a stop codon (UAA, UAG or UGA) reaches the A-site. In eubacteria, two class I release factors (RFs), namely RF1 and RF2, recognize either the codon triplets UAG/UAA or UGA/UAA, respectively (Scolnick, Tompkins *et al.* 1968), and bind to the A-site contacting both subunits (Petry, Brodersen *et al.* 2005a; Korostelev, Asahara *et al.* 2008; Laurberg, Asahara *et al.* 2008; Weixlbaumer, Jin *et al.* 2008; Jin, Kelley *et al.* 2010; Korostelev, Zhu *et al.* 2010). However, the situation is different in mitochondria where organelle-specific stop codons exist (AGG and AGA) (Soleimanpour-Lichaei, Kuhl *et al.* 2007). The action of RFs leads to release of the polypeptide chain from the P-site bound tRNA, producing a deacetylated tRNA at this position. The RFs contain highly conserved

motifs for both stop codon specificity and peptide hydrolysis (Frolova, Tsivkovskii *et al.* 1999; Song, Mugnier *et al.* 2000). In particular, the first base of each stop codon, uridine, is recognized by a certain amino acid motif (GxxE, located in helix $\alpha 5$) in both release factors, RF1 and RF2, while the second nucleobase is monitored by either the PVT motif in RF1 or the SPF motif in RF2 and the third stop codon position is screened by a specific threonine and another amino acid residue (T194 and Q181 in RF1, T216 and V203 in RF2) (Korostelev, Asahara *et al.* 2008; Laurberg, Asahara *et al.* 2008; Weixlbaumer, Jin *et al.* 2008; Korostelev, Zhu *et al.* 2010). Upon stop codon recognition, RF1/2 induce conformational changes in H69 of 23S rRNA, and then the switch loop of the RFs undergoes significant rearrangements, which leads to the docking of the universally conserved GGQ motif (located in domain 3 of the RF) into the PTC (Weixlbaumer, Jin *et al.* 2008; Korostelev, Zhu *et al.* 2010). It could be shown that the glutamine residue of the GGQ motif directly contributes to the catalysis of peptidyl tRNA hydrolysis (Shaw and Green 2007; Korostelev, Asahara *et al.* 2008). The main-chain amide nitrogen of the glutamine residue interacts with the 2' OH group of A76 of the peptidyl tRNA (Laurberg, Asahara *et al.* 2008). Cryo-EM analyses of 70S·RF complexes show that the RF resembles a tRNA bound at the A-site by connecting the decoding center on the 30S subunit (by interacting with the conserved PVT motif of RF1 or SPF motif of RF2) with the PTC on the 50S subunit (by interacting with the GGQ motif of RF1/2) (Klaholz, Pape *et al.* 2003; Rawat, Zavialov *et al.* 2003).

A third factor is required in the termination stage of translation, namely the GTPase RF3. Free RF3 in the cell is bound to GDP and the class I RF bound to the ribosome promotes the rapid nucleotide exchange in RF3 to GTP (Zavialov, Buckingham *et al.* 2001). In this state, RF3·GTP is able to bind to the ribosome and therefore releases the class I RF from the ribosome (Zavialov, Buckingham *et al.* 2001). GTP hydrolysis by RF3 is necessary so that RF3·GDP can dissociate from the ribosome (Zavialov, Buckingham *et al.* 2001; Gao, Zhou *et al.* 2007). RF3 induces a ratchet-like movement within the ribosome and interacts with the sarcin-ricin-loop of 23S rRNA via its G domain (Zhou, Lancaster *et al.* 2012). The RF3-induced ribosomal subunit rotation stabilizes the tRNA in a hybrid P/E conformation, therefore promoting the release of class I RFs (Jin, Kelley *et al.* 2011). Recently, it could be shown that RF3 has a primary role in monitoring translation fidelity by prematurely releasing peptides carrying mistakes in their sequence (Zaher and Green 2011). The remaining complex consisting of the 70S ribosome as well as the mRNA and deacetylated tRNA in the P/E-site has to be recycled for a new round of translation. This process is catalyzed by RRF

and EF-G (Hirashima and Kaji 1973). There is no structural data available showing the 70S post-termination ribosomal complex with both factors bound, however, there is a structure determined with RRF and EF-G bound to the large ribosomal subunit (Gao, Zavialov *et al.* 2005). The group of R.K. Agrawal could show by cryo-EM analysis that RRF is able to move from its initial binding site on the 70S ribosome to a different one that is located exclusively on the 50S subunit (Barat, Datta *et al.* 2007). A more recent analysis presents an intact 70S-RRF structure in a fully ratcheted conformation stabilizing the tRNA in the P/E hybrid state, which is in agreement to the recent studies on RF3 (Dunkle, Wang *et al.* 2011). Upon EF-G binding to the post-termination complex bound with RRF, RRF undergoes a translocation-like movement which promotes significant conformational changes within the ribosome resulting in the disruption of essential intersubunit bridge(s) with bridge B2a and B3 as the most important ones (Agrawal, Sharma *et al.* 2004; Barat, Datta *et al.* 2007; Pai, Zhang *et al.* 2008). EF-G-dependent GTP hydrolysis is required for the ribosomal subunit dissociation (Peske, Rodnina *et al.* 2005) and IF3 then associates with the 30S subunit to prevent re-association with the 50S subunit (Karimi, Pavlov *et al.* 1999), but also has a role in the recycling of pre-termination complexes which still harbor a peptidyl tRNA (Singh, Das *et al.* 2005). The ribosomal components are now ready for a new round of translation.

1.6 Inhibition of Translation: Antibiotics

Antibiotics are small compounds that were originally produced by certain bacteria or fungi to inhibit the growth or even kill other bacteria. Therefore antibiotics can be distinguished as bacteriostatic compounds – the majority of antibiotics belong to this section - that inhibit growth of bacteria without killing them, in contrast to bacteriocidal substances which lead to cell death (Davis 1987; Kohanski, Dwyer *et al.* 2007).

One of the first used and maybe most important discoveries in history was the compound penicillin which is naturally produced by the fungus *Penicillium notatum* and was first described by Alexander Fleming in 1929. Today, a huge number of different compounds are in medical usage against bacterial infections of humans as well as of animals. Most often these antibiotics are produced in a semi-synthetic way, i.e. the compounds are isolated from natural sources and are chemically modified afterwards.

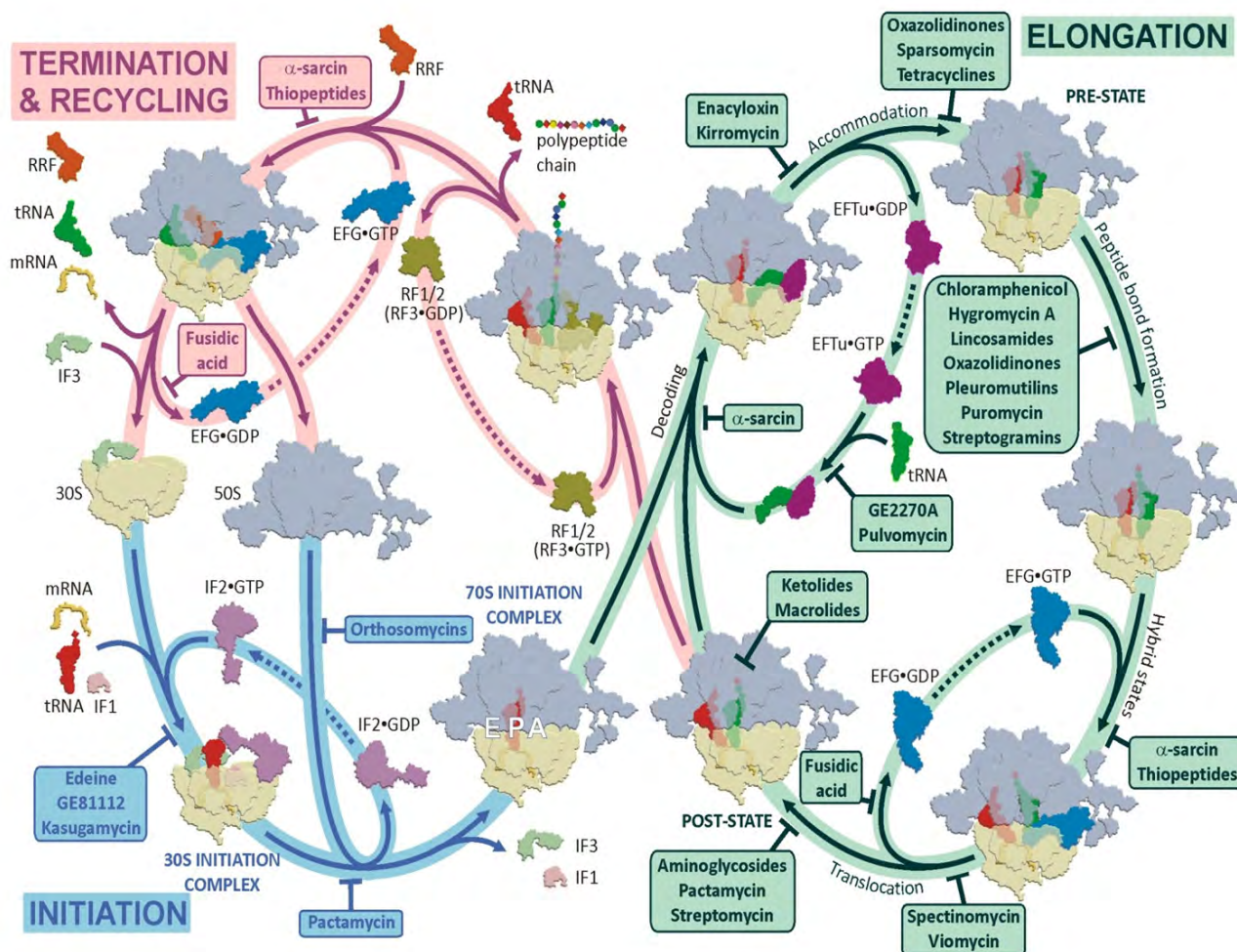


Figure 2: Inhibition of translation by antibiotics. The cycle of protein synthesis can be affected at every step of translation as indicated by square boxes. The different steps of translation – initiation, elongation, termination & recycling are highlighted in blue, green and red, respectively. The figure was taken from (Wilson 2009).

In general, antibiotics have several different targets in the cell, including cell wall synthesis (e.g. Penicillins, Cephalosporins), cell wall integrity (β -lactamases) and cell membrane function (Polymyxins), as well as affecting folate metabolism (Sulfonamides, Trimethoprim), DNA and RNA synthesis (Quinolones, Rifampicin) and protein synthesis (Fischbach and Walsh 2009). The process of translation is one of the major points of action for a wide range of antibiotics, to an extent that almost every single step in protein synthesis can be affected by a specific drug (**Figure 2**).

In addition, almost all clinically used antibiotics that target the ribosome have been structurally visualized in complex with their specific subunit target, either bound to the 30S (e.g. (Brodersen, Clemons *et al.* 2000; Carter, Clemons *et al.* 2000)) or 50S subunit (e.g.

(Schlünzen, Zarivach *et al.* 2001); for summary see review (Wilson 2009)). With the help of these structures, it was shown that most antibiotics target – not surprisingly – the functional centers of the ribosome, namely the tRNA-mRNA binding sites on the 30S subunit as well as the PTC on the 50S subunit. Moreover, the majority of interactions between the compound and the ribosome involve rRNA, which is predominantly present in the functional centers of the ribosome.

1.6.1 Stages of Inhibition during Translation

There are five different classes of antibiotics that target the small or the large ribosomal subunit during the initiation phase of translation. All of them differ slightly in their mode of action: (i) kasugamycin inhibits the stable binding of the initiator tRNA with the start codon by directly blocking the path of the mRNA (Schlunzen, Takemoto *et al.* 2006), (ii) in contrast to edeine which overlaps the peptidyl tRNA binding site (Pioletti, Schlunzen *et al.* 2001; Dinos, Wilson *et al.* 2004) and prevents the interaction of the initiator tRNA with the 30S subunit (Moazed and Noller 1987). (iii) Early studies suggest that pactamycin inhibits the formation of the 70S initiation complex (reviewed by (Gale, Cundliffe *et al.* 1981), however more recent studies implicate this compound in inhibition of translocation (Dinos, Wilson *et al.* 2004). (iv) Oligosaccharide antibiotics like the orthosomycins, with evernimicin as a prominent member, prevent the formation of the 70S-IC in an IF2-dependent manner by interacting with the large ribosomal subunit (Belova, Tenson *et al.* 2001; Burakovskii, Smirnova *et al.* 2007). (v) The tetrapeptide antibiotics, like GE81112, are very effective in the inhibition of 30S-IC formation by preventing the binding of the initiator tRNA to the 30S subunit in an mRNA-independent manner (Brandi, Fabbretti *et al.* 2006).

The elongation phase of translation is targeted by a huge number of antibiotics and therefore can be affected in several different ways: Firstly, tRNA delivery to the ribosome can be affected by either inhibiting accommodation of A-site tRNA upon EF-Tu-dependent GTP hydrolysis (tetracycline) (Blanchard, Gonzalez *et al.* 2004), trapping EF-Tu on the ribosome (kirromycin) or by binding to the elongation factor and thereby inhibiting the interaction of EF-Tu with aa-tRNAs (pulvomycin) (Parmeggiani and Nissen 2006). In contrast, aminoglycosides and streptomycins are known to introduce translational misreading: aminoglycosides stabilize tRNA binding and facilitate accommodation of near-cognate tRNAs at the A-site, whereas streptomycins discriminate the selection of cognate tRNAs and therefore promote near-

cognate tRNA binding to the A-site (Karimi and Ehrenberg 1994; Pape, Wintermeyer *et al.* 2000). The PTC itself can be affected through the binding of compounds in this specific region, resulting in the prevention of peptide-bond formation (e.g. chloramphenicol (Pestka 1969; Rheinberger and Nierhaus 1990), hygromycin A (Guerrero and Modolell 1980), lincomycin (Fernandez-Munoz, Monro *et al.* 1971) and linezolid (Wilson, Schlutzen *et al.* 2008)). A different way of targeting the PTC is achieved by puromycin that binds to the A-site and releases the nascent polypeptide chain from the ribosome (Darken 1964). Another target in the elongation phase is the translocation step where the tRNAs move in a cyclic fashion through the A-, P- and E-site on the ribosome after peptide-bond formation occurred. This is the target of many different classes of antibiotics, including aminoglycosides, spectinomycin, viomycin, ribotoxins and thiopeptides. Aminoglycosides are strong translocation inhibitors (Cabanas, Vazquez *et al.* 1978; Misumi, Nishimura *et al.* 1978), and also facilitate back-translocation (Shoji, Walker *et al.* 2006; Borovinskaya, Shoji *et al.* 2007). Binding of spectinomycin to the ribosome prevents the swiveling of the 30S head region and thereby inhibits the translocation reaction (Borovinskaya, Shoji *et al.* 2007). The compound viomycin stabilizes the peptidyl tRNA in the A-site and the uncharged tRNA in a P/E hybrid state and therefore prevents the translocation reaction (Liou and Tanaka 1976; Modolell and Vazquez 1977; Feldman, Terry *et al.* 2010). Ribotoxins like α -sarcin target H95 of 23S rRNA (known as the sarcin-ricin-loop (SRL)) resulting in a cleavage of the SRL with A2660 as a key component in the GTPase activation of EF-G (Clementi, Chirkova *et al.* 2010). The thiopeptide family of antibiotics, with thiostrepton as a well-known member, prevent the stable binding of EF-G on the ribosome, thus resulting in translocation inhibition (Seo, Kiel *et al.* 2004). Additionally, thiopeptides inhibit IF2 by causing a fast recycling from the initiation factor from the ribosome (Brandi, Marzi *et al.* 2004), EF-Tu dependent tRNA delivery (Gonzalez, Chu *et al.* 2007) as well as the GTPase RF3 (Cameron, Thompson *et al.* 2002). A different way to affect elongation is carried out by macrolides that bind within the ribosomal tunnel exit and prevent the elongation of most nascent polypeptide chains (Otaka and Kaji 1975; Tenson, Lovmar *et al.* 2003).

Several compounds mentioned here affect more than one step during translation, thus no specific inhibitors are known to exclusively target the termination & recycling phase during translation. Examples would be the aminoglycosides as well as streptomycins that affect translational fidelity by inducing misreading, but are also known as potent translocation inhibitors. Moreover, compounds like thiostrepton and α -sarcin target elongation factors EF-

Tu and EF-G and, in addition, other translational GTPases, like IF2. EF-G is mainly responsible for translocation but is also participating in ribosome recycling together with RRF and therefore, antibiotics like viomycin and fusidic acid (FA) were shown to target both translocation and termination (Hirokawa, Kiel *et al.* 2002). For FA, it could be shown that the drug has a more significant effect on the recycling process since the P_i release is obligatory for ribosome disassembly (Savelsbergh, Rodnina *et al.* 2009).

1.6.2 Mechanisms of Antibiotic Resistance and Strategies to overcome this Problem

Resistance to antibiotics is already a significant and still increasing problem in our society also due to an unnecessary over-usage of these compounds. Bacteria utilize multiple strategies to obtain resistance against antibiotics, which causes problems due to the increasing number of resistant bacteria (Davies and Davies 2010). This issue will be discussed here with one specific example, the compound tetracycline (for review see (Griffin, Fricovsky *et al.* 2010)). Tetracycline was first introduced for medical usage in the late 1940s. Since Tet is a broad-spectrum antibiotic, it was heavily used against a wide range of Gram-positive and Gram-negative bacteria as well as chlamydiae and protozoan parasites for many years. Bacteria have developed several strategies to obtain resistance to this compound, including efflux pumps, ribosome protection proteins (RPPs), enzymatic inactivation of Tet and some uncharacterized mechanisms of resistance (for review see (Chopra and Roberts 2001)).

In 1948, the first member of the group of tetracyclines was isolated, namely chlortetracycline, that is naturally produced by *Streptomyces aureofaciens* (Duggar 1948). In general, the chemical structure of this class consists of a four-ring system (with the individual rings designated as A, B, C and D) and functional groups attached to it. Later, other tetracyclines were discovered, like the compound tetracycline (Tet) from several *Streptomyces* species (1953), but also semi-synthetic approaches were accomplished with the production and marketing of doxycycline (Winkler and Weih 1967) and minocycline (Klastersky and Daneau 1972) which were essentially well tolerated. These compounds are known and can be referred to as first-generation (1948 to 1963) and second-generation tetracyclines (1965 to 1972). The next generation consists of the semi-synthetic group of

glycylcyclines (Chopra 2002), with tigecycline (Tgc) as one of the commercially used compounds (Tygacil®). In comparison to Tet, Tgc possesses a substitution at the C7 and C9 position of the chemical structure and displays an enhanced antimicrobial activity, including resistance against *tet* genes (Rasmussen, Gluzman *et al.* 1994; Bergeron, Ammirati *et al.* 1996).

As of 2001, twenty-nine different tetracycline resistance (*tet*) and three oxytetracycline resistance (*otr*) genes have been characterized, which encode either efflux proteins or RPPs. Efflux proteins have been extensively studied and all *tet* efflux genes encode for membrane-associated proteins which transport the drug via the cell membrane out of the cell. The pump functions with the help of a proton gradient, which means one H⁺ is exchanged against one molecule of tetracycline (Yamaguchi, Ono *et al.* 1990) resulting in a reduction of the intracellular drug concentration. In general, efflux proteins have a size of approximately 46 kDa and are divided into six groups according to their sequence identity. Tet efflux pumps show sequence and structure similarities to other known efflux proteins, for example AraB, an arabinose transporter described in *Escherichia coli* (Sheridan and Chopra 1991). Due to the encoding of many *tet* genes on plasmids, together with other favorable selection markers, the efflux genes are already widely distributed and this might increase even more during the next years.

Ribosome protection proteins (RPPs) are soluble, cytoplasmic proteins that confer resistance to tetracyclines by releasing the compound from the ribosome. In general, RPPs show homology to elongation factors EF-Tu and EF-G, including the GTP-binding domain (Sanchez-Pescador, Brown *et al.* 1988; Taylor and Chau 1996). Both proteins, Tet(O) and Tet(M), are well-characterized. It has been shown that EF-G and Tet(M) bind to the same region of the ribosome, however, Tet(M) has a higher affinity in comparison to EF-G (Dantley, Dannelly *et al.* 1998). Hence, there are functional differences between Tet(M) and EF-G, since the RPP cannot compensate for the function of EF-G *in vivo* and *in vitro* (Burdett 1996). GTP hydrolysis might be crucial for the release of the compound from the ribosome (Taylor and Chau 1996; Trieber, Burkhardt *et al.* 1998), but the exact mechanism as to how the compound is released from the ribosome is so far not well understood. Structural investigations using cryo-EM were performed on a complex consisting of *E. coli* 70S, Tet(O) and a non-hydrolyzable GTP analogue resulting in a structure at 16 Å resolution (Spahn, Blaha *et al.* 2001). It could be shown that the binding position of Tet(O) is close to the ribosomal A-site and adjacent to the Tet1 binding site similar to EF-G, however, the tip of

domain IV of EF-G reaches further into the A-site contacting intersubunit bridge B2a in the case of EF-G (Agrawal, Heagle *et al.* 1999) suggesting that Tet release from the ribosome is catalyzed by Tet(O) indirectly, probably due to conformational rearrangements in h34 (Spahn, Blaha *et al.* 2001).

Tet can also be inactivated in an enzymatic way by the function of *tet(X)*. Tet(X) is a 44 kDa cytoplasmic protein that encodes for an oxidoreductase and modifies the chemical structure of Tet in the presence of oxygen and NADPH. So far this gene was only found in anaerobic *Bacteroides* (Speer, Bedzyk *et al.* 1991; Yang, Moore *et al.* 2004). Additionally, one more gene is known to be involved in conferring Tet resistance, however, the mechanism is not described to date. *tet(U)* encodes for a small protein that shows some sequence similarity to known *tet* genes excluding the GTP binding domain (Ridenhour, Fletcher *et al.* 1996).

Due to bacterial strategies to obtain resistance against Tet, there was some time and effort invested to find and develop new tetracycline derivatives, such as the third- and fourth-generation glycylicyclines, that are immune to some of the above-mentioned resistance mechanisms (Chopra 2002). The most prominent and commercially used member of this group is tigecycline (Tgc, Tygacil®) that differs from the original Tet structure by having extensions at the C9 position (of ring D). This new compound shows higher affinity to the ribosome in comparison to the original compound (Bauer, Berens *et al.* 2004) and is immune against bacteria harboring *tet* resistance genes (Rasmussen, Gluzman *et al.* 1994; Bergeron, Ammirati *et al.* 1996). However, in recent studies it could be shown that TetX represents the first identified resistance mechanism against the broad-spectrum antibiotic Tgc (Volkers, Palm *et al.* 2011).

2 Objectives and Aims of the Thesis

The ribosome and the process of translation are central to the life of the cell and are therefore highly regulated. To date, a multitude of factors involved in ribosome function have been identified. This includes a variety of proteins that play a role during ribosome biogenesis, such as RNA modification enzymes and chaperones (see section 3: Dönhöfer, Sharma *et al.*, 2009), but also protein factors that participate directly in the essential process of translation, e.g. the elongation factors EF-Tu and EF-G. Furthermore, the binding and interaction of factors to the ribosome can be modulated by the composition of the ribosome itself and therefore insights into translation regulation in different organisms, such as archaea or eukaryotic organelles (chloroplasts and mitochondria) can arise from differences in composition of their respective ribosomes. Finally, translation itself can be inhibited due to the action and binding of antibiotics to the ribosome. Interestingly, resistance to some antibiotics, such as the tetracyclines, can arise from the binding of specialized protein factors to the ribosome.

With this in mind, the thesis presented here aims to investigate these different regulatory events and is divided into four topics:

(I) Ribosome Biogenesis

The role of a group of factors involved in bacterial ribosome biogenesis has been so far only partially understood. This thesis concentrates on two different modification enzymes, namely the *E. coli* methyltransferase YhhF and RlmH as well as one chaperone-like protein, *E. coli* RimM (see section 4). The aim for these projects was (i) to identify their exact binding position on either the 70S ribosome (in case of RlmH) or the small ribosomal subunit (in case of YhhF and RimM) by cryo-EM analysis and (ii) to gain more insights in the functional roles of these proteins. Moreover, ribosome assembly can be affected by the presence of several antibiotics. Here it was shown that premature ribosomal particles treated with specific compounds are able to mature, but exhibit differences in the r-protein content in comparison to standard intermediate particles determined mainly by pulse labeling and mass spectrometry (see section 3: Siibak, Peil *et al.*, 2011).

(II) Translation Factors

During the process of translation, the growth of the nascent polypeptide chain is facilitated through the movement of tRNAs on the ribosome in a cyclic manner accompanied by the connection of amino acids via peptide-bond formation. This process is catalyzed by EF-G in a GTP-dependent manner. One part of the thesis focuses on the translocation mechanism, in particular showing two structural sub-steps of translocation analyzed by cryo-EM (see section 3: Ratje, Loerke *et al.*, 2010).

(III) Ribosome Composition

In a more global perspective, the composition of archaeal ribosomes was investigated with a particular focus on the r-protein content. This analysis elucidated the presence of novel r-proteins in general and identified possible binding positions of these proteins determined by cryo-EM (see section 3: Márquez, Fröhlich *et al.*, 2011). Moreover, this work addresses the composition of ribosomes present in intracellular organelles, such as chloroplasts and mitochondria. Both organelles possess specific r-proteins that exhibit novel features or have a specific function on the ribosome. In chloroplasts, six plastid-specific ribosomal proteins (PSRPs) are known and one of these factors, called PSRP1, was studied here in detail from a biochemical and structural point of view (see section 3: Sharma, Dönhöfer *et al.*, 2010). In mitochondria, a larger number of additional factors have been identified, but their functions and binding positions on the ribosome are only partially understood. Therefore, one part of this thesis also focuses on this topic (see section 5).

(IV) Antibiotic Resistance Proteins

One specific protein conferring resistance to the antibiotic tetracycline, namely Tet(M), was also investigated in this thesis (see section 6). The aim here was to confirm the binding position on the *E. coli* 70S ribosome in terms of ribosomal contacts as well as to obtain better insight into the exact mechanism of how the antibiotic is released from the ribosome due to the action of this protein factor.

3 Cumulative Thesis: Summary of published Results

3.1 Paper I

Dönhöfer A, Sharma MR, Datta PP, Nierhaus KH, Agrawal RK, Wilson DN.

***Factor-mediated ribosome assembly in bacteria.* Encyclopedia of Life Sciences (ELS), 2009. Review.**

Ribosome biogenesis is a crucial process in all living organisms since protein synthesis is dependent on the correct folding of rRNA and the assembly of the ribosome in general. Although both bacterial ribosomal subunits can be reconstituted *in vitro*, the conditions to do so are far from physiological. *In vivo*, the process of ribosome assembly is supported by a multitude of additional factors, including enzymes that are involved in rRNA processing, unwinding and modification, but also factors that facilitate the assembly process itself. This review focuses mainly on the latter protein factors with the aim to provide an overview of the enzymes that are known so far in eubacteria and their functional roles in ribosome assembly.

Non-ribosomal factors that are identified to be involved in the assembly of the small ribosomal subunit are RbfA, Era, RsgA, RimM and RimN. Structural data is available from both crystallography presenting the free protein structure and cryo-EM showing 30S-factor complexes for RbfA (Huang, Swapna *et al.* 2003; Datta, Wilson *et al.* 2007), Era (Chen, Court *et al.* 1999; Sharma, Barat *et al.* 2005) and RsgA (Shin, Lou *et al.* 2004; Guo, Yuan *et al.* 2011). For the two remaining factors, RimM and RimN, crystal structures of the free proteins were determined (*P. aeruginosa* RimM: PDB2F1L, *T. thermophilus* RimM: PDB2DYI; RimN (Teplova, Tereshko *et al.* 2000)), as well as a crystal structure of *T. thermophilus* RimM and r-protein S19 (PDB3A1P), but structural data for 30S-RimM and 30S-RimN complexes is still missing. Many GTPases are involved in the biogenesis of the 50S subunit, such as Obg, EngA, EngB and RbgA. Crystal structures for all of the free proteins have been determined and summarized here (for Obg (Buglino, Shen *et al.* 2002; Kukimoto-Niino, Murayama *et al.* 2004), EngA (Robinson, Hwang *et al.* 2002; Muench, Xu *et al.* 2006), EngB (Ruzheinikov, Das *et al.* 2004) and RbgA (Kim do, Jang *et al.* 2008)), accompanied by biochemical data.

In summary, there is still some information missing, including the exact binding position for RimM and RimN on the 30S subunit, as well as insights in all structural complexes between the 50S assembly factors and the large ribosomal subunit. In particular, it will be interesting to see in which step and order these factors participate in the assembly process.

3.2 Paper II

Siibak T, Peil L, Dönhöfer A, Tats A, Remm M, Wilson DN, Tenson T, Remme J.

Antibiotic-induced ribosomal assembly defects result from changes in the synthesis of ribosomal proteins. Mol Microbiol. 2011 Apr; 80(1): 54-67.

The biogenesis of bacterial ribosomes is a highly coordinated and efficient process. During the assembly of both the small and large ribosomal subunit, distinct intermediate particles are formed. Due to the treatment of cells with antibiotics, in particular chloramphenicol (cam) and erythromycin (ery), sub-ribosomal particles are observed, which are different in r-protein composition to known assembly intermediates. In earlier days, the prevailing idea in the field was that antibiotics have the ability to directly inhibit ribosome assembly (Dagley and Sykes 1959). Champney and colleagues proposed that ery leads to an accumulation of damaged ribosomal particles (Chittum and Champney 1995) due to the binding of the drug to the large ribosomal subunit, suggesting a direct mechanism for the inhibition of ribosome assembly (Usary and Champney 2001).

In this study, novel results for cam and ery could be obtained with regards to ribosome assembly defects that differ to earlier studies from Champney. It could be shown that the accumulation of defective ribosomal particles is an indirect effect caused by a disturbed balance in the synthesis of r-proteins. These results were based on pulse-labeling experiments where the maturation of sub-ribosomal particles in the presence and absence of both drugs was examined. The assembly of *E. coli* 70S ribosomes could be observed in the presence of the compounds, but at significant slower rates. When intermediates were analyzed by negative-stain EM, the particles were highly heterogeneous due to their diverse r-protein content, in agreement with complementary analysis using quantitative mass spectrometry. The production of individual r-proteins was shown to differ significantly from

each other and, furthermore, correlates with the amounts of individual r-proteins within the sub-ribosomal particles. Since the genes encoding for r-proteins are organized into operons, it was interesting to observe that antibiotic treatment disturbs the r-protein balance by progressively decreasing the translation of the first to the last cistron. In contrast, only a small number of non-ribosomal genes organized into operons show a similar behavior (e.g. translational coupling within the *atp* operon (Hellmuth, Rex *et al.* 1991; Rex, Surin *et al.* 1994)) probably due to smaller expression levels compared to r-proteins.

In conclusion, the before-mentioned hypothesis of Champney could be refuted at least for ery and cam, since the effect of both antibiotics used in this study was shown to be indirect with respect to defects in ribosome assembly and caused through the imbalance in the levels of r-protein production.

3.3 Paper III

Márquez V, Fröhlich T, Armache JP, Sohmen D, Dönhöfer A, Mikolajka A, Berninghausen O, Thomm M, Beckmann R, Arnold GJ, Wilson DN.

***Proteomic characterization of archaeal ribosomes reveals the presence of novel archaeal specific ribosomal proteins.* J. Mol. Biol. 2011 Feb 4; 405(5): 1215-32.**

Most of the analyses regarding the ribosome, in particular the composition of r-proteins, have been done using either the bacterial or eukaryotic system. However, no systematic analysis has been performed on archaeal ribosomes.

Here, ribosomes from two different archaeal species, namely the thermophilic crenarchaeon *Pyrobaculum aerophilum* and the thermoacidophilic crenarchaeon *Sulfolobus acidocaldarius*, were investigated in a systematic approach using two-dimensional PAGE and mass spectrometry techniques. In this analysis, all 66 r-proteins from *P. aerophilum* and 62 out of 64 r-proteins from *S. acidocaldarius* could be identified with regards to genomic predictions. Moreover, three novel r-proteins, namely L45a, L46a and L47a that associate with the *S. acidocaldarius* 50S subunit could be identified. The purified ribosomal subunits from *S. acidocaldarius* were analyzed by negative-stain EM and confirmed to be homogeneous, so that the putative binding positions of the novel r-proteins could be determined in preliminary cryo-EM reconstructions. However, there are probably a large

number of additional r-proteins existing in other archaeal species that have not been identified so far. These differences in the third domain of life may be due to extreme and often unfavorable conditions that archaea have to deal with.

3.4 Paper IV

Sharma MR*, Dönhöfer A*, Barat C, Marquez V, Datta PP, Fucini P, Wilson DN, Agrawal RK.

PSRP1 is not a ribosomal protein but a ribosome-binding factor that is recycled by the ribosome-recycling factor (RRF) and elongation factor G (EF-G). J. Biol. Chem. 2010 Feb 5; 285(6): 4006-14.

*Both authors contributed equally to this work.

Chloroplasts are intracellular organelles that are responsible for the essential process of photosynthesis in higher plants and algae. During a systematic proteomic approach performed for *Spinacea oleracea*, six plastid-specific ribosomal proteins (PSRPs) were identified without an r-protein counterpart in bacteria (Somanchi and Mayfield 1999). Four of these proteins associate with the small ribosomal subunit, whereas PSRP5 and PSRP6 bind to the large ribosomal subunit. However, the functional role of these proteins has been so far only poorly understood.

Here, the protein factor PSRP1 was studied in detail and shown not to be a ribosomal protein *per se* but rather have functions similar to protein Y (pY) in *E. coli*, which is mainly to stabilize 70S ribosomes from degradation under conditions of cold shock. In this study, PSRP1 was demonstrated to be able to bind to both *E. coli* 70S ribosomes and 30S ribosomal subunits *in vivo* as well as *in vitro*. Using cryo-EM, the exact binding position of the factor could be determined showing PSRP1 positioned in the neck region between the head and the platform of the 30S subunit in a position overlapping the binding sites of A- and P-site tRNAs. This position is similar to the localization of pY on the ribosome, suggesting that both protein factors prevent tRNA binding to the ribosome and thus - not surprisingly - inhibit translation. More interestingly was the question of how PSRP1/ pY inactivated ribosomes are able to return to the actively translating pool once optimal growth conditions are restored. PSRP1 stabilizes the 70S ribosome from dissociation due to conformational alterations,

mainly within intersubunit bridge B2a, and *in vitro* binding assays indicate that this is influenced by several factors which are known to be involved in ribosome recycling, such as RRF, EF-G and IF3: RRF seems to stabilize PSRP1 on the ribosome, but does not interact with IF3 on the 30S subunit. However, in the presence of RRF and EF-G, PSRP1 was released from the ribosome and the subunits were able to dissociate from each other. These biochemical experiments were done in comparison with *E. coli* protein Y and the results were strongly comparable to each other probably due to the high sequence similarity between the two factors. This work was summarized in a model describing the mechanism of how PSRP1/pY inactivated ribosomes return to a new round of translation after environmental conditions improve.

3.5 Paper V

Ratje AH, Loerke J, Mikolajka A, Brünner M, Hildebrand PW, Starosta AL, Dönhöfer A, Connell SR, Fucini P, Mielke T, Whitford PC, Onuchic JN, Yu Y, Sanbonmatsu KY, Hartmann RK, Penczek PA, Wilson DN, Spahn CM.

Head swivel on the ribosome facilitates translocation by means of intra-subunit tRNA hybrid sites. Nature. 2010 Dec 2; 468(7324): 713-6.

The process of translation can be divided into three major parts – initiation, elongation as well as termination & recycling. During the elongation phase, aminoacyl tRNAs are delivered by EF-Tu·GTP to the appropriate binding site on the ribosome (A-site) followed by peptide-bond formation. Subsequently, the ribosome contains a peptidyl tRNA at the A-site and an uncharged tRNA at the P-site. However, both tRNAs are oscillating at this specific step between classical states (A/A and P/P sites on 30S/50S) and hybrid states (A/P and P/E sites on 30S/50S). Then, the translocation reaction takes place, which involves the movement of tRNAs from their initial A- and P- sites (via hybrid states) to their final P- and E-site position. Translocation is facilitated by EF-G in a GTP-dependent manner.

Structural data is available presenting the ribosome in either the pre- or post-translocational state bound with EF-G as well as during hybrid state formation (Frank and Agrawal 2000; Valle, Zavialov *et al.* 2003; Connell, Takemoto *et al.* 2007; Gao, Selmer *et al.* 2009). However, the precise mechanism of translocation, including distinct and subsequent

tRNA intermediate states on the ribosome, is not structurally investigated and remains unclear so far. The study addresses this particular question by focusing on the tRNA-mRNA movement on the small ribosomal subunit including the ratcheting and 30S head swivel movement.

The translocation process was investigated in detail using multi-particle cryo-EM. For this purpose, a complex was formed using *Thermus thermophilus* 70S ribosomes, EF-G and the antibiotic fusidic acid (FA) to prevent the dissociation of the elongation factor from the ribosome. Two translocation intermediates of the 70S-EF-G-GDP-FA complex in a ratcheted conformation (referring to sub-state I and II) were identified that showed significant differences to each other with regards to the magnitude of subunit ratcheting and the position of the L1 protuberance as well as the swivel action of the head region with respect to the rest of the 30S subunit. Both intermediates have only one tRNA present in the reconstruction, with sub-state I representing a ratcheted complex in a pre-translocational state, with the tRNA bound in a hybrid P/E state. In contrast, the tRNA in sub-state II adopts a novel hybrid state, namely a pe/E state, where the tRNA contacts the P-site on the head and the E-site on the platform of the 30S subunit as well as the E-site on the 50S subunit - suggesting that this unique intermediate is related to a post-translocational state. In addition, it was possible to superimpose a second tRNA in an ap/P state in that reconstruction which confirms this specific state as valid. Moreover, it could be shown that the conformation of EF-G differs slightly between the two intermediates with respect to domain IV of EF-G. In comparison, EF-G domain IV shows extensive contacts to h34 of 16S rRNA in sub-state II (due to the swivel movement of the head) in contrast to sub-state I, where this interaction does not occur. The conformational changes within the ribosome observed in sub-state II lead to an opening of the latch of the mRNA entry channel (formed by h34 as well as the nucleotide 530 region of 16S rRNA) promoting the movement of the mRNA and tRNAs.

In summary, a model could be presented explaining the process of translocation including novel intermediate states that were discovered in this study: The binding of EF-G-GTP stabilizes the oscillating tRNA-ribosome complex in a ratcheted conformation (sub-state I). EF-G-dependent GTP hydrolysis facilitates the translocation event accompanied by 30S back-ratcheting as well as a swivel movement of the 30S head resulting in the new identified intra-subunit hybrid state (sub-state II). Translocation finishes when the 30S subunit establishes a completely un-ratcheted conformation and EF-G-GDP dissociates from the ribosome.

4 *Extra-ribosomal Factors in Ribosome Biogenesis*

Overall Aim

The general goal in this projects dealing with extra-ribosomal factors in ribosome biogenesis is to visualize the binding sites of *E. coli* methyltransferase YhhF and RlmH, as well as *E. coli* assembly factor RimM on the ribosome using cryo-EM.

4.1 *Project Aims*

E. coli YhhF

The aim of this project was to visualize the [*Eco*30S Δ *yhhF*·YhhF] complex by cryo-EM and to gain insights about the binding position and the mechanism of the *E. coli* site-specific methyltransferase YhhF on the small ribosomal subunit.

E. coli RlmH

Due to the uniqueness of m³Ψ1915 in eubacteria and the location of the residue in a functional important region, namely Helix 69, the [*Eco*70S Δ *rluD/rlmH*·RlmH] complex was assembled *in vitro* and used for further cryo-EM analysis.

E. coli RimM

So far, RimM crystal structures determined from two different species accompanied by biochemical studies are available to characterize this specific 30S assembly factor. However, a complex structure showing RimM bound to the small ribosomal subunit is still missing. Therefore, the aim of this project was to assemble the [*Eco*30S Δ *rimM*·RimM] complex *in vitro* to visualize the distinct binding position of the factor on the small ribosomal subunit using cryo-EM.

4.2 *Introduction*

There is experimental evidence that bacterial ribosomal subunits can be reconstituted *in vitro* from purified rRNA and r-protein components but the required conditions for this

process are highly non-physiological (Traub and Nomura 1968; Nierhaus 1991; Culver 2003). *In vivo*, ribosome assembly is supported by a multitude of extra-ribosomal factors to facilitate highly efficient ribosome biogenesis. This is particularly well-characterized for *S. cerevisiae* where over 200 supporting factors have been identified so far (Hage and Tollervey 2004). In eubacteria, an ever-increasing number of proteins appear to be involved in ribosome biogenesis. These factors can be classified into different groups according to their specific functions during the assembly process, including RNA modification enzymes, RNA helicases, heat shock proteins, ribosome-dependent GTPases and RNA chaperones (see review (Dönhöfer, Sharma *et al.* 2009)). Some of these factors are discussed here in detail, in particular *E. coli* YhhF, RlmH and RimM.

4.2.1 Post-transcriptional modification by methyltransferases

Modification of rRNA is taking place after rRNA transcription and two main types of modifications are known in *E. coli*, methylation and pseudouridylation. In total, thirty-five of those rRNA modifications are present on the *E. coli* ribosome divided into 24 methylated nucleosides (10 in 16S rRNA and 14 in 23S rRNA) and 11 pseudouridines (Ψ) (1 in 16S and 10 in 23S rRNA). In addition, one 5-hydroxycytidine modification at position 2501 of 23S rRNA was found more recently (Havelund, Giessing *et al.* 2011). The enzymes modifying nucleotides on *E. coli* 16S rRNA are already studied. However, two methyltransferases and one dihydrouridine synthase responsible for 23S rRNA modifications at positions A2030, G2069 and U2449 remain to be elucidated.

Regarding the functional role of the rRNA modifications, this aspect is still under intensive discussion as well as investigation. Most of the modification sites are located in close proximity to the functional centers on both the small and the large ribosomal subunit, namely, the mRNA and tRNA binding sites on the 30S and the PTC on the 50S (Decatur and Fournier 2002) (**Figure 3**). It was shown that the absence of most of the modifications does not have any impact on the cell, neither cell growth nor ribosome function, with one well-known exception presented by the *E. coli* methylase KsgA. Deletion of this enzyme results in severe defects in cell growth and 30S subunit biogenesis (Connolly, Rife *et al.* 2008).

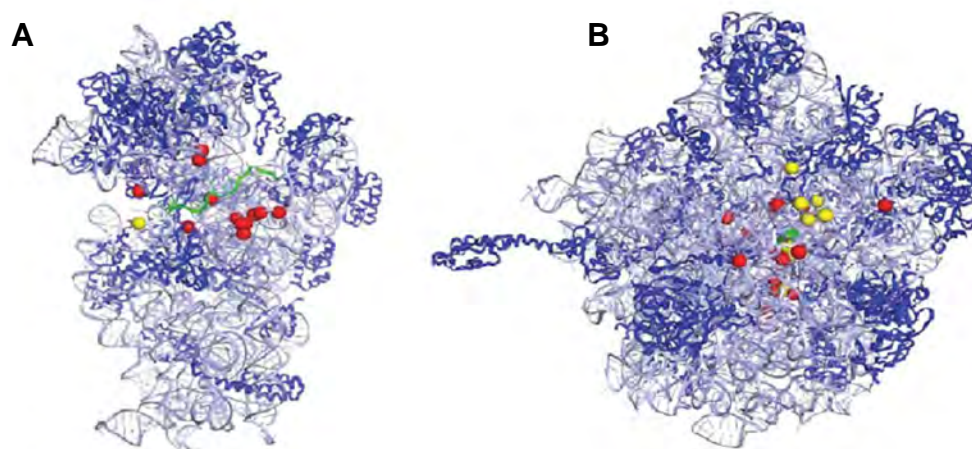


Figure 3: Sites of modification on the small (A) and large (B) ribosomal subunit. Methylations and pseudouridylation are highlighted as red and yellow spheres and rRNA and r-proteins are shown in light and dark blue, respectively. The path of the mRNA through the small ribosomal subunit is depicted in green (A) and the antibiotic chloramphenicol is shown as a green sphere in (B) to demonstrate the location of the PTC. The figure is taken from (Dönhöfer, Sharma *et al.* 2009).

4.2.2 Guanine 966 specific methyltransferase YhhF (RsmD)

One important area on the ribosome is the P-site tRNA binding pocket that is comprised of a number of modified bases. Helix 31 (h31) of the 16S rRNA is located in the head region of the 30S subunit and contains two modified bases, m²G966 and m⁵C967, in which guanine 966 is specifically modified by the methyltransferase YhhF (**Figure 4A**). It has been shown that YhhF, which was recently renamed to RsmD (ribosome small subunit methyltransferase D) according to common nomenclature (Lesnyak, Osipiuk *et al.* 2006), functions on assembled 30S ribosomal subunits (Weitzmann, Tumminia *et al.* 1991). Four ribosome-specific guanine-(N2)-methyltransferases have been identified with similar AdoMet-binding sites. However, these enzymes can be divided into two groups since RlmG and RlmL are using naked 16S rRNA as a ribosomal substrate and are relatively large in comparison to RsmC and YhhF/RsmD, both of which act on late assembly intermediates (Sergiev, Bogdanov *et al.* 2007). Methylguanine 966 has direct contact with the anticodon stem-loop of the P-site bound tRNA (Yusupov, Yusupova *et al.* 2001; Petry, Brodersen *et al.* 2005b). Although the modification at position 966 in 16S rRNA appears to be conserved (Youvan and Hearst 1981; Kowalak, Bruenger *et al.* 2000), a knock-out of *yhhF* does not produce any

phenotypical alterations (Jemiolo, Taurence *et al.* 1991). Recently, the crystal structure of YhhF/RsmD was determined (**Figure 4B**) (Lesnyak, Osipiuk *et al.* 2006), revealing it to be highly similar to another methyltransferase, RsmC, which specifically methylates m²G1207 in the 16S rRNA (Huang, Hung *et al.* 2002). However, no structure of the 30S-YhhF complex was determined so far.

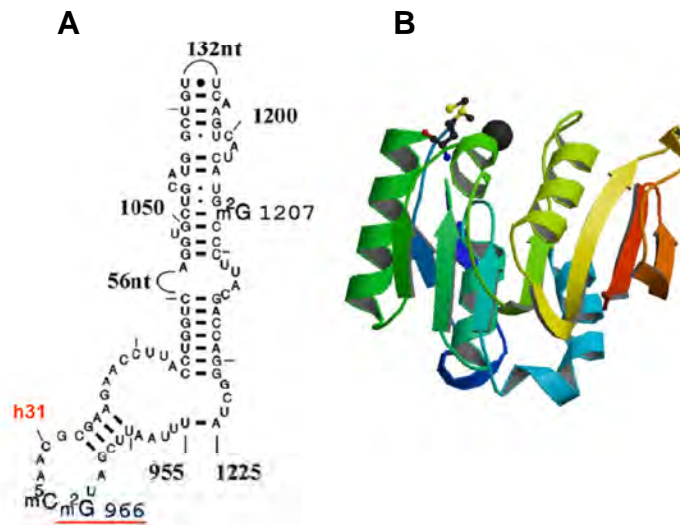


Figure 4: Location of m²G966 in the 30S ribosomal subunit and crystal structure of YhhF/RsmD. (A) Secondary structure of parts of *E. coli* 16S rRNA with helix 31(h31) and m²G966 highlighted in red. m²G966 is one of two modified bases in h31. **(B)** Crystal structure of the *E. coli* YhhF/RsmD protein (PDB2FPO).

4.2.3 Ψ1915 specific methyltransferase RlmH (YbeA)

rlmH (former *ybeA*, according to uniform nomenclature renamed to rRNA large subunit methyltransferase H) encodes for an *E. coli* methyltransferase that methylates one out of 11 pseudouridines (Ψ) in *E. coli* rRNA (Ero, Peil *et al.* 2008), specifically, the N³-position of pseudouridine 1915 in the 23S rRNA (Kowalak, Bruenger *et al.* 1996) (**Figure 5A**). Ψ1915 is located in stem-loop 69 (H69) of the 23S rRNA, together with two other pseudouridines (Ψ1911 and Ψ1917) (**Figure 5B**) that are all isomerized from uridine with the help of one specific pseudouridine synthase, RluD (Huang, Ku *et al.* 1998; Raychaudhuri, Conrad *et al.* 1998). Deletion of *rluD* shows reduced growth rates and defects in ribosome assembly, which confirms the importance of these modifications. RlmH belongs to the SPOUT (SpoU-TrmD)

superfamily of methyltransferases, is conserved in bacteria, and exist in plants as well as several archaeal genomes (Ero, Peil *et al.* 2008).

H69 is a significantly important region on the ribosome since it is involved in formation of inter-subunit bridge B2a (Yusupov, Yusupova *et al.* 2001). It could be shown that RlmH is involved in a very late step in ribosome biogenesis since the methylation reaction on the 70S ribosome takes place after the subunits are assembled together, most probably during translation initiation (Ero, Peil *et al.* 2008). Moreover, the enzyme is specific for pseudouridine, since uridine gets methylated less efficiently (Ero, Leppik *et al.* 2010). Recently, it was shown that RlmH is active as a homodimer and binds to the interface region of the 70S ribosome overlapping with the A-tRNA binding site (Purta, Kaminska *et al.* 2008), however, no structural data showing the 70S ribosome in complex with the methyltransferase RlmH is available so far.

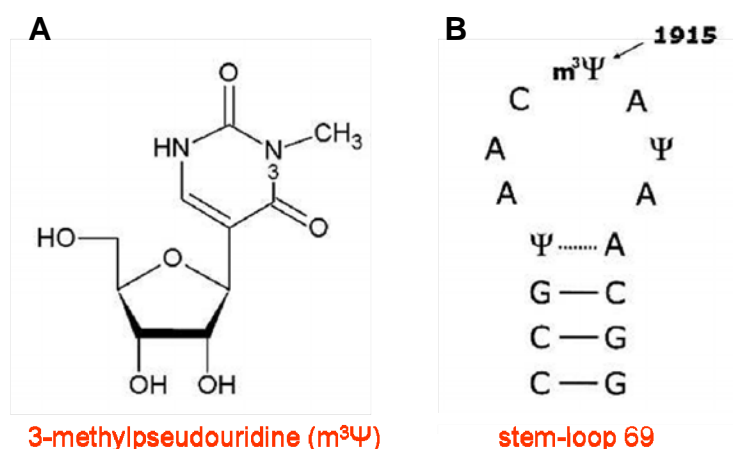


Figure 5: (A) Chemical structure of 3-methylpseudouridine (m³Ψ) and (B) secondary structure of *E. coli* 23S rRNA stem-loop 69. Helix 69 contains three post-transcriptional modifications: two pseudouridines (Ψ) at position 1911 and 1917 and one 3-methylpseudouridine (m³Ψ) at position 1915. Positions are according to *E. coli* numbering.

4.2.4 Ribosome maturation factor M (RimM)

A multitude of factors are known to be involved in ribosome biogenesis including rRNA processing (RNases and helicases) and modification (methylases, acetylases and pseudouridinyllases) enzymes. During the last years, several additional factors were identified to associate with the immature small ribosomal subunit including factors like RimM, RbfA and Era.

RimM (former called 21K or YfiA) (Byström, Hjalmarsson *et al.* 1983) is one out of four proteins encoded by the *trmD* operon, together with r-protein S16 (*rpsP*), the tRNA (m¹G37) methyltransferase TrmD (*trmD*) and r-protein L19 (*rpL5*) (Bylund, Persson *et al.* 1997). The assembly factor associates with free 30S ribosomal subunits but not with the fully assembled 70S ribosome, which implicates the factor to be involved in ribosome maturation (Bylund, Persson *et al.* 1997). A multitude of suppressor mutations for a $\Delta rimM$ strain have been identified and the majority of these characterized alterations have been linked to another ribosome assembly factor, namely RbfA (Bylund, Wipemo *et al.* 1998a; Bylund, Lövgren *et al.* 2001). Deletion of the *rimM* gene shows defects in growth and decreases translational efficiency (Persson, Bylund *et al.* 1995; Bylund, Persson *et al.* 1997; Bylund, Wipemo *et al.* 1998b). A mutation in the RimM protein containing alanine substitutions for two adjacent and conserved tyrosine residues (**Figure 6A**) has been identified and results in the inability to bind to 30S subunits as well as an accumulation of 17S rRNA, a precursor form of 16S rRNA.

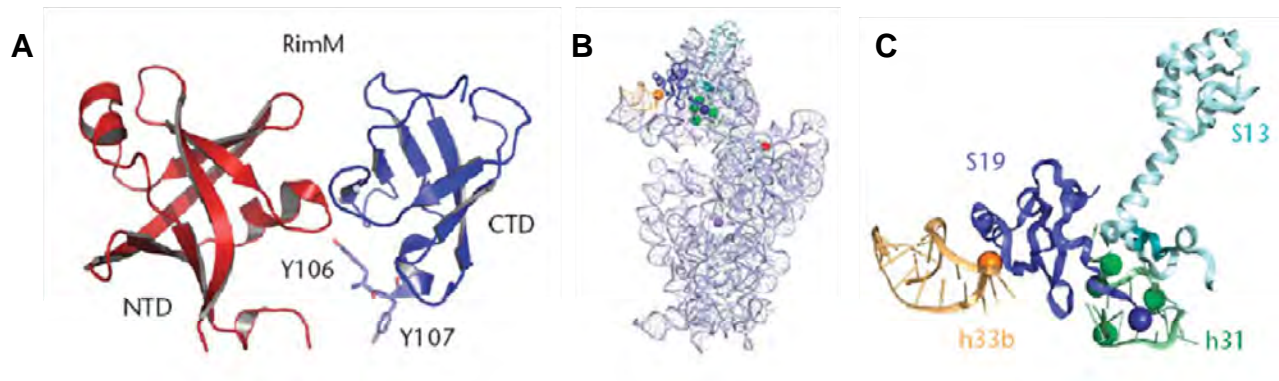


Figure 6: Assembly factor RimM. (A) Crystal structure of *Pseudomonas aeruginosa* RimM homologue (PDB2F1L), showing N- and C-terminal domains (NTD, red and CTD, blue) with two adjacent tyrosine residues (Y106/Y107). (B) and (C) Location of RimM suppressor mutations in the *E. coli* 30S subunit (PDB2AW4). G1015A in h33b (orange), D974A in h31 (green), D89–99 in S13 (cyan) and R81 in S19 (blue) are shown with spheres. On the 30S subunit, the 5' and 3' termini of the 16S rRNA are indicated with a blue and red sphere, respectively. Figure taken from (Dönhöfer, Sharma *et al.* 2009).

The slow growth phenotype could be overcome by expression of a S16-RimM hybrid protein (Lövgren and Wikström 2001). Moreover, this mutation could be suppressed by alterations in helices 31 and 33b as well as r-proteins S13 and S19 (**Figure 6B, 6C**), which led to the suggestion that the assembly factor RimM binds to the head region of the small ribosomal subunit. A GST-RimM fusion protein associates strongly with r-protein S19, which

confirms the interaction and a probable binding position of the assembly factor in the head region of the 30S subunit (Lövgren, Bylund *et al.* 2004). In a structural characterization, it could be shown that *Thermus thermophilus* RimM (PDB2DYI) has a two-domain structure in which the N-terminal domain closely resembles the N-terminal domain of *Pseudomonas aeruginosa* RimM determined by crystallization (PDB2F1L) (**Figure 6A**, (Suzuki, Tatsuguchi *et al.* 2007). However, a complex structure showing RimM bound to the small ribosomal subunit is still missing.

4.3 Results

4.3.1 Purification of *E. coli* YhhF protein

The expression and purification of *E. coli* YhhF was essentially carried out as described before (Lesnyak, Osipiuk *et al.* 2006).

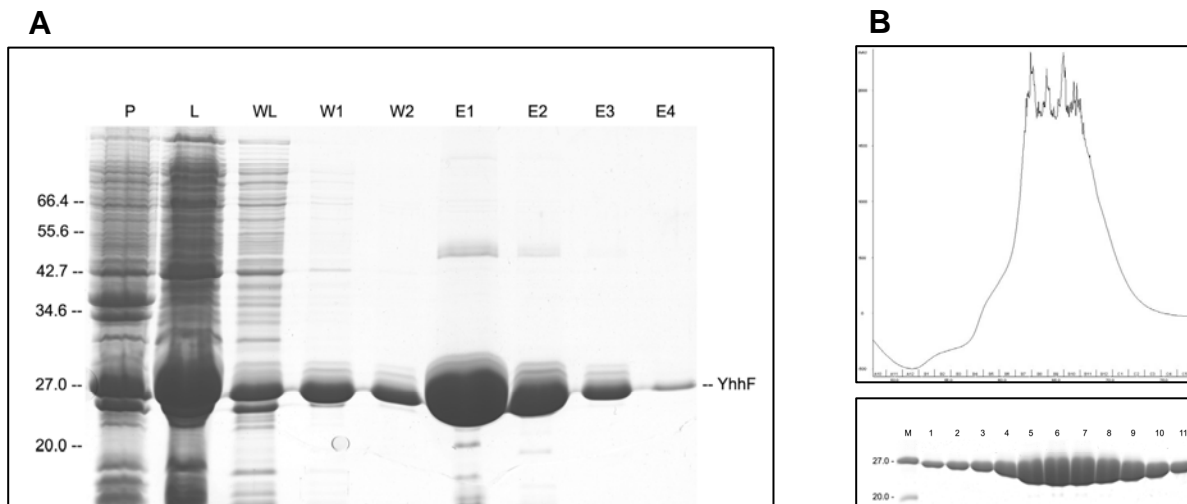


Figure 7: Purification of *E. coli* YhhF protein. (A) SDS-PAGE of Ni-NTA affinity purification. Various steps of purification are indicated: P: pellet, L: lysate, WL: wash step with lysis buffer, W1/2: wash step 1/2 with wash buffer, E1/2/3/4: elution step 1/2/3/4 with elution buffer. (B) Gel filtration profile of size-exclusion chromatography. Fractions are indicated on the horizontal axis and milli absorption units (mAU) on the vertical axis. Fractions 5 – 8 as indicated in the SDS-PAGE of purified YhhF protein were pooled.

After ultrasonification of cells overexpressing *E. coli* YhhF, the cleared lysate was applied to His-affinity chromatography (Ni²⁺-NTA-Agarose) and subsequent gel filtration (HiLoad 16/60 Superdex 75 pg, GE Healthcare, in buffer 20 mM Hepes-KOH, pH 7.5, 1 mM MgCl₂, 200 mM NH₄Cl, 0.1% Triton X-100, 10% Glycerin, 5 mM DTT) (**Figure 7A** and **7B**). YhhF eluted as a sharp, almost clean band with a calculated mass of 21.7 kDa from the column. After gel filtration, protein fractions were pooled and stored at -80°C with a concentration of 158 µM in the before-mentioned buffer.

4.3.2 *In vitro* binding assay: Eco30SΔyhhF + YhhF + sinefungin

For the 3D-reconstruction, the complex consisting of purified 30S ribosomal subunits derived from a *yhhF* knock-out strain and purified, soluble YhhF protein was assembled *in vitro* in the presence of sinefungin, a methyltransferase-specific inhibitor, in order to trap the enzyme on the 30S ribosomal subunit and maintain the complex for further cryo-EM analysis.

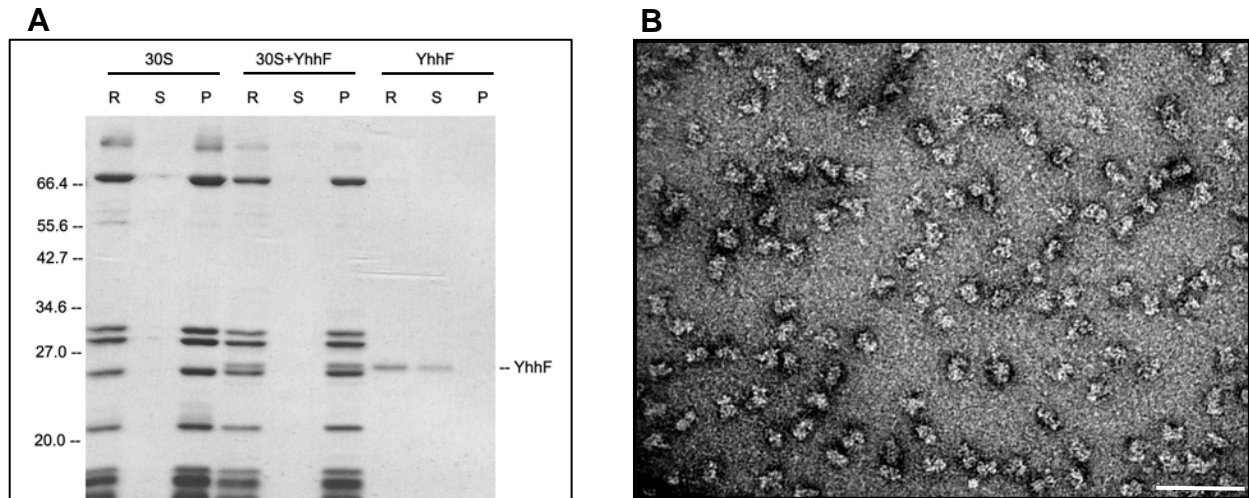


Figure 8: *In vitro* binding assay and negative-stain EM. (A) *In vitro* binding experiment with *Eco30SΔyhhF* ribosomal subunits in the absence (30S) and presence (30S+YhhF) of 2x excess of YhhF protein and YhhF protein alone (YhhF). The SDS-PAGE shows the initial reaction (R) before the samples were centrifuged through a 10% sucrose cushion and aliquots were taken from supernatant (S) and pellet (P) fraction. (B) Negative-stain EM of the *in vitro* assembled [*Eco30SΔyhhF*-YhhF] complex. The scale bar represents 10 nm.

Figure 8A shows the binding of *E. coli* YhhF protein to purified 30SΔ*yhhF* ribosomal subunits in comparison to empty 30S ribosomal subunits, visualized by the additional band in

the pellet fraction (**Figure 8A**, “30S+YhhF/P” in comparison to “30S/P”). As a control, *E. coli* YhhF protein does not precipitate by itself, which is confirmed by the absence of a protein signal in the appropriate pellet fraction (**Figure 8A**, “YhhF/P”). As a result, the binding of YhhF protein to 30S ribosomal subunits can be noted as a valid ribosome-protein association. The [*Eco*30S Δ *yhhF*-YhhF] complex was taken for negative-stain EM to analyze the homogeneity and concentration of the sample (**Figure 8B**). The sample was confirmed to be homogenous without or only minor tendency for aggregation. Therefore the sample was used for a further cryo-EM reconstruction.

4.3.3 3D-reconstruction of the [*Eco*30S Δ *yhhF*-YhhF] complex

A preliminary low-resolution structure of the *E. coli* [30S Δ *yhhF*-YhhF] complex was determined with a Spirit FEI 120 kV transmission electron microscope (LMU Biocenter, Munich, Germany). 55 out of 71 initially collected micrographs were used for the reconstruction, resulting in a small dataset of 3871 particles divided into 14 defocus groups. After several rounds of refinement, the map showed a resolution of approximately 28 Å according to the FSC_{0.5} cut-off criterion (**Figure 9**). The reconstruction showed a little bit of extra density in comparison to an empty 30S ribosomal subunit reference (taken from *E. coli*) due to low resolution and the small size of the dataset (**Figure 10A**). Nevertheless, the extra density is in close proximity to h31 (consisting of residues 956 – 983 according to *E. coli* 16S rRNA secondary structure numbering, shown in red) harboring guanine 966, the residue that is methylated by YhhF during 30S subunit biogenesis (**Figure 10B and 10C**).

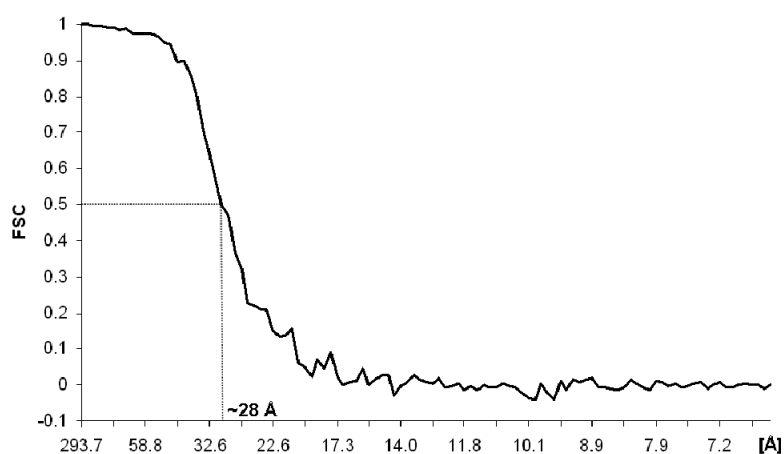


Figure 9: Cryo-EM reconstruction of the [*Eco*30S Δ *yhhF*-YhhF] complex. Resolution curve of the cryo-EM reconstruction. The map has a resolution of ~28 Å based on the 0.5 FSC cut-off criterion.

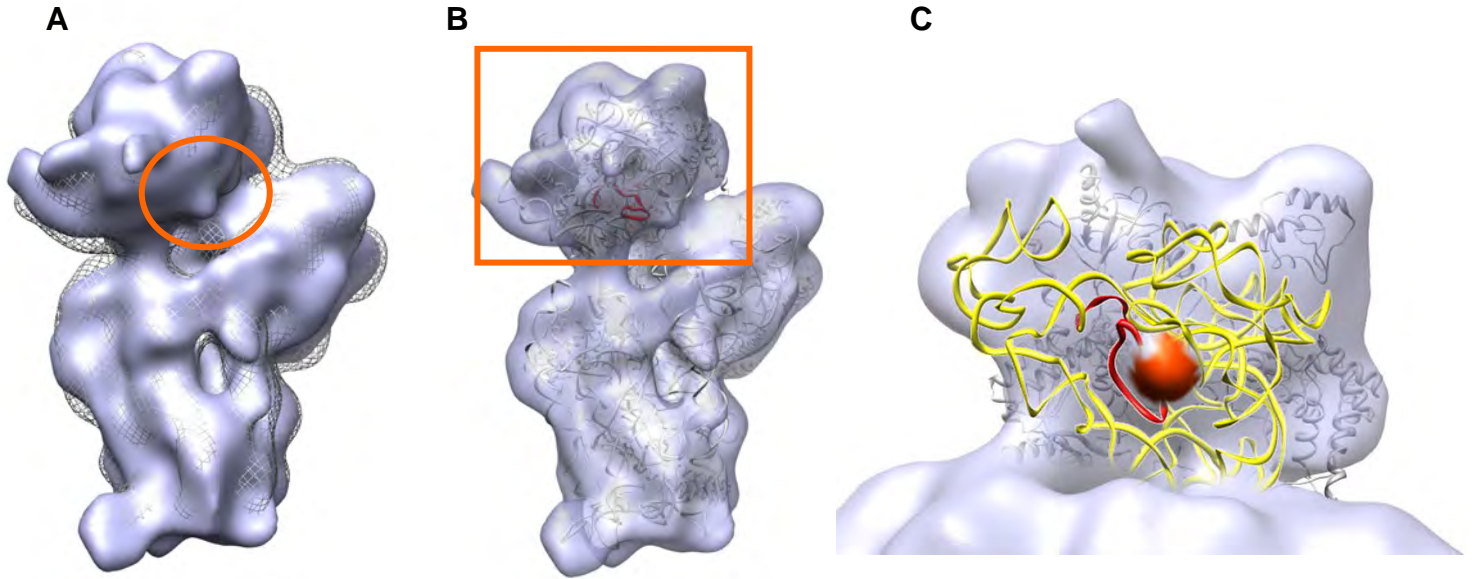


Figure 10: Cryo-EM reconstruction of the [Eco30S Δ yhhF-YhhF] complex. (A) Comparison of the volume obtained from the reconstruction (light purple) with an empty *E. coli* 30S ribosomal subunit (grey mesh). An orange circle highlights the extra density assigned to YhhF. (B) Reconstruction of the [Eco30S Δ yhhF-YhhF] complex shown in transparent purple fitted with PDB2YKR. 16S rRNA and r-proteins are shown in grey and h31 is highlighted in red. (C) Detailed view of the head region of the 30S ribosomal subunit from (B). 16S rRNA h31 is shown in red being in close proximity to the extra density of the cryo-EM reconstruction, highlighted in orange. 16S rRNA and r-proteins are depicted in yellow and light grey, respectively.

4.3.4 *In vitro* binding assay: Eco70S Δ rluD/rlmH + RlmH + sinefungin

The *in vitro* binding assay was performed with three different types of knock-out strains: Δ rlmH, a single knock-out strain for the Ψ 1915 specific methyltransferase (70S Δ rlmH+RlmH), Δ rluD, a single knock-out strain for the pseudouridine synthase RluD, which isomerizes uridine at position 1911, 1915 and 1917 in *E. coli* 23S rRNA to pseudouridine (70S Δ rluD+RlmH) and a double knock-out strain Δ ruD/rlmH for both enzymes (70S Δ rluD/rlmH+RlmH). For each reaction, a 5x excess of RlmH protein was added and the reactions were carried out in the presence of sinefungin, a specific methyltransferase inhibitor to retain the enzyme on the 70S ribosome. RlmH protein was purified as described in Material and Methods (7.2.2) without using any specific purification tags due to an activity loss of the protein by applying tag-purification. The *in vitro* binding assay was performed together with a

ribosome (70S) and a protein control (RlmH) reaction according to Material and Methods (7.2.6). The sample [70S Δ rluD/rlmH-RlmH] was confirmed by negative-stain EM and high-resolution data collection was carried out on a FEI Tecnai F30 field emission gun microscope (Max- Planck Institute of Molecular Genetics, Berlin, Germany) operated at 300 kV using a magnification of 39,000.

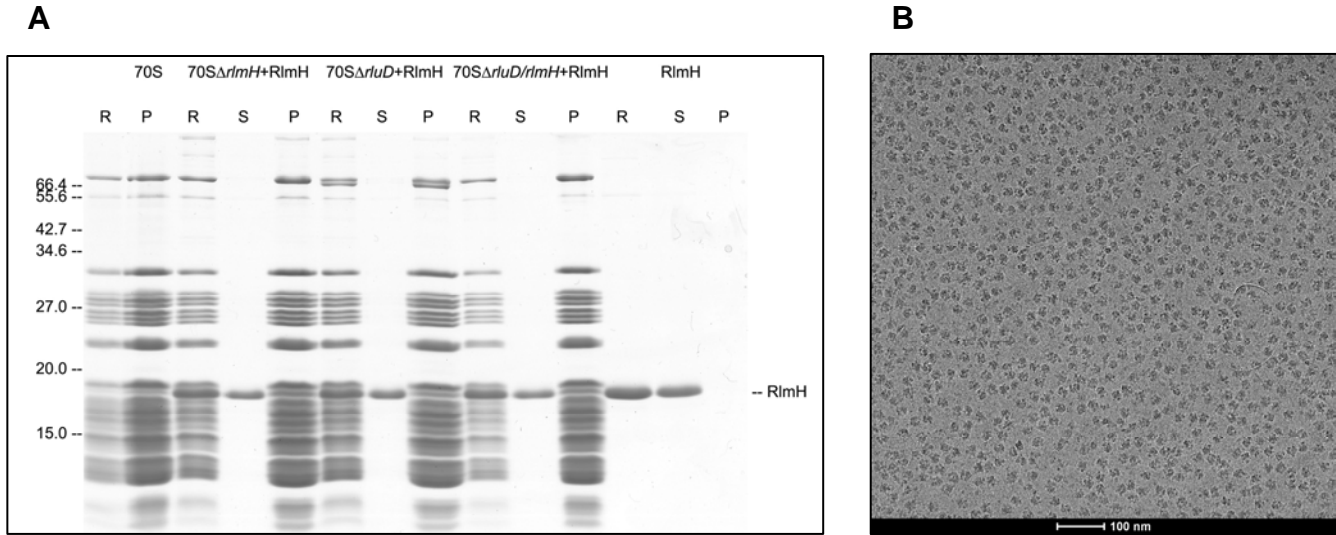


Figure 11: *In vitro* binding assay and cryo-EM data collection of the [70S Δ rluD/rlmH-RlmH] complex.

(A) The experiment was performed as described before (7.2.6). For each reaction, samples for initial reaction (R), supernatant (S) and pellet (P) were analyzed on an 18% SDS-PAGE. **(B)** Example of a micrograph recorded with a Tecnai Polara F30 field emission gun microscope. The scale bar represents 100 nm.

The binding efficiency (**Figure 11A**) was hardly visible because of a similar migration position of the RlmH protein on an SDS-PAGE gel with some ribosomal proteins. No western blot analysis could be applied due to the absence of tags on RlmH protein. Binding of RlmH to 70S ribosomes was therefore verified using radioactively labeled experiment (performed by laboratory of Prof. J. Remme). To do this, ^{35}S Met/ ^{35}S Cys-labeled RlmH and streptavidin-tagged ribosomes were purified (Leonov, Sergiev *et al.* 2003). After incubation of protein, ribosomes and sinefungin, one part of the sample was TCA precipitated and analyzed on a SDS-PAGE, the other half was taken for radioactivity counting. RlmH protein was shown to bind to both Δ rluD and Δ rluD/ Δ rlmH purified ribosomes, but not to Δ rlmH or WT ribosomes. Overall, the binding efficiency showed modest protection by RlmH in chemical footprinting experiments (performed by the laboratory of Prof. J. Remme).

4.3.5 3D-reconstruction of the [*Eco*70S Δ *rluD*/*rlmH*-RlmH] complex

For the reconstruction of the [*Eco*70S Δ *rluD*/*rlmH*-RlmH] complex, a dataset consisting of 278 micrographs was collected. For a preliminary analysis, 71 micrographs were used for processing, resulting in a dataset of 135887 particles divided into 59 defocus groups. Images were calculated with a 2x decimation factor resulting in a pixel size of 2.475 Å/pixel. After several rounds of refinement the dataset obtained a resolution of 10.4 Å (resolution curve **Figure 12A**, map **Figure 13**, shown in grey). Since no extra density was present in the inter-subunit space most probably due to the heterogeneity of the dataset, sorting techniques were applied to subdivide the dataset. This resulted in a major dataset (~ 85%) with an “empty” 70S ribosome (resolution curve **Figure 12B**, map **Figure 13**, shown in yellow) without any extra density in the inter-subunit region, and a minor dataset (~ 15%) with a ratcheted 30S ribosomal subunit relative to the 50S subunit and an E-site tRNA present in the reconstruction (resolution curve **Figure 12C**, map **Figure 13**, shown in cyan; comparison of the two sub-datasets, see **Figure 14**). Unfortunately, no extra density for RlmH could be observed in both datasets after sorting.

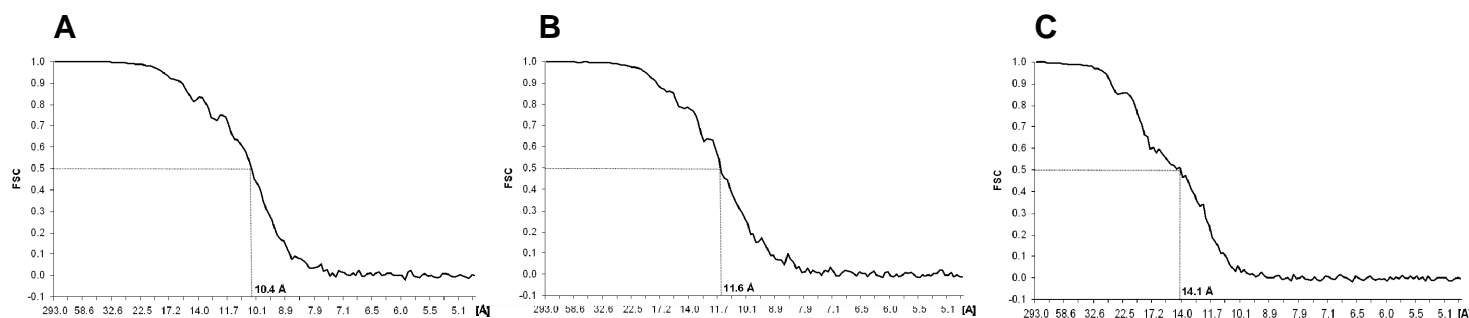


Figure 12: FSC curves for the [*Eco*70S Δ *rluD*/*rlmH*-RlmH] complex before (A) and after (B and C) sorting. (A) Whole dataset (Figure 13, shown in grey) before sorting was applied. (B) After sorting, the major portion of the dataset showed a map with 11.6 Å resolution (Figure 13, yellow). (C) The 70S ribosome with a ratcheted 30S subunit and an E-site tRNA present in the map had a resolution of 14.1 Å (Figure 13, cyan). Resolution is calculated based on the FSC_{0.5} cut-off criterion.

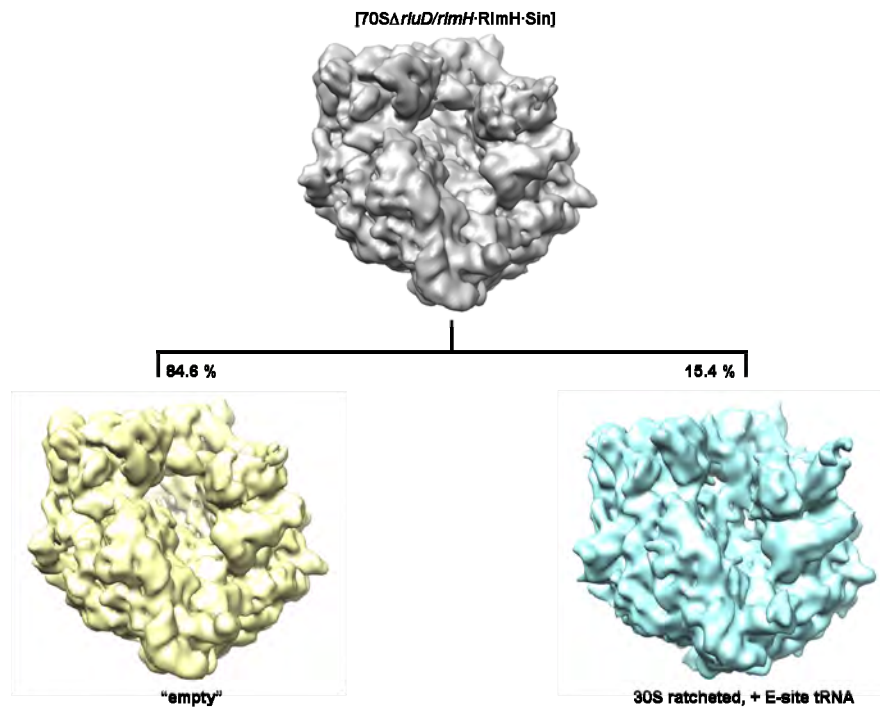


Figure 13: Cryo-EM reconstruction of the [70S Δ rluD/rlmH-RlmH] complex. The whole dataset (135887 particles, shown in grey) was sub-divided into one major dataset (84.6%, ~114930 particles, yellow) that showed no extra density for RlmH and a minor dataset shown in blue (15.4%, 20990 particles). The latter map showed the 30S subunit ratcheted relative to the 50S subunit and, in addition, an E-site tRNA.

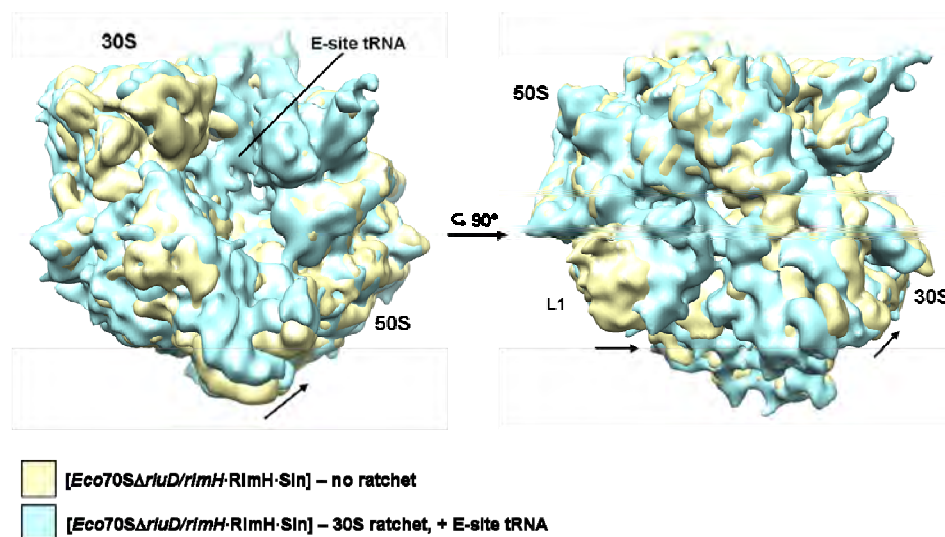


Figure 14: Comparison of volumes after sorting. It is clearly visible that the small ribosomal subunit of the cyan sub-dataset is ratcheted relative to the large ribosomal subunit in comparison to the yellow sub-dataset. In addition, an E-site tRNA is present in the ratcheted volume. Colors are similar to Figure 13.

4.3.6 Ribosome profiles and purification of *E. coli* RimM

In order to determine the structure of RimM bound to the 30S ribosomal subunit, the $\Delta rimM$ strain was analyzed and the protein had to be purified. $\Delta rimM$ shows a slow growth phenotype in comparison to a WT MC4100 strain (data not shown). Ribosome profiles exhibit and increase in free 30S and 50S ribosomal subunits (in the presence of 30 mM $MgCl_2$) as well as a significant loss in polysomes (**Figure 15**). Mature 30S ribosomal subunit derived from *E. coli* MC4100 and premature 30S ribosomal subunits derived from *E. coli* $\Delta rimM$ were collected and purified for further *in vitro* binding attempts.

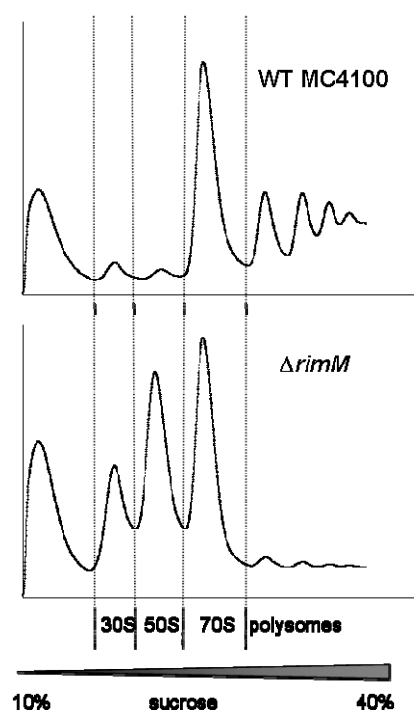


Figure 15: Ribosomal profiling of a WT MC4100 and $\Delta rimM$ strain. 10 OD of S30 extracts were loaded on 10 – 40% sucrose gradients in buffer $H_{10}M_{30}N_{150}SH_6$ (SW40, 15500 rpm, 16.5 h, 4°C).

The expression and purification of RimM was carried out according to Material and Methods (7.2.2). After cell breakage, the cleared lysate containing soluble RimM protein was applied to Ni^{2+} -NTA-affinity chromatography and subsequent gel filtration (**Figure 16A** and **16B**). RimM eluted as a prominent band from the Ni-NTA column. After gel filtration, clean protein fractions were pooled and stored at -80°C with a concentration of 74 μM .

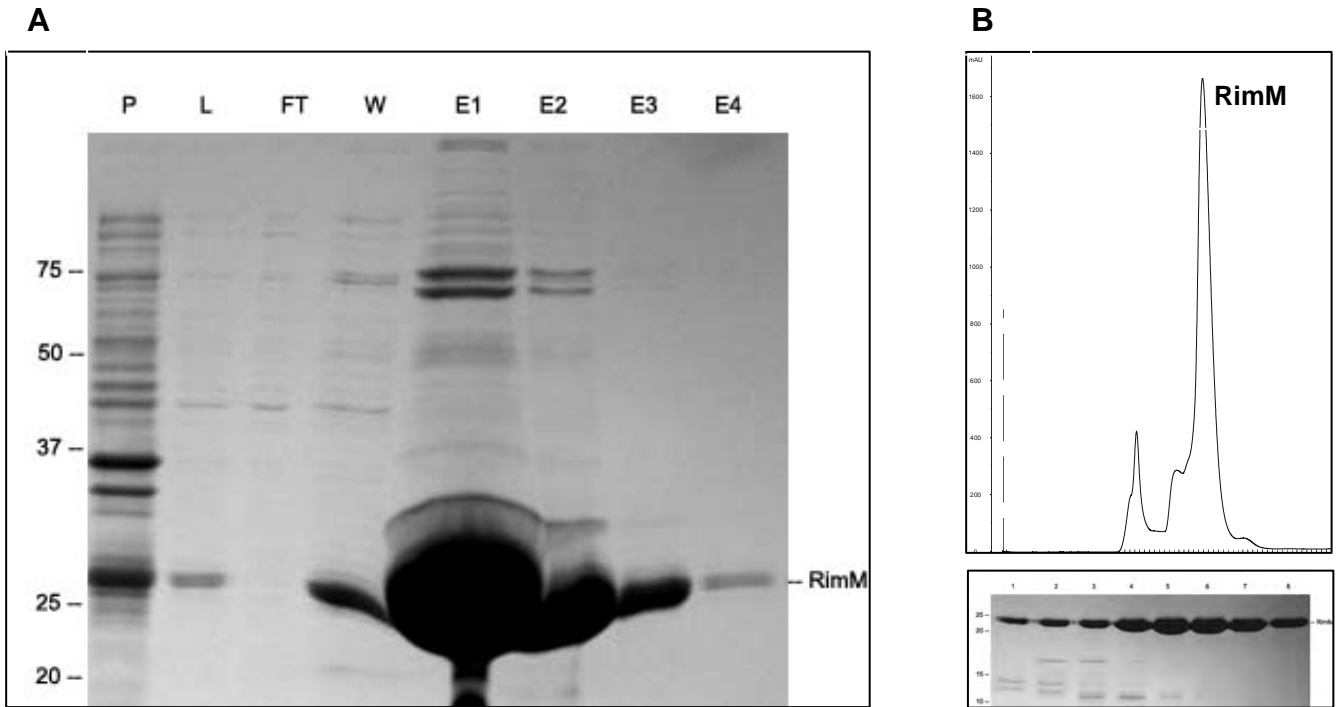


Figure 16: Purification of *E. coli* RimM protein. (A) SDS-PAGE of Ni-NTA affinity purification. Various steps of purification are indicated: P: pellet, L: lysate, FT: flow-through, W: wash step with wash buffer, E1/2/3/4: elution step 1/2/3/4 with elution buffer. (B) Gel filtration profile of size-exclusion chromatography. Fractions 6 – 8 as indicated in the SDS-PAGE of purified RimM protein were pooled.

4.3.7 *In vitro* binding assay: *Eco30S/Eco30SΔrimM* + RimM

30S ribosomal subunits (from WT and $\Delta rimM$ strain) and purified RimM protein (added in an excess of 10 times over ribosomes to the reactions) were assembled to a complex as described before (Material and Methods 7.2.6). The complex was formed successfully with both mature 30S ribosomal subunits derived from WT strain (30S) and premature 30S ribosomal subunits (30S $\Delta rimM$) as shown in **Figure 17A**. The results were confirmed by western blot analysis (**Figure 17B**) and the [*Eco30SΔrimM*-RimM] complex was verified by negative-stain EM as homogeneous and being worth pursuing further by cryo-EM analysis (**Figure 17C**).

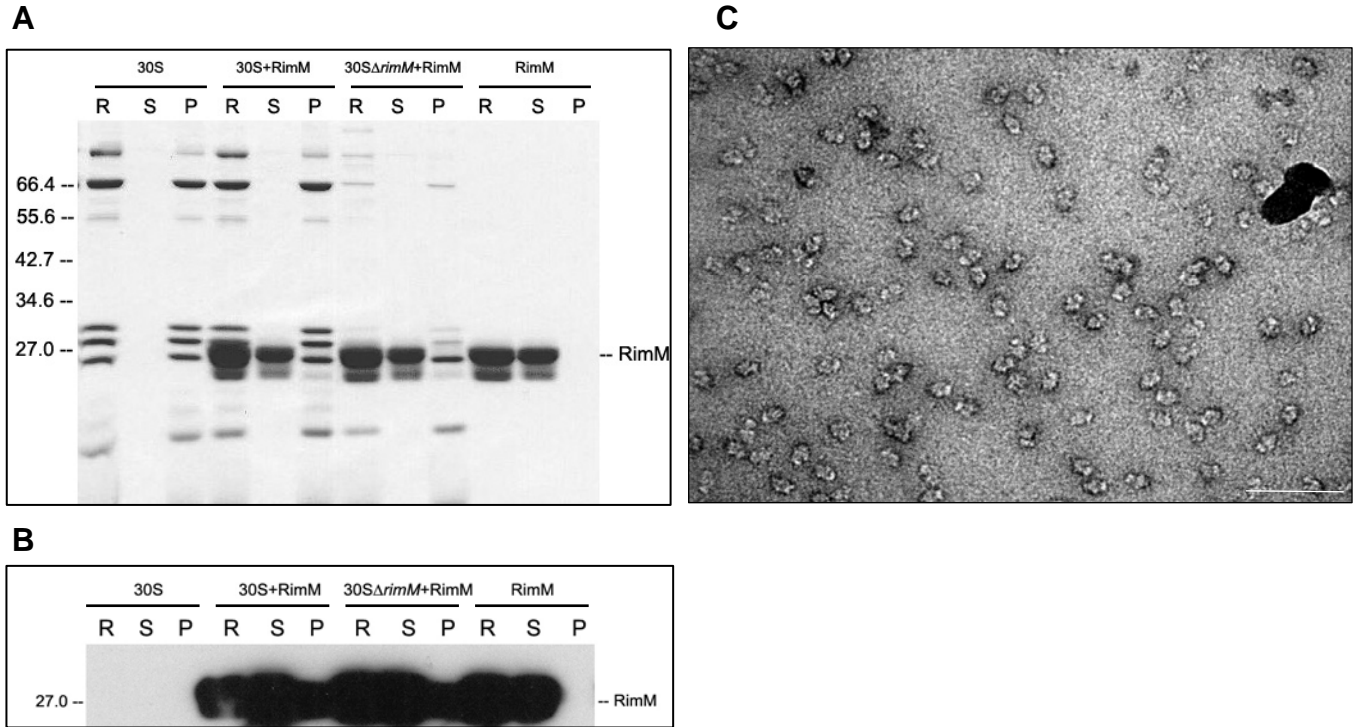


Figure 17: *In vitro* binding assay and negative-stain EM. (A) *In vitro* binding experiment with mature 30S ribosomal subunits as a control reaction (30S). In the presence of mature (30S+RimM) and premature (30S Δ rimM+RimM) 30S ribosomal subunits, 10x excess of RimM protein (over ribosomes) was added. In addition, RimM protein alone was included as a control reaction (RimM). The SDS-PAGE stained with Coomassie blue shows the initial reaction (R) before the samples were centrifuged through a 10% sucrose cushion and aliquots were taken from supernatant (S) and pellet (P) fraction. **(B)** Signal detection of the *in vitro* binding experiment by western blotting against α His antibody. **(C)** Negative-stain EM of the *in vitro* assembled [Eco30S Δ rimM-RimM] complex. The scale bar represents 15 nm.

4.3.8 3D-reconstruction of the [Eco30S Δ rimM-RimM] complex

For the reconstruction of the complex, data was collected on a FEI Tecnai F30 field emission gun microscope at 300 kV (Max-Planck Institute of Molecular Genetics, Berlin, Germany). 33 out of 96 micrographs were used for a preliminary cryo-EM analysis, which resulted in a dataset of 57047 particles with a pixel size of 4.95 Å/pixel (with a 4x decimation factor). Particles were divided into 16 defocus groups and after refinement, the map showed a resolution of ~19 Å (**Figure 18**). The volume exhibited a small extra density on top of the head of the small ribosomal subunit (**Figure 19A**, red circle) in comparison to an *E. coli* 30S

ribosomal subunit reference without any factors bound (**Figure 19A**, grey mesh). The RimM protein exhibit a two-domain structure with the N- and C-terminal domain resembling a (PRC) β -barrel like topology as could be shown by the crystal structure of a RimM homologue from *Pseudomonas aeruginosa* (PDB2F1L). The extra density shown here (**Figure 19C**, highlighted in red) resembles two roundish blobs that could not be refined to better resolution due to heterogeneity of the dataset and preferred orientations of the complex on the grid.

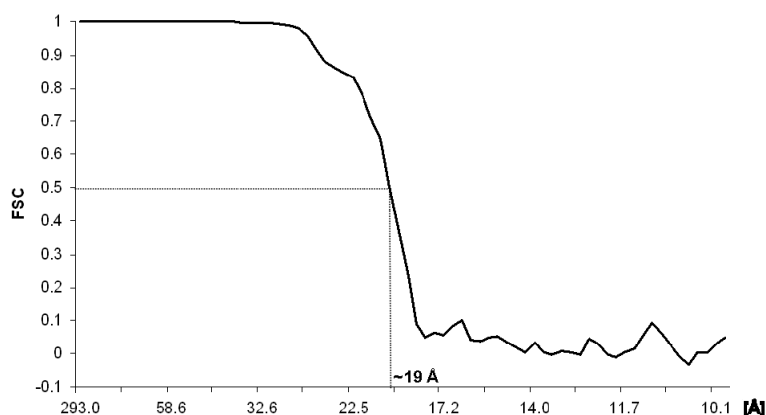


Figure 18: Cryo-EM reconstruction of a [*Eco30S* Δ *rimM*-RimM] complex. Resolution curve of the map based on the 0.5 FSC cut-off criterion.

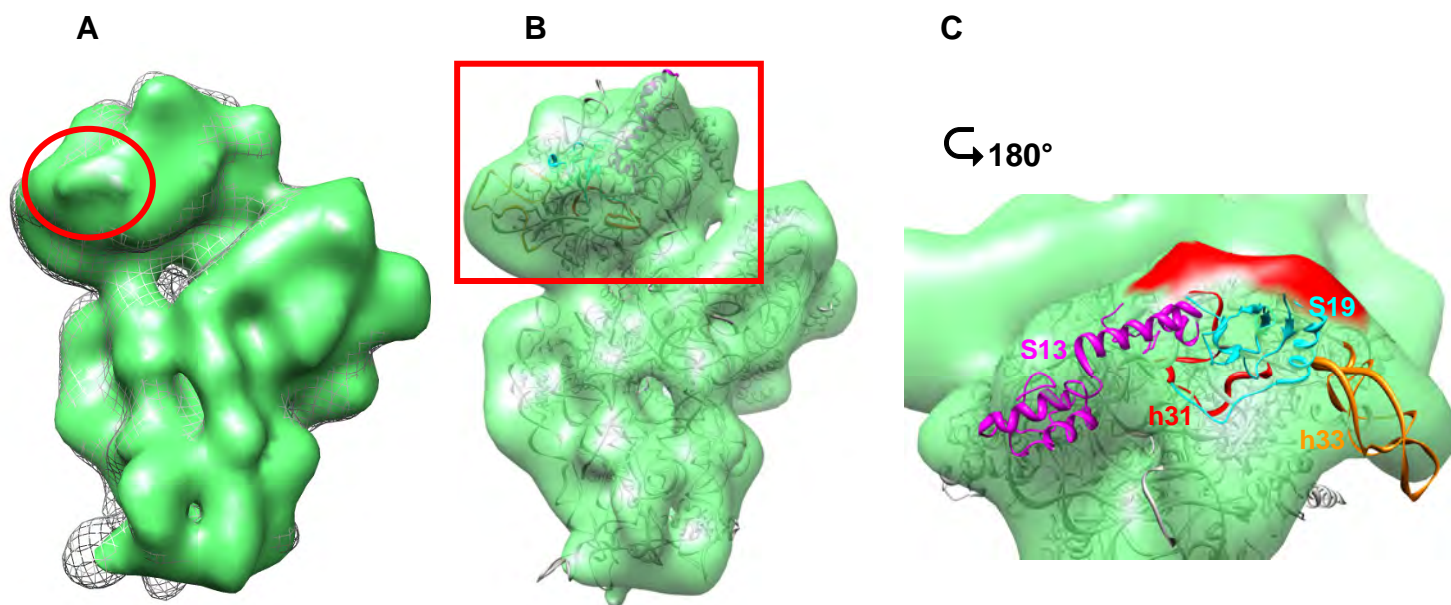


Figure 19: Cryo-EM reconstruction of the [Eco30SΔrimM-RimM] complex. (A) Comparison of the volume obtained from the reconstruction (green) with an *E. coli* 30S reference (grey mesh). A red circle highlights the extra density assigned to RimM. (B) 3D-reconstruction of the [Eco30SΔrimM-RimM] complex shown in transparent green fitted with PDB2YKR. 16S rRNA and r-proteins are shown in grey and main components are highlighted in color. (C) Detailed view of the head region of the 30S ribosomal subunit from (B) turned by 180°. 16S rRNA h31 and h33 are shown in red and orange, respectively, and r-proteins S13 and S19 in pink and cyan, respectively. The extra density of the cryo-EM reconstruction is highlighted in red.

4.4 Conclusions and Outlook

The *E. coli* G966 specific methyltransferase YhhF has been obtained in high purity and the complex consisting of purified 30S ribosomal subunits derived from the *yhhF* deletion strain together with recombinant YhhF protein has been assembled *in vitro* in the presence of sinefungin (**Figure 8A**). A low-resolution cryo-EM analysis of the complex (collected at 120 kV) showed extra density in the head region of the 30S subunit (**Figure 10A**), in close proximity to helix 31 that harbors the guanine nucleobase, which is specifically methylated by YhhF (**Figure 10C**). The results obtained here are promising and a large dataset of the

[30S Δ yhhF-YhhF] complex has to be collected (on the Titan Krios TEM at 200kV) in the future to have the possibility to gain more insights in the 30S-YhhF interactions. In addition, additional sorting techniques should be applied on the dataset to separate the 30S-protein complex from small ribosomal subunits with unbound factor. The dataset should be then more homogeneous and improve in resolution.

E. coli RlmH specifically methylates Ψ 1915 in the 23S rRNA, which is located in the stem-loop of H69. The [*Eco*70S Δ rluD/*rlmH*-RlmH] complex has been successfully assembled in an *in vitro* binding assay in the presence of sinefungin (**Figure 11A**). Thus, the occupancy of the factor bound to the 70S ribosome could not be directly verified in this experiment. A high-resolution cryo-EM dataset was obtained and sorting strategies were used to visualize the structural complex (**Figure 13 and 14**). However, the RlmH factor could not be detected in this cryo-EM reconstruction, probably due to the low binding efficiency of the factor to the ribosome. For the future, the binding capacity of the factor to the ribosome has to be improved and should be thoroughly monitored using specific tags which allow the binding and the detection of the factor to the ribosome and simultaneously maintain RlmH activity.

E. coli RimM is known to be involved in small subunit biogenesis, in particular in the maturation of the 30S head region. The protein factor has been successfully purified and assembled in an *in vitro* binding assay with purified small ribosomal subunits derived from a *rimM* deletion strain (**Figure 17A**). A subsequent cryo-EM reconstruction of this complex could visualize extra density located on top of the head of the 30S subunit (**Figure 19A**). Lövgren *et al.* (2004) could show that a double mutant in the interdomain linker region of RimM (Y106A-Y107A) produces a phenotype similar to a Δ *rimM* knock-out strain due to the inability of the protein to bind to the 30S subunit any longer. Several suppressor mutations could be identified for the double mutation, including modifications in ribosomal proteins S13 and S19 as well as alterations in 16S rRNA helices 31 and 33b (Lövgren, Bylund *et al.* 2004). These components of the 30S subunit are in close proximity to the extra density found in the cryo-EM reconstruction determined here (**Figure 19C**). Therefore, the results obtained in this project are encouraging to collect high-resolution data (at the Titan Krios TEM at 200 kV) in the future. The amount of data collected has to be increased to achieve better resolution and sorting techniques has to be applied to get the dataset more homogeneous.

5 Organellar-specific ribosomal Proteins

5.1 Project Aims

The aim of this project is to determine the binding position of several yeast MSRPs on the ribosome in order to elucidate the specific functional and/or structural roles of these proteins. The binding ability of specific MSRPs to *E. coli* ribosomes will be analyzed and verified by western blot analysis and mass spectrometry, and their binding positions should be visualized by cryo-EM.

5.2 Introduction

5.2.1 Mitochondrion-specific ribosomal proteins (MSRPs)

Mitochondria originated from an early endosymbiotic event and still possess a translational apparatus in a significant reduced version compared to the proteobacterium, mitochondria derive from (Gray, Burger *et al.* 2001). Mitochondrial ribosomes (mitoribosomes) exhibit striking differences in comparison to their bacterial ribosome ancestor and one of them is the huge acquisition of mitochondrion-specific ribosomal proteins (MSRPs).

In *S. cerevisiae*, a still-increasing number of individual mitochondrial ribosomal proteins exist, which were identified by mass-spectrometry and tag-assisted purification techniques (Gan, Kitakawa *et al.* 2002) as well as in biochemical and mutational studies (Graack and Wittmann-Liebold 1998). Some MSRPs have been identified to be involved in the composition of the yeast mitochondrial ribosomal tunnel exit including Mba1, MRPL3, MRPL13 and MRPL27 (Gruschke, Grone *et al.* 2010). Several hypothesis persist for the presence of these proteins: (1) they might compensate for a loss in rRNA sequence (O'Brien 2002), (2) MSRPs help to stabilize the mitoribosome or (3) these proteins exhibit novel features and have a specific function on the mitoribosome. While analyzing yeast mitochondrial ribosomes, it became clear that they resemble closely the mass of the 55S mammalian mitoribosomes (molecular mass of the bovine 55S mitoribosome: 2.71 MDa), however yeast organellar ribosomes exhibit no reduction in their rRNA content compared to mammalian mitoribosomes (Gan, Kitakawa *et al.* 2002). This finding indicates on the one hand that the long-standing replacement hypothesis saying that the multitude of additional proteins compensate for the

loss in rRNA is unlikely to be correct (O'Brien 2002). On the other hand, MSRPs might indeed have specific, yet so far unknown, functional roles on the mitochondrial ribosome. However, no structural data is available so far determining the specific binding site of individual MSRPs on the ribosome which would also help to suggest a probable function of the protein.

5.3 Results

5.3.1 Expression and purification of yeast MSRPs

To specifically identify the binding sites of MSRPs, nine individual MSRPs were selected from *S. cerevisiae* that have no bacterial counterpart, but do have a homologue in both *Neurospora crassa* and *Homo sapiens*. Furthermore, yeast MSRPs were selected that are larger than 20 kDa in size for an ease of detection by cryo-EM analysis and have an isoelectric point (pI) larger than 8.0, since basic proteins are more likely to interact directly with the negatively charged rRNA (**Table 5**).

Table 5: Nine mitochondrion-specific ribosomal proteins from *S. cerevisiae* were selected and cloned for expression and purification in *Escherichia coli*. The table summarizes the name of the protein in yeast together with its respective ORF, the binding priority of the protein to either the small (SSU) or the large ribosomal subunit (LSU), the name of the construct together with the respective restriction sites for cloning and finally the length of the mature protein in aa and the molecular mass in kDa.

Yeast Name	ORF	Subunit protein binding	Construct	Restriction sites	Length (aa)	Molecular Mass (kDa)
RSM22	YKL155C	SSU	pET28-HisTEV-rsm22	<i>Bam</i> HI, <i>Xho</i> I	651	74.9
RSM23	YGL129C	SSU	pET28-HisTEV-rsm23	<i>Bam</i> HI, <i>Xho</i> I	511	58.3
RSM24	YDR175C	SSU	pET28-HisTEV-rsm24	<i>Eco</i> RI, <i>Xho</i> I	344	40.4
RSM25	YIL093C	SSU	pET28-HisTEV-rsm25	<i>Sac</i> I, <i>Hind</i> III	291	33.8
Ppe1	YHR075C	SSU	pET28-HisTEV-ppe1	<i>Eco</i> RI, <i>Xho</i> I	425	47.9
MRPL35	YDR322W	LSU	pET28-HisTEV-mrpl35	<i>Eco</i> RI, <i>Xho</i> I	392	45.9
MRPL3	YMR024W	LSU	pET28-HisTEV-mrpl3	<i>Bam</i> HI, <i>Sac</i> I	413	46.8
MBA1	YBR185C	LSU	pET28-HisTEV-mba1	<i>Bam</i> HI, <i>Sal</i> I	301	34.6
MRPL17	YNL252C	LSU	pET28-HisTEV-mrpl17	<i>Eco</i> RI, <i>Xho</i> I	306	35.2

Genes were cloned from yeast genomic DNA into both a modified pET28 vector providing the construct with an N-terminal 6x His-tag separated from the mature protein by a short linker sequence and a TEV cleavage site, as well as into a pET32b vector. Individual constructs were expressed in *E. coli* in different strains (BL21 (DE3), Rosetta, Lemo 21) under different conditions (temperature, IPTG concentration, growth time) and in different media (LB, TB) to find optimal conditions for protein expression. The best expression pattern could be achieved when cells were grown in LB media at 37°C for 1 hour and then shifted to 25°C for overnight growth. Cells were induced at mid-log phase with 1 mM IPTG.

Protein expression was successful for all MSRPs shown here by the overexpression of MRPL3 in *E. coli* (**Figure 20A**). Unfortunately, none of the proteins could be purified by Ni²⁺-NTA affinity purification, since the proteins tended to aggregate and were found almost exclusively in inclusion bodies in the pellet fraction (**Figure 20B**, “P”). Protein purification was carried out under native conditions using varying salt and imidazole concentrations but no optimal condition could be found to achieve soluble protein. Protein purification attempts were also tried under denaturing conditions using 6 M GuHCl or 8 M urea. Here, the purification strategies basically worked, however, the protein precipitated after refolding. The MSRP-pET32b constructs harbor an N-terminal thioredoxin tag that is fused to the MSRP to increase protein solubility during protein expression. However, also these attempts failed, since no optimization in protein solubility could be achieved with these constructs.

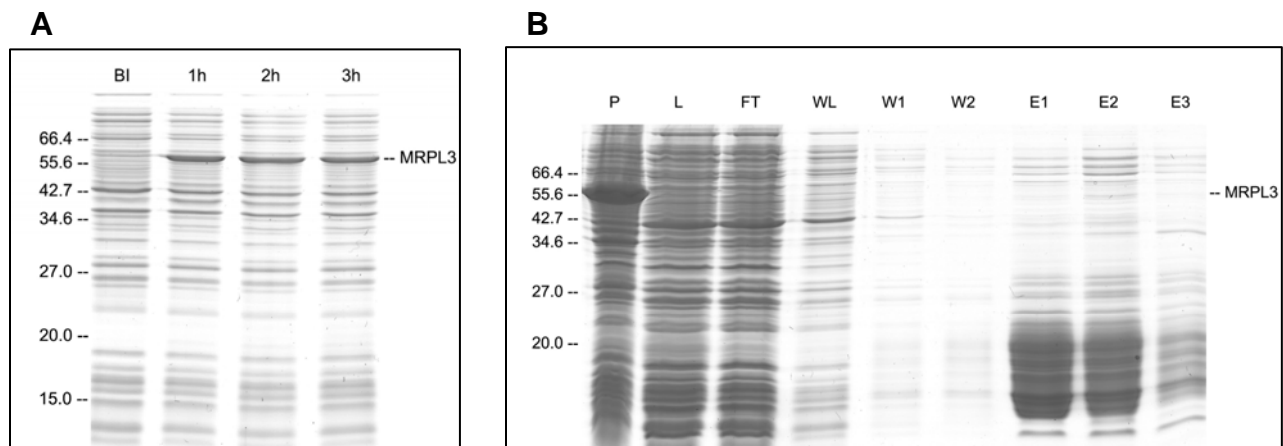


Figure 20: Expression of yeast MRPL3 in *E. coli* and small-scale purification attempts of overexpressed MRPL3. (A) Cells were induced with 1 mM IPTG and samples were taken for SDS-PAGE before induction (BI), 1, 2 and 3 hours after induction. Overexpressed MRPL3 is indicated on the righthand sight. (B) Ni²⁺-NTA purification of overexpressed MRPL3. Purification steps are indicated as P (pellet), L (lysate), FT (flow-through), WL (wash step with lysis buffer), W1/2 (subsequent wash steps with wash buffer) and E1/2/3 (subsequent elution steps with elution buffer).

Due to the failure of protein purification, no *in vitro* binding assays could be performed. Therefore, attempts for the association of individual MSRPs with *E. coli* ribosomes were carried out *in vivo* to show the binding of the individual protein to 70S ribosomes and the assigned subunit.

5.3.2 *In vivo* association of individual MSRPs with *E. coli* ribosomes

The *in vivo* association of individual MSRPs with *E. coli* ribosomes (Material and Methods 7.2.7) was successfully performed for yeast MRPL3 (**Figure 21A**) and MRPL17 (data not shown). Cells overexpressing yeast MRPL3 were grown and *E. coli* 70S ribosomes and ribosomal subunits were isolated as described before (Material and Methods 7.2.1). MRPL3 showed binding to both 70S ribosomes and the large ribosomal subunit (**Figure 21A**, 70S (S) and 50S (S)). No binding could be observed for the small ribosomal subunit that confirms the binding of MRPL3 as specific (**Figure 21A**, 30S (S)). In addition, the binding of MRPL3 to 70S ribosomes and 50S ribosomal subunits was confirmed by western blot (**Figure 21B**) and mass-spectrometry (data not shown, performed by Dr. T. Fröhlich, Gene Center,

LMU). *In vivo* attempts for all other MSRPs were either non-specific, e.g. showed binding to both ribosomal subunits or did not show any binding at all (data not shown).

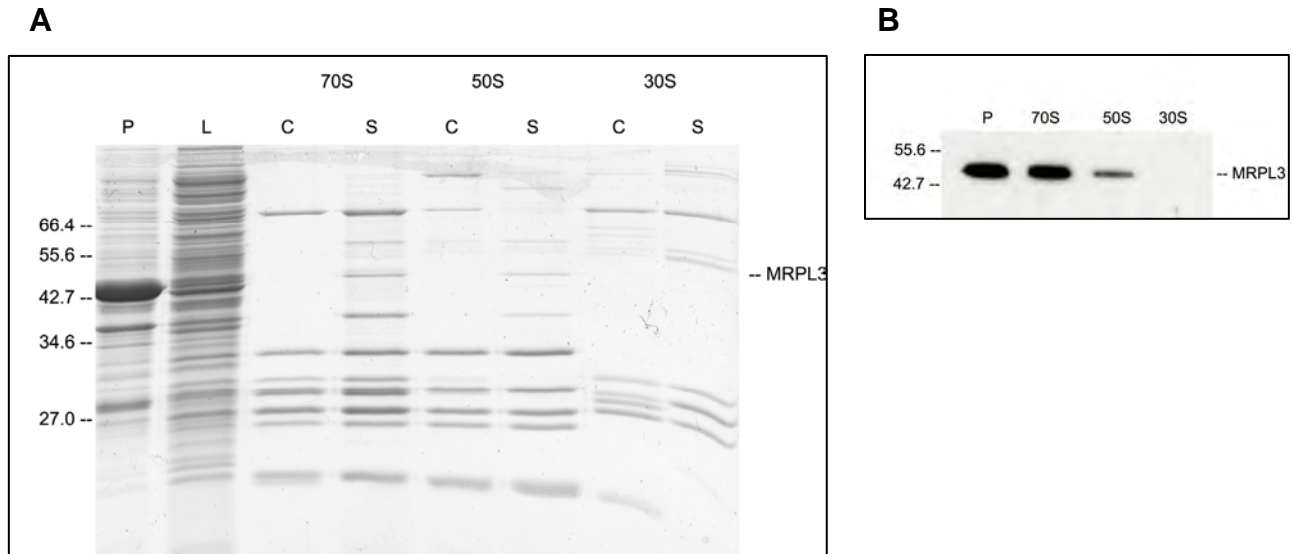


Figure 21: *In vivo* association of yeast MRPL3 with *E. coli* 70S ribosomes and 50S ribosomal subunits in accordance to western blots analysis. (A) SDS-PAGE with samples (S) for 70S ribosomes and both 50S and 30S ribosomal subunits with overexpressed MRPL3 loaded next to ribosome controls (C). MRPL3 is represented in the pellet fraction (P) as a prominent band but far less in the lysate (L) as indicated on the righthand site. **(B)** Detection of MRPL3 via the α His antibody by western blot analysis.

5.3.3 Purification of [*Eco*70S-MRPL3] complexes

[*Eco*70S-MRPL3] complexes were purified as described in Material and Methods (7.2.3) (**Figure 22A**). For this purification attempt, TALON resin was used due to higher binding specificity in comparison to nickel-based IMAC resin. Moreover, TALON shows a significantly lower unspecific binding capacity for non-tagged proteins, which was preferred in this case to obtain highly pure complexes. After elution from the column, both elution fractions were pooled and pelleted through a sucrose cushion in order to remove imidazole and to concentrate the sample. Out of 550 OD that were initially loaded on the TALON column, ~3 OD of pure [*Eco*70S-MRPL3] complex could be obtained for further cryo-EM analysis. The homogeneity of the [*Eco*70S-MRPL3] sample was verified by negative-stain EM (**Figure 22B**).

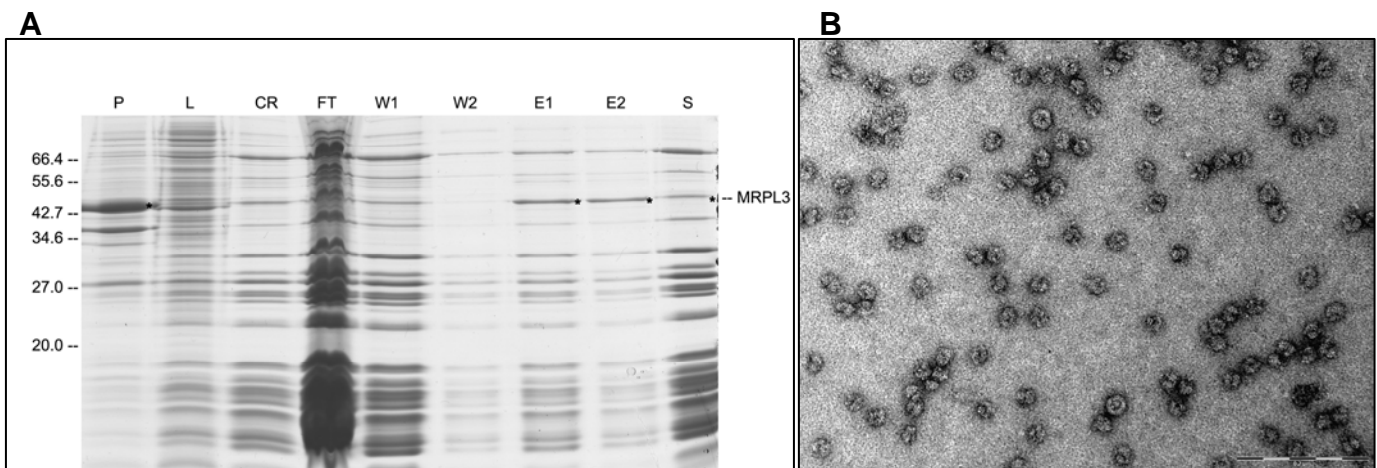


Figure 22: TALON purification and negative-stain EM of [*Eco*70S-MRPL3] complexes. (A) SDS-PAGE from TALON metal affinity chromatography with 70S ribosomes associated with MRPL3. Lanes are indicated as pellet (P), lysate (L), crude ribosomes (CR), flow-through (FT), wash step with equilibration buffer (W1), wash step with wash buffer (W2), elution step 1 and 2 (E1/2) and the [*Eco*70S-MRPL3] complex after pelleting the sample (S) through a sucrose cushion. (B) Negative-stain EM of the [*Eco*70S-MRPL3] complex. The scale bar represents 20 nm.

5.3.4 3D-reconstruction of [*Eco*70S-MRPL3] complexes

98 micrographs were collected on the Spirit microscope (LMU Biocenter, Munich, Germany). 17 micrographs were used for the reconstruction resulting in a small dataset with 16137 particles divided into 6 defocus groups. After several refinements, the reconstructed volume obtained a resolution of ~ 24 Å based on the $FSC_{0.5}$ cut-off criterion (**Figure 23**). Unfortunately, there was no prominent extra density visible on the large ribosomal subunit in comparison with a 70S *E. coli* reference volume probably due to low resolution and low occupancy of the factor bound to the ribosome (**Figure 24**).

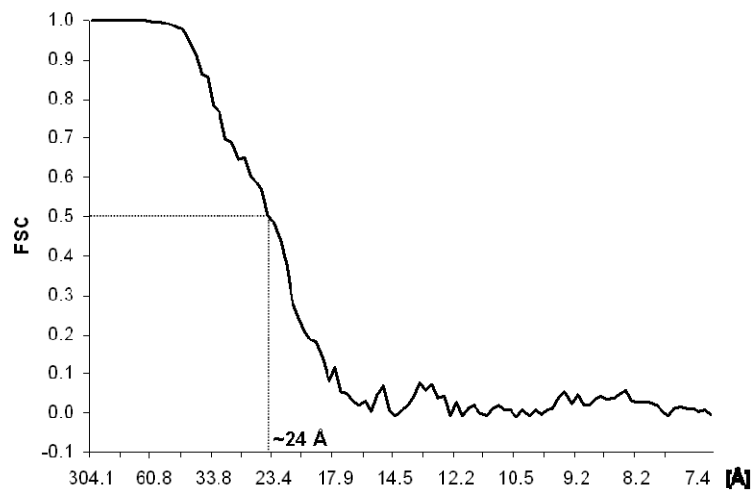


Figure 23: Resolution curve of the [*Eco*70S-MRPL3] complex. The resolution of the map was calculated to be ~ 24 Å according to $FSC_{0.5}$.

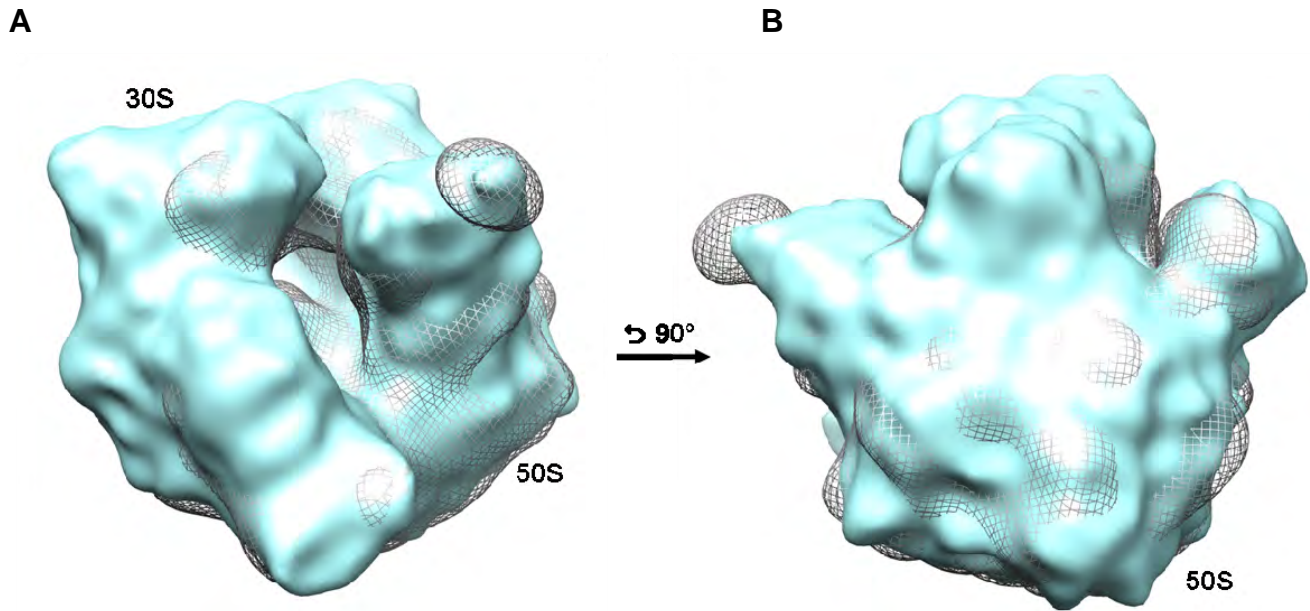


Figure 24: Cryo-EM reconstruction of the [Eco70S-MRPL3] complex. (A) Front-view of the *E. coli* [70S-MRPL3] complex shown in cyan in comparison with an *E. coli* 70S reference (grey mesh). The ribosomal subunits (30S and 50S) are indicated. (B) View on the large ribosomal subunit. In comparison, there is no extra density visible for MRPL3.

5.4 Conclusions and Outlook

In this project, individual MSRPs from yeast were chosen due to their presence in other eukaryotes, such as the fungus *N. crassa* or humans, and their simultaneous absence in eubacteria as well as based on their size and their basic character with the aim of identifying the binding sites of these protein factors on the *E. coli* ribosome. Since mitochondrial ribosomes are difficult to purify and are only achieved in low amounts, we tried to bind individual yeast MSRPs to the *E. coli* ribosome since the chosen proteins are absent in bacteria. Nine MSRPs were successfully cloned and overexpressed in *E. coli* cells, however, the purification attempts for these proteins failed. Therefore, the association of the individual factors with the *E. coli* ribosome and the appropriate subunit was monitored *in vivo* and could be shown for MRPL3 (**Figure 21A**) and MRPL17. Both of the proteins, MRPL3 and MRPL17, were found to associate with the *E. coli* 70S ribosome as well as the large ribosomal subunit which could be confirmed by western blot analysis (**Figure 21B**, data not shown for

MRPL17). Therefore, these results were in agreement to earlier mass-spectrometry analyses that were performed for the characterization of yeast MSRPs (Graack and Wittmann-Liebold 1998). The [*Eco*70S-MRPL3] complex was purified (**Figure 22A**), the homogeneity of the sample was confirmed by negative-stain EM (**Figure 22B**) and a preliminary cryo-EM reconstruction was accomplished for the complex (**Figure 24**). Unfortunately, no extra density could be visualized in this reconstruction on the large ribosomal subunit, due to low-resolution data and probably low occupancy of the factor on the ribosome. For the future, the purification and therefore the complex stoichiometry should be improved so that in a larger high-resolution dataset (Titan Krios TEM, 200 kV), the resolution of the complex could be improved to visualize the factor bound to the ribosome. Moreover, the same procedure should be performed with the [*Eco*70S-MRPL17] complex that should be purified and visualized by cryo-EM.

6 Antibiotic Resistance Proteins

6.1 Project Aims

For this project, *Enterococcus faecalis* Tet(M) protein should be overexpressed in *E. coli* cells and purified. The complex consisting of *E. coli* 70S ribosomes, Tet(M) protein, GDPNP and the compound tigecycline (Tgc) should be assembled *in vitro* and detected by cryo-EM. On the one hand, the structure should confirm the previous low resolution cryo-EM studies on Tet(O) performed by Spahn, Blaha *et al.* (2001), but at higher resolution additional new insights are expected to be obtained, such as more details into the binding position of Tet(M) (including protein-ribosome contacts) as well as the mechanism of how the drug might get released from the ribosome. So far, an indirect mechanism has been proposed as to how tetracycline is released from the ribosome by Tet(M), however, higher resolution structural information will be necessary to validate this. On the other hand, Tgc will also be used in this cryo-EM reconstruction to investigate the interplay between the drug and Tet(M). Although challenging, direct visualization of small molecules by cryo-EM analysis will provide additional insight into the mechanism of action of the drug.

6.2 Introduction

6.2.1 Ribosome protection protein Tet(M)

Tetracyclines are a group of antibiotics that target the ribosome during the elongation phase of translation. Tetracycline (Tet) (**Figure 25C**) is naturally produced by *Streptomyces aureofaciens* and has been in medical usage since the late 1940s. Although several binding sites on the small ribosomal subunit were identified for this drug (**Figure 25A**), the primary and most occupied position of tetracycline (Tet1) is located in the head region of the 30S subunit making contacts to h34 and h31 (**Figure 25A und B**) (Brodersen, Clemons *et al.* 2000; Pioletti, Schlunzen *et al.* 2001). In contrast to Tet1, additional binding sites for tetracycline on the 30S subunit (Tet2 and three other binding sites) seem to be less important for translation inhibition. The mechanism of translation inhibition by Tet is well understood: The antibiotic overlaps with the anticodon stem-loop of the tRNA bound to the A-site and therefore inhibits the stable association of the ternary complex (consisting of aa-tRNA, EF-Tu

and GTP) with the ribosome as well as preventing the accommodation of the delivered aa-tRNA (Blanchard, Gonzalez et al. 2004).

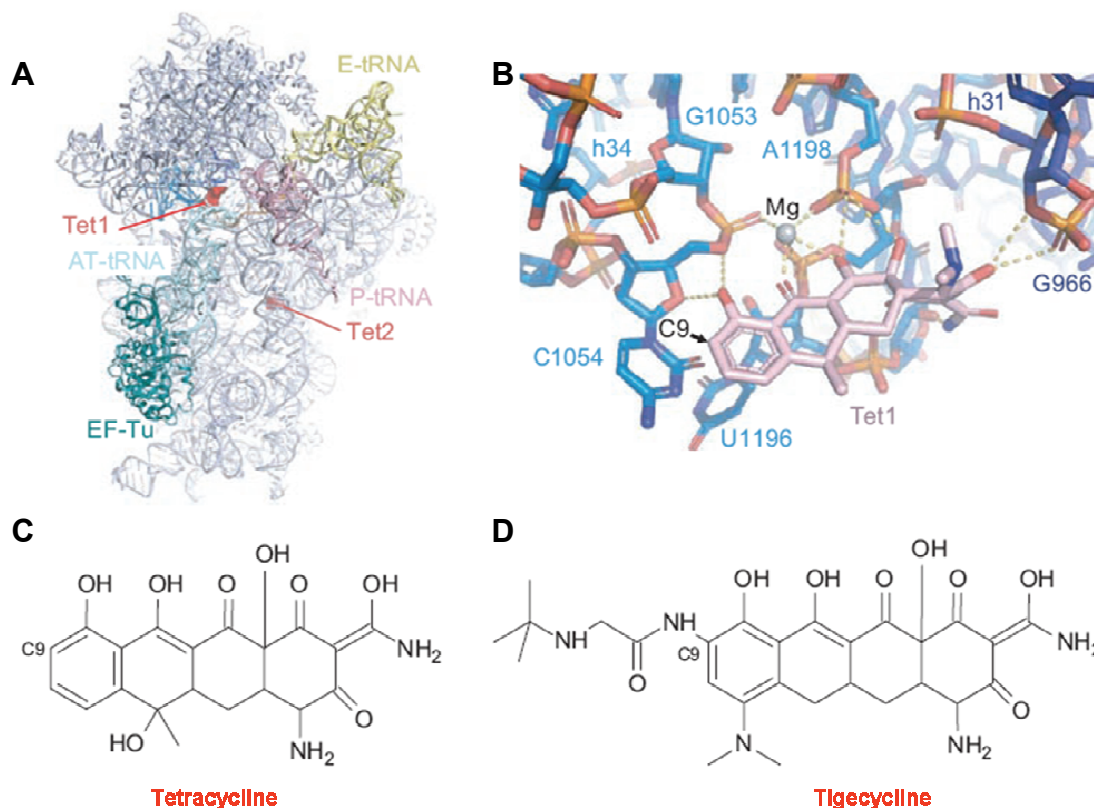


Figure 25: Inhibition of translation by tetracycline and derivatives. **(A)** 30S ribosomal subunit with the primary (Tet1) and secondary binding sites (Tet2) of tetracycline highlighted. E-, P- and A/T-tRNAs together with EF-Tu are shown in yellow, pink and blue-green, respectively. **(B)** Tet1 contacts the phosphate-sugar-backbone of helix 34 (h34, light blue) and helix 31 (h31, dark blue) of the 16S rRNA. **(C)** and **(D)** Chemical structures of tetracycline and a third-generation derivative of tetracycline, tigecycline.

Tet is a broad-spectrum antibiotic active against a variety of Gram-positive and Gram-negative bacteria. However, since Tet was in extensive usage for a long time, the effectiveness of this drug today is rather limited due to emergence of several prevalent antimicrobial resistance determinants. In general, common resistance mechanisms include energy-dependent efflux-pumps that transport the drug out of the cell as well as enzymatic inactivation of the antibiotic inside the cell (Chopra and Roberts 2001). One unique strategy

against Tet resistance that is becoming more prevalent in pathogenic bacteria involves ribosome protection proteins (RPPs) encoded by *tet* genes (Connell, Tracz *et al.* 2003).

RPPs are GTPases that bind to the ribosome and are suggested to confer Tet resistance by promoting the release of the compound from the ribosome (Connell, Trieber *et al.* 2002). Two well-studied RPPs are Tet(M) and Tet(O) (Burdett 1996; Dantley, Dannelly *et al.* 1998; Trieber, Burkhardt *et al.* 1998). These enzymes show about 75% sequence similarity (Taylor and Courvalin 1988) to each other and have 51% sequence similarity with EF-G (Taylor and Chau 1996). Ten years ago, a cryo-EM structure at 16 Å resolution of a [fMet-tRNA-70S-Tet(O)] complex was published (Spahn, Blaha *et al.* 2001). This structure showed high similarity to a previously determined [70S-EF-G-GMPPCP] complex (Agrawal, Heagle *et al.* 1999) regarding the binding position of Tet(O) on the ribosome. However, due to the low resolution of the existing structure, only limiting insights could be gained regarding the contacts of the factor on the ribosome and the mechanism of drug release.

6.3 Results

6.3.1 Purification of *E. faecalis* Tet(M)

The *tet*(M) gene was cloned from *E. faecalis* genomic DNA into the pET-46 Ek/LIC vector system. The construct was kindly provided by Dr. Aleksandra Mikolajka (Wilson Lab, Gene Center, LMU). Protein purification was carried out as described before (Material and Methods 7.2.2) with the following alterations: 3 liters of LB medium were inoculated with an overnight culture and substituted with ampicillin before induction of protein expression in mid-log phase. After induction with 1 mM IPTG, cell cultures were shifted from 37°C to 25°C and grown overnight.

Protein purification was carried out via the N-terminal His-tag of the construct on a column containing Ni²⁺-NTA resin. As seen in **Figure 26A**, the Tet(M) protein showed good overexpression indicated by prominent protein bands around 70 kDa on the Coomassie-stained SDS-PAGE and was eluted from the Ni²⁺-NTA-column (**Figure 26A**, E1 – E5). For higher purity, elution fractions 1 and 2 were applied onto a S200 gel filtration column. The protein showed a clean, sharp peak in the gel filtration elution profile (**Figure 26B**, upper part, indicated with Tet(M)). However, when samples were loaded on a SDS-PAGE, the purified

Tet(M) protein already exhibited minor degradation products (**Figure 26B**, lower part). Tet(M) was stored at 4°C, since previous purification attempts showed that the protein tend to degrade even faster when the purified protein was stored at -20°C or -80°C. Therefore, the *in vitro* binding assay was performed immediately to avoid further degradation.

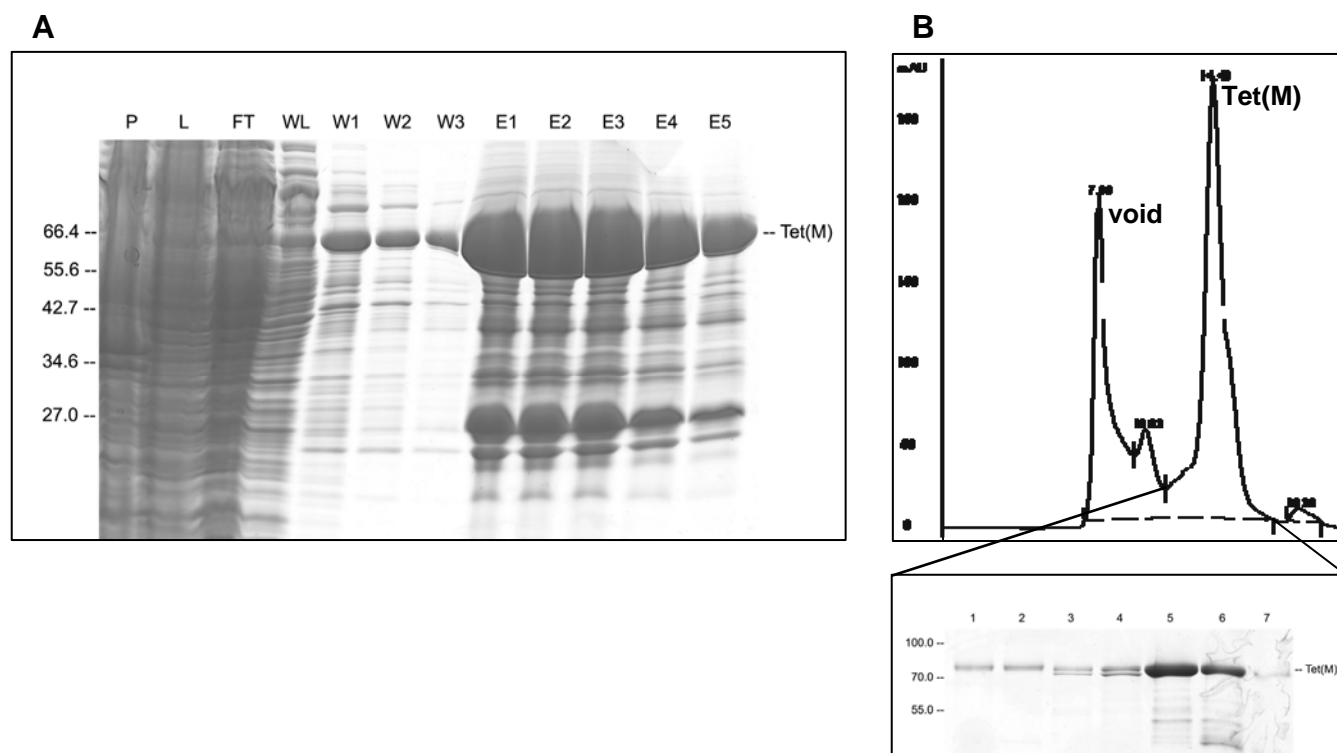


Figure 26: Purification of *E. faecalis* Tet(M). (A) SDS-PAGE of Ni^{2+} -NTA affinity purification. Various steps of purification are indicated: P: pellet, L: lysate, FT: flow-through, WL: wash step with lysis buffer, W1/2/3: subsequent wash steps with wash buffer, E1/2/3/4: subsequent elution steps with elution buffer. 72 kDa Tet(M) protein is indicated on the right-hand side. (B) S200 gel filtration profile of size-exclusion chromatography. Fraction 5 as indicated in the SDS-PAGE was used in further *in vitro* binding assays without any concentration attempts.

6.3.2 *In vitro* binding assay: Eco70S + Tet(M) + GDPNP +/- Tgc

The complex was assembled as described in Material and Methods (7.2.6) with the following components being used: 60 pmol of purified *E. coli* 70S ribosomes alone (70S) as well as in the presence of 10x excess of purified Tet(M) protein over ribosomes and a non-hydrolysable GTP analogue, GDPNP, with a final concentration of 0.5 mM in the reaction (70S+Tet(M)). In addition, one reaction was performed in the presence of Tgc with a final

concentration of 10 μ M in the reaction (70S+Tet(M)+Tgc). Both antibiotics, Tet and Tgc, should occupy the same binding site on the 30S subunit. However, in contrast to Tet, Tet(M) is not able to restore translation in the presence of Tgc, which could be shown recently in an *E. coli in vitro* coupled transcription/ translation assay (Grossman, Starosta et al., 2012, in press) and also confirms earlier studies (Rasmussen, Gluzman et al. 1994; Bergeron, Ammirati et al. 1996). Therefore, a complex was assembled *in vitro* with Tet(M) and Tgc bound to *E. coli* 70S ribosomes.

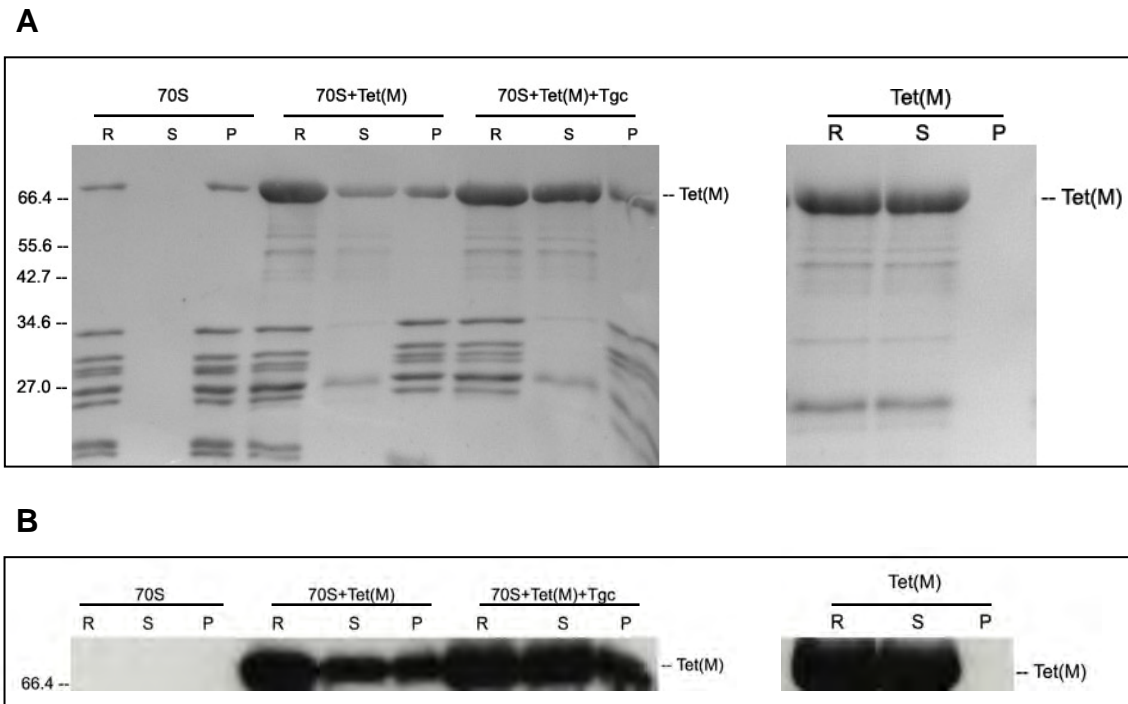


Figure 27: *In vitro* binding assay and western blot analysis. (A) *In vitro* binding experiment with *E. coli* 70S ribosomes alone (70S) and in the presence of 10x excess of Tet(M) protein (70S+Tet(M)). In one reaction, 10 μ M of Tgc was added (70S+Tet(M)+Tgc) and one reaction was carried out as protein control (Tet(M)). The amidoblack-stained membrane shows the initial reaction (R) before the samples were centrifuged through a 10% sucrose cushion and aliquots were taken from supernatant (S) and pellet (P) fraction. **(B)** Western blot analysis of the *in vitro* binding experiment shown in (A). Tet(M) protein was detected using antibodies raised against α His.

6.3.3 3D-reconstruction of [*Eco*70S-Tet(M)-GDPNP-Tgc] complex

Dataset 1 contained in total 145275 particles, organized into 99 defocus groups with approximately 1500 particles/defocus group. Image calculation started with 3x decimated particles and was finalized without decimation factor using a pixel size of 1.0489 Å/pixel. The final map volume obtained from this dataset contained 40776 particles with an estimated resolution of 8.1 Å. Since the final particle number of dataset 1 was very small and the density for the Tet(M) factor was fragmented, a second dataset was collected. Dataset 2 comprised 261412 particles in total, sub-divided into 122 defocus groups with approximately 2200 particles/defocus group. The workflow of data processing is summarized in **Figure 28**, and is exemplified using the second dataset. After several rounds of refinement, particles of the initial volume obtained for this reconstruction (**Figure 28**, grey, 100%) were sorted into healthy ribosomal particles (**Figure 28**, yellow, 56.2%), noisy/edged particles (**Figure 28**, cyan, 15.8%) as well as 50S ribosomal subunits (**Figure 28**, light purple, 28.0%), which appeared to be over-represented in the dataset. With 56.2% of the initial dataset remaining, more refinements were applied, including a second round of sorting. Here, the particles were sub-divided into datasets containing ribosomes in a non-ratcheted conformation and without the protein factor bound (**Figure 28**, dark purple, 18.6%), ribosomal particles in a ratcheted conformation where the 30S subunit has a rotated conformation relative to the 50S subunit (without Tet(M)) (**Figure 28**, light green, 22.3%) and ribosomal particles in an un-ratcheted conformation bound with Tet(M) (**Figure 28**, yellow, 15.3%). The particles from the latter volume containing Tet(M) were combined with the Tet(M) containing particles from dataset 1.

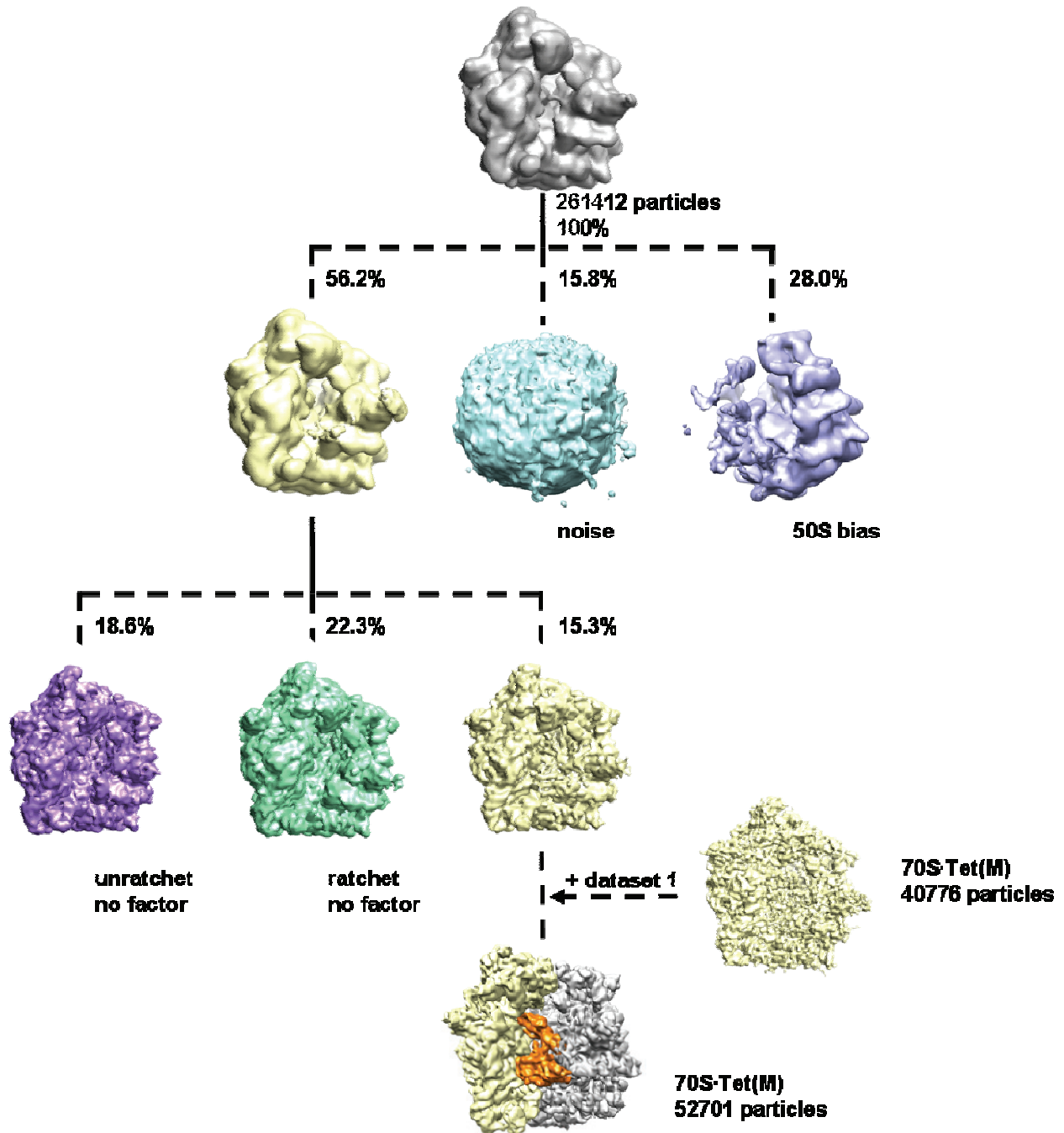


Figure 28: Workflow of data processing described on dataset 2. The initial dataset (261412 particles, shown in grey, 100%) was sorted into sub-datasets containing healthy ribosomal particles (56.2%, yellow), noisy/edged particles (15.8%, cyan) as well as 50S ribosomal subunits (28.0%, light purple). After several rounds of refinement, particles were sorted based on the following criteria: un-ratcheted ribosomes without Tet(M) (18.6%, dark purple), ratcheted ribosomal particles without Tet(M) (22.3%, light green) and Tet(M)-bound ribosomes (15.3%, yellow). 70S-Tet(M) particles from dataset 1 were then joined with this dataset and after improvement, a final map could be visualized showing Tet(M) (highlighted in orange) bound to the ribosome determined at a resolution of 8.1 Å.

The combined dataset was subjected to several further rounds of refinement resulting in a final dataset containing 52701 particles, which represents 13% of the initial particle number (**Figure 28**, bottom volume, 30S is shown in yellow, 50S in grey, Tet(M) in orange; **Figure 30**). The final map had a resolution of 8.1 Å (**Figure 29**).

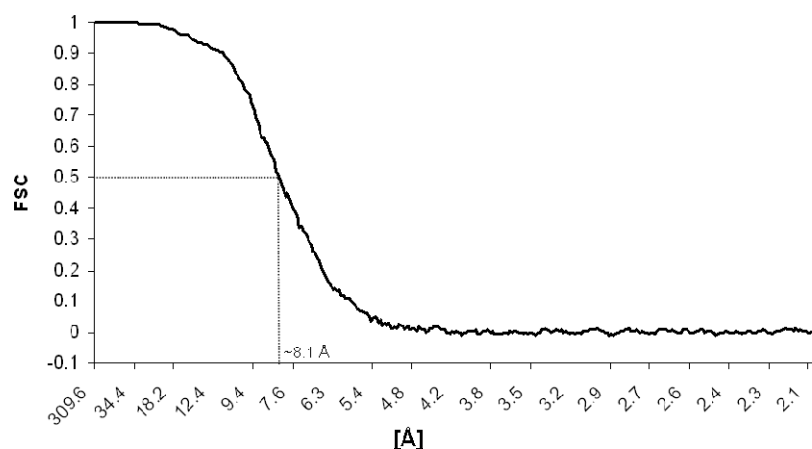


Figure 29: Resolution curve of the combined and processed datasets 1 and 2 collected on a Titan Krios TEM (200 kV). The final dataset contained 52701 particles and showed a resolution of 8.1 Å based on the $FSC_{0.5}$ cut-off criterion.

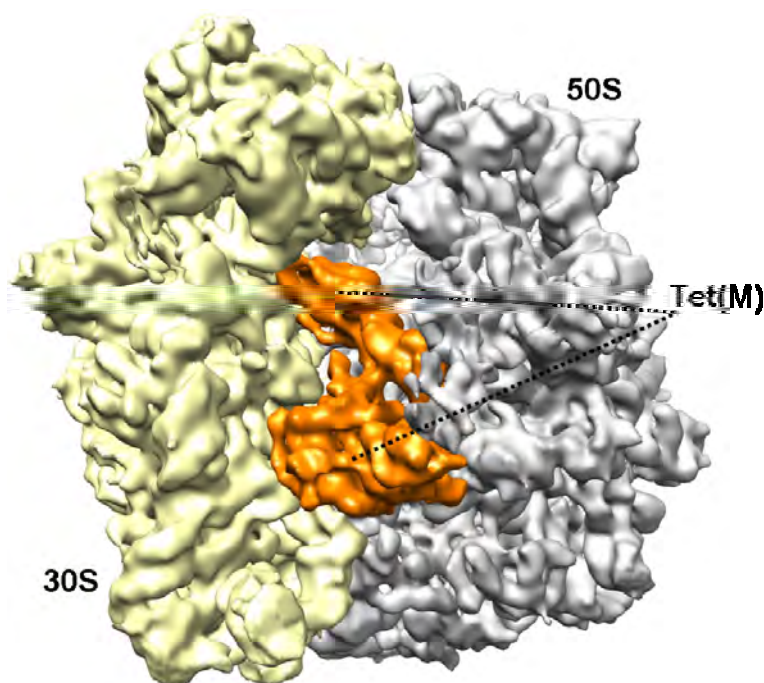


Figure 30: Overview of the final map obtained from the 3D-reconstruction of the [Eco70S-Tet(M)-GDPNP-Tgc] complex. The small and the large ribosomal subunit are shown in yellow and grey, respectively. Protein factor Tet(M) is highlighted in orange.

The final map volume exhibited extra density in the inter-subunit space between the small and the large ribosomal subunit, which was assigned to Tet(M) (**Figure 30**). The binding position is in agreement with earlier studies on Tet(O) (Spahn, Blaha *et al.* 2001) and shows similarities in terms of binding site and shape to EF-G (Agrawal, Penczek *et al.* 1998; Agrawal, Heagle *et al.* 1999).

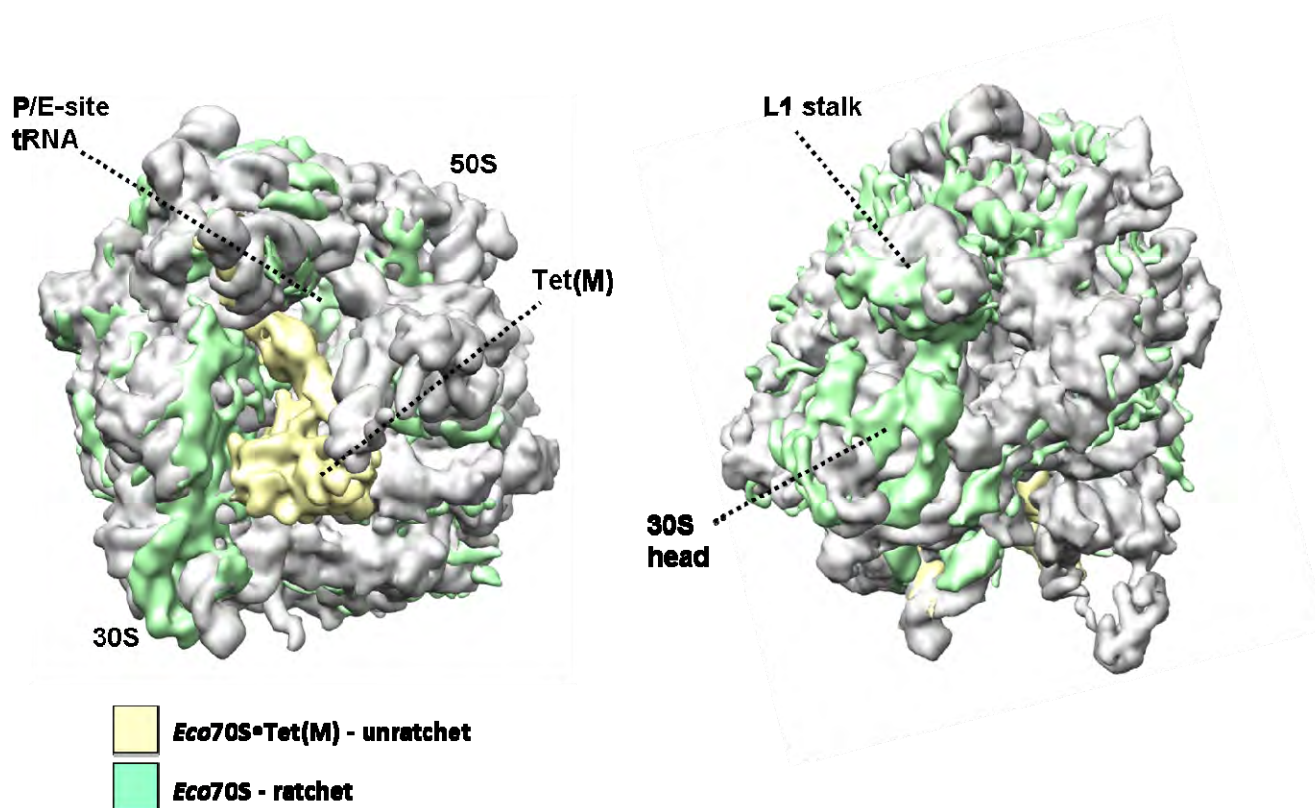


Figure 31: Difference map illustrating alterations of two sub-datasets that were separated during sorting. The reference structure, shown in grey, was calculated as a molecular map at 8 Å from PDB2WRI and PDB2WRJ using Chimera. The 30S and 50S subunit are indicated. By calculating a difference map, clear differences could be visualized between the sub-volume in a ratcheted conformation (shown in green) and the un-ratcheted sub-volume containing Tet(M), highlighted in yellow. The difference map is shown in (A) a front-view and by tilting the map about 90° in (B) a top-view, indicated with the 30S head and the L1 stalk.

The implementation of sorting strategies revealed that the dataset could be separated into various sub-volumes with ribosomes exhibiting different conformations in the presence or absence of Tet(M). During the second sorting step, particles harboring Tet(M) were separated from particles that were found in a rotated conformation, i.e. the small ribosomal subunit was rotated relative to the large ribosomal subunit (**Figure 31A**). This ribosomal conformation therefore appears to be unfavorable for Tet(M) binding. Moreover, the rotated sub-volume

showed a tRNA bound in a P/E hybrid state (**Figure 31A**, shown in green). Tilting the map about 90° to the front results in a presentation of the map in a top-view. Here, it is clearly visible that the 30S head underwent a swivel movement towards L1 and is accompanied by a conformational change of the L1 stalk on the large subunit when compared to the reference map (**Figure 31 B**, shown in green). In comparison, the sub-volume containing density for Tet(M) showed a completely un-rotated conformation (**Figure 31**, shown in yellow).

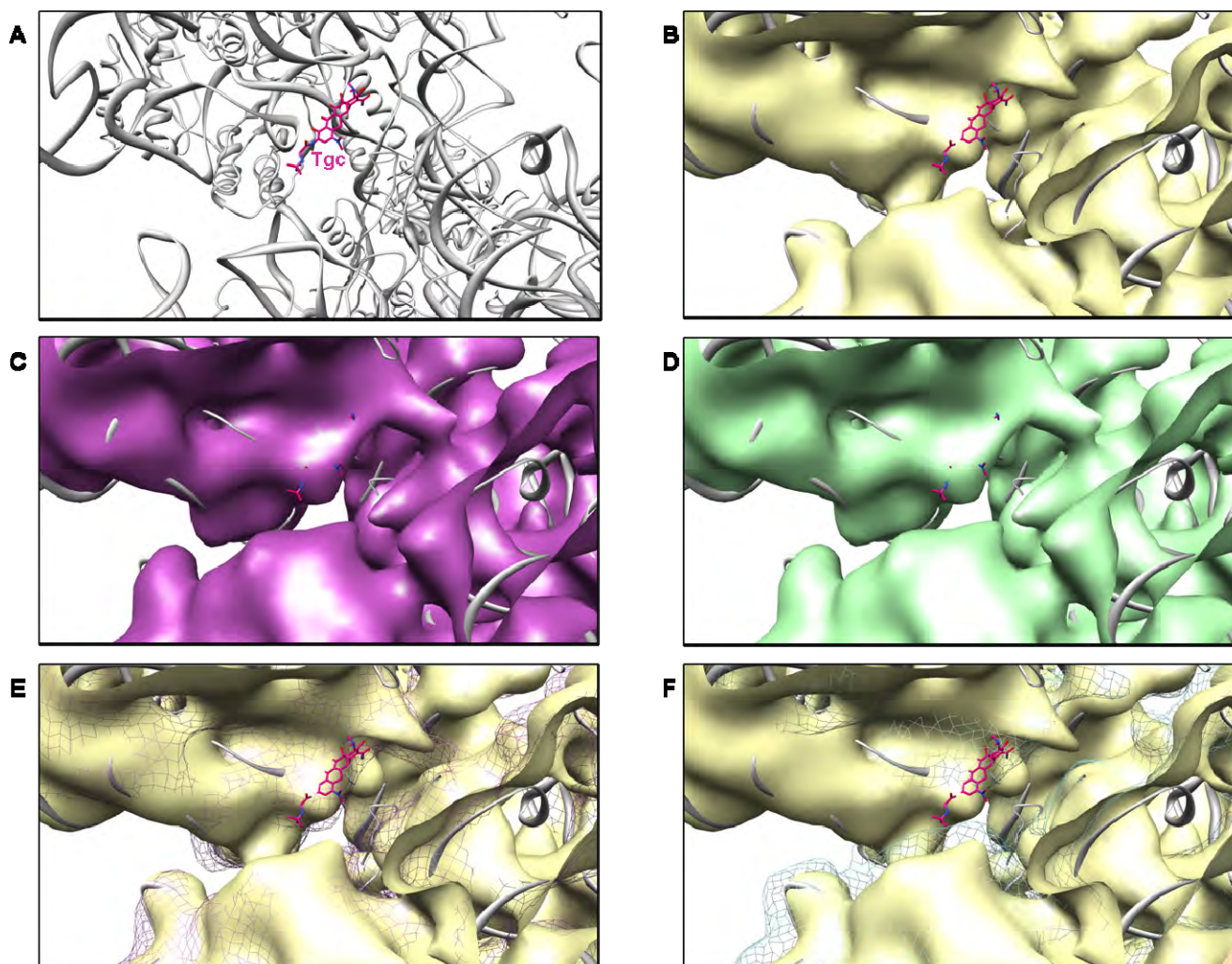


Figure 32: Sub-datasets from sorting step 2 in relation to the presence and absence of the compound Tgc. (A) For the *in vitro* binding assay, the antibiotic tigecycline (Tgc) was included in the reaction, which occupies a binding site on the 30S subunit, similar to tetracycline. (B) Interestingly, the map containing 70S-Tet(M) particles (yellow) did not show any density for Tgc. (C) and (D) Sub-datasets with non-rotated ribosomes without Tet(M) (C, purple) and ribosomes in a rotated conformation in the absence of Tet(M) (D, green) showed density for the compound Tgc. (E) and (F) Overlay of the 70S-Tet(M) sub-dataset (yellow) with the sub-datasets shown in (C) and (D), represented here in (E) purple and (F) green mesh to highlight the differences for the compound density in the sub-volumes.

Since Tgc was included in the *in vitro* binding assay, the sub-datasets from the second sorting application were also analyzed with regard to the presence of the compound. Interestingly, Tgc density could only be visualized in two of the three sub-volumes (**Figure 32**). As illustrated in **Figure 32**, Tgc occupies a binding site in the head region of the 30S subunit, similar to Tet (**Figure 32A**). In the sub-dataset containing 70S-Tet(M) particles, no density for the compound could be visualized (**Figure 32B**), in contrast to the sub-volumes with un-rotated ribosomes (**Figure 32C** and **32E** as an overlay) and ribosomes in a rotated conformation (**Figure 32D** and **32F** as an overlay). The two latter sub-datasets did not contain any density for Tet(M), which leads us to the suggestion that both Tet(M) and the compound could not bind together to the same 70S ribosome.

Since no crystal structure of any RPP has been determined so far, a model for Tet(M) was generated using HHpred (Söding, Biegert *et al.* 2005) based on homology with elongation factor G (both proteins share 51% sequence similarity (Taylor and Chau 1996), see sequence alignment, **Figure 41**) (Material and Methods 7.3.4). The final model was based on a sequence alignment with *Thermus thermophilus* EF-G and a crystal structure of EF-G bound with GDP (PDB1DAR) (al-Karadaghi, Aevvarsson *et al.* 1996), as shown in **Figure 33A**. The N-terminal region of Tet(M) (G domain) is similar to EF-G encompassing five well-conserved sequence motifs, namely G1 to G5 (Grewal, Manavathu *et al.* 1993), that function in nucleotide binding. Moreover, the G domain of EF-G contains a G' sub-domain (Aevvarsson, Brazhnikov *et al.* 1994) (**Figure 33A-C**, shown in dark blue), whereas the RPPs also contain a G' sub-domain with several sequence stretches missing (**Figure 41**). Domain II and III are also well conserved between elongation factors, such as EF-G, and RPPs. Domain IV and V of EF-G are essential for tRNA translocation and factor release (Savelsbergh, Matassova *et al.* 2000), whereas domain IV of Tet(M) is involved in the release of Tet from the Tet1 binding site (Spahn, Blaha *et al.* 2001)

The individual domains of the homology model were fitted separately into the isolated Tet(M) density of the cryo-EM reconstruction using the “Fit in Map” function of Chimera (Material and Methods, 7.3.4). The domains fit very nicely into the density (**Figure 33B** and **33C**), with the exception of some flexible loop regions that were not in density with the initial rigid-body fit. However, it can be shown that there is in fact extra density for these loop regions, indicated by the black arrows in **Figure 33B** and **33C**, and therefore remodeling will be required in the future. The C-terminus of Tet(M) (**Figure 33A-C**, domain V, shown in light blue) is absent in EF-G and is therefore predicted to be unstructured from the homology

model. However, the C-terminus is well conserved between various Tet proteins (**Figure 41**). Moreover, applying a secondary structure prediction on the C-terminal sequence of Tet(M) indicates that 11 C-terminal amino acids have the potential to adopt an α -helix (**Figure 33D**).

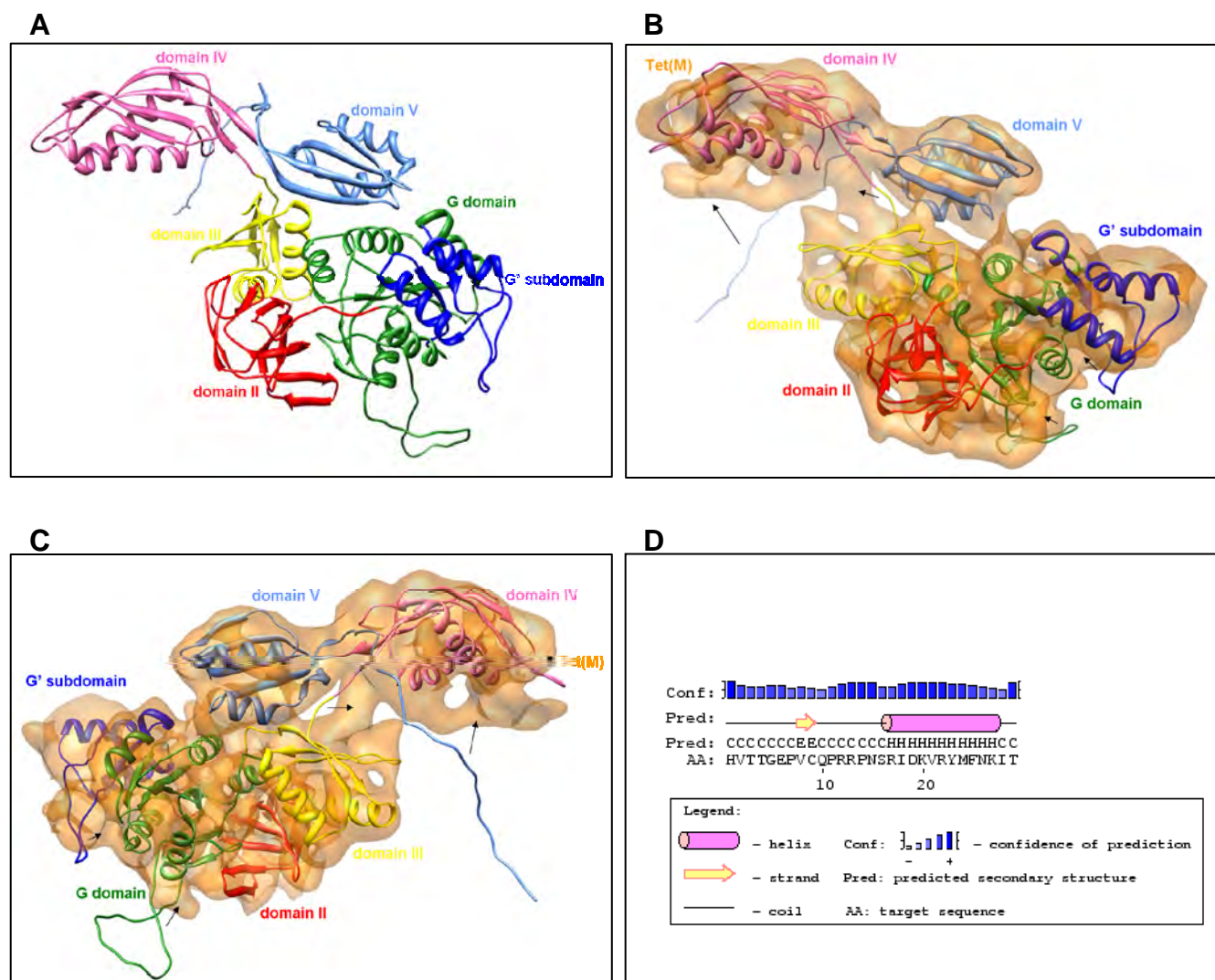


Figure 33: (A) Homology model of *E. faecalis* Tet(M), based on comparison with *T. thermophilus* EF-G.

(A) The protein can be sub-divided into 5 domains. The G domain is highlighted in green and contains the G' sub-domain (indicated in dark blue) that is responsible for a rapid nucleotide exchange. Domain II, III, IV and V are shown in red, yellow, pink and light blue, respectively. **(B)** and **(C)** Model fitted into isolated density of Tet(M), shown in transparent orange, using the "Fit in Map" function of Chimera. Domains are indicated as in (A). Several flexible loop regions, which are located outside of Tet(M) density are indicated with an arrow. **(D)** The unstructured C-terminus of domain V can form a helical structure as indicated by the secondary structure prediction using PSIPRED.

This is also in agreement with secondary structure predictions on the C-terminal sequence of other RPPs, which all have the potential to form a helical structure within the corresponding sequence region (with the exception of Tet(Q) from *Bacteroides thetaiotaomicron*, where the prediction is not entirely clear, i.e. the C-terminal sequence is predicted to form an α -helix by using the programs JPred and PredictProtein, but forms a β -strand using PSIPRED and CFSSP, respectively; data not shown) (**Figure 42**). There is strong extra density visualized in this cryo-EM reconstruction, which is consistent with the α -helical structure of the Tet(M) C-terminus. Moreover, additional density is also observed connecting the end of domain V of Tet(M) to the helical density that reaches towards the tip of domain IV (**Figure 33B** and **33C**).

The contacts between Tet(M) and the small and large ribosomal subunit visualized in this cryo-EM reconstruction are summarized in **Table 6** in comparison to the protein-ribosome contacts observed for EF-G on the ribosome bound in a post-translocational state (Connell, Takemoto *et al.* 2007; Gao, Selmer *et al.* 2009) as well as Tet(O) in complex with the P_i-state ribosome (Spahn, Blaha *et al.* 2001).

Table 6: Comparison of the ribosomal components that interact with the corresponding domains of Tet(O), EF-G and Tet(M). Tet(M) – ribosomal contacts were identified by fitting atomic models from the 30S and 50S ribosomal subunit (PDB2WRJ and PDB2WRJ) into isolated densities from this cryo-EM reconstruction, together with the Tet(M) model and density. The contact(s) of individual domains of Tet(M) are described with the ribosomal subunit (30S and 50S) together with the corresponding structural element (e.g. H95 or S12) and the individual region of Tet(M) contacting the ribosome (e.g. α -helix, β -sheet, loop). The exact interaction site is described according to the *E. faecalis* Tet(M) sequence with the closest contacts highlighted in red. The loop region contacting the Tet1 binding site is shown in blue, probable contacts via the C-terminus in green.

Domain	Tet(O)	EF-G	Tet(M)
G	50S: H95	50S: H95 (SRL)	<u>50S: H95 (SRL)</u> loop K ₁₂₉ LDQNGID ₁₃₆
G'	---	50S: L12 CTD (bridge to L11 NTD)	<u>50S: L12 CTD</u> (bridge to L11 NTD)
II	30S: h5	30S: h5 and h15	<u>30S: h5</u> β -hairpin structure D ₂₇₉ SV ₂₈₁ and I ₂₈₉ KV ₂₉₁
III	30S: S12	50S: H95 (SRL)	<u>30S: S12</u>

III		30S: h5 and S12	α -helix P ₃₅₅ EQREMLLDALLEISDS ₃₇₁ loop D ₃₈₀ STTHE ₃₈₅ <u>50S: H95 (SRL)</u>
IV	30S: h18/34	<u>30S decoding center:</u> contacts to P-site tRNA and mRNA interaction via two loops: - loop I (496 to 509) K ₄₉₆ FIRQTGGRGQYGH ₅₀₉ - loop II (570 to 577) G ₅₇₀ SYHEVDS ₅₇₇ contacts to h35 and h44	<u>30S: h18</u> α -helix P ₅₁₃ ADFRMLAPIVLEQVLKKA ₅₃₁ <u>30S: h34</u> loop S ₄₆₃ VSLGYLN ₄₇₀ <u>contact to C-terminal α-helix:</u> loop I V ₄₃₆ PPNPV ₄₄₁ <u>contact to Tet1/ clash with Tgc:</u> loop II Y ₅₀₆ YSPVST ₅₁₂
V	50S: H43/44	50S: H95 (SRL) 50S: L11-binding region (H43/44) 50S: H89	<u>50S: H43/44</u> α -helix Q ₅₄₈ EYLSRAYNDAPKY ₅₆₁ <u>50S: L11 NTD</u> first strand of a β -hairpin T ₅₆₈ QLK ₅₇₁
C-term	---	---	<u>50S: H89</u> α -helix R ₆₂₇ IDKVR YM FNK ₆₃₇ <u>50S: H69</u> α -helix R ₆₂₇ IDKVR YM FNK ₆₃₇ <u>30S: h44</u> α -helix R ₆₂₇ IDKVR YM FNK ₆₃₇

The interaction sites visualized for Tet(O) with ribosomal components in a previous cryo-EM study (Spahn, Blaha *et al.* 2001) were in agreement with those described here for Tet(M). In addition, the higher resolution enabled a more precise description of the contacts including the observation of novel contacts between the ribosome and Tet(M). Overall, the sites of contact are remarkably similar to the interaction sites that have been identified for EF-G (Connell, Takemoto *et al.* 2007; Gao, Selmer *et al.* 2009): The G-domain and domain III of Tet(M) contact and surround the sarcin-ricin loop of 23S rRNA (H95), which is the closest ribosomal component to the nucleotide binding site of Tet(M) (**Figure 36B**). Domain II interacts with h5 of the 16S rRNA via a β -hairpin structure (**Figure 34B**). Domain III, which is involved in GTP hydrolysis (Martemyanov and Gudkov 2000), contacts the 30S subunit by interacting with r-protein S12 via the start of an α -helix, precisely P355, and a following loop region (D₃₈₀STTHE₃₈₅) as well as H95 of the 23S rRNA (**Figure 34B** and **36B**). By contacting

both ribosomal subunits, domain III of Tet(M) might be involved in triggering GTP hydrolysis, similar to previous suggestions for EF-G and EF-Tu (Gao, Selmer *et al.* 2009; Schmeing, Voorhees *et al.* 2009). Domain V interacts with the 50S subunit, in particular with the L11 binding region (H43/44 of the 23S rRNA) and the N-terminal domain of L11 (**Figure 37A**). The major difference in the interactions of Tet(M) and EF-G with the ribosome are related to domain IV (**Figure 34** and **35**). Here, Tet(M) domain IV contacts a region located between the head and the shoulder of the 30S subunit, partially consisting of helices 18 and 34 (Wimberly, Brodersen *et al.* 2000) (**Figure 34**, h34 and h18 are shown in green and cyan, respectively). Domain IV of EF-G is mainly involved in translocation and the tip of domain IV overlaps more significantly with the position of A-site bound tRNA in comparison to Tet(M). Moreover, domain IV of EF-G interacts with both h35 in the head of the 30S subunit and h44 at the decoding center as well as contacts the bridge B2a region of the 50S subunit, which is formed partially by H69 of the 23S rRNA (Cate, Yusupov *et al.* 1999; Gao, Selmer *et al.* 2009) (**Figure 35**). Domain IV contains two conserved loop regions in EF-G (loop I (K₄₉₆FIRQTGGRGQYGH₅₀₉) and loop II (G₅₇₀SYHEVDS₅₇₇)), which mutational analysis have shown to be essential for the translocation event (Martemyanov, Yarunin *et al.* 1998; Savelsbergh, Matassova *et al.* 2000). Domain IV of EF-G contacts h44 (via loop I), in particular the conserved bases G530, A1492 and A1493, that are involved in cognate tRNA binding at the decoding center (Ogle, Brodersen *et al.* 2001), suggesting a displacement of these bases and therefore allowing translocation (Ogle, Brodersen *et al.* 2001). In contrast, the corresponding loops in Tet(M) domain IV do not show any sequence conservation to EF-G (loop I (V₄₃₆PPNPV₄₄₁) and loop II (Y₅₀₆YSPVST₅₁₂)). In Tet(M), loop I seems to make contact with the C-terminal α -helix of domain V (**Figure 38**) and loop II interacts directly with the tetracycline binding site (**Figure 39** and **40A**), illustrating the different roles of these proteins. Regarding domain V, it seems that the C-terminus of Tet(M), which forms a helical structure according to secondary structure predictions and the presence of strong extra density in the volume map, interacts with h44 with the proximal part of the α -helix whereas the distal part contacts H69 and H89 of the 23S rRNA (**Figure 38**). As shown in **Figure 37**, Tet(M) contacts both the L11 region and the CTD of L12, similar to previous EF-G studies (Datta, Sharma *et al.* 2005; Gao, Selmer *et al.* 2009) (**Figure 37A** and **37B**). Moreover, an interaction of domain V of Tet(M) with the NTD of L11 via the first strand of a β -hairpin could be visualized (**Figure 37A**).

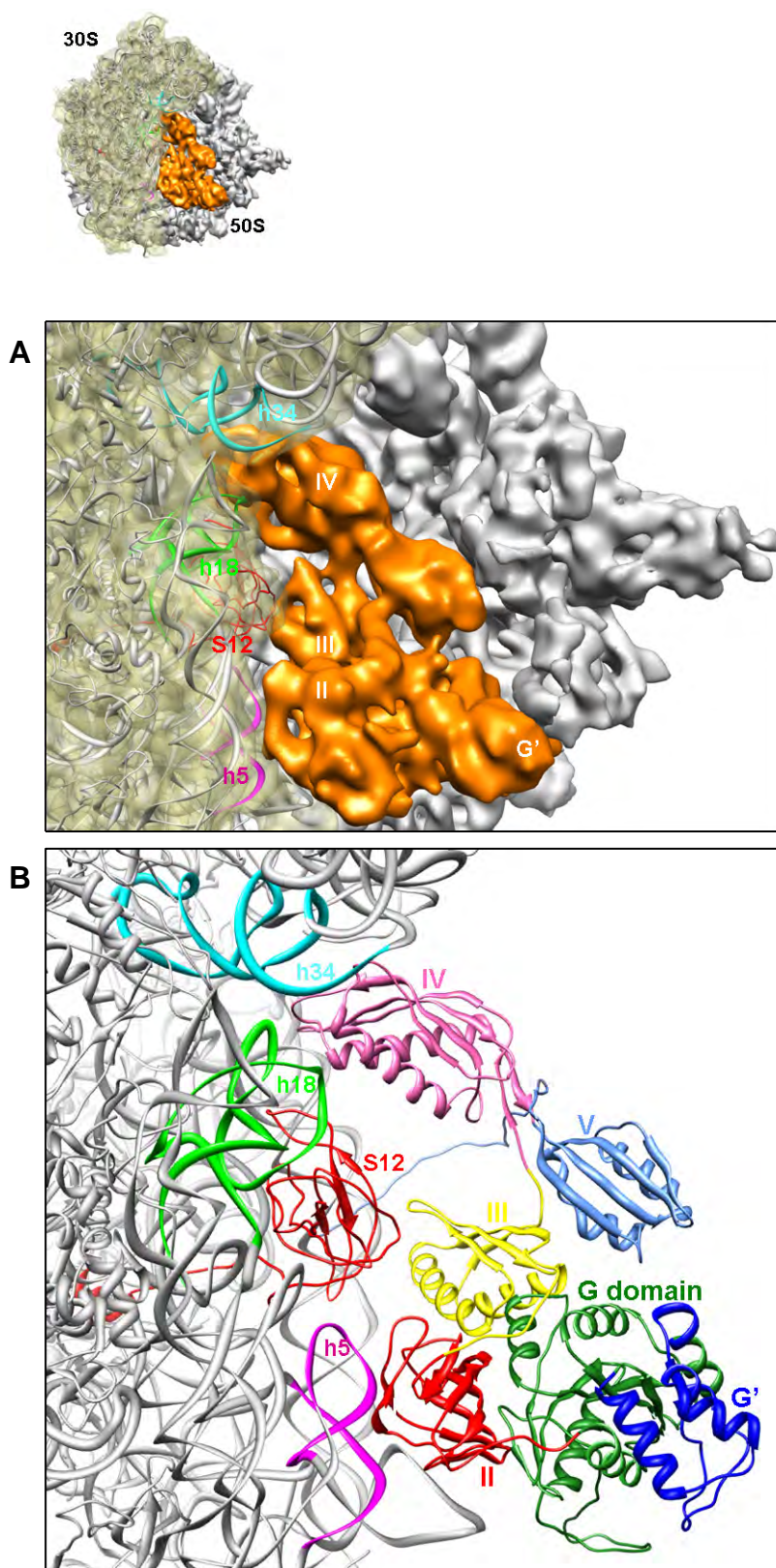


Figure 34: Contacts between the 30S ribosomal subunit and Tet(M). (A) and (B) present a close-up of the overview shown on top. (A) The *E. coli* 30S subunit is shown in transparent yellow, fitted with PDB2WRI. The 50S subunit and density for Tet(M) are shown in grey and orange, respectively, with various domains of Tet(M) indicated. 30S contact sites are highlighted in pink (h5), red (S12), green (h18) and cyan (h34). (B) Contact sites represented without the densities for the 30S subunit and Tet(M).

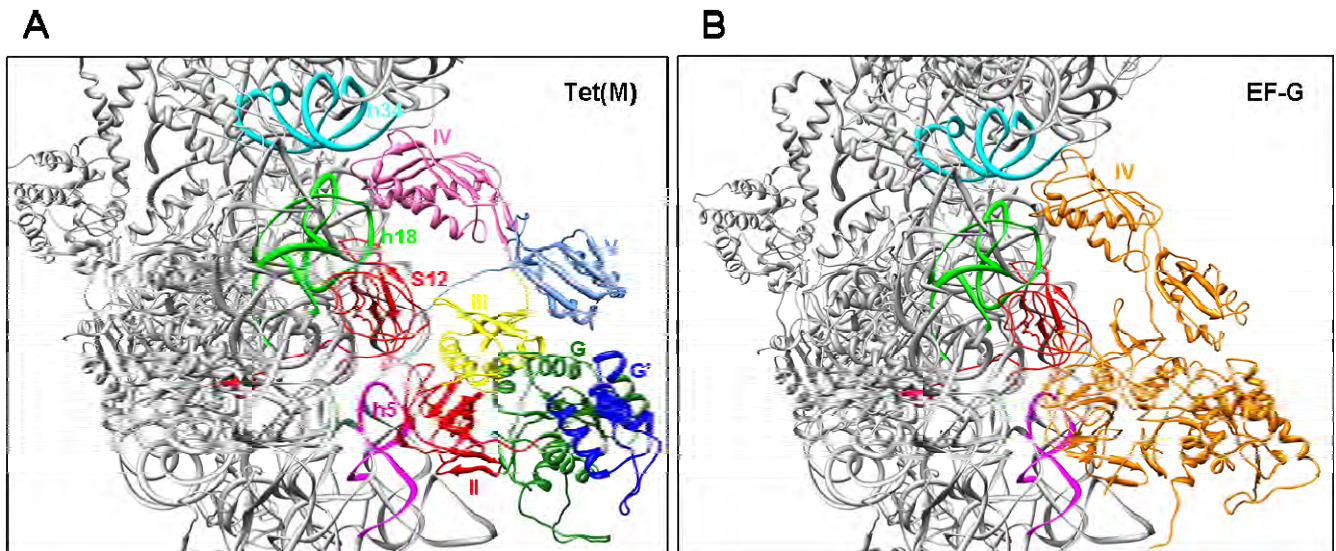


Figure 35: Comparison of domain IV of Tet(M) and EF-G contacting the 30S subunit. (A) The figure is similar to Figure 34B with domain VI of Tet(M) highlighted in pink. (B) Contact sites between EF-G and the 30S ribosomal subunit (PDB2WRI). Colors are identical to (A), with EF-G presented in orange. Ribosomal components are highlighted in cyan (h34), green (h18), red (r-protein S12) and pink (h5).

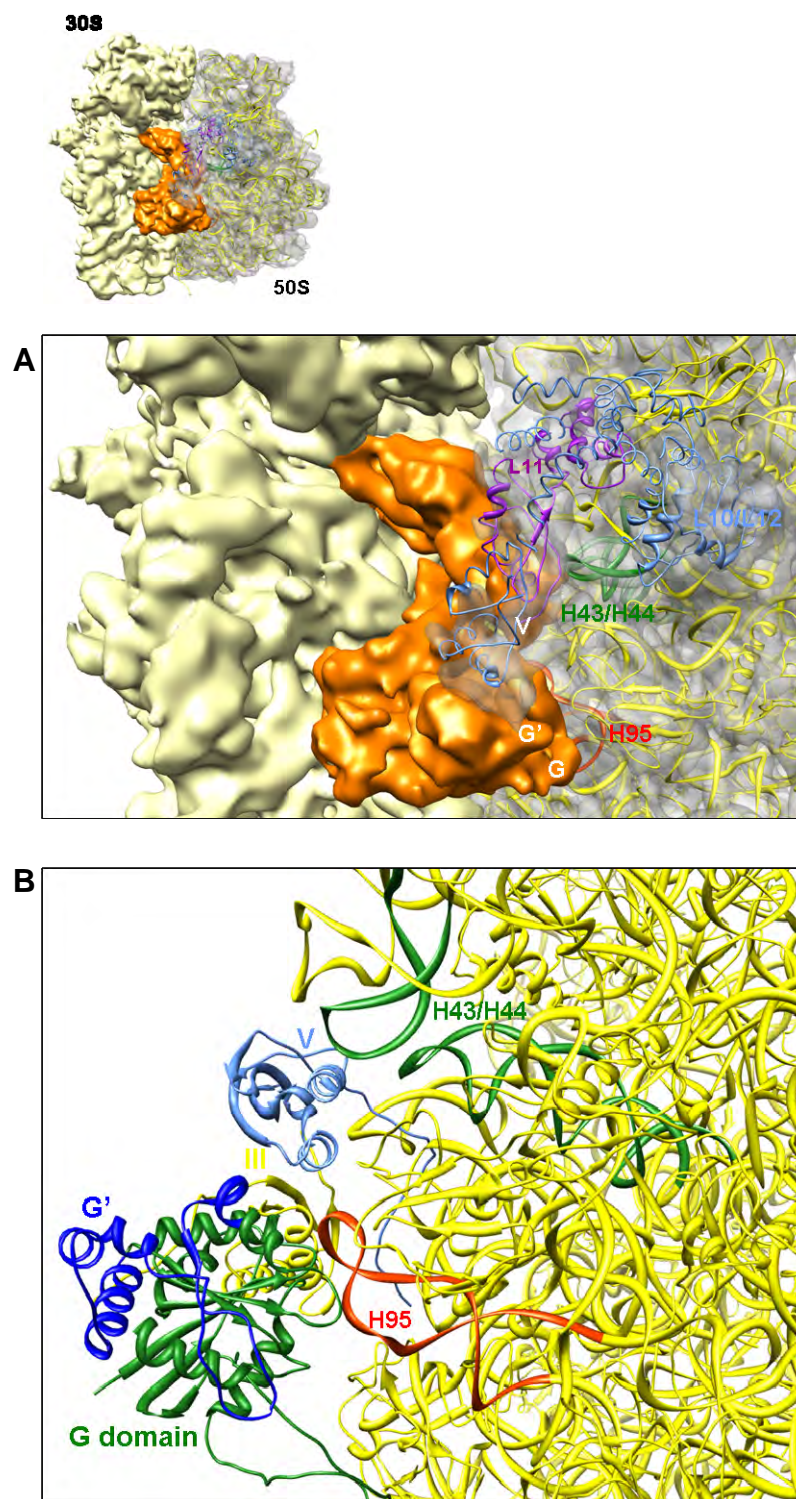


Figure 36: Contacts between the 50S ribosomal subunit and Tet(M). (A) and (B) present a close-up of the overview shown on top. (A) The *E. coli* 50S subunit is shown in transparent grey, fitted with PDB2WRJ. The 30S subunit and density for Tet(M) are shown in yellow and orange, respectively, with various domains of Tet(M) indicated. 50S contact sites are highlighted in red (H95) and green (H43/H44). (B) Contact sites represented without the densities for the 50S subunit and Tet(M).

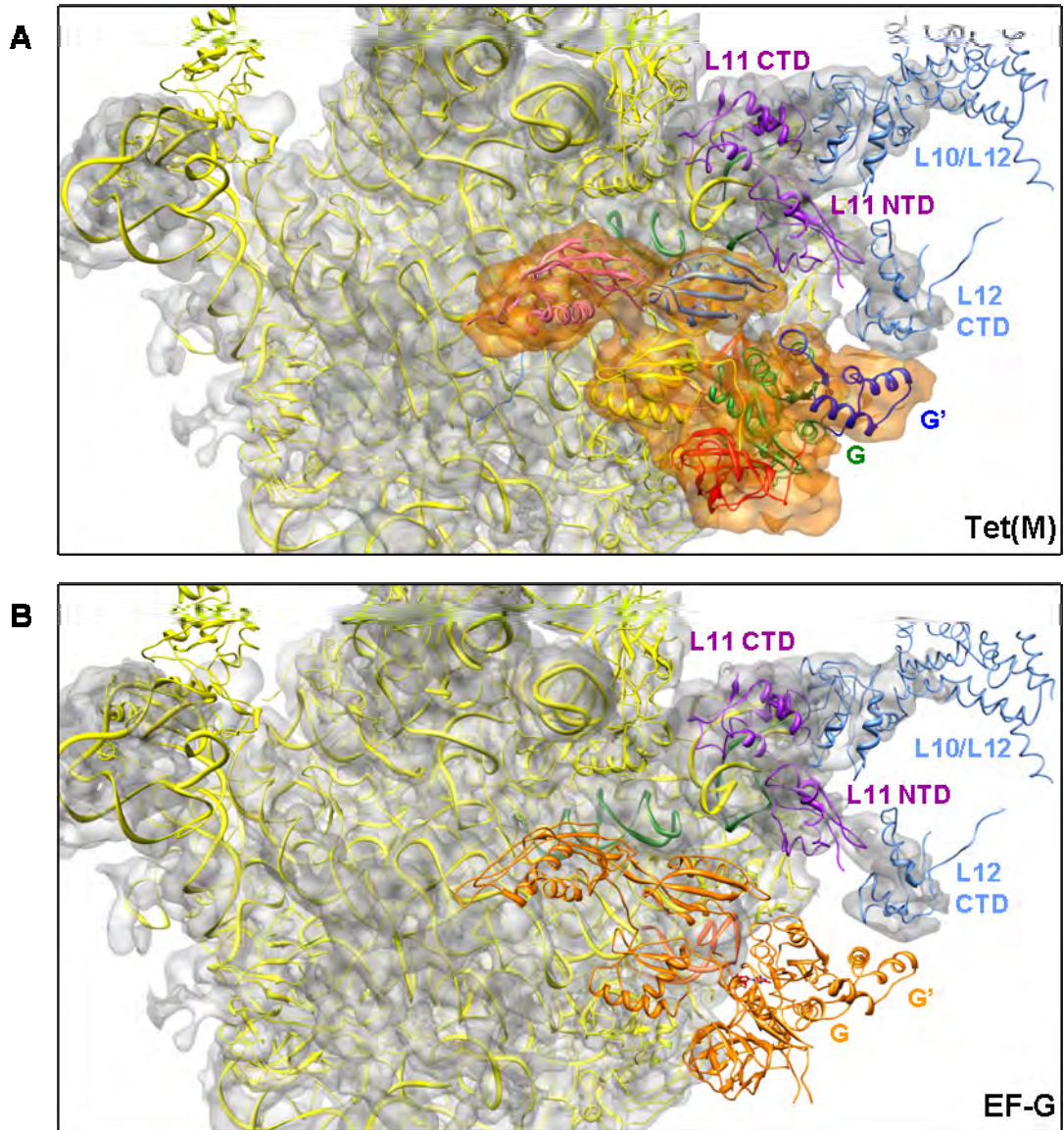


Figure 37: Comparison of the G' sub-domain of Tet(M) and EF-G contacting the C-terminal domain of L12. (A) The densities for the 50S subunit and Tet(M) are shown in transparent grey and orange, respectively. PDB2WRJ is fitted into the 50S density, contact sites highlighted in light blue (L12 CTD) and purple (L11 NTD). (B) Contact sites between EF-G and the 50S ribosomal subunit (PDB2WRJ).

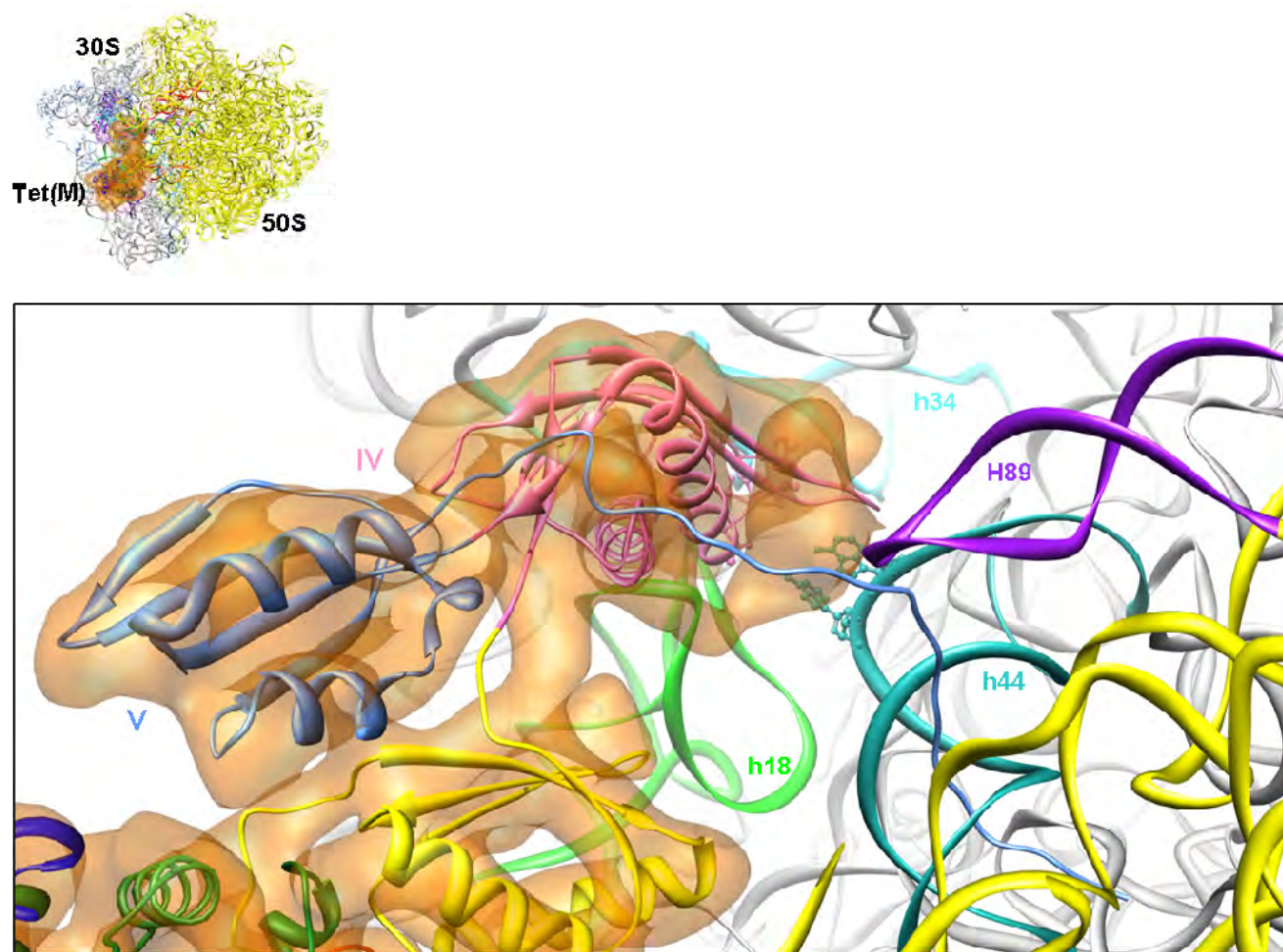


Figure 38: Contacts between the C-terminus of Tet(M) and structural elements of the small and the large ribosomal subunit. The figure presents a close-up of the overview shown on top. Tet(M) density is shown in transparent orange, fitted with the model (domain VI is shown in pink, domain V in light blue). The 30S subunit is presented in grey, with h44 highlighted in turquoise and A1492/A1493 shown in ball and stick representation. The 50S subunit is presented in yellow, with H89 shown in purple.

Tgc is a third-generation tetracycline derivative and was included in complex formation for this cryo-EM reconstruction. The compound is highly similar to the chemical structure of Tet, with the exception of two alterations at the C7 and C9 position of ring D (**Figure 25C** and **25D**). Therefore, the structure of the 30S subunit crystallized with Tet (PDB1HNW) was used as a reference model to demonstrate the distance of Tet(M), in particular domain IV, to the primary binding site for tetracycline (Tet1), in comparison to EF-G (**Figure 40A-C**). As seen in **Figure 40A**, Tet1 is presented as a ball-and-stick model. The Tet1 binding site is mainly built up of the sugar-phosphate backbone of helix 34 (**Figure 40**, highlighted in cyan), together

with parts of helix 31. Loop II of Tet(M) domain IV (Y₅₀₆YSPVST₅₁₂) is in very close proximity to Tet1, and overlaps with ring D of Tet (**Figure 39 and 40A**). In comparison, domain IV of EF-G is located slightly different (**Figure 40B**), which is also demonstrated in an overlay of Tet(M) and EF-G domain IV with Tet1 (**Figure 40C**). In contrast, replacing the chemical structure of Tet with Tgc produces an even larger steric clash between the side chains of loop II of Tet(M) domain IV and the additional substitution at position C9 of Tgc (**Figure 40D**). This would explain why Tet(M) and Tgc could not be visualized in the same sub-dataset of this cryo-EM reconstruction.

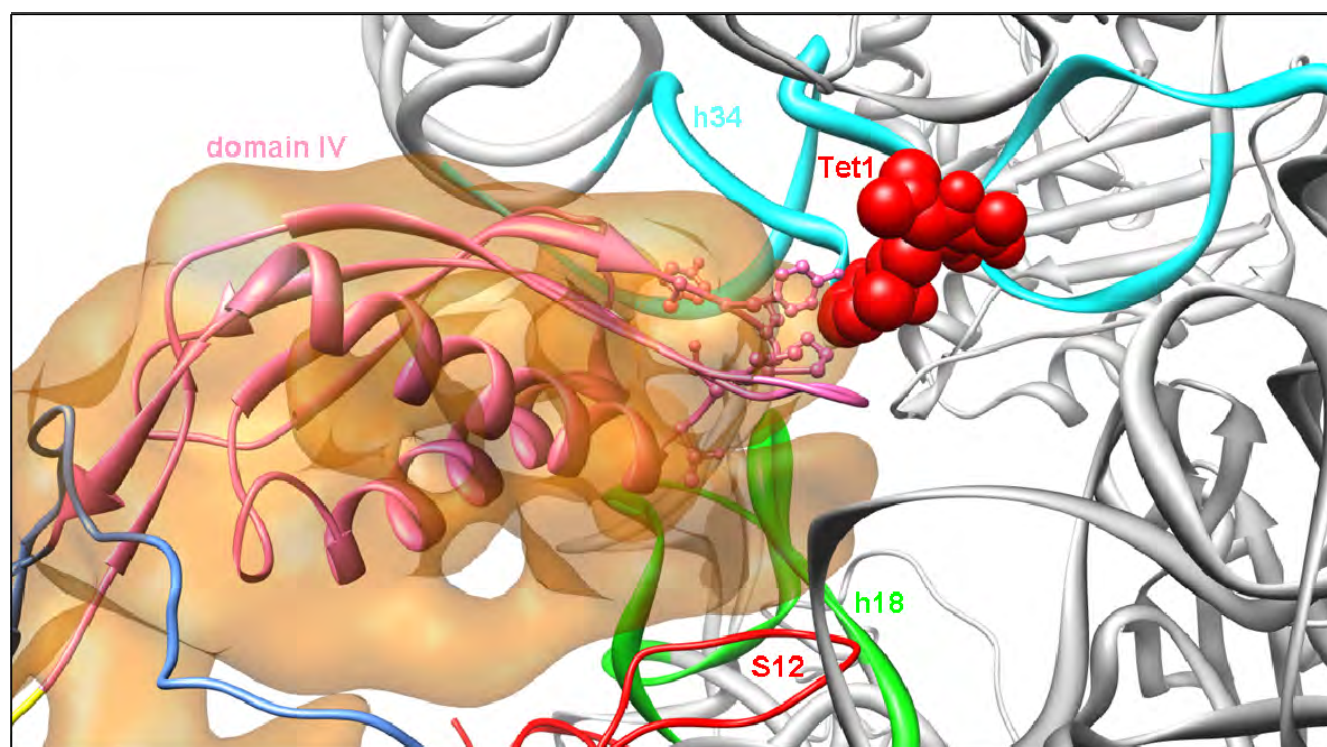


Figure 39: Contact of Tet(M) domain IV to the Tet1 binding site on the 30S subunit. The 30S subunit (PDB1HNW) is shown with the primary binding site for tetracycline (Tet1, shown using red spheres), with the contact sites of Tet(M) (the isolated density of Tet(M) is shown in transparent orange) highlighted in cyan (h34), green (h18) and red (r-protein S12). Domain IV of Tet(M) (highlighted in pink) contacts Tet1 via a direct interaction.

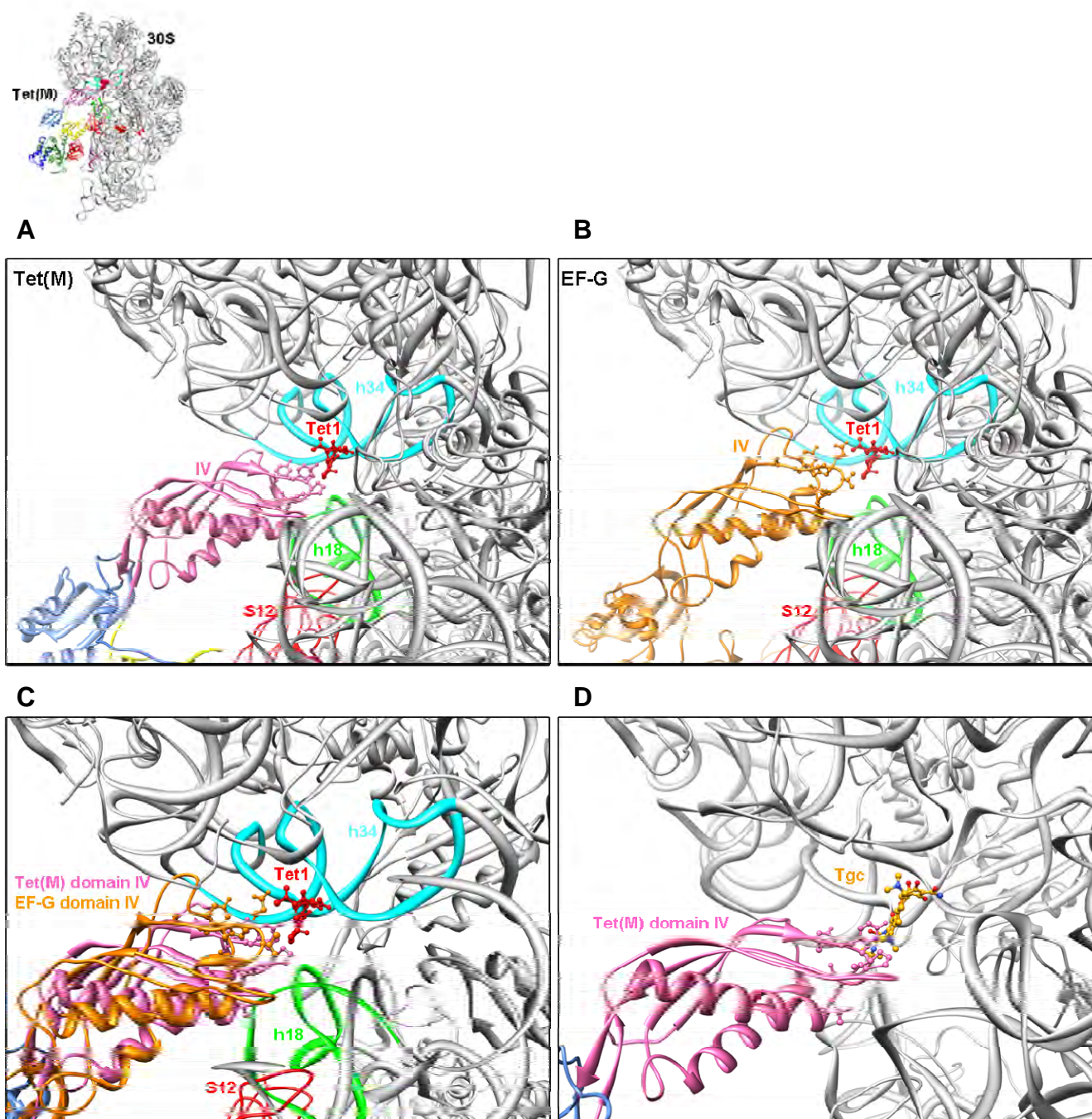


Figure 40: Contact of Tet(M) to the Tet1 binding site on the 30S subunit – occupied with Tet or Tgc - in comparison to EF-G. (A) to (D) present a close-up of the overview shown on the top. The 30S subunit (PDB1HNW) is shown with the primary binding site for tetracycline (Tet1), with the contact sites of Tet(M) highlighted in cyan (h34), green (h18) and red (r-protein S12). Tet1 and Tgc are shown using a ball-and-stick representation. (A) Domain IV of Tet(M) (highlighted in pink) contacting Tet1 via a direct interaction. (B) In comparison, domain IV of EF-G (shown in orange) does not reach as far as Tet(M) into the Tet1 binding site. (C) Overlay of Tet(M) and EF-G domain IV demonstrating the distance to Tet1. (D) Domain IV of Tet(M) clashes with Tgc due to a substitution at the C9 position of the compound.


```

gi|81251419|TetM_ENTFA -----MKIINIGVLAHVVDAGKTTLTESLLYNSGAITELGVSVDRTGT 41
gi|6094461|Tets_LACLL ----MEEIKLKIINIGILAHVDAGKTTLTESLLYSSGRIKELGVSVDSTGT 46
gi|32189795|TetO_CAMJE -----MKIINIGILAHVDAGKTTLTESLLYTSGAIALGVSVDDEGT 41
gi|58326|TetQ_BACTHE -----MNIINLGILAHVDAGKTSVTENLLFASGATEKCGCVDNGDT 41
gi|6094458|TETP_CLOPE -----MKKIINIGIVAHVDAGKTTITENLLYYSGAIKSVGRVDLGNT 42
gi|47473|OtrA_STRRI -----MNKLNLGILAHVDAGKTSLTERLLHRTGVIDEVGSVDAGTT 41
gi|119190|EFG_THTHE MAVKVEYDLKRLRNIGIAAHIDAGKTTTTERILYYTGRIHKIGEVHEGAA 50
      . *: *: **:*****: *: *: . *: . *: *: *:

gi|81251419|TetM_ENTFA KTDNTLLERQRGITITQTAITSFQWKNTKINIIDTPGHMDFLAEVYRSLSV 91
gi|6094461|Tets_LACLL KTDTMFLERQRGITITQTAITSFQRENKVNIVDTPGHMDFLADVYRSLSV 96
gi|32189795|TetO_CAMJE RTDTMNLERQRGITITQTAITSFQWEDVKVNIIDTPGHMDFLAEVYRSLSV 91
gi|58326|TetQ_BACTHE ITDSMDIEKRKGITVRASTTSIIWNGVKCNIIDTPGHMDFIAEVERTFKM 91
gi|6094458|TETP_CLOPE QTDSMELERKRGITIKSSTISFNWNNVKVNIIDTPGHVDFISEVERSLNS 92
gi|47473|OtrA_STRRI TTDSMELERQRGITIRSAVATFVLDLKVNLIDTPGHSDFISEVERALGV 91
gi|119190|EFG_THTHE TMDFMEQERERGITITAAVTTCFWKDHRIINIDTPGHVDFITIEVERSMRV 100
      * *:*****: :: : .. : *:***** *: *: *:

gi|81251419|TetM_ENTFA LDGAILLISAKDGVQAQTRILFHALRKIGIPTIFFINKIDQNGIDLSTVY 141
gi|6094461|Tets_LACLL LDGAILLISAKDGVQSQTTRILFHALRKMNIPITIFFINKIDQNGINLPDVY 146
gi|32189795|TetO_CAMJE LDGAVLLVSAKDGIQAQTRILFHALQIMKIPTIFFINKIDQEGIDLPVMY 141
gi|58326|TetQ_BACTHE LDGAVLILSAKEGIQAQTKLLFNTLQKLQIPTITIFFINKIDRAGVNLRLY 141
gi|6094458|TETP_CLOPE LDGAILVISGVEGQSQTTRILFDLTKELNIPITIFFVNLKLDRIAGFNKVF 142
gi|47473|OtrA_STRRI LDGAVLVVSAVEGVQPTTRILMRTLRLGIPTLVFVNKIDRGGARPDGV 141
gi|119190|EFG_THTHE LDGAVLVVSSQGVFPQSETVWRQAKEYKVPRIAFANKMDKTGADLWIVI 150
      *****:..... :*::*::: . :*: * **:*: * :

gi|81251419|TetM_ENTFA QDIKEKLSAEIVIKQKVELH-----PNMRVMNFT----- 170
gi|6094461|Tets_LACLL QDIKDKLSDDIIKQTVNLN-----LKPVIDYT----- 175
gi|32189795|TetO_CAMJE REMKAKLSSEIIVKQKVGQH-----PHINVTND----- 170
gi|58326|TetQ_BACTHE LDIKANLSQDVLFMQNVVDG-----SVYPVCSQTY----- 171
gi|6094458|TETP_CLOPE EEIKKNMSNKVVRLQEVYDVGSKAVYIKKLFDTCI----- 177
gi|47473|OtrA_STRRI REIRDRLTPAAVALSAVADAGTPPARAIALGPDTP----- 177
gi|119190|EFG_THTHE RTMQERLGARPVVMQLPIGREDTFSGIIDVLRMKAYTYGNDLGTDIRIIP 200
      :: :: : . :

gi|81251419|TetM_ENTFA -----ESEQWDMVIEGNDYLLKEYTSGK-LLEALELEQEEISIR 207
gi|6094461|Tets_LACLL -----EPEQWETVIVGNDYLLKEYTIGK-TLNIAELEKEENER 212
gi|32189795|TetO_CAMJE -----DMEQWDAVIMGNDELLEKYMVGK-PFKMSELEQENNR 207
gi|58326|TetQ_BACTHE -----IKEFYKEFVCNHDNILERYLADS-EISPADYWNTHIAL 209
gi|6094458|TETP_CLOPE -----INDDAINVLSDLEAFLEFYIGGI-EPDKKEIQEKLSLY 215
gi|47473|OtrA_STRRI -----DFAIVGVELLADHDAFLTAYLDEEHVLTKEKYAEELAAQ 217
gi|119190|EFG_THTHE IPPEEYLDQAREYHEKLVVAADFENIMLKYLEGE-EPTEEELVAAIRKG 249
      : :: :: * :

gi|81251419|TetM_ENTFA FHNCSLFPVYHGSANKNIGIDNLEIVITNKFY----- 240
gi|6094461|Tets_LACLL IQSCSLYPVYHGSANKNIGIKQLIEVITSKLFS----- 245
gi|32189795|TetO_CAMJE FQNGTLFPVYHGSANKNLTGRQLIEVIASKFY----- 240
gi|58326|TetQ_BACTHE VAKAKVYPVLHGSAMFNIGINELDAITSFILP----- 242
gi|6094458|TETP_CLOPE AREGSLYPVFCGAAAGLGIEDLLDGICSYFPF----- 248
gi|47473|OtrA_STRRI TARGLVHPVYFGSALTGEGLDHLVHGIRELLPS----- 250
gi|119190|EFG_THTHE TIDLKIPVFLGSAKKNKGVLQLLDVAVDYLPSPLDIPPIKGTTPGEVV 299
      : ** *: * * *: . *: . :

gi|81251419|TetM_ENTFA -STHRGQSELCKGVFKIEYSEKRRQLAYIRLYSGVLHLRDSVRISEKEK- 288
gi|6094461|Tets_LACLL -PTQLNSDKLCGNVFKVEYSDDGQRLVYVRLYSGTLHLRDSVNISEKEK- 293
gi|32189795|TetO_CAMJE -STPEGQSELCKGVFKIEYSEKRRRFVYVRIYSGTLHLRDLVIRISEKEK- 288
gi|58326|TetQ_BACTHE -PASVSN-RLSSYLKIEHDPKGHKRSFLKIIDGSLRLRDVVRINDSEKF 290
gi|6094458|TETP_CLOPE -ASNDCESDLGCVFKIERTSKNEKKVYVRLFGGKISVRDKIQVPNKIEA 297
gi|47473|OtrA_STRRI -VHASQDAPLFRATVFKVDRGARGEAVAYLRLVSGTLGTRDSVTLHRVDHT 299
gi|119190|EFG_THTHE BIHPDPNGPLAALAFKIMADPYVGRLTFFIRVYSGTLTSGSYVNTTKGRK 349
      . * . :*: :::: . * : . :

gi|81251419|TetM_ENTFA -----IKITEMYTSINGELCKIDKAYSGEIVILQN-EFLKLNS-VLGD 329
gi|6094461|Tets_LACLL -----IKVTEMYTSINGELRQIDKAEPGEIILKN-ELLKLNN-VLGD 334
gi|32189795|TetO_CAMJE -----IKITEMYVTNGELYSSDTACSGDIVILPN-DVLQLNS-ILGN 329
gi|58326|TetQ_BACTHE -----IKIKNLKTINQGREINVEVGANDIAIVEDMDDFRIGN-YLGA 332
gi|6094458|TETP_CLOPE -----EKVKKINRLENGGVVEAQRIEAGDIGILYGLTSFQVGD-VIGI 339
gi|47473|OtrA_STRRI GRVTEHAGRITALRVFEHGSATSETRATAGDIAQAWGLKDVVRGD-RAGH 348
gi|119190|EFG_THTHE -----ERVARLLRMHANHREEVEELKAGDLGAVVGLKETITGDTLVGE 392
      :: : . . ::: . . *

gi|81251419|TetM_ENTFA TKLLPQRIENPLPLLQTTVEPSKPQQREMILLALLEISDSDPLLRYV 379
gi|6094461|Tets_LACLL KKRLPHREILENPLPMLQTTIEPCSVQREKLLDALFEISDSDPLLQYV 384
gi|32189795|TetO_CAMJE EILLPQKRIENPLPMIQTITIAVKKSEQREILLGALTEISDCDPLLKYV 379
gi|58326|TetQ_BACTHE EPCLIQG--LSHQHPALKSSVRPDRPEERSKVISALNTLWIEDPSLSFIS 380
gi|6094458|TETP_CLOPE SNDKIKN--ISIAKPAKTTISADKEKNPELFKALTLLAEEDPLLFAM 387
gi|47473|OtrA_STRRI LDGPPPR--NFFAPPSLETVIRPERPEEAGRLHAALRLDEQDPSIDLRQ 396
gi|119190|EFG_THTHE DAPRVILESIEVPEVIDVAIEPKTKADQEKLSQALARLAEEDPTFRVST 442
      * :: : . : ** : ** :

```

```

gi|81251419|TetM_ENTFA      D-SATHEIILSFLGKQMEVTCALLQEKYHVEIEIKEPTVIYMERPLKKA 428
gi|6094461|TetS_LACLL      D-TVTHEIVLSFLGEVQMEVTCITLIQEKYHIEIETRKPTVIYMERPLKKS 433
gi|32189795|TetO_CAMJE     D-TTTHEIILSFLGNVQMEVICALEEKYHVEAEIKEPTVIYMERPLRKA 428
gi|58326|TetQ_BACTHE       N-SYSDELEISLYGLTQKEIIQTLLERFSVKVHFDEIKTIYKERPVKKV 429
gi|6094458|TetP_CLOPE      N-DIDKEIYVNLFGVQMEILSSMLDDLYGIKVEFSNIETIYKETPKGFG 436
gi|47473|OtrA_STRRI        DEENAGAVVRLYGEVQKEILGSTLAESFGVVRVREDPTRTVCIEKPVGTG 446
gi|119190|EFG_THTHE        H-PETGQTTISGMGELHLEIIVDRLKREFKVDANVGKPKQVAYRETITKPV 491
      .      :      *      :      *      :      :      .      *

gi|81251419|TetM_ENTFA      EYTIHIEVPPN--PFWASIGLSVAPLPL-GSGVQYESSVSLGYLNQSFQN 475
gi|6094461|TetS_LACLL      EFTIDIEVPPN--PFWASIGLSVTPPLPL-GSGIQYESLVSGLGYLNQSFQN 480
gi|32189795|TetO_CAMJE     EYTIHIEVPPN--PFWASVGLSIEPLPI-GSGVQYESRVSLGYLNQSFQN 475
gi|58326|TetQ_BACTHE       NKIIQIEVPPN--PYWATIGLTLEPLPL-GTGLQIESDISYGYLNHNSFQN 476
gi|6094458|TetP_CLOPE      ASIMHMQEDLN--PFWATVGLIEEPAGR-GEGLRYSISNVSVGSLPKSFQN 483
gi|47473|OtrA_STRRI        EALIELDTRTHN-YFWGAPWVCASDRPSPARAITFRLAVALGSLPLAFHK 495
gi|119190|EFG_THTHE        DVEGKFIRQTGGRGQYGHVKIKVEPLPR-GSGFEFVNAIVGGVIPKEYIP 540
      ..      :      :      .      .      :      *      :      :

gi|81251419|TetM_ENTFA      AVMEGIRYGCQGG-LYGWNVTDCKICFKYGLIYSPVSTPADFRMLAP-IV 523
gi|6094461|TetS_LACLL      AVMEGIRYGCQGG-LYGWKLTDCKICFKYGLIYSPVSTPADFRMLAP-IV 528
gi|32189795|TetO_CAMJE     AVMEGVLYGCQGG-LYGWKTDCCKICFEYGLIYSPVSTPADFRLLSP-IV 523
gi|58326|TetQ_BACTHE       AVFEGIRMSCQSG-LHGWEVTDLKVFTTQAEYYSVPVSTPADFRQLTP-YV 524
gi|6094458|TetP_CLOPE      AIEEAVIKTSKQG-LFGWEVTDVKVTLSCGEFFSPASTPADFRNVTP-MV 531
gi|47473|OtrA_STRRI        AIEETVHTTTLRHG-LYGWQVTDCAVTLTRTGVRSPVSAADDFRKANARLV 544
gi|119190|EFG_THTHE        AVQKGIEEAMQSGPLIGFPVVDIKVTLYDGSYHEVDSEMAFKIAGS-MA 589
      * : : : . * * * : . * : : . * : * : . .

gi|81251419|TetM_ENTFA      LEQVLKKAGTELLEPYLSFKIYAPQEYLSRAYNDAPKYCANIVDTQLKNN 573
gi|6094461|TetS_LACLL      LEQAFRKSGTELLEPYLSFEIYVPQEYLSRAYNDASKYCANILNTKLKGN 578
gi|32189795|TetO_CAMJE     LEQALKKAGTELLEPYLHFEIYAPQEYLSRAYHDAPRYCADIVSTQIKND 573
gi|58326|TetQ_BACTHE       FRLALQQSGVDILEPMLYFELQIPQAASSKAITDLQKMMSEIEDISCNNE 574
gi|6094458|TetP_CLOPE      FMEALYKAQTVLLEPLHEFELKIPQNALSKAVWDLTMRATFDNPIVIGD 581
gi|47473|OtrA_STRRI        LMDALGRAGTEVHPEVSSFELEVPAARLSPVLAKLAELGATPGVPTAEGD 594
gi|119190|EFG_THTHE        IKEAVQKGDVPVILEPIMRVEVTTPEEYMGDVGIDLNARRGQILGMEPRGN 639
      : . . : . : ** . : : * . . . . . : :

gi|81251419|TetM_ENTFA      EVILSGEIPARCIQEYRSDLTFFTNGRSVCLTELKGYHVTGTEP-VCQPR 622
gi|6094461|TetS_LACLL      EVILIGEIPARCIQEYRNSLTFFTNGRSVCLTELKGYQVTNIKS-AFQPR 627
gi|32189795|TetO_CAMJE     EVILKGEIPARCIQEYRNDLTFTNGQGVCLTELKGYQPAIGKF-ICQPR 622
gi|58326|TetQ_BACTHE       WCHIKGKVPLNTSKDYASEVSSYTKGLGIFMVKPCGYQITKGGY-SDNIR 623
gi|6094458|TetP_CLOPE      EFSIKGLIPVENSKEYKMKIASYTEGRGMFVTKFYGYKEASAEFSKARKK 631
gi|47473|OtrA_STRRI        VFRLEGTMPSTSLVHDFNQRPVPLTQGEVFLAEHRGYPVAVGQPPVPRP 644
gi|119190|EFG_THTHE        AQVIRAFVPLAEMFGYATDLRSKTQGRGSFVMFFDHYQEVKQVQEKLIK 689
      : . : * : : : * . : : * : .

gi|81251419|TetM_ENTFA      RPNSRIDKVRVMFNKIT---- 639
gi|6094461|TetS_LACLL      RPNNRIDKVRHMFNKNLH-- 646
gi|32189795|TetO_CAMJE     RPNSRIDKVRHMFHKLKLA---- 639
gi|58326|TetQ_BACTHE       --MNEKDKLLFMFQKSMSSK- 641
gi|6094458|TetP_CLOPE      TTYDPLNKKEYLLHKLNAIRD 652
gi|47473|OtrA_STRRI        EGPNPLNRDEYILHVLKRV-- 663
gi|119190|EFG_THTHE        GQ----- 691

```

Figure 41: Amino acid sequence alignment of various Tet proteins and EF-G. Each line represents a gap inserted because of dissimilarities in the alignment. The alignment includes sequences from *Enterococcus faecalis* Tet(M), *Lactococcus lactis* subsp. *lactis* Tet(S), *Campylobacter jejuni* Tet(O), *Bacteroides thetaiotaomicron* Tet(Q), *Clostridium perfringens* Tet(P), *Streptomyces rimosus* OtrA and *Thermus thermophilus* EF-G. The alignment was generated using ClustalW2. The symbols below the alignment represent 100% conservation indicated by an asterisk with decreasing conservation, symbolized by two dots, one dot and an open space for no conservation. The sequences highlighted in yellow refer to the first and second functional loop regions of domain IV of Tet(M) as well as the C-terminal region that forms a helical structure according to secondary structure predictions.

6.4 Conclusions and Outlook

For this project, *E. faecalis* Tet(M) protein was successfully purified and a complex was assembled *in vitro* consisting of *E. coli* 70S ribosomes, Tet(M) protein, GDPNP and Tgc. Two high-resolution datasets were collected on the Titan Krios TEM (200kV), processed separately according to standard protocols and joined after optimization of both datasets. The final volume map showed strong extra density for Tet(M) (**Figure 30**) with an estimated resolution of 8.1 Å (**Figure 29**). Due to the usage of empty 70S ribosomes for complex formation, different sorting strategies had to be applied to separate various sub-populations of ribosomes from Tet(M)-bound 70S particles, such as a sub-dataset in an un-rotated and a rotated conformation without Tet(M) bound to it (**Figure 28** and **Figure 31**). Tet(M) was found exclusively bound to non-rotated ribosomes, which is in agreement to earlier studies on Tet(O) (Spahn, Blaha *et al.* 2001). Indeed, in the cell, Tet(M) would be expected to bind to POST state ribosomes harboring tRNAs in the P- and E-site accompanied by an empty A-site due to the presence of Tet (Connell, Trieber *et al.* 2003). One approach for the future to reduce heterogeneity and obtain higher resolution would be to use ribosome-nascent chain complexes (RNCs), since RNCs adopt preferentially a non-ratcheted state that appears to be favored by Tet(M).

Since no crystal structures of Tet(M) are available, neither bound to the ribosome nor in solution, a homology model was created for Tet(M) based on high sequence similarities to EF-G (**Figure 33A** and **41**). The homology model could be nicely fitted into the isolated Tet(M) density from the cryo-EM reconstruction (**Figure 33B** and **33C**). The interaction sites between Tet(M) and the ribosome are remarkably similar to the contacts found for EF-G bound to the ribosome in a POST-state, probably due to the before mentioned high sequence similarities and near identical domain organization. However, the conformation of EF-G in solution (in the presence or absence of GDP) (Aevarsson, Brazhnikov *et al.* 1994; Czworkowski, Wang *et al.* 1994) is rather different to the bound form, resulting from conformational alterations in domain IV, but also in domain III and V, relative to the G domain (Hansson, Singh *et al.* 2005). Moreover, the contact sites with the ribosomal subunits described previously for Tet(O) could also be confirmed and visualized for Tet(M) in more detail in this study (**Table 6**, **Figure 34 - 38**), including the revealing of novel interaction sites between the ribosome and the Tet(M) G' sub-domain (**Figure 37**), domain V (**Figure 38**) and domain IV (**Figure 35**, **39** and **40**).

The G' sub-domain of Tet(M) interacts directly with a copy of the C-terminal domain (CTD) of L12 via two α -helices (D₁₇₆TVIEG₁₈₁ and D₁₈₃DLLEKYMS₁₉₁) (**Figure 37A**). In comparison, a similar mode of interaction has been shown for EF-G in previous studies (Datta, Sharma *et al.* 2005; Gao, Selmer *et al.* 2009) (**Figure 37B**). The EF-G G' sub-domain also contacts r-protein L7/L12 via two helical structures (E₂₀₄YLDQAREYHEKLVEVAADF₂₂₃ and E₂₂₅NIMLKYLE₂₃₃), however, the interaction sites between the G' sub-domain of EF-G and Tet(M) to L7/L12 do not share a similar sequence do not seem to have a significant sequence conservation. This interaction site was shown to be highly important, since ribosomes lacking the CTD of L12 show an approximately 90% inhibition on the GTP hydrolysis reaction of EF-G and EF-Tu under multiple turnover conditions (Mohr, Wintermeyer *et al.* 2002; Diaconu, Kothe *et al.* 2005). In addition, mutations in the CTD of L7/L12 affect the release of inorganic phosphate (P_i) from ribosome-bound EF-G·GDP·P_i complexes (Savelsbergh, Mohr *et al.* 2005). Similar experiments could be performed with Tet(M) to identify whether the Tet(M) G' sub-domain has a function analogous to the EF-G G' sub-domain. Mutational studies within the *E. coli* EF-G G' sub-domain revealed two well conserved glutamic acid residues that cause large defects in EF-G-dependent GTP hydrolysis and minor defects in translocation when substituted to lysine (E224K and E228K, according to *E. coli* numbering) (Nechifor, Murataliev *et al.* 2007). In *E. faecalis* Tet(M), these residues correspond to D₁₇₅ and E₁₈₀, respectively, and therefore seem to be conserved. In the future, mutational studies on these two residues should also be performed to investigate the involvement of these residues in the GTPase activation or P_i release activities of the factor.

Another novel interaction site between Tet(M) and the ribosome could be visualized for the C-terminal end of Tet(M), which is not predicted to form any secondary structure according to the homology model (**Figure 33A**). Indeed, the C-terminus of Tet(M) is absent in EF-G but is well conserved between various Tet proteins (**Figure 41**). According to secondary structure predictions, 11 residues of the C-terminal sequence of Tet(M) form an α -helix (**Figure 33D**). Formation of an α -helix is also predicted for the corresponding C-terminal sequences of several other RPPs, with the exception of *Bacteroides thetaiotaomicron* Tet(Q), which shows predictions for both, α -helices and β -strands (**Figure 42**, additional predictions for Tet(Q) are not shown). The observed extra density for the C-terminal α -helix of Tet(M) is sandwiched between loop I at the tip of domain IV and bridge B2a (h44 in the 16S rRNA and

H69 of the 23S rRNA) (**Figure 33B, 33C and 38**). This interaction was not observed in the previous cryo-EM study on Tet(O) (Spahn, Blaha *et al.* 2001), however chemical probing studies using DMS observed an enhancement in accessibility for A1408 located in h44 upon Tet(O) binding (Connell, Trieber *et al.* 2002). A similar effect could be visualized for EF-G and could be explained by the general dynamic nature of h44. Within h44, A1408 is base-paired with A1493 (Fourmy, Recht *et al.* 1996), which, together with A1492, is important for decoding. The function of this C-terminal region is not understood so far and the C-terminus of Tet(M) is located in significant distance to the remaining domain V (**Figure 38**). However, there are similar examples like the Dom34-Hbs1 complex that is involved in a no-go decay mechanism in eukaryotic cells dealing with mRNA quality control. Here, Hbs1 binds to the translation factor binding site together with Dom34, whereas the N-terminal domain (NTD) of Hbs1 is found in significant large distance, near the mRNA entry site of the 40S subunit, where it contacts rpS3 and monitors the presence of the stem-loop in the mRNA of stalled ribosomes (Becker, Armache *et al.* 2011). It might be that the C-terminus of Tet(M) has a similar function to the NTD of Hbs1 by monitoring tetracycline-bound ribosomes in an un-rotated conformation. Therefore, the C-terminal region of domain V should be intensively investigated by mutational studies, for example by deletion of the C-terminal α -helix to elucidate the functional importance of this conserved region. The location of the α -helix in close proximity to h44, including the conserved bases A1492/A1493, is very interesting, since A1492 and A1493 are universally conserved within the decoding center being involved in the cognate codon-anticodon interaction (Yoshizawa, Fourmy *et al.* 1999; Ogle, Brodersen *et al.* 2001). These two bases flip out of h44 to interact with a cognate fit between the mRNA codon and the tRNA anticodon, together with base G530. In contrast, if there is a mismatch in the codon-anticodon interaction, A1492 and A1493 do not participate in that interaction and therefore do not adopt a flipped-out conformation. In this cryo-EM reconstruction, A1492 and A1493 are not completely flipped in and flip out of h44, but rather adapt a half flipped out conformation.

Regarding domain IV of Tet(M), the interaction sites with the ribosome show differences to the contacts of EF-G when bound to the ribosome (Gao, Selmer *et al.* 2009). Tet(M) density is in close proximity to h34, involving an interaction between a loop region of Tet(M) (S₄₆₃VSLGYLN₄₇₀) and the bases G₁₂₀₇CCC₁₂₁₀ of h34 (according to *E. coli* numbering). Studies on Tet(O) showed that C1214, which is located in h34 of the 16S rRNA and is part of the Tet1 binding site, is protected in the presence of the factor using chemical

probing with DMS (Connell, Trieber *et al.* 2002). A superimposition of Tet(M) density with the model and an atomic structure bound with Tet (PDB1HNW) illustrate that Tet(M) density, which can be assigned to side chains of loop II domain IV (Y₅₀₆YSPVST₅₁₂) encroaches directly into the Tet1 binding site and overlaps slightly with the compound, in particular the three side chains of residues Y₅₀₇SP₅₀₉ (**Figure 39** and **40A**). In contrast, the corresponding loop region of EF-G is slightly different in its location (G₅₇₀SYHEVDS₅₇₇) (**Figure 40B**). In a previous study, Tet(O) domain IV was estimated to be located in 6 Å distance to the Tet1 binding site and therefore it was concluded that the distance would be too large for a direct interaction between Tet(O) and Tet (Spahn, Blaha *et al.* 2001). Based on that, it was suggested that Tet is released from the ribosome due to conformational changes within the Tet1 binding site induced by Tet(O) binding (Spahn, Blaha *et al.* 2001). This previous model could not be validated by our study. In contrast, our findings suggest that the mechanism of Tet release from the ribosome by Tet(M) is based on a direct interaction between the RPP and the drug. However, due to limitations in resolution of this reconstruction it cannot be ruled out that the direct interaction of Tet(M) with the ribosome induces indirect conformational changes within the Tet1 binding site (h43 and h31), that in turn leads to release of the drug from the ribosome. Indeed, the hypothesis of a conformational change within the Tet1 binding site and the ribosome would be tempting to prevent the rebinding of the drug. A model for Tet(O)-mediated tetracycline release was suggested before (Spahn, Blaha *et al.* 2001), wherein Tet(O) triggers the release of the bound drug by inducing conformational changes in the Tet1 binding site. Then, the GTPase activity of Tet(O) is stimulated and the factor is released from the ribosome, leaving the Tet1 binding site in a conformation that disfavors rebinding of Tet but allows binding of the ternary complex to restart translation (Connell, Trieber *et al.* 2003). Therefore, in the future, the functional loop II of Tet(M) domain IV should be studied by single amino acid substitution experiments, in particular Y₅₀₇SP₅₀₉, to identify in detail, which residues are involved and functionally important for the release of Tet from the ribosome. A similar approach was performed for EF-G, where substitution of a highly conserved histidine residue (His583) at the tip of domain IV for lysine or arginine led to a dramatic decrease in tRNA translocation ability. In addition, various small deletions in the tip region of domain IV decreased the translocation activity of EF-G even more (Savelsbergh, Matassova *et al.* 2000). His583 in *E. coli* EF-G corresponds to the well conserved Tyr507 in *E. faecalis* Tet(M) (**Figure 41**), which is one out of three residues contacting the tetracycline binding site.

In contrast to Tet, Tgc, which was used in this cryo-EM reconstruction, harbors one long extension at the C9 position of ring D (**Figure 25D**). Here, it could be shown that Tgc prevents the binding of Tet(M) to the ribosome and *vice versa*. The compound Tgc is not visible in the final dataset containing 70S-Tet(M) particles (**Figure 32B**), however, density for the compound is observable in the different sub-datasets during sorting that do not contain Tet(M) (**Figure 32C** and **32D**). Obviously, this does not conform to the *in vitro* binding assay (**Figure 27**) that was performed for complex formation, however, you could argue that the supernatant fraction of the “70S+Tet(M)+Tgc” reaction contains more unbound protein in comparison to the “70S+Tet(M)” reaction in the absence of the compound (**Figure 27**). In conclusion, the pellet fraction of the “70S+Tet(M)+Tgc” reaction might contain a mixture of ribosomes bound exclusively with Tgc or Tet(M), which is in agreement to the sub-datasets derived from sorting (**Figure 32**). Moreover, the replacement of the chemical structure of Tet with Tgc in the model results in a more significant steric clash due to the extended substitution at the C9 position of Tgc (**Figure 40D**). Consistently, Tgc and Tet(M) could not be visualized in the same sub-dataset. Since Tgc has a ten times higher affinity for the ribosome than Tet (Bauer, Berens *et al.* 2004), Tet(M) binding was prevented on Tgc occupied ribosomes explaining the low occupancy of Tet(M) within dataset 1 and 2 (13% in total). These findings are not entirely in agreement to earlier studies on glycylcyclines, where it was shown that Tgc was unaffected by the presence of Tet(M) and Tet(O) (Bergeron, Ammirati *et al.* 1996). Here, it could be shown, that Tet(M) is able to release Tgc from the ribosome, since Tet(M) could be visualized in this cryo-EM reconstruction, but rather in a very inefficient way.

In summary, this study has led to a change in our understanding of the mechanism of Tet(M)-mediated Tet resistance: In the presence of Tet, the ribosome is inhibited in a post-translocational state, since the compound prevents the delivery of the aa-tRNA within the ternary complex and therefore the accommodation of the tRNA into the A-site. Tet(M) binds favorably to un-rotated ribosomes, such as the POST-state, and utilizing residues in the tip of domain IV directly chases Tet from its primary binding site. This process may also induce a conformational change within the tetracycline binding site that prevents rebinding of the drug and, in addition, favors the stable binding of the ternary complex to return the Tet-inhibited ribosome to the actively translating pool.

7 Material and Methods

7.1 Methods in Molecular Biology

7.1.1 Media and Supplements

Luria Broth (LB) and Terrific Broth (TB) liquid media as well as LB Agar plates were prepared according to standard protocols (Sambrook, Fritsch *et al.* 1989). Media was supplemented with the respective antibiotics using stock solutions of ampicillin (100 mg/mL; Roth), kanamycin (50 mg/mL; Roth) and chloramphenicol (34 mg/mL; Roth).

7.1.2 Strains

As a reference and wild-type strain, *E. coli* MC4100 was used. The single gene knock-out strains $\Delta yhhF$ and $\Delta rimM$ were originally derived from Keio collection. $\Delta rlmH$ was also originally derived from Keio collection and then transferred to an *E. coli* MG1655 background. $\Delta rluD$ was generated by Dr. Lauri Peil as described before (Leppik, Peil *et al.* 2007). The $\Delta rlmH/\Delta rluD$ double knock-out strain (*rlmH* and *rluD* are replaced by a kanamycin and chloramphenicol resistance cassette, respectively) was constructed as described before (Ero, Peil *et al.* 2008).

7.1.3 Polymerase Chain Reaction (PCR)

Primers were designed by the program Sci Ed Central (Clone Manager 6, version 6.00) and ordered at Metabion (Munich, Germany). DNA was amplified by Polymerase Chain Reaction (PCR) using Phusion High-Fidelity DNA Polymerase (Finnzymes) according to manufacturer's instructions. In general, 50 μ L reactions were set up consisting of 0.5 μ M forward and reverse primer, respectively (Table 6), 1 ng of template DNA, 1x Phusion HF Buffer (final concentration), 200 μ M of each dNTP and 1 U enzyme. Reactions were conducted using appropriate cycling programs. Samples were analyzed subsequently by

agarose gel electrophoresis and purified using the QIAquick® PCR purification kit (Qiagen) according to the manufacturer's protocol.

Table 7: Name and sequences of used oligonucleotides.

Name	Sequence [5' to 3' direction]
Cloning of pET28-His-TEV-<i>rimM</i> construct	
rimM_s_add_EcoRI	AGCTATAATGAATTCATGAGCAAACAA
rimM_as_add_XhoI	AGCTGTATACTCGAGTTAAAAACCAGG
Cloning of yeast mitochondrial proteins of the large ribosomal subunit	
mrpl3_s_addBamHI	GAGATATTAGGATCCATGGGCATAGTTTTGAAAAGAGCA
mrpl3_as_addSacI	TCGACAATAGAGCTCTTAAACAACAACAGTGCCAGGATC
mrpl17_s_addEcoRI	AGCTATAATGAATTCATGAAGGTAAATTTA
mrpl17_as_addXhoI	AGCTGTATACTCGAGTTAATTATCCGCTAA
mba1_s_addBamHI	AGCTATAATGGATCCATGAGTGTATTAAGA
mba1_as_addSall	AGATGTATAGTCGACTTAGCTTGGAGGTAA
mrpl35_s_addEcoRI	AGCTATAATGAATTCATGTTACGAAGATCT
mrpl35_as_addXhoI	AGCTGTATACTCGAGTTACCTTCTAAC
Cloning of yeast mitochondrial proteins of the small ribosomal subunit	
rsm22_s_addBamHI	AGCTATAATGGATCCATGATGAAAAGATGC
rsm22_as_addXhoI	AGCTGTATACTCGAGTTATTTTCTATTTAC
rsm23_s_addBamHI	AGCTATAATGGATCCATGTACAAGAATATA
rsm23_as_addXhoI	AGCTGTATACTCGAGTTACCTATGGGAAAG
rsm24_s_addEcoRI	AGCTATAATGAATTCATGAAAGTACCATTG
rsm24_as_addXhoI	AGATGTATCCTCGAGTTAAAGAGTGCTCAA
rsm25_s_addSacI	AGATATAATGAGCTCATGAAGATACAAACA
rsm25_as_addHindIII	AGATGTATAAAGCTTTTAGAAGTGGAGGTT
ppe1_s_addEcoRI	AGCTATAATGAATTCATGTCTGACGATTTG
ppe1_as_addXhoI	AGATGTATACTCGAGTTATGTATTTTGCAC

For cloning of the pET28-His-TEV-*rimM* construct, genomic DNA from *E. coli* served as a template. All yeast mitochondrial proteins were cloned from yeast genomic DNA into the

pET28-His-TEV vector. Yeast genomic DNA was generated by the Wizard Genomic DNA Purification Kit (Promega) according to manufacturer's instructions.

7.1.4 Agarose Gel Electrophoresis

Agarose gel electrophoresis was used to separate DNA according to their size and to analyze the purity of PCR products. Gels were made with 1% (w/v) agarose (Invitrogen) in TAE buffer (40 mM Tris/HCl pH 8.0, 20 mM acetic acid, 2 mM EDTA) and run for 30-45 min at 100 V. DNA molecules were stained with SYBR® Green I (for DNA) and visualized at a wavelength of 300 nm with a UV light gel documentation system (INTAS UV system, INTAS). A DNA marker (NEB) was used as molecular weight standard.

7.1.5 Cloning

tet(M) was cloned from *Enterococcus faecalis* genomic DNA into a pET-46 Ek/LIC vector (Novagen) containing an N-terminal cleavable His-tag. The construct was provided by Dr. Aleksandra Mikolajka (Wilson Lab, Munich, Germany).

Several restriction endonucleases (NEB) were used to digest DNA in order to prepare defined ends in both the PCR product and the destination vector. In general, two restriction endonucleases (1-2 U each) were incubated with 1-2 µg of PCR product or vector, respectively, together with the according 10x reaction buffer for 2 hours at 37°C. Reactions were subjected to agarose gel electrophoresis and DNA fragments of interest were cut out from the gel and purified using the QIAquick® gel extraction kit (Qiagen) according to the manufacturer's protocol.

Ligation of digested DNA fragments was performed with T4 DNA Ligase (Fermentas) according to the protocol instructions for 3 hours at 16°C.

For transformation of chemically competent *E. coli* cells (XL1 blue or BL21 (DE3)), 1 µl of plasmid DNA or the ligation reaction was incubated with one aliquot of thawed cells for 30 min on ice. Cells were heat-shocked for 30 sec at 42°C, and then chilled on ice for 2 min. 600-800 µL of LB medium was added, and cells were incubated for 30-45 min at 37°C in a shaking incubator. After short centrifugation, the cell pellet was resuspended in 100 µl LB

medium and plated on LB agar plates (containing the appropriate antibiotic) for overnight growth at 37°C. Plasmid DNA was isolated from a 5 mL overnight culture using the QIAprep® Spin Miniprep Kit (Qiagen). DNA sequencing was performed by Eurofins MWG (Munich, Germany).

7.2 Methods in Biochemistry

7.2.1 Isolation of *E. coli* 70S ribosomes and ribosomal subunits

E. coli strains $\Delta rlmH$, $\Delta rluD$ and $\Delta rlmH/\Delta rluD$ were grown in 2.4 liters of 2xTY (tryptone/yeast) media containing 25 µg/mL kanamycin and 20 µg/mL chloramphenicol. Cells were harvested in mid-log phase and resuspended in Lysis Buffer (20 mM Tris-HCl, pH 7.5, 100 mM NH₄Cl, 10 mM Mg(Ac), 0.5 mM EDTA, 6 mM β-Mercaptoethanol, 20 U/mL DNase I, 2 mg/mL Lysozyme) before ran through a French Press. Cell lysate was cleared by centrifugation and diluted two-fold with TKNM-10 buffer (10 mM Tris-HCl, pH 8.0, 60 mM NH₄Cl, 60 mM KCl, 10 mM Mg(Ac), 6 mM β-Mercaptoethanol). 3500 A₂₆₀ units of cell lysate were layered onto 10 – 35% sucrose density gradients in TKNM-10 buffer (Ti 14, 25.000 rpm, 18.5 h, 4°C). Sucrose density gradients were analyzed by continuous monitoring of absorbance at 254 nm, the 70S fractions were collected and pelleted (Ti 45, 34.000 rpm, 22 h, 4°C). 70S ribosomal pellets were resuspended in TKNM-12 buffer (10 mM Tris-HCl, pH 8.0, 60 mM NH₄Cl, 60 mM KCl, 12 mM Mg(Ac), 6 mM β-Mercaptoethanol), concentrated and stored at -80°C.

In general, cells (WT MC4100, $\Delta rimM$) were grown at 37°C and harvested in mid-log phase (SLC-6000, 5.000 rpm, 15 min, 4°C). Cell pellets were resuspended in 2 volumes of cell buffer (10 mM Hepes-KOH, pH 7.8, 30 mM MgCl₂, 150 mM NH₄Cl) and incubated on ice in the presence of lysozyme (1 µg/mL, Sigma) and DNase I (0.2 µg/mL, RNase free). Cells were lysed by two runs with a Microfluidizer (18 kpsi, Microfluidics, USA) and lysate was clarified by centrifugation (SS-34, 25.000 rpm, 20 min, 4°C). RNA concentration was measured (A₂₆₀) and 10 OD of the sample was loaded on an analytical SW40 gradient (10-40 % sucrose in buffer H₁₀M₃₀N₁₅₀SH₆, 17.000 rpm, 15 h, 4°C). The remaining S30 was loaded on a 30 % sucrose cushion (1.1 M sucrose in H₁₀M₃₀N₁₅₀SH₆) and centrifuged (Ti 45, 36.000 rpm, 24 h, 4°C). Pellets were resuspended in a minimal volume of cell buffer (supplemented

with 6 mM β -Mercaptoethanol) and 200 OD of ribosomes were loaded on SW32 gradients (10-40% sucrose in buffer $H_{10}M_{xx}N_{150}SH_6$, 18.000 rpm, 14 h, 4°C). Fractions of 70S ribosomes were pooled in the presence of 30 mM $MgCl_2$ and ribosomal subunits (30S and 50S) were collected while using a magnesium concentration of 1 mM in the buffer. Ribosomal fractions were pelleted (Ti 70, 38.000 rpm, 24 h, 4°C), resuspended in cell buffer, aliquoted and stored at -80°C.

7.2.2 Protein purification: Ni^{2+} -NTA-Agarose

The YhhF construct (the gene encoding mature YhhF was cloned into pCA24N (Cam^R) with an N-terminal 6x histidine tag) was provided by the laboratory of Dr. Petr Sergiev (Moskow, Russia).

The mature RlmH protein was provided by the laboratory of Prof. Jaanus Remme (Tartu, Estonia). It was necessary to purify non-tagged RlmH protein since both the N- and C-terminally His-tagged protein versions were 1000-fold less active and completely inactive, respectively. RlmH protein was purified from *E. coli* TOP10 cells harboring the pBAD-*rlmH* plasmid and grown in 2xTY (tryptone/yeast) media in the presence of 1 mM arabinose. Cells were harvested and resuspended in buffer (20 mM Tris-HCl, pH 7.5, 200 mM NaCl, 10% glycerol, 0.5 mM PMSF, 1 mM DTT) before cells were disrupted with a French Press. The supernatant was applied to a Q-Sepharose anion-exchange column in order to remove contaminants. The flow-through containing RlmH protein was concentrated and the buffer was exchanged to 50 mM sodium acetate, pH 5.8, 125 mM KCl, 5% glycerol, 0.5 mM PMSF and 1 mM DTT. Protein was loaded onto a SP-Sepharose cation-exchange column and eluted from the column with a 0 – 0.5 M NaCl linear gradient over 20 column volumes. Fractions containing RlmH protein were pooled, concentrated and dialyzed into 50 mM Tris-HCl, pH 7.5, 200 mM KCl, 10% glycerol and 1 mM DTT. The purity of RlmH protein was verified by SDS-PAGE and Mass Spec analysis. The protein concentration was determined by the Bradford method and protein was stored at -80°C.

The genes encoding the mature mitochondrion-specific ribosomal proteins (MSRPs) were amplified from yeast genomic DNA and cloned into a modified pET28 vector, thus introducing an N-terminal 6x histidine-tag together with a TEV cleavage site combined via a short linker sequence.

In general, plasmids were transformed into BL21 (DE3) cells, protein expression was induced at mid-log phase with 1 mM isopropyl-1-thio- β -D-galactopyranoside (IPTG, Roth) and cells were grown for 3 hours at 37°C (in the case of YhhF) or overnight at 25°C (in the case of MSRPs) before harvested in a SLC-6000 rotor (5.000 rpm, 15 min, 4°C). Cell pellets containing overexpressed protein were resuspended in Lysis Buffer (50 mM NaH₂PO₄, 300 mM NaCl, 10 mM Imidazole, 5 mM β -Mercaptoethanol) and mechanically disrupted using ultrasonification (5x 15 sec (35-40%), on ice, HD200, Bandelin, Germany) or 2 runs in a French Press (18 kpsi, Microfluidics, USA) in the presence of lysozyme (1 μ g/mL) and phenylmethylsulfonyl fluoride (PMSF, 0.1 mM). Lysates were clarified by centrifugation in a SS-34 rotor (25.000 rpm, 20 min, 4°C). The supernatant (S30) was used for protein purification.

Purified protein was obtained by metal affinity purification using the N-terminal 6x His-tag for binding to Ni-NTA-Agarose beads (Qiagen) followed by gel filtration. The protein was washed and eluted from the resin with increasing concentrations of imidazole in the wash and elution buffers (with 20 mM and 250 mM Imidazole, respectively). Aliquots from each purification step were taken for subsequent SDS-PAGE analysis. Elution fractions of purified protein were pooled and applied to an equilibrated gel filtration column (HiLoad 16/60 Superdex 75 pg, GE Healthcare) using ÄKTA buffer (20 mM Hepes-KOH, pH 7.5, 1 mM MgCl₂, 200 mM NH₄Cl, 0.1% Triton X-100, 10% Glycerin, 5 mM DTT) in the case of YhhF purification and RimM buffer (10 mM Hepes-KOH, pH 7.8, 100 mM NaCl, 10 mM β -Mercaptoethanol) in the case of RimM purification. An ÄKTA purifier liquid chromatography system was used for gel filtration. Peak fractions were analyzed by SDS-PAGE and purified protein was aliquoted, snap-frozen at -80°C and used for further binding experiments.

7.2.3 Protein purification: TALON[®]

TALON[®] is an immobilized metal ion affinity chromatography (IMAC) resin with a Co²⁺ ion in the reactive core that binds polyhistidine-tagged proteins more specifically than nickel-based IMAC resin. Therefore, TALON resin was used for the purification of [Eco70S-MRPL3] complexes. 550 OD of *E. coli* 70S ribosomes purified from cells overexpressing yeast MRPL3 were loaded on 500 μ L of TALON slurry prewashed with 2 mL of autoclaved water and equilibrated with 2.5 mL of Equilibration Buffer (50 mM Hepes, pH 7.0, 20 mM MgCl₂, 250 mM

NH₄Cl, 5 mM β -Mercaptoethanol) containing 10 μ g/mL tRNA and incubated overnight at 4°C. The column was washed once with 2 mL of Equilibration Buffer, then twice with 2 mL of Wash Buffer (50 mM Hepes, pH 7.0, 20 mM MgCl₂, 250 mM NH₄Cl, 7.5 mM Imidazole, 5 mM β -Mercaptoethanol) before His-tagged MRPL3 bound to 70S ribosomes was eluted from the column. Elution fractions (E1 and E2) were collected after 5 min incubation with Elution Buffer (50 mM Hepes, pH 7.0, 20 mM MgCl₂, 250 mM NH₄Cl, 150 mM Imidazole, 5 mM β -Mercaptoethanol) on the column. Each elution fraction (500 μ L) was pelleted through 2.5 mL of sucrose cushion (1 M sucrose final concentration in Equilibration Buffer) to concentrate the sample and remove the remaining imidazole (TLA 110, 100.000 rpm, 55 min, 4°C). Pellets were resuspended, aliquoted and stored at -80°C.

7.2.4 SDS-PAGE

A SDS-PAGE (Sodiumdodecylsulfate polyacrylamide gel electrophoresis) was performed in order to separate proteins according to their molecular weights using standard protocols (Laemmli 1970). Samples were denatured at 95°C for 5 min and loaded on 15% polyacrylamide gels. Electrophoresis was performed at constant voltage of 120-160 V in standard running buffer (25 mM Tris, 192 mM Glycine, 0.1% (w/v) SDS) for 1 hour. In addition, a broad range protein marker (NEB) was loaded. Gels were stained with Coomassie staining solution (50% (v/v) methanol, 10% (v/v) acetic acid, 0.25% (w/v) Coomassie Brilliant blue R-250) and afterwards destained with destaining solution (40% (v/v) methanol, 10% (v/v) acetic acid).

7.2.5 Western blot Analysis

Western blot analysis was used for the qualitative detection of tagged proteins. For His-tag detection, SDS gels were blotted for 55 min in transfer buffer (20% (v/v) methanol, 50 mM Tris, 40 mM Glycine, 0.037% (w/v) SDS) at 1 mA/cm² (50 mA) on Nitrocellulose membranes, using a standard semi-dry blotting apparatus. Membranes were then stained for 1-2 min in Amidoblack (Merck), digitized, destained and blocked with 10 % (w/v) milk (Roth) in

TBS buffer (50 mM Tris-HCl, pH 7.5, 150 mM NaCl) for 30 min at RT to prevent unspecific binding of the first antibody. The primary antibody (His Tag Monoclonal Antibody, Novagen) was used in a 1:1000 dilution in 10 % milk-TBS and incubated overnight at 4°C. The membrane was washed twice for 10 min with 1x TBS-T buffer (50 mM Tris-HCl, pH 7.5, 150 mM NaCl, 0.1% (v/v) Tween 20) and once with 1x TBS buffer before the second antibody (goat anti-mouse HRP antibody, Santa Cruz Biotechnology) was used in a 1:5000 dilution in 10 % milk-TBS and incubated for 1 h at RT. Membranes were washed again four times with TBS-T buffer and signals were detected by ECL reaction (Chemiluminescent Detection Kit, AppliChem) and films (GE Healthcare).

7.2.6 *In vitro* binding assay

Binding assays were performed to characterize the binding *in vitro* of purified protein to both purified ribosomal subunits and 70S ribosomes, respectively.

In general, the assay was performed as following: 2.5 OD of purified 70S ribosomes (1OD of 70S = 24 pmol) or ribosomal subunits (1OD of 30S = 72 pmol or 1 OD of 50S = 36 pmol) were incubated with an excess of purified protein (3 – 10x excess over ribosomes) for 20 min at 37°C in binding buffer (20 mM Hepes-KOH, pH 7.5, 10 mM MgCl₂, 30 mM NH₄Cl) before being loaded on a 10% sucrose cushion in binding buffer and centrifuged in a TLN 100 rotor at 75.000 rpm for 30 min at 4°C. For each reaction, aliquots of the initial reaction (R), supernatant (S) and pellet (P) after centrifugation were taken and analyzed by SDS-PAGE or Western Blot. In all cases, controls were performed with both ribosomes without addition of protein and protein factors alone (no ribosomes present).

In case of binding studies of protein factors YhhF and RlmH, sinefungin was applied to the reaction (0.02 mM final concentration). Sinefungin is a nucleoside antibiotic that acts as an S-adenosyl-L-methionine (SAM) methyltransferase-specific inhibitor.

7.2.7 *In vivo* association of individual MSRPs with *E. coli* ribosomes

BL21 (DE3) carrying the plasmid with individual MSRP constructs were grown at 37°C to mid-log phase, induced with 1 mM IPTG and continued growth overnight at 25°C before

harvested (SLC-6000, 5.000 rpm, 15 min, 4°C). Cell pellets were resuspended in 2 volumes of buffer A (20 mM Hepes-KOH, pH 7.8, 10 mM MgCl₂, 60 mM NH₄Cl, 4 mM β-Mercaptoethanol) and were incubated on ice in the presence of lysozyme (1 µg/mL) and DNase I (0.2 µg/mL, RNase free). Cells were lysed by three runs with a Microfluidizer (18 kpsi, Microfluidics, USA) and the lysate was clarified by centrifugation (SS-34, 25.000 rpm, 30 min, 4°C) before applied to a 5-30% sucrose gradient (SW40, in buffer A, 19.000 rpm, 16 h, 4°C). 70S fractions were pooled and ribosomes were pelleted (RP-80-AT, 34.000 rpm, 3 h, 4°C). In case of ribosomal subunit collection, buffer A was supplemented with 1 mM MgCl₂. Binding of overexpressed MSRPs to 70S ribosomes and ribosomal subunits was determined by SDS-PAGE and Western blot analysis in comparison to control ribosomes (in the absence of the overexpressed MSRP).

7.3 Electron microscopy (EM)

7.3.1 Negative-Stain Electron Microscopy

Negative-stain EM was used to visually inspect the samples taken from binding assays and to pre-analyze the samples prior to grid preparation for cryo-EM. The grids (Quantifoil) were washed with chloroform, floated with a thin carbon layer and glow discharged in a plasma cleaner chamber (Harrick Plasma, USA) at 0.22 Torr for 45 sec. 3.5 µl of the sample was applied onto the grid and incubated for 45 sec. The grid was washed with five drops of water and subsequently stained with three drops of 2% uranyl acetate (Ted Pella, Inc., USA) for 15 sec. Then, the grid was dried with blotting paper to remove excess sample and uranyl acetate. Analysis of the negative-stain grids were carried out on a Morgagni microscope (100 kV FEI Morgagni electron microscope, Biocenter, Munich, Germany).

7.3.2 Cryo-Electron Microscopy (Cryo-EM)

3,5 µl of sample was applied to carbon coated holey grids as described before (Grassucci, Taylor *et al.* 2007) and vitrified using a Vitrobot Mark IV (FEI Company). Data was collected on a FEI Tecnai F30 field emission gun microscope at 300 kV (Max-Planck Institute of Molecular Genetics, Berlin, Germany) in the case of the “[Eco70SΔ*rluD/rlmH*·RlmH]” and

“[*Eco30S Δ rimM*·RimM]” datasets or on a FEI Tecnai G2 Spirit 120 kV cryo-microscope (Biocenter, Munich, Germany) in case of the “[*Eco30S Δ yhhF*·YhhF]” and the “[*Eco70S*·MRPL3]” datasets under low dose conditions with $\sim 20 \text{ e}^-/\text{\AA}^2$ in a defocus range between 1.0 μm and 4.5 μm . Micrographs taken from the FEI Tecnai F30 were developed and digitized on a Heidelberg drum scanner resulting in a pixel size of 1.24 \AA /pixel on object scale.

The “[*Eco70S*·TetM-GDPNP·Tgc]” dataset was collected on a Titan Krios TEM (FEI Company, Biocenter, Munich, Germany) at 200 kV under low dose conditions ($20 \text{ e}^-/\text{\AA}^2$) at a nominal magnification of 75.000. Data was recorded on a TemCam F416 camera (4096 x 4096 pixel, 15.6 μm pixel size, 1 sec/full frame, TVIPS GmbH) leading to a final magnification of 148,721 x at the plane of CCD resulting in a image pixel size of 1.049 \AA (object scale). The nominal defocus was set between -1 μm and -3.5 μm . Data collection was done semi-automatically using the software EM-TOOLS (TVIPS).

7.3.3 Image Processing and 3D-reconstruction

Pre-processing the dataset comprises several semi-automated steps using scripts based on the SPIDER software package (Frank, Radermacher *et al.* 1996): Firstly, micrographs were converted into spider readable files and the CTF was determined using the SPIDER TF ED command. Visual inspection of power spectra and micrographs was done using JWEB. Micrographs showing significant ice contamination, high drift or astigmatism were excluded from the dataset. Coordinates of particles were automatically determined with a modified version of SIGNATURE (Chen and Grigorieff 2007) using projections of a eukaryotic ribosome as reference. Based on the coordinates the particles were taken from each micrograph. An automated learning based algorithm (MAPPOS) was used for classification of ribosomal and non-ribosomal particles like contaminations, noise or carbon edges. The program was trained with manually selected good and bad particles. The remaining ribosomal particles were initially aligned using a cross-correlation based projection matching technique with an angular accuracy of 15° (83 reference projections). The initial reference was obtained from an *E. coli* 70S ribosome. The organization of the dataset was changed from micrograph-based to defocus-based for the following refinements. 1500 to

2200 particles with similar defocus values were merged into one defocus group. In each refinement round all particles were aligned against the volume generated in the previous round. For the first round of refinement the initial reference was used. Sub-volumes for each defocus group based on the angle and shift values obtained in the alignment were calculated. The defocus-dependent sub-volumes were CTF-corrected and combined into a single volume. The resolution was calculated by comparing sub-volumes of all even and odd particles in each defocus group. The Fourier shell correlation (FSC) was calculated and a cut-off at 0.5 indicated the resolution. For sorting a dataset, up to three distinct reference volumes were offered during a refinement and the particles were separated according to their best cross correlation with one of these references. Based on the particles assigned to each reference, the back-projections were done separately and used as references for the next round of sorting.

7.3.4 Structural Modeling and Preparation of Figures

Atomic models for the 30S and 50S ribosomal subunit (PDB2YKR was used for the structural interpretation of the [*Eco*30S Δ *yhhF*-YhhF] and [*Eco*30S Δ *rimM*-RimM] complex; PDB2WRI, PDB2WRJ and PDB1HNW were used for the structural interpretation of the [*Eco*70S-TetM-GDPNP-Tgc] complex) were fitted into the cryo-EM reconstructions and isolated densities. An *E. faecalis* Tet(M) homology model was created using HHpred (Söding, Biegert et al. 2005), based on a sequence alignment of *T. thermophilus* EF-G and an EF-G crystal structure (PDB1DAR). Densities for the *E. coli* 50S and 30S ribosomal subunits and Tet(M) were isolated using the color zone function of Chimera (Pettersen, Goddard et al. 2004). The individual domains of the Tet(M) model were fitted into the isolated protein density using the “Fit in Map” function of Chimera and the Tet(M) domains were reconnected using Coot (crystallographic object-oriented toolkit). The secondary structure prediction on the C-terminal part of Tet(M) as well as on various other RPPs was performed using PSIPRED. The sequence alignment of various Tet proteins and *T. thermophilus* EF-G was performed using ClustalW2.

8 References

- Adams, K. L. and J. D. Palmer (2003). "Evolution of mitochondrial gene content: gene loss and transfer to the nucleus." Mol Phylogenet Evol **29**(3): 380-395.
- AEvarsson, A., E. Brazhnikov, M. Garber, J. Zheltonosova, Y. Chirgadze, S. Alkaradaghi, L. A. Svensson and A. Liljas (1994). "Three-dimensional structure of the ribosomal translocase: Elongation factor G from *Thermus thermophilus*." EMBO J. **13**(16): 3669-3677.
- Agirrezabala, X., J. Lei, J. L. Brunelle, R. F. Ortiz-Meoz, R. Green and J. Frank (2008). "Visualization of the hybrid state of tRNA binding promoted by spontaneous ratcheting of the ribosome." Mol Cell **32**(2): 190-197.
- Agrawal, R. K., P. Penczek, R. Grassucci and J. Frank (1998). "Visualization of elongation factor G on the *Escherichia coli* 70S ribosome: The mechanism of translocation." Proc Natl Acad Sci USA **95**: 6134 - 6138.
- Agrawal, R. K., M. Sharma, M. Kiel, G. Hirokawa, T. Booth, C. Spahn, R. Grassucci, A. Kaji and J. Frank (2004). "Visualization of ribosome-recycling factor on the *Escherichia coli* 70S ribosome: Functional implications." Proc Natl Acad Sci USA **101**(24): 8900–8905.
- Agrawal, R. K., A. B. Heagle, P. Penczek, R. A. Grassucci and J. Frank (1999). " EF-G-dependent GTP hydrolysis induces translocation accompanied by large conformational changes in the 70S ribosome." Nature Struct. Biol. **6**(7): 643-647.
- al-Karadaghi, S., A. Aevansson, M. Garber, J. Zheltonosova and A. Liljas (1996). "The structure of elongation factor G in complex with GDP: Conformational flexibility and nucleotide exchange." Structure **4**(5): 555-565.
- Al Refaii, A. and J. H. Alix (2009). "Ribosome biogenesis is temperature-dependent and delayed in *Escherichia coli* lacking the chaperones DnaK or DnaJ." Mol Microbiol **71**(3): 748-762.
- Alix, J. H. and M. F. Guerin (1993). "Mutant DnaK chaperones cause ribosome assembly defects in *Escherichia coli*." Proc Natl Acad Sci USA **90**: 9725-9729.
- Allen, G. S., A. Zavialov, R. Gursky, M. Ehrenberg and J. Frank (2005). "The Cryo-EM Structure of a Translation Initiation Complex from *Escherichia coli*." Cell **121**(5): 703-712.
- Allen, J. F. (2003). "The function of genomes in bioenergetic organelles." Philos Trans R Soc Lond B Biol Sci **358**(1429): 19-37; discussion 37-18.

- Alonso, J. and J. F. Santaren (2006). "Characterization of the *Drosophila melanogaster* ribosomal proteome." J Proteome Res **5**(8): 2025-2032.
- Antoun, A., M. Y. Pavlov, M. Lovmar and M. Ehrenberg (2006). "How initiation factors tune the rate of initiation of protein synthesis in bacteria." EMBO J. **25**(11): 2539-2550.
- Armache, J. P., A. Jarasch, A. M. Anger, E. Villa, T. Becker, S. Bhushan, F. Jossinet, M. Habeck, G. Dindar, S. Franckenberg, V. Marquez, T. Mielke, M. Thomm, O. Berninghausen, B. Beatrix, J. Söding, E. Westhof, D. N. Wilson and R. Beckmann (2010). "Cryo-EM structure and rRNA model of a translating eukaryotic 80S ribosome at 5.5-Å resolution." Proc Natl Acad Sci U S A **107**(46): 19748-19753.
- Arnold, R. J. and J. P. Reilly (1999). "Observation of *Escherichia coli* ribosomal proteins and their posttranslational modifications by mass spectrometry." Anal. Biochem. **269**(1): 105-112.
- Ban, N., P. Nissen, J. Hansen, P. B. Moore and T. A. Steitz (2000). "The complete atomic structure of the large ribosomal subunit at 2.4 Å resolution." Science **289**: 905-920.
- Barat, C., P. P. Datta, V. S. Raj, M. R. Sharma, H. Kaji, A. Kaji and R. K. Agrawal (2007). "Progression of the Ribosome Recycling Factor through the Ribosome Dissociates the Two Ribosomal Subunits." Mol Cell **27**(2): 250-261.
- Bauer, G., C. Berens, S. Projan and W. Hillen (2004). "Comparison of tetracycline and tigecycline binding to ribosomes mapped by dimethylsulphate and drug-directed Fe²⁺ cleavage of 16S rRNA." J. Antimicrob. Chemother. **53**(4): 592-599.
- Becker, T., J. P. Armache, A. Jarasch, A. M. Anger, E. Villa, H. Sieber, B. A. Motaal, T. Mielke, O. Berninghausen and R. Beckmann (2011). "Structure of the no-go mRNA decay complex Dom34-Hbs1 bound to a stalled 80S ribosome." Nat Struct Mol Biol **18**(6): 715-720.
- Belova, L., T. Tenson, L. Q. Xiong, P. M. McNicholas and A. S. Mankin (2001). "A novel site of antibiotic action in the ribosome: Interaction of evernimicin with the large ribosomal subunit." Proc Natl Acad Sci USA **98**(7): 3726-3731.
- Ben-Shem, A., N. Garreau de Loubresse, S. Melnikov, L. Jenner, G. Yusupova and M. Yusupov (2011). "The Structure of the Eukaryotic Ribosome at 3.0 Å Resolution." Science **334**: 1524-1529.
- Berg, O. G. and C. G. Kurland (2000). "Why mitochondrial genes are most often found in nuclei." Mol Biol Evol **17**(6): 951-961.

- Bergeron, J., M. Ammirati, D. Danley, L. James, M. Norcia, J. Retsema, C. A. Strick, W. G. Su, J. Sutcliffe and L. Wondrack (1996). "Glycylcyclines bind to the high-affinity tetracycline ribosomal binding site and evade Tet(M)- and Tet(O)-mediated ribosomal protection." Antimicrob Agents Chemother **40**(9): 2226-2228.
- Blanchard, J. L. and M. Lynch (2000). "Organellar genes: why do they end up in the nucleus?" Trends Genet **16**(7): 315-320.
- Blanchard, S. C., R. L. Gonzalez, H. D. Kim, S. Chu and J. D. Puglisi (2004). "tRNA selection and kinetic proofreading in translation." Nat Struct Mol Biol **11**(10): 1008-1014.
- Blanchard, S. C., H. D. Kim, R. L. Gonzalez, Jr., J. D. Puglisi and S. Chu (2004). "tRNA dynamics on the ribosome during translation." Proc Natl Acad Sci USA **101**(35): 12893-12898.
- Borovinskaya, M. A., S. Shoji, J. M. Holton, K. Fredrick and J. H. Cate (2007). "A steric block in translation caused by the antibiotic spectinomycin." ACS Chem Biol **2**(8): 545-552.
- Borst, P. and L. A. Grivell (1971). "Mitochondrial ribosomes." FEBS Lett. **13**(2): 73-88.
- Brandi, L., A. Fabbretti, A. La Teana, M. Abbondi, D. Losi, S. Donadio and C. Gualerzi (2006). "Specific, efficient, and selective inhibition of prokaryotic translation initiation by a novel peptide antibiotic." Proc Natl Acad Sci USA **103**(1): 39-44.
- Brandi, L., S. Marzi, A. Fabbretti, C. Fleischer, W. Hill, J. Lodmell and C. Gualerzi (2004). "The translation initiation functions of IF2: Targets for thiostrepton inhibition." J Mol Biol **335**: 881-894.
- Brimacombe, R., P. Mitchell, M. Osswald, K. Stade and D. Bochkariov (1993). "Clustering of Modified Nucleotides at the Functional Center of Bacterial Ribosomal RNA." FASEB J **7**(1): 161-167.
- Brodersen, D. E., W. M. Clemons, A. P. Carter, R. J. Morgan-Warren, B. T. Wimberly and V. Ramakrishnan (2000). "The structural basis for the action of the antibiotics tetracycline, pactamycin, and hygromycin B on the 30S ribosomal subunit." Cell **103**(7): 1143-1154.
- Buglino, J., V. Shen, P. Hakimian and C. D. Lima (2002). "Structural and biochemical analysis of the Obg GTP binding protein." Structure **10**: 1581-1592.
- Burakovskii, D. E., A. S. Smirnova, D. V. Lesniak, S. V. Kiparisov, A. A. Leonov, P. V. Sergiev, A. A. Bogdanov and O. A. Dontsova (2007). "Interaction of 23S ribosomal RNA helices 89 and 91 of *Escherichia coli* contributes to the activity of IF2 but is insignificant for elongation factors functioning." Mol Biol (Mosk) **41**(6): 1031-1041.

- Burdett, V. (1996). "Tet(M)-promoted release of tetracycline from ribosomes is GTP dependent." J Bacteriol **178**(11): 3246-3251.
- Bylund, G. O., L. Wipemo, L. Lundberg and P. Wikström (1998a). "RimM and RbfA are essential for efficient processing of 16S rRNA in *Escherichia coli*." J Bacteriol **180**(1): 73-82.
- Bylund, G. O., J. M. Lövgren and P. M. Wikström (2001). "Characterization of Mutations in the *metY-nusA-infB* Operon That Suppress the Slow Growth of a $\Delta rimM$ Mutant." J Bacteriol **183**(20): 6095-6106.
- Bylund, G. O., B. C. Persson, L. A. Lundberg and P. M. Wikström (1997). "A novel ribosome-associated protein is important for efficient translation in *Escherichia coli*." J Bacteriol **179**(14): 4567-4574.
- Byström, A. S., K. J. Hjalmarsson, P. M. Wikström and G. R. Björk (1983). "The nucleotide sequence of an *Escherichia coli* operon containing genes for the tRNA(m¹G)methyltransferase, the ribosomal proteins S16 and L19 and a 21-K polypeptide." EMBO J **2**(6): 899-905.
- Cabanas, M. J., D. Vazquez and J. Modolell (1978). "Inhibition of ribosomal translocation by aminoglycoside antibiotics." Biochem Biophys Res Commun **83**(3): 991-997.
- Caldon, C. E. and P. E. March (2003). "Function of the universally conserved bacterial GTPases." Curr Opin Microbiol **6**(2): 135-139.
- Cameron, D. M., J. Thompson, P. E. March and A. E. Dahlberg (2002). "Initiation factor IF2, thiostrepton and micrococin prevent the binding of elongation factor G to the *Escherichia coli* ribosome." J Mol Biol **319**(1): 27-35.
- Campbell, T. L. and E. D. Brown (2008). "Genetic Interaction Screens with Ordered Overexpression and Deletion Clone Sets Implicate the *Escherichia coli* GTPase YjeQ in Late Ribosome Biogenesis." J Bacteriol **190**(7): 2537-2545.
- Carter, A. P., W. M. Clemons, D. E. Brodersen, R. J. Morgan-Warren, B. T. Wimberly and V. Ramakrishnan (2000). "Functional insights from the structure of the 30S ribosomal subunit and its interactions with antibiotics." Nature **407**(6802): 340-348.
- Carter, A. P., W. M. Clemons, Jr., D. E. Brodersen, R. J. Morgan-Warren, T. Hartsch, B. T. Wimberly and V. Ramakrishnan (2001). "Crystal structure of an initiation factor bound to the 30S ribosomal subunit." Science **291**(5503): 498-501.

- Cate, J. H., M. M. Yusupov, G. Z. Yusupova, T. N. Earnest and H. F. Noller (1999). "X-ray crystal structures of 70S ribosome functional complexes." Science **285**: 2095-2104.
- Cedergren, R., M. W. Gray, Y. Abel and D. Sankoff (1988). "The evolutionary relationships among known life forms." J Mol Evol **28**(1-2): 98-112.
- Chandramouli, P., M. Topf, J. F. Menetret, N. Eswar, J. J. Cannone, R. R. Gutell, A. Sali and C. W. Akey (2008). "Structure of the mammalian 80S ribosome at 8.7 Å resolution." Structure **16**(4): 535-548.
- Chen, J. Z. and N. Grigorieff (2007). "SIGNATURE: a single-particle selection system for molecular electron microscopy." J Struct Biol **157**(1): 168-173.
- Chen, X., D. Court and X. Ji (1999). "Crystal structure of ERA: a GTPase-dependent cell cycle regulator containing an RNA binding motif." Proc Natl Acad Sci USA **96**(15): 8396-8401.
- Chittum, H. S. and W. S. Champney (1995). "Erythromycin inhibits the assembly of the large ribosomal subunit in growing *Escherichia coli* cells." Curr Microbiol **30**(5): 273-279.
- Chopra, I. (2002). "New developments in tetracycline antibiotics: glycylcyclines and tetracycline efflux pump inhibitors." Drug Resist Updates **5**(3-4): 119-125.
- Chopra, I. and M. Roberts (2001). "Tetracycline Antibiotics: Mode of Action, Applications, Molecular Biology, and Epidemiology of Bacterial Resistance." Microbiol Mol Biol Rev **65**(2): 232-260.
- Clementi, N., A. Chirkova, B. Puffer, R. Micura and N. Polacek (2010). "Atomic mutagenesis reveals A2660 of 23S ribosomal RNA as key to EF-G GTPase activation." Nat Chem Biol **6**(5): 344-351.
- Connell, S. R., C. Takemoto, D. N. Wilson, H. Wang, K. Murayama, T. Terada, M. Shirouzu, M. Rost, M. Schuler, J. Giesebrecht, M. Dabrowski, T. Mielke, P. Fucini, S. Yokoyama and C. M. Spahn (2007). "Structural basis for interaction of the ribosome with the switch regions of GTP-bound elongation factors." Mol Cell **25**(5): 751-764.
- Connell, S. R., D. M. Tracz, K. H. Nierhaus and D. E. Taylor (2003). "Ribosomal Protection Proteins and Their Mechanism of Tetracycline Resistance." Antimicrob Agents Chemother **47**(12): 3675-3681.
- Connell, S. R., C. A. Trieber, G. P. Dinos, E. Einfeldt, D. E. Taylor and K. H. Nierhaus (2003). "Mechanism of Tet(O)-mediated tetracycline resistance." EMBO J **22**(4): 945-953.

- Connell, S. R., C. A. Trieber, U. Stelzl, E. Einfeldt, D. E. Taylor and K. H. Nierhaus (2002). "The tetracycline resistance protein Tet(O) perturbs the conformation of the ribosomal decoding centre." Mol Microbiol **45**(6): 1463-1472.
- Connolly, K., J. P. Rife and G. Culver (2008). "Mechanistic insight into the ribosome biogenesis functions of the ancient protein KsgA." Mol Microbiol **70**(5): 1062-1075.
- Cordin, O., J. Banroques, N. K. Tanner and P. Linder (2006). "The DEAD-box protein family of RNA helicases." Gene **367**: 17-37.
- Culver, G. M. (2003). "Assembly of the 30S ribosomal subunit." Biopolymers **68**(2): 234-249.
- Curgy, J. J. (1985). "The mitoribosomes." Biol Cell **54**(1): 1-38.
- Czworkowski, J., J. Wang, T. A. Seitz and P. B. Moore (1994). "The crystal structure of elongation factor G complexed with GDP, at 2.7 Å resolution." EMBO J **13**: 3661-3668.
- Dagley, S. and J. Sykes (1959). "Effect of drugs upon components of bacterial cytoplasm." Nature **183**(4675): 1608-1609.
- Dantley, K., H. Dannelly and V. Burdett (1998). "Binding interaction between Tet(M) and the ribosome: Requirements for binding." J Bacteriol **180**(16): 4089-4092.
- Darken, M. A. (1964). "Puromycin Inhibition of Protein Synthesis." Pharmacol Rev **16**: 223-243.
- Datta, P. P., M. R. Sharma, L. Qi, J. Frank and R. K. Agrawal (2005). "Interaction of the G' Domain of Elongation Factor G and the C-Terminal Domain of Ribosomal Protein L7/L12 during Translocation as Revealed by Cryo-EM." Mol Cell **20**(5): 723-731.
- Datta, P. P., D. N. Wilson, M. Kawazoe, N. K. Swami, T. Kaminishi, M. R. Sharma, T. M. Booth, C. Takemoto, P. Fucini, S. Yokoyama and R. K. Agrawal (2007). "Structural Aspects of RbfA Action during Small Ribosomal Subunit Assembly." Mol Cell **28**(3): 434-445.
- Davies, J. and D. Davies (2010). "Origins and evolution of antibiotic resistance." Microbiol Mol Biol Rev **74**(3): 417-433.
- Davis, B. D. (1987). "Mechanism of bactericidal action of aminoglycosides." Microbiol Rev **51**(3): 341-350.
- De Rijk, P., Y. Van de Peer, I. Van den Broeck and R. De Wachter (1995). "Evolution according to large ribosomal subunit RNA." J Mol Evol **41**(3): 366-375.
- Decatur, W. A. and M. J. Fournier (2002). "rRNA modifications and ribosome function." Trends Biochem Sci **27**(7): 344-351.

- Deutscher, M. P. (2009). "Maturation and degradation of ribosomal RNA in bacteria." Prog Mol Biol Transl Sci **85**: 369-391.
- Diaconu, M., U. Kothe, F. Schlünzen, N. Fischer, J. M. Harms, A. G. Tonevitsky, H. Stark, M. V. Rodnina and M. C. Wahl (2005). "Structural Basis for the Function of the Ribosomal L7/12 Stalk in Factor Binding and GTPase Activation." Cell **121**(7): 991-1004.
- Dinos, G., D. N. Wilson, Y. Teraoka, W. Szaflarski, P. Fucini, D. Kalpaxis and K. H. Nierhaus (2004). "Dissecting the ribosomal inhibition mechanisms of edeine and pactamycin: the universally conserved residues G693 and C795 regulate P-site tRNA binding." Mol Cell **13**(1): 113-124.
- Dönhöfer, A., M. R. Sharma, P. P. Datta, K. H. Nierhaus, R. K. Agrawal and D. N. Wilson (2009). "Factor-Mediated Ribosome Assembly in Bacteria." Encyclopedia of Life Sciences (ELS).
- Duggar, B. M. (1948). "Aureomycin; a product of the continuing search for new antibiotics." Ann N Y Acad Sci **51**(Art. 2): 177-181.
- Dunkle, J. A., L. Wang, M. B. Feldman, A. Pulk, V. B. Chen, G. J. Kapral, J. Noeske, J. S. Richardson, S. C. Blanchard and J. H. Cate (2011). "Structures of the bacterial ribosome in classical and hybrid states of tRNA binding." Science **332**(6032): 981-984.
- El Hage, A. and J. H. Alix (2004). "Authentic precursors to ribosomal subunits accumulate in *Escherichia coli* in the absence of functional DnaK chaperone." Mol Microbiol **51**(1): 189-201.
- El Hage, A., M. Sbai and J. H. Alix (2001). "The chaperonin GroEL and other heat-shock proteins, besides DnaK, participate in ribosome biogenesis in *Escherichia coli*." Mol Gen Genet **264**(6): 796-808.
- Emelyanov, V. V. (2001). "Evolutionary relationship of Rickettsiae and mitochondria." FEBS Lett **501**(1): 11-18.
- Erlacher, M. D. and N. Polacek (2008). "Ribosomal catalysis: the evolution of mechanistic concepts for peptide bond formation and peptidyl-tRNA hydrolysis." RNA Biol **5**(1): 5-12.
- Ero, R., M. Leppik, A. Liiv and J. Remme (2010). "Specificity and kinetics of 23S rRNA modification enzymes RlmH and RluD." RNA **16**(11): 2075-2084.
- Ero, R., L. Peil, A. Liiv and J. Remme (2008). "Identification of pseudouridine methyltransferase in *Escherichia coli*." RNA **14**(10): 2223-2233.

- Feldman, M. B., D. S. Terry, R. B. Altman and S. C. Blanchard (2010). "Aminoglycoside activity observed on single pre-translocation ribosome complexes." Nat Chem Biol **6**(1): 54-62.
- Fernandez-Munoz, R., R. E. Monro, R. Torres-Pinedo and D. Vazquez (1971). "Substrate- and antibiotic-binding sites at the peptidyl transferase centre of *E. coli* ribosomes. Studies on the chloramphenicol, lincomycin and erythromycin sites." Eur J Biochem **23**: 185-193.
- Feunteun, J., B. R. Jordan and R. Monier (1972). "Study of the maturation of 5 s RNA precursors in *Escherichia coli*." J Mol Biol **70**(3): 465-474.
- Fischbach, M. A. and C. T. Walsh (2009). "Antibiotics for emerging pathogens." Science **325**(5944): 1089-1093.
- Frank, J. and R. K. Agrawal (2000). "A ratchet-like inter-subunit reorganization of the ribosome during translocation." Nature **406**: 318-322.
- Frank, J., M. Radermacher, P. Penczek, J. Zhu, Y. Li, M. Ladjadj and A. Leith (1996). "SPIDER and WEB: processing and visualization of images in 3D electron microscopy and related fields." J Struct Biol **116**(1): 190-199.
- Frolova, L., R. Tsivkovskii, G. Sivolobova, N. Oparina, O. Serpinski, V. Blinov, S. Tatkov and L. Kisselev (1999). "Mutations in the highly conserved GGQ motif of class 1 polypeptide release factors abolish the ability of human eRF1 to trigger peptidyl-tRNA hydrolysis." RNA **5**: 1014-1020.
- Gale, E. F., E. Cundliffe, P. E. Reynolds, M. H. Richmond and M. J. Waring (1981). Antibiotic inhibitors of ribosome function. The molecular basis of antibiotic action. Bristol, UK, John Wiley and sons: 278-379.
- Gan, X., M. Kitakawa, K. Yoshino, N. Oshiro, K. Yonezawa and K. Isono (2002). "Tag-mediated isolation of yeast mitochondrial ribosome and mass spectrometric identification of its new components." Eur J Biochem **269**(21): 5203-5214.
- Gao, H., Z. Zhou, U. Rawat, C. Huang, L. Bouakaz, C. Wang, Z. Cheng, Y. Liu, A. Zavialov, R. Gursky, S. Sanyal, M. Ehrenberg, J. Frank and H. Song (2007). "RF3 induces ribosomal conformational changes responsible for dissociation of class I release factors." Cell **129**(5): 929-941.

- Gao, N., A. V. Zavialov, W. Li, J. Sengupta, M. Valle, R. P. Gursky, M. Ehrenberg and J. Frank (2005). "Mechanism for the disassembly of the posttermination complex inferred from cryo-EM studies." Mol Cell **18**(6): 663-674.
- Gao, Y. G., M. Selmer, C. M. Dunham, A. Weixlbaumer, A. C. Kelley and V. Ramakrishnan (2009). "The structure of the ribosome with elongation factor G trapped in the posttranslocational state." Science **326**(5953): 694-699.
- Giavalisco, P., D. Wilson, T. Kreitler, H. Lehrach, J. Klose, J. Gobom and P. Fucini (2005). "High heterogeneity within the ribosomal proteins of the *Arabidopsis thaliana* 80S ribosome." Plant Molecular Biology **57**(4): 577-591.
- Gonzalez, R. L., Jr., S. Chu and J. D. Puglisi (2007). "Thiostrepton inhibition of tRNA delivery to the ribosome." RNA **13**(12): 2091-2097.
- Graack, H. R. and B. Wittmann-Liebold (1998). "Mitochondrial ribosomal proteins (MRPs) of yeast." Biochem J **329** (Pt 3): 433-448.
- Grassucci, R. A., D. J. Taylor and J. Frank (2007). "Preparation of macromolecular complexes for cryo-electron microscopy." Nat Protoc **2**(12): 3239-3246.
- Gray, M. W., G. Burger and B. F. Lang (2001). "The origin and early evolution of mitochondria." Genome Biol **2**(6): REVIEWS1018.
- Gregory, S. T. and A. E. Dahlberg (1999). "Erythromycin resistance mutations in ribosomal proteins L22 und L4 perturb the higher order structure of 23S ribosomal RNA." J Mol Biol **289**: 827-834.
- Grewal, J., E. K. Manavathu and D. E. Taylor (1993). "Effect of Mutational Alteration of Asn-128 in the Putative GTP-Binding Domain of Tetracycline Resistance Determinant Tet(O) from *Campylobacter Jejuni*." Antimicrob Agents Chemother **37**: 2645-2649.
- Griffin, M. O., E. Fricovsky, G. Ceballos and F. Villarreal (2010). "Tetracyclines: a pleiotropic family of compounds with promising therapeutic properties. Review of the literature." Am J Physiol Cell Physiol **299**(3): C539-548.
- Grigoriadou, C., S. Marzi, S. Kirillov, C. O. Gualerzi and B. S. Cooperman (2007a). "A quantitative kinetic scheme for 70 S translation initiation complex formation." J Mol Biol **373**(3): 562-572.
- Grigoriadou, C., S. Marzi, D. Pan, C. O. Gualerzi and B. S. Cooperman (2007b). "The translational fidelity function of IF3 during transition from the 30 S initiation complex to the 70 S initiation complex." J Mol Biol **373**(3): 551-561.

- Gruschke, S., K. Gröne, M. Heublein, S. Hölz, L. Israel, A. Imhof, J. M. Herrmann and M. Ott (2010). "Proteins at the Polypeptide Tunnel Exit of the Yeast Mitochondrial Ribosome." J Biol Chem **285**(25): 19022-19028.
- Guerrero, M. D. and J. Modolell (1980). "Hygromycin A, a novel inhibitor of ribosomal peptidyltransferase." Eur J Biochem **107**: 409-414.
- Guo, Q., Y. Yuan, Y. Xu, B. Feng, L. Liu, K. Chen, M. Sun, Z. Yang, J. Lei and N. Gao (2011). "Structural basis for the function of a small GTPase RsgA on the 30S ribosomal subunit maturation revealed by cryoelectron microscopy." Proc Natl Acad Sci USA **108**(32): 13100-13105.
- Guttsell, N. S., M. P. Deutscher and J. Ofengand (2005). "The pseudouridine synthase RluD is required for normal ribosome assembly and function in *Escherichia coli*." RNA **11**: 1141–1152.
- Hage, A. E. and D. Tollervey (2004). "A surfeit of factors: why is ribosome assembly so much more complicated in eukaryotes than bacteria?" RNA Biol **1**(1): 10-15.
- Havelund, J. F., A. M. Giessing, T. Hansen, A. Rasmussen, L. G. Scott and F. Kirpekar (2011). "Identification of 5-hydroxycytidine at position 2501 concludes characterization of modified nucleotides in *E. coli* 23S rRNA." J Mol Biol **411**(3): 529-536.
- Hayes, F. and M. Vasseur (1976). "Processing of the 17S *Escherichia coli* precursor RNA in the 27S pre-ribosomal particle." Eur J Biochem **61**(2): 433-442.
- Hellmuth, K., G. Rex, B. Surin, R. Zinck and J. E. McCarthy (1991). "Translational coupling varying in efficiency between different pairs of genes in the central region of the *atp* operon of *Escherichia coli*." Mol Microbiol **5**(4): 813-824.
- Hiller, D. A., V. Singh, M. Zhong and S. A. Strobel (2011). "A two-step chemical mechanism for ribosome-catalysed peptide bond formation." Nature **476**(7359): 236-239.
- Hirashima, A. and A. Kaji (1973). "Role of elongation factor G and a protein factor on the release of ribosomes from messenger ribonucleic acid." J Biol Chem **248**(21): 7580-7587.
- Hirokawa, G., M. C. Kiel, A. Muto, M. Selmer, V. S. Raj, A. Liljas, K. Igarashi, H. Kaji and A. Kaji (2002). "Post-termination complex disassembly by ribosome recycling factor, a functional tRNA mimic." EMBO J **21**(9): 2272-2281.
- Huang, C. Y., M. A. Ayliffe and J. N. Timmis (2003). "Direct measurement of the transfer rate of chloroplast DNA into the nucleus." Nature **422**(6927): 72-76.

- Huang, L., L. Hung, M. Odell, H. Yokota, R. Kim and S. H. Kim (2002). "Structure-based experimental confirmation of biochemical function to a methyltransferase, MJ0882, from hyperthermophile *Methanococcus jannaschii*." J Struct Funct Genomics **2**(3): 121-127.
- Huang, L., J. Ku, M. Pookanjanatavip, X. Gu, D. Wang, P. J. Greene and D. V. Santi (1998). "Identification of two *Escherichia coli* pseudouridine synthases that show multisite specificity for 23S RNA." Biochemistry **37**(45): 15951-15957.
- Huang, Y. J., G. V. T. Swapna, P. K. Rajan, H. Ke, B. Xia, K. Shukla, M. Inouye and G. T. Montelione (2003). "Solution NMR Structure of Ribosome-binding Factor A (RbfA), A Cold-shock Adaptation Protein from *Escherichia coli*." J Mol Biol **327**(2): 521-536.
- Inoue, K., J. Alsina, J. Chen and M. Inouye (2003). "Suppression of defective ribosome assembly in a *rbfA* deletion mutant by overexpression of Era, an essential GTPase in *Escherichia coli*." Mol Microbiol **48**(4): 1005-1016.
- Inoue, K., J. Chen, Q. Tan and M. Inouye (2006). "Era and RbfA Have Overlapping Function in Ribosome Biogenesis in *Escherichia coli*." J Mol Microbiol Biotechnol **11**(1-2): 41-52.
- Iost, I. and M. Dreyfus (2006). "DEAD-box RNA helicases in *Escherichia coli*." Nucleic Acids Res. **34**(15): 4189–4197.
- Jemiolo, D. K., J. S. Taurence and S. Giese (1991). "Mutations in 16S rRNA in *Escherichia coli* at methyl-modified sites: G966, C967, and G1207." Nucleic Acids Res **19**(15): 4259-4265.
- Jenner, L. B., N. Demeshkina, G. Yusupova and M. Yusupov (2010). "Structural aspects of messenger RNA reading frame maintenance by the ribosome." Nat Struct Mol Biol **17**(5): 555-560.
- Jin, H., A. C. Kelley, D. Loakes and V. Ramakrishnan (2010). "Structure of the 70S ribosome bound to release factor 2 and a substrate analog provides insights into catalysis of peptide release." Proc Natl Acad Sci USA **107**(19): 8593-8598.
- Jin, H., A. C. Kelley and V. Ramakrishnan (2011). "Crystal structure of the hybrid state of ribosome in complex with the guanosine triphosphatase release factor 3." Proc Natl Acad Sci USA **108**(38): 15798-15803.
- Julian, P., A. L. Konevega, S. H. Scheres, M. Lazaro, D. Gil, W. Wintermeyer, M. V. Rodnina and M. Valle (2008). "Structure of ratcheted ribosomes with tRNAs in hybrid states." Proc Natl Acad Sci USA **105**(44): 16924-16927.

- Julian, P., P. Milon, X. Agirrezabala, G. Lasso, D. Gil, M. V. Rodnina and M. Valle (2011). "The Cryo-EM structure of a complete 30S translation initiation complex from *Escherichia coli*." PLoS Biol **9**(7): e1001095.
- Kaczanowska, M. and M. Ryden-Aulin (2007). "Ribosome Biogenesis and the Translation Process in *Escherichia coli*." Microbiol Mol Biol Rev **71**(3): 477-494.
- Kaltschmidt, E. and H. G. Wittmann (1970). "Ribosomal proteins XII. Number of proteins in small and large subunits of *Escherichia coli* as determined by two-dimensional gel electrophoresis." Proc Natl Acad Sci USA **67**: 1276-1282.
- Kaminishi, T., D. N. Wilson, C. Takemoto, J. M. Harms, M. Kawazoe, F. Schlutzen, K. Hanawa-Suetsugu, M. Shirouzu, P. Fucini and S. Yokoyama (2007). "A snapshot of the 30S ribosomal subunit capturing mRNA via the Shine-Dalgarno interaction." Structure **15**(3): 289-297.
- Kang, W. K., T. Icho, S. Isono, M. Kitakawa and K. Isono (1989). "Characterization of the gene *rimK* responsible for the addition of glutamic acid residues to the C-terminus of ribosomal protein S6 in *Escherichia coli* K12." Mol Gen Genet **217**(2-3): 281-288.
- Karbstein, K. (2007). "Role of GTPases in ribosome assembly." Biopolymers **87**(1): 1-11.
- Karimi, R. and M. Ehrenberg (1994). "Dissociation rate of cognate peptidyl-tRNA from the A-site of hyper-accurate and error-prone ribosomes." Eur J Biochem **226**: 355-360.
- Karimi, R., M. Pavlov, R. Buckingham and M. Ehrenberg (1999). "Novel roles for classical factors at the interface between translation termination and initiation." Mol Cell **3**: 601-609.
- Kim do, J., J. Y. Jang, H. J. Yoon and S. W. Suh (2008). "Crystal structure of YlqF, a circularly permuted GTPase: implications for its GTPase activation in 50 S ribosomal subunit assembly." Proteins **72**(4): 1363-1370.
- King, T. C., R. Sirdeshmukh and D. Schlessinger (1984). "RNase III cleavage is obligate for maturation but not for function of *Escherichia coli* pre-23S rRNA." Proc Natl Acad Sci USA **81**(1): 185-188.
- Kino, K., T. Arai and Y. Arimura (2011). "Poly-alpha-glutamic acid synthesis using a novel catalytic activity of RimK from *Escherichia coli* K-12." Appl Environ Microbiol **77**(6): 2019-2025.
- Kitakawa, M. and K. Isono (1991). "The Mitochondrial Ribosomes." Biochimie **73**: 813-825.

- Klaholz, B. P., T. Pape, A. V. Zavialov, A. G. Myasnikov, E. V. Orlova, B. Vestergaard, M. Ehrenberg and M. Van Heel (2003). "Structure of the *Escherichia coli* ribosomal termination complex with release factor 2." Nature **421**(6918): 90-94.
- Klastersky, J. and D. Daneau (1972). "Bacteriological evaluation of minocycline, a new tetracycline." Chemotherapy **17**(1): 51-58.
- Klinge, S., F. Voigts-Hoffmann, M. Leibundgut, S. Arpagaus and N. Ban (2011). "Crystal structure of the eukaryotic 60S ribosomal subunit in complex with initiation factor 6." Science **334**(6058): 941-948.
- Koc, E. C., W. Burkhart, K. Blackburn, A. Moseley and L. L. Spremulli (2001a). "The small subunit of the mammalian mitochondrial ribosome. Identification of the full complement of ribosomal proteins present." J Biol Chem **276**(22): 19363-19374.
- Koc, E. C., W. Burkhart, K. Blackburn, M. B. Moyer, D. M. Schlatzer, A. Moseley and L. L. Spremulli (2001b). "The large subunit of the mammalian mitochondrial ribosome. Analysis of the complement of ribosomal proteins present." J Biol Chem **276**(47): 43958-43969.
- Kohanski, M. A., D. J. Dwyer, B. Hayete, C. A. Lawrence and J. J. Collins (2007). "A common mechanism of cellular death induced by bactericidal antibiotics." Cell **130**(5): 797-810.
- Korostelev, A., H. Asahara, L. Lancaster, M. Laurberg, A. Hirschi, J. Zhu, S. Trakhanov, W. G. Scott and H. F. Noller (2008). "Crystal structure of a translation termination complex formed with release factor RF2." Proc Natl Acad Sci USA **105**(50): 19684-19689.
- Korostelev, A., J. Zhu, H. Asahara and H. F. Noller (2010). "Recognition of the amber UAG stop codon by release factor RF1." Embo J **29**(15): 2577-2585.
- Kowalak, J. A., E. Bruenger, P. F. Crain and J. A. McCloskey (2000). "Identities and phylogenetic comparisons of posttranscriptional modifications in 16 S ribosomal RNA from *Haloferax volcanii*." J Biol Chem **275**(32): 24484-24489.
- Kowalak, J. A., E. Bruenger, T. Hashizume, J. M. Peltier, J. Ofengand and J. A. McCloskey (1996). "Structural characterization of U^{*}-1915 in domain IV from *Escherichia coli* 23S ribosomal RNA as 3-methylpseudouridine." Nucleic Acids Res **24**(4): 688-693.
- Kukimoto-Niino, M., K. Murayama, M. Inoue, T. Terada, J. R. Tame, S. Kuramitsu, M. Shirouzu and S. Yokoyama (2004). "Crystal structure of the GTP-binding protein Obg from *Thermus thermophilus* HB8." J Mol Biol **337**: 761-770.

- Laemmli, U. K. (1970). "Cleavage of structural proteins during the assembly of the head of bacteriophage T4." Nature **227**: 680-685.
- Laurberg, M., H. Asahara, A. Korostelev, J. Zhu, S. Trakhanov and H. F. Noller (2008). "Structural basis for translation termination on the 70S ribosome." Nature **454**(7206): 852-857.
- Lecompte, O., R. Ripp, J. C. Thierry, D. Moras and O. Poch (2002). "Comparative analysis of ribosomal proteins in complete genomes: an example of reductive evolution at the domain scale." Nucleic Acids Res. **30**(24): 5382-5390.
- Lee, S., S. Berger, S. Martinovic, L. Pasa-Tolic, G. Anderson, Y. Shen, R. Zhao and R. Smith (2002). "Direct mass spectrometric analysis of intact proteins of the yeast large ribosomal subunit using capillary LC/FTICR." Proc Natl Acad Sci USA **99**(9): 5942-5947.
- Leonov, A. A., P. V. Sergiev, A. A. Bogdanov, R. Brimacombe and O. A. Dontsova (2003). "Affinity purification of ribosomes with a lethal G2655C mutation in 23 S rRNA that affects the translocation." J Biol Chem **278**(28): 25664-25670.
- Leppik, M., L. Peil, K. Kipper, A. Liiv and J. Remme (2007). "Substrate specificity of the pseudouridine synthase RluD in *Escherichia coli*." Febs J **274**(21): 5759-5766.
- Lesnyak, D. V., J. Osipiuk, T. Skarina, P. V. Sergiev, A. A. Bogdanov, A. Edwards, A. Savchenko, A. Joachimiak and O. A. Dontsova (2006). "Methyltransferase That Modifies Guanine 966 of the 16 S rRNA: Functional Identification and tertiary structure." J Biol Chem **282**(8): 5880-5887.
- Lewicki, B. T. U., T. Margus, J. Remme and K. H. Nierhaus (1993). "Coupling of rRNA transcription and ribosomal assembly *in vivo* - formation of active ribosomal subunits in *Escherichia coli* requires transcription of rRNA genes by host RNA polymerase which cannot be replaced by bacteriophage-T7 RNA polymerase." J Mol Biol **231**: 581-593.
- Li, Z., S. Pandit and M. P. Deutscher (1999a). "Maturation of 23S ribosomal RNA requires the exoribonuclease RNase T." RNA **5**(1): 139-146.
- Li, Z., S. Pandit and M. P. Deutscher (1999b). "RNase G (CafA protein) and RNase E are both required for the 5' maturation of 16S ribosomal RNA." EMBO J **18**(10): 2878-2885.
- Li, Z. W. and M. P. Deutscher (1995). "The tRNA processing enzyme RNase T is essential for maturation of 5S RNA." Proc Natl Acad Sci USA **92**(15): 6883-6886.

- Link, A., J. Eng, D. Schieltz, E. Carmack, G. Mize, D. Morris, B. Garvik and J. r. Yates (1999). "Direct analysis of protein complexes using mass spectrometry." Nat Biotechnol **17**(7): 676-682.
- Liou, Y. and N. Tanaka (1976). "Dual actions of viomycin on the ribosomal functions." Biochem Biophys Res Commun **71**: 477-483.
- Lövgren, J. M., G. O. Bylund, M. K. Srivastava, L. A. Lundberg, O. P. Persson, G. Wingsle and P. M. Wikström (2004). "The PRC-barrel domain of the ribosome maturation protein RimM mediates binding to ribosomal protein S19 in the 30S ribosomal subunits." RNA **10**(11): 1798-1812.
- Lövgren, J. M. and P. M. Wikström (2001). "Hybrid Protein between Ribosomal Protein S16 and RimM of *Escherichia coli* Retains the Ribosome Maturation Function of Both Proteins." J Bacteriol **183**(18): 5352-5357.
- Maguire, B. A., A. D. Beniaminov, H. Ramu, A. S. Mankin and R. A. Zimmermann (2005). "A protein component at the heart of an RNA machine: the importance of protein I27 for the function of the bacterial ribosome." Mol Cell **20**(3): 427-435.
- Maki, J. A., D. J. Schnobrich and G. M. Culver (2002). "The DnaK chaperone system facilitates 30S ribosomal subunit assembly." Mol Cell **10**(1): 129-138.
- Maki, J. A., D. R. Southworth and G. M. Culver (2003). "Demonstration of the role of the DnaK chaperone system in assembly of 30S ribosomal subunits using a purified *in vitro* system." RNA **9**(12): 1418-1421.
- Martemyanov, K. A. and A. T. Gudkov (2000). "Domain III of elongation factor G from *Thermus thermophilus* is essential for induction of GTP hydrolysis on the ribosome." J Biol Chem **275**(46): 35820-35824.
- Martemyanov, K. A., A. S. Yarunin, A. Liljas and A. T. Gudkov (1998). "An intact conformation at the tip of elongation factor G domain IV is functionally important." FEBS Lett **434**(1-2): 205-208.
- Martin, W. and R. G. Herrmann (1998). "Gene transfer from organelles to the nucleus: how much, what happens, and Why?" Plant Physiol **118**(1): 9-17.
- Maslov, D. A., M. R. Sharma, E. Butler, A. M. Falick, M. Gingery, R. K. Agrawal, L. L. Spremulli and L. Simpson (2006). "Isolation and characterization of mitochondrial ribosomes and ribosomal subunits from *Leishmania tarentolae*." Mol Biochem Parasitol **148**(1): 69-78.

- Milon, P., M. Carotti, A. L. Konevega, W. Wintermeyer, M. V. Rodnina and C. O. Gualerzi (2010). "The ribosome-bound initiation factor 2 recruits initiator tRNA to the 30S initiation complex." EMBO Rep
- Milon, P., A. L. Konevega, C. O. Gualerzi and M. V. Rodnina (2008). "Kinetic Checkpoint at a Late Step in Translation Initiation." Mol Cell **30**(6): 712-720.
- Misumi, M., T. Nishimura, T. Komai and N. Tanaka (1978). "Interaction of kanamycin and related antibiotics with the large subunit of ribosomes and the inhibition of translocation." Biochem Biophys Res Commun **84**(2): 358-365.
- Mittelstaet, J., A. L. Konevega and M. V. Rodnina (2011). "Distortion of tRNA upon near-cognate codon recognition on the ribosome." J Biol Chem **286**(10): 8158-8164.
- Moazed, D. and H. F. Noller (1987). "Interaction of antibiotics with functional sites in 16S ribosomal RNA." Nature **327**: 389-394.
- Moazed, D. and H. F. Noller (1989). "Intermediate states in the movement of transfer RNA in the ribosome." Nature **342**: 142-148.
- Moazed, D. and H. F. Noller (1990). "Binding of tRNA to the ribosomal A and P sites protects two distinct sets of nucleotides in the 16S rRNA." J Mol Biol **211**: 135-145.
- Modolell, J. and D. Vazquez (1977). "The inhibition of ribosomal translocation by viomycin." Eur J Biochem **81**: 491-497.
- Mohr, D., W. Wintermeyer and M. V. Rodnina (2002). "GTPase activation of elongation factors Tu and G on the ribosome." Biochemistry **41**: 12520-12528.
- Moore, V. G., R. E. Atchison, G. Thomas, M. Moran and H. F. Noller (1975). "Identification of a ribosomal protein essential for peptidyl transferase activity." Proc Natl Acad Sci USA **72**(3): 844-848.
- Muench, S. P., L. Xu, S. E. Sedelnikova and D. W. Rice (2006). "The essential GTPase YphC displays a major domain rearrangement associated with nucleotide binding." Proc Natl Acad Sci USA **103**: 12359-12364.
- Myasnikov, A., S. Marzi, A. Simonetti, A. Giuliadori, C. Gualerzi, G. Yusupova, M. Yusupov and B. Klaholz (2005). "Conformational transition of initiation factor 2 from the GTP- to GDP-bound state visualized on the ribosome." Nat Struct Mol Biol **12**(12): 1145-1149.
- Nakamoto, T. (2009). "Evolution and the universality of the mechanism of initiation of protein synthesis." Gene **432**(1-2): 1-6.

- Nechifor, R., M. Murataliev and K. S. Wilson (2007). "Functional interactions between the G' subdomain of bacterial translation factor EF-G and ribosomal protein L7/L12." J Biol Chem **282**(51): 36998-37005.
- Nierhaus, K. H. (1991). "The assembly of prokaryotic ribosomes." Biochimie **73**(6): 739-755.
- Noller, H. F. and C. R. Woese (1981). "Secondary structure of 16S ribosomal RNA." Science **212**(4493): 403-411.
- Nomura, M., R. Gourse and G. Baughman (1984). "Regulation of the synthesis of ribosomes and ribosomal components." Ann Rev Biochem **53**: 75-117.
- O'Brien, T. W. (2002). "Evolution of a protein-rich mitochondrial ribosome: implications for human genetic disease." Gene **286**(1): 73-79.
- Odintsova, T. I., E. C. Muller, A. V. Ivanov, T. A. Egorov, R. Bienert, S. N. Vladimirov, S. Kostka, A. Otto, B. Wittmann-Liebold and G. G. Karpova (2003). "Characterization and analysis of posttranslational modifications of the human large cytoplasmic ribosomal subunit proteins by mass spectrometry and Edman sequencing." J Protein Chem **22**(3): 249-258.
- Ogle, J. M., D. E. Brodersen, W. M. Clemons Jr, M. J. Tarry, A. P. Carter and V. Ramakrishnan (2001). "Recognition of cognate transfer RNA by the 30S ribosomal subunit." Science **292**(5518): 897-902.
- Ogle, J. M., F. V. Murphy, M. J. Tarry and V. Ramakrishnan (2002). "Selection of tRNA by the ribosome requires a transition from an open to a closed form." Cell **111**(5): 721-732.
- Ortiz-Meoz, R. F. and R. Green (2010). "Functional elucidation of a key contact between tRNA and the large ribosomal subunit rRNA during decoding." RNA **16**(10): 2002-2013.
- Otaka, T. and A. Kaji (1975). "Release of (oligo)peptidyl-tRNA from ribosomes by erythromycin A." Proc Natl Acad Sci USA **72**(7): 2649-2652.
- Pai, R. D., W. Zhang, B. S. Schuwirth, G. Hirokawa, H. Kaji, A. Kaji and J. H. D. Cate (2008). "Structural Insights into Ribosome Recycling Factor Interactions with the 70S Ribosome." J Mol Biol **376**(5): 1334-1347.
- Pape, T., W. Wintermeyer and M. V. Rodnina (2000). "Conformational switch in the decoding region of 16S rRNA during aminoacyl-tRNA selection on the ribosome." Nat Struct Biol **7**(2): 104-107.

- Parmeggiani, A. and P. Nissen (2006). "Elongation factor Tu-targeted antibiotics: four different structures, two mechanisms of action." FEBS Lett **580**(19): 4576-4581.
- Pel, H. J. and L. A. Grivell (1994). "Protein synthesis in mitochondria." Mol Biol Rep **19**(3): 183-194.
- Persson, B. C., G. O. Bylund, D. E. Berg and P. M. Wikström (1995). "Functional analysis of the *ffh-trmD* region of the *Escherichia coli* chromosome by using reverse genetics." J Bacteriol **177**(19): 5554-5560.
- Peske, F., M. Rodnina and W. Wintermeyer (2005). "Sequence of steps in ribosome recycling as defined by kinetic analysis." Mol Cell **18**(4): 403-412.
- Pestka, S. (1969). "Studies on the formation of transfer ribonucleic acid-ribosome complexes. X. Phenylalanyl-oligonucleotide binding to ribosomes and the mechanism of chloramphenicol action." Biochem Biophys Res Commun **36**: 589-595.
- Petry, S., D. Brodersen, F. t. Murphy, C. Dunham, M. Selmer, M. Tarry, A. Kelley and V. Ramakrishnan (2005a). "Crystal structures of the ribosome in complex with release factors RF1 and RF2 bound to a cognate stop codon." Cell **123**(7): 1255-1266.
- Pettersen, E. F., T. D. Goddard, C. C. Huang, G. S. Couch, D. M. Greenblatt, E. C. Meng and T. E. Ferrin (2004). "UCSF Chimera - A Visualization System for Exploratory Research and Analysis." J Comput Chem **25**(13): 1605-1612.
- Pioletti, M., F. Schlunzen, J. Harms, R. Zarivach, M. Gluhmann, H. Avila, A. Bashan, H. Bartels, T. Auerbach, C. Jacobi, T. Hartsch, A. Yonath and F. Franceschi (2001). "Crystal structures of complexes of the small ribosomal subunit with tetracycline, edeine and IF3." EMBO J **20**(8): 1829-1839.
- Purta, E., K. H. Kaminska, J. M. Kasprzak, J. M. Bujnicki and S. Douthwaite (2008). "YbeA is the m3 methyltransferase RlmH that targets nucleotide 1915 in 23S rRNA." RNA **14**(10): 2234-2244.
- Rabl, J., M. Leibundgut, S. F. Ataide, A. Haag and N. Ban (2010). "Crystal structure of the eukaryotic 40S ribosomal subunit in complex with initiation factor 1." Science **331**(6018): 730-736.
- Ramirez, C., K. A. Louie and A. T. Matheson (1991). "A small basic ribosomal protein from the extreme thermophilic archaeobacterium *Sulfolobus solfataricus* that has no equivalent in *Escherichia coli*." FEBS Lett **284**(1): 39-41.

- Rasmussen, B. A., Y. Gluzman and F. P. Tally (1994). "Inhibition of protein synthesis occurring on tetracycline-resistant, TetM-protected ribosomes by a novel class of tetracyclines, the glycylcyclines." Antimicrob Agents Chemother **38**(7): 1658-1660.
- Ratje, A. H., J. Loerke, A. Mikolajka, M. Brunner, P. W. Hildebrand, A. L. Starosta, A. Dönhöfer, S. R. Connell, P. Fucini, T. Mielke, P. C. Whitford, J. N. Onuchic, Y. Yu, K. Y. Sanbonmatsu, R. K. Hartmann, P. A. Penczek, D. N. Wilson and C. M. Spahn (2010). "Head swivel on the ribosome facilitates translocation by means of intra-subunit tRNA hybrid sites." Nature **468**(7324): 713-716.
- Rawat, U. B., A. V. Zavialov, J. Sengupta, M. Valle, R. A. Grassucci, J. Linde, B. Vestergaard, M. Ehrenberg and J. Frank (2003). "A cryo-electron microscopic study of ribosome-bound termination factor RF2." Nature **421**(6918): 87-90.
- Raychaudhuri, S., J. Conrad, B. G. Hall and J. Ofengand (1998). "A pseudouridine synthase required for the formation of two universally conserved pseudouridines in ribosomal RNA is essential for normal growth of *Escherichia coli*." RNA **4**(11): 1407-1417.
- Reeh, S. and S. Pedersen (1979). "Post-translational modification of *Escherichia coli* ribosomal protein S6." Mol Gen Genet **173**(2): 183-187.
- Rex, G., B. Surin, G. Besse, B. Schneppe and J. E. G. McCarthy (1994). "The mechanism of translational coupling in *Escherichia coli* - Higher order structure in the atpHA mRNA acts as a conformational switch regulating the access of *de novo* initiating ribosomes." J Biol Chem **269**(27): 18118-18127.
- Rheinberger, H. J. and K. H. Nierhaus (1990). "Partial release of AcPhe-Phe-transfer RNA from ribosomes during Poly(U)-dependent Poly(Phe) synthesis and the effects of chloramphenicol." Eur J Biochem **193**: 643-650.
- Ridenhour, M. B., H. M. Fletcher, J. E. Mortensen and L. Daneo-Moore (1996). "A novel tetracycline-resistant determinant, tet(U), is encoded on the plasmid pKq10 in *Enterococcus faecium*." Plasmid **35**(2): 71-80.
- Robertson, H. D., R. E. Webster and N. D. Zinder (1968). "Purification and properties of ribonuclease III from *Escherichia coli*." J Biol Chem **243**(1): 82-91.
- Robinson, V., J. Hwang, E. Fox, M. Inouye and A. Stock (2002). "Domain arrangement of Der, a switch protein containing two GTPase domains." Structure **10**(12): 1649-1658.

- Rodnina, M. V., R. Fricke and W. Wintermeyer (1994). "Transient conformational states of aminoacyl-tRNA during ribosome binding catalyzed by elongation factor Tu." Biochemistry **33**(40): 12267-12275.
- Rodnina, M. V., A. Savelsbergh, V. I. Katunin and W. Wintermeyer (1997). "Hydrolysis of GTP by elongation factor G drives tRNA movement on the ribosome." Nature **385**(6611): 37-41.
- Roy, M. K., B. Singh, B. K. Ray and D. Apirion (1983). "Maturation of 5S rRNA: ribonuclease E cleavages and their dependence on precursor sequences." Eur J Biochem **131**(1): 119-127.
- Ruusala, T., M. Ehrenberg and C. G. Kurland (1982). "Catalytic effects of elongation factor Ts on polypeptide synthesis." Embo J **1**(1): 75-78.
- Ruzheinikov, S. N., S. K. Das, S. E. Sedelnikova, P. J. Baker, P. J. Artymiuk, J. Garcia-Lara, S. J. Foster and D. W. Rice (2004). "Analysis of the open and closed conformations of the GTP-binding protein Ysx C from *Bacillus subtilis*." J Mol Biol **339**: 265-278.
- Sambrook, J., E. F. Fritsch and T. Maniatis (1989). Molecular Cloning, a laboratory manual: 2nd edition. Cold Spring Harbour, NY, Cold Spring Harbour Laboratory Press.
- Sanchez-Pescador, R., J. T. Brown, M. Roberts and M. S. Urdea (1988). "Homology of the TetM with translational elongation factors: implications for potential modes of tetM-conferred tetracycline resistance." Nucleic Acids Res **16**(3): 1218.
- Savelsbergh, A., N. B. Matassova, M. V. Rodnina and W. Wintermeyer (2000). "Role of domains 4 and 5 in elongation factor G functions on the ribosome." J Mol Biol **300**(4): 951-961.
- Savelsbergh, A., D. Mohr, U. Kothe, W. Wintermeyer and M. V. Rodnina (2005). "Control of phosphate release from elongation factor G by ribosomal protein L7/12." EMBO J **24**: 4316–4323.
- Savelsbergh, A., M. V. Rodnina and W. Wintermeyer (2009). "Distinct functions of elongation factor G in ribosome recycling and translocation." RNA **15**(5): 772-780.
- Schlutzen, F., C. Takemoto, D. N. Wilson, T. Kaminishi, J. M. Harms, K. Hanawa-Suetsugu, W. Szaflarski, M. Kawazoe, M. Shirouzu, K. H. Nierhaus, S. Yokoyama and P. Fucini (2006). "The antibiotic kasugamycin mimics mRNA nucleotides to destabilize tRNA binding and inhibit canonical translation initiation." Nat Struct Mol Biol **13**(10): 871-878.

- Schlünzen, F., R. Zarivach, J. Harms, A. Bashan, A. Tocilj, R. Albrecht, A. Yonath and F. Franceschi (2001). "Structural basis for the interaction of antibiotics with the peptidyl transferase centre in eubacteria." Nature **413**(6858): 814-821.
- Schmeing, T. M. and V. Ramakrishnan (2009). "What recent ribosome structures have revealed about the mechanism of translation." Nature **461**(7268): 1234-1242.
- Schmeing, T. M., R. M. Voorhees, A. C. Kelley, Y. G. Gao, F. V. t. Murphy, J. R. Weir and V. Ramakrishnan (2009). "The crystal structure of the ribosome bound to EF-Tu and aminoacyl-tRNA." Science **326**(5953): 688-694.
- Schuetz, J. C., F. V. t. Murphy, A. C. Kelley, J. R. Weir, J. Giesebrecht, S. R. Connell, J. Loerke, T. Mielke, W. Zhang, P. A. Penczek, V. Ramakrishnan and C. M. Spahn (2009). "GTPase activation of elongation factor EF-Tu by the ribosome during decoding." Embo J **28**(6): 755-765.
- Scolnick, E., R. Tompkins, T. Caskey and M. Nirenberg (1968). "Release factors differing in specificity for terminator codons." Proc Natl Acad Sci USA **61**: 768-774.
- Seo, H., M. Kiel, D. Pan, V. Raj, A. Kaji and B. Cooperman (2004). "Kinetics and thermodynamics of RRF, EF-G, and thiostrepton interaction on the *Escherichia coli* ribosome." Biochemistry **43**(40): 12728-12740.
- Sergiev, P. V., A. A. Bogdanov and O. A. Dontsova (2007). "Ribosomal RNA guanine-(N2)-methyltransferases and their targets." Nucleic Acids Res **35**(7): 2295-2301.
- Sharma, M. R., C. Barat, D. N. Wilson, T. M. Booth, M. Kawazoe, C. Hori-Takemoto, M. Shirouzu, S. Yokoyama, F. P. and R. K. Agrawal (2005). "Interaction of Era with the 30S Ribosomal Subunit: Implications for 30S Subunit Assembly." Mol Cell **18**(3): 319-329.
- Sharma, M. R., T. M. Booth, L. Simpson, D. A. Maslov and R. K. Agrawal (2009). "Structure of a mitochondrial ribosome with minimal RNA." Proc Natl Acad Sci USA **106**(24): 9637-9642.
- Sharma, M. R., E. C. Koc, P. P. Datta, T. M. Booth, L. L. Spemulli and R. K. Agrawal (2003). "Structure of the mammalian mitochondrial ribosome reveals an expanded functional role for its component proteins." Cell **115**(1): 97-108.
- Sharma, M. R., D. N. Wilson, P. P. Datta, C. Barat, F. Schlunzen, P. Fucini and R. K. Agrawal (2007). "Cryo-EM study of the spinach chloroplast ribosome reveals the

- structural and functional roles of plastid-specific ribosomal proteins." Proc Natl Acad Sci USA **104**(49): 19315-19320.
- Shaw, J. J. and R. Green (2007). "Two distinct components of release factor function uncovered by nucleophile partitioning analysis." Mol Cell **28**(3): 458-467.
- Sheridan, R. P. and I. Chopra (1991). "Origin of tetracycline efflux proteins: conclusions from nucleotide sequence analysis." Mol Microbiol **5**(4): 895-900.
- Shin, D. H., Y. Lou, J. Jancarik, H. Yokota, R. Kim and S.-H. Kim (2004). "Crystal structure of YjeQ from *Thermotoga maritima* contains a circularly permuted GTPase domain." Proc Natl Acad Sci USA **101**(36): 13198-13203.
- Shine, J. and L. Dalgarno (1974). "The 3'-terminal sequence of *E. coli* 16S rRNA: Complementarity to nonsense triplets and ribosome binding sites." Proc Natl Acad Sci USA **71**(4): 1342-1346.
- Shoji, S., S. E. Walker and K. Fredrick (2006). "Reverse translocation of tRNA in the ribosome." Mol Cell **24**(6): 931-942.
- Simonetti, A., S. Marzi, A. G. Myasnikov, A. Fabbretti, M. Yusupov, C. O. Gualerzi and B. P. Klaholz (2008). "Structure of the 30S translation initiation complex." Nature **455**(7211): 416-420.
- Singh, N., G. Das, A. Seshadri, R. Sangeetha and U. Varshney (2005). "Evidence for a role of initiation factor 3 in recycling of ribosomal complexes stalled on mRNAs in *Escherichia coli*." Nucleic Acids Res **33**(17): 5591-5601.
- Sirdeshmukh, R. and D. Schlessinger (1985). "Ordered processing of *Escherichia coli* 23S rRNA *in vitro*." Nucleic Acids Res **13**: 5041-5054.
- Skeggs, P. A., J. Thompson and E. Cundliffe (1985). "Methylation of 16 S ribosomal RNA and resistance to aminoglycoside antibiotics in clones of *Streptomyces lividans* carrying DNA from *Streptomyces tenjimariensis*." Mol Gen Genet **200**(3): 415-421.
- Söding, J., A. Biegert and A. N. Lupas (2005). "The HHpred interactive server for protein homology detection and structure prediction." Nucleic Acids Res **33**(Web Server issue): W244-248.
- Soleimanpour-Lichaei, H. R., I. Kuhl, M. Gaisne, J. F. Passos, M. Wydro, J. Rorbach, R. Temperley, N. Bonnefoy, W. Tate, R. Lightowlers and Z. Chrzanowska-Lightowlers (2007). "mtRF1a is a human mitochondrial translation release factor decoding the major termination codons UAA and UAG." Mol Cell **27**(5): 745-757.

- Somanchi, A. and S. P. Mayfield (1999). "Nuclear-chloroplast signalling." Curr Opin Plant Biol **2**(5): 404-409.
- Song, H., P. Mugnier, A. Das, H. Webb, D. Evans, M. Tuite, B. Hemmings and D. Barford (2000). "The crystal structure of human eukaryotic release factor eRF1 - Mechanism of stop codon recognition and peptidyl-tRNA hydrolysis." Cell **100**: 311-321.
- Spahn, C. M., G. Blaha, R. K. Agrawal, P. Penczek, R. A. Grassucci, C. A. Trieber, S. R. Connell, D. E. Taylor, K. H. Nierhaus and J. Frank (2001). "Localization of the ribosomal protection protein Tet(O) on the ribosome and the mechanism of tetracycline resistance." Mol Cell **7**(5): 1037-1045.
- Spahn, C. M., E. Jan, A. Mulder, R. A. Grassucci, P. Sarnow and J. Frank (2004). "Cryo-EM visualization of a viral internal ribosome entry site bound to human ribosomes; the IRES functions as an RNA-based translation factor." Cell **118**(4): 465-475.
- Speer, B. S., L. Bedzyk and A. A. Salyers (1991). "Evidence that a novel tetracycline resistance gene found on two *Bacteroides* transposons encodes an NADP-requiring oxidoreductase." J Bacteriol **173**(1): 176-183.
- Suzuki, S., A. Tatsuguchi, E. Matsumoto, M. Kawazoe, T. Kaminishi, M. Shirouzu, Y. Muto, C. Takemoto and S. Yokoyama (2007). "Structural Characterization of the Ribosome Maturation Protein, RimM." J Bacteriol **189**(17): 6397-6406.
- Tan, J., U. Jakob and J. C. A. Bardwell (2002). "Overexpression of Two Different GTPases Rescues a Null Mutation in a Heat-Induced rRNA Methyltransferase." J Bacteriol **184**(10): 2692-2698.
- Taylor, D. E. and A. Chau (1996). "Tetracycline resistance mediated by ribosomal protection." Antimicrob Agents Chemother **40**(1): 1-5.
- Tenson, T., M. Lovmar and M. Ehrenberg (2003). "The mechanism of action of macrolides, lincosamides and streptogramin B reveals the nascent peptide exit path in the ribosome." J Mol Biol **330**(5): 1005-1014.
- Teplova, M., V. Tereshko, R. Sanishvili, A. Joachimiak, T. Bushueva, W. F. Anderson and M. Egli (2000). "The structure of the *yrdC* gene product from *Escherichia coli* reveals a new fold and suggests a role in RNA binding." Protein Sci **9**: 2557-2566.
- Timmis, J. N., M. A. Ayliffe, C. Y. Huang and W. Martin (2004). "Endosymbiotic gene transfer: organelle genomes forge eukaryotic chromosomes." Nat Rev Genet **5**(2): 123-135.

- Tomsic, J., L. A. Vitali, T. Daviter, A. Savelsbergh, R. Spurio, P. Striebeck, W. Wintermeyer, M. V. Rodnina and C. O. Gualerzi (2000). "Late events of translation initiation in bacteria: a kinetic analysis." EMBO J **19**(9): 2127-2136.
- Traub, P. and M. Nomura (1968). "Reconstitution of functionally active 30S ribosomal particles from RNA and proteins." Proc Natl Acad Sci USA **59**: 777-784.
- Trieber, C. A., N. Burkhardt, K. H. Nierhaus and D. E. Taylor (1998). "Ribosomal Protection from Tetracycline Mediated by Tet(O): Tet(O) Interaction with Ribosomes Is GTP-Dependent." Biol Chem **379**: 847-855.
- Trobro, S. and J. Aqvist (2008). "Role of ribosomal protein L27 in peptidyl transfer." Biochemistry **47**(17): 4898-4906.
- Usary, J. and W. S. Champney (2001). "Erythromycin inhibition of 50S ribosomal subunit formation in *Escherichia coli* cells." Mol Microbiol **40**(4): 951-962.
- Valle, M., A. Zavialov, J. Sengupta, U. Rawat, M. Ehrenberg and J. Frank (2003). "Locking and unlocking of ribosomal motions." Cell **114**(1): 123-134.
- Vanet, A., J. A. Plumbridge, M. F. Guerin and J. H. Alix (1994). "Ribosomal protein methylation in *Escherichia coli*: The gene *prmA*, encoding the ribosomal protein L11 methyltransferase, is dispensable." Mol Microbiol **14**: 947-958.
- Villa, E., J. Sengupta, L. G. Trabuco, J. LeBarron, W. T. Baxter, T. R. Shaikh, R. A. Grassucci, P. Nissen, M. Ehrenberg, K. Schulten and J. Frank (2009). "Ribosome-induced changes in elongation factor Tu conformation control GTP hydrolysis." Proc Natl Acad Sci USA **106**(4): 1063-1068.
- Vladimirov, S. N., A. V. Ivanov, G. G. Karpova, A. K. Musolyamov, T. A. Egorov, B. Thiede, B. Wittmannliedbold and A. Otto (1996). "Characterization of the human small-ribosomal-subunit proteins by N-terminal and internal sequencing, and mass spectrometry." Eur J Biochem **239**(1): 144-149.
- Volkers, G., G. J. Palm, M. S. Weiss, G. D. Wright and W. Hinrichs (2011). "Structural basis for a new tetracycline resistance mechanism relying on the TetX monooxygenase." FEBS Lett **585**(7): 1061-1066.
- Voorhees, R. M., T. M. Schmeing, A. C. Kelley and V. Ramakrishnan (2010). "The mechanism for activation of GTP hydrolysis on the ribosome." Science **330**(6005): 835-838.

- Voorhees, R. M., A. Weixlbaumer, D. Loakes, A. C. Kelley and V. Ramakrishnan (2009). "Insights into substrate stabilization from snapshots of the peptidyl transferase center of the intact 70S ribosome." Nat Struct Mol Biol **16**(5): 528-533.
- Weinger, J. S., K. M. Parnell, S. Dorner, R. Green and S. A. Strobel (2004). "Substrate-assisted catalysis of peptide bond formation by the ribosome." Nat Struct Mol Biol **11**(11): 1101-1106.
- Weisblum, B. (1995). "Insights into erythromycin action from studies of its activity as inducer of resistance." Antimicrob Agents Chemother **39**: 797-805.
- Weitzmann, C., S. J. Tumminia, M. Boublik and J. Ofengand (1991). "A paradigm for local conformational control of function in the ribosome: binding of ribosomal protein S19 to *Escherichia coli* 16S rRNA in the presence of S7 is required for methylation of m²G966 and blocks methylation of m⁵C967 by their respective methyltransferases." Nucleic Acids Res **19**(25): 7089-7095.
- Weixlbaumer, A., H. Jin, C. Neubauer, R. M. Voorhees, S. Petry, A. C. Kelley and V. Ramakrishnan (2008). "Insights into Translational Termination from the Structure of RF2 Bound to the Ribosome." Science **322**(5903): 953-956.
- Wilson, D. N. (2009). "The A–Z of bacterial translation inhibitors." Crit Rev Biochem Mol Biol **44**(6): 393-433.
- Wilson, D. N. and K. H. Nierhaus (2005). "Ribosomal Proteins in the Spotlight." Crit Rev Biochem Mol Biol **40**(5): 243-267.
- Wilson, D. N. and K. H. Nierhaus (2007). "The Weird and Wonderful World of Bacterial Ribosome Regulation." Crit Rev Biochem Mol Biol **42**(3): 187-219.
- Wilson, D. N., F. Schlutzen, J. M. Harms, A. L. Starosta, S. R. Connell and P. Fucini (2008). "The oxazolidinone antibiotics perturb the ribosomal peptidyl-transferase center and effect tRNA positioning." Proc Natl Acad Sci USA **105**(36): 13339-13344.
- Wimberly, B. T., D. E. Brodersen, W. M. Clemons, R. J. Morgan-Warren, A. P. Carter, C. Vornrhein, T. Hartsch and V. Ramakrishnan (2000). "Structure of the 30S ribosomal subunit." Nature **407**: 327-339.
- Winkler, E. and H. Weih (1967). "[Doxycycline. Results of basic studies]." Med Klin **62**(33): 1257-1262.
- Xu, Z., H. C. O'Farrell, J. P. Rife and G. M. Culver (2008). "A conserved rRNA methyltransferase regulates ribosome biogenesis." Nat Struct Mol Biol **15**(5): 534-536.

- Yamaguchi, A., N. Ono, T. Akasaka, T. Noumi and T. Sawai (1990). "Metal-tetracycline/H⁺ antiporter of *Escherichia coli* encoded by a transposon, Tn10." J Biol Chem **265**(26): 15525-15530.
- Yamaguchi, K. and A. R. Subramanian (2000). "The plastid ribosomal proteins. Identification of all the proteins in the 50 S subunit of an organelle ribosome (chloroplast)." J Biol Chem **275**(37): 28466-28482.
- Yamaguchi, K., K. von Knoblauch and A. R. Subramanian (2000). "The plastid ribosomal proteins. Identification of all the proteins in the 30 S subunit of an organelle ribosome (chloroplast)." J Biol Chem **275**(37): 28455-28465.
- Yang, W., I. F. Moore, K. P. Koteva, D. C. Bareich, D. W. Hughes and G. D. Wright (2004). "TetX is a flavin-dependent monooxygenase conferring resistance to tetracycline antibiotics." J Biol Chem **279**(50): 52346-52352.
- Yoshizawa, S., D. Fourmy and J. D. Puglisi (1999). "Recognition of the codon-anticodon helix by ribosomal RNA." Science, **285**(5434): 1722-1725.
- Young, R. A. and J. A. Steitz (1978). "Complementary sequences 1700 nucleotides apart form a ribonuclease III cleavage site in *Escherichia coli* ribosomal precursor RNA." Proc Natl Acad Sci USA **75**(8): 3593-3597.
- Youvan, D. C. and J. E. Hearst (1981). "A sequence from *Drosophila melanogaster* 18S rRNA bearing the conserved hypermodified nucleoside am psi: analysis by reverse transcription and high-performance liquid chromatography." Nucleic Acids Res **9**(7): 1723-1741.
- Yusupov, M. M., G. Z. Yusupova, A. Baucom, K. Lieberman, T. N. Earnest, J. H. Cate and H. F. Noller (2001). "Crystal structure of the ribosome at 5.5 Å resolution." Science **292**(5518): 883-896.
- Zaher, H. S. and R. Green (2011). "A primary role for release factor 3 in quality control during translation elongation in *Escherichia coli*." Cell **147**(2): 396-408.
- Zavialov, A. V., R. H. Buckingham and M. Ehrenberg (2001). "A posttermination ribosomal complex is the guanine nucleotide exchange factor for peptide release factor RF3." Cell **107**(1): 115-124.
- Zhou, J., L. Lancaster, S. Trakhanov and H. F. Noller (2012). "Crystal structure of release factor RF3 trapped in the GTP state on a rotated conformation of the ribosome." RNA **18**(2): 230-240.

Zhou, Z. and M. P. Deutscher (1997). "An essential function for the phosphate-dependent exoribonucleases RNase PH and polynucleotide phosphorylase." J Bacteriol **179**(13): 4391-4395.

9 Acknowledgements

At this point I would like to thank many people for their presence, support and help during the last years:

First of all I would like to thank Dr. Daniel Wilson for offering me a PhD position and giving me the opportunity to work in his group. I appreciated all the advices and discussions you gave me for my huge number of projects during the last years and I am grateful for the never-ending motivation and criticism you offered me which made my projects sometimes more difficult but successful at the end. Dankeschön!

I would like to thank Prof. Roland Beckmann for his support during my PhD as well as being part of his lab. Lots of projects wouldn't be possible without this great scientific environment.

I am grateful to my collaboration partners who participated in some of my projects and contributed to publications: Prof. R.K. Agrawal for the PSRP1 story, Prof. C.M. Spahn for the collaboration on EF-G and Prof. J. Remme for collaborations on RImH and ribosome assembly defective particles.

I would like to thank Dr. Daniel Wilson, Prof. Roland Beckmann, Prof. Jaanus Remme and PD Dietmar Martin for being part of my thesis committee.

Special thanks to people and friends from my group whom I had the pleasure to meet and work with: Dr. Aleksandra Mikolajka who helped me a lot to get started and was always nice to work with as well as Agata Starosta and Daniel Sohmen who accompanied me during my PhD, during the usual and sometimes annoying time in lab and lots of seminars☺. Without you guys it would be much harder to survive! Thanks to Daniel, Ola, Agata, and DanielS for the great atmosphere!

I also want to mention my students I supervised during my time at the Gene Center: Mika Scheler, Catharina von Nicolai and Camilla Godlee.

Thanks to the whole Beckmann group, especially Sibylle Franckenberg who always helped me with my processing work as well as during the other small or large crisis I had to deal with during the last years. Thanks a lot Sibylle for the great time, all the fun we had in lab and in kitchen during teatime. I will definitely miss it. I also want to thank Julian Deeng, Stephan Wickles, Dr. Jean Paul Armache and Dr. Alexander Jarasch for the great help with all the computer and SPIDER issues and of course for your company. Also, I want to mention and thank Charlotte Ungewickell and Dr. Otto Berninghausen for the amazing work at the

microscope, Christoph Leidig and the cooking team for great lunchtimes☺ as well as the rest of the Beckmann group. It was a pleasure to work with all of you! Thanks for the great time we had and still have together, also during retreats, parties and other events.

Vielen Dank an die besten Freunde dieser Welt: Steffi, Vroni und Johannes, Lucky, Flo, Jonny, Martin und Guku, ebenso an Niklas, Verena, Captn und Celine. Ich wüsste nicht was ich ohne euch machen würde!

Danke Michi, für einfach Alles, für deine Liebe, Motivation und Zuversicht, dass alles gut werden wird. Ohne dich wäre ich sicher nicht so weit gekommen.

Zuletzt möchte ich meinen Eltern und meiner Familie danken. Vielen Dank, dass ihr immer für mich da seid und mich in jeder Lebenslage ausnahmslos unterstützt. Ohne euch wäre vieles nicht möglich gewesen. Vielen, vielen Dank!

10 Publications

Paper I

**Dönhöfer A, Sharma MR, Datta PP,
Nierhaus KH, Agrawal RK, Wilson DN.
Factor-mediated ribosome assembly in bacteria.
Encyclopedia of Life Sciences (ELS), 2009. Review.**

Factor-Mediated Ribosome Assembly in Bacteria

A Dönhöfer, *Gene Center and Department of Chemistry and Biochemistry, University of Munich, Germany*

MR Sharma, *Wadsworth Center, New York State Department of Health, Albany, New York, USA*

PP Datta, *Wadsworth Center, New York State Department of Health, Albany, New York, USA*

KH Nierhaus, *Max-Planck-Institute for Molecular Genetics, Berlin, Germany*

RK Agrawal, *Wadsworth Center, New York State Department of Health, Albany, New York, USA*

DN Wilson, *Gene Center and Department of Chemistry and Biochemistry, University of Munich, Germany*

Advanced article

Article Contents

- Introduction
- Processing
- Processing of rRNA
- Modification
- Unwinding
- Chaperoning
- The hierarchy of small subunit assembly
- GTPases that affect large subunit assembly

Online posting date: 15th September 2009

The ribosome is a structurally and functionally conserved macromolecular machine responsible for translating messenger ribonucleic acid (mRNA) into proteins. Composed of two independently assembled subunits, the bacterial ribosome is approximately 2.5 MDa in size. The process of translation, catalysed by the ribosome, is central to gene expression in the cell. Correspondingly, the regulation of ribosome biogenesis is paramount to cell viability, growth and differentiation. Moreover, the ribosome is the target of numerous clinically relevant therapeutic agents, several of which are known to affect ribosome assembly. Although, *in vitro* reconstitution of bacterial ribosomal subunits can be achieved using purified ribosomal RNA (rRNA) and r-protein components, the process occurs at nonphysiological conditions. It is suggested that a specific order of processing and assembly events and regulatory factors is required to achieve fully functional particles. This article focuses on the protein factors that are involved in the process of bacterial ribosome biogenesis.

Introduction

Bacterial ribosomes are macromolecular machines of more than 2.3 MDa that translate the genetic information into functional proteins. Because up to 40% of an *Escherichia coli* cell's total energy turnover goes towards protein synthesis, the translational apparatus must be strictly regulated. One fundamental way of modulating gene expression is by regulating the biogenesis of the translational apparatus itself. In bacteria, the 70S ribosome is composed of two subunits, a small 30S subunit and a large 50S subunit. Each subunit is composed of ribosomal ribonucleic acid (rRNA) and ribosomal proteins (r-proteins). In *E. coli*, for example, the 30S subunit contains a single 1542 nucleotide (nt) 16S rRNA and 21 r-proteins, whereas the 50S subunit contains two RNAs, a 120 nt 5S rRNA and 2904 nt 23S rRNA, together with 33 r-proteins. Therefore, the challenge for the cell is to ensure the coordinated synthesis and binding of r-proteins to the rRNA in the correct manner so as to form an active ribosomal particle. Although, bacterial ribosomal subunits can be reconstituted *in vitro* from purified rRNA and r-protein components, the conditions required to do this, namely high magnesium and long incubations at elevated temperatures, are far from physiological. Instead, it is likely that a plethora of protein factors are involved *in vivo* to facilitate the assembly process. Indeed, the assembly process of eukaryotic, particularly yeast, ribosomes has been well characterized, revealing that nearly 200 auxiliary proteins are associated with pre-ribosomal particles (reviewed by Dez and Tollervey, 2004). In bacteria, a number of protein factors have been identified that are involved in processing, such as RNases and helicases, or modification of the ribosomal components by methylases, acetylases and pseudouridinyases; however, accumulating evidence suggests that there are in fact many more protein factors that appear to be directly involved in

ELS subject area: Biochemistry

How to cite:

Dönhöfer, A; Sharma, MR; Datta, PP; Nierhaus, KH; Agrawal, RK; and, Wilson, DN (September 2009) Factor-Mediated Ribosome Assembly in Bacteria. In: Encyclopedia of Life Sciences (ELS). John Wiley & Sons, Ltd: Chichester.

DOI: 10.1002/9780470015902.a0021836

Table 1 Protein factors involved in ribosome biogenesis

Factor ^a	Possible functions
CsdA (DeaD)	Cold shock DeaD A (CsdA) is an ATP-dependent RNA helicase that binds to large ribosomal subunit to mediate unwinding of 23S rRNA during assembly. Previously called DeaD
DbpA	DEAD box protein A (DbpA) is an ATP-dependent RNA helicase that mediates unwinding of 23S rRNA during assembly. Termed YxiN in <i>Bacillus subtilis</i>
Der	See EngA
EngA (Der/YphC)	Unique G protein with tandem G-domains and RNA binding KH-domain. Probably involved in assembly of the large ribosomal subunit. Also known as Der/YfgK (<i>E. coli</i>) or YphC (<i>B. subtilis</i>)
EngB (YihA, YsxC)	<i>E. coli</i> YihA and the <i>B. subtilis</i> homologue YsxC are essential proteins that appear to have a role in assembly of the large ribosomal subunit
Era	<i>E. coli</i> Ras-like protein is a GTPase that binds to (pre-)30S subunit to facilitate processing of the 3' end of the 16S rRNA precursor. Orthologue in <i>B. subtilis</i> termed Bex
KsgA	Also regarded as a late-stage ribosome biogenesis factor, and methylation is a trigger for release of KsgA from the assembling small ribosomal subunit
Obg (CgtA)	SpoOB-associated GTP-binding protein (OBG) binds ppGpp and appears to monitor levels of G-nucleotides in the cell. Obg also binds the large ribosomal subunit and may link the stress response, DNA replication and ribosome assembly. Also known as CgtA or YhbZ
RbfA (P15B)	Ribosome-binding factor A (RbfA) binds to 30S subunit to facilitate subunit assembly. Overexpression suppresses cold sensitive C23U mutation in the 16S rRNA. Previously termed P15B
RbgA (YlqF)	Ribosome biogenesis GTPase A (RbgA) is involved in a late assembly step of <i>B. subtilis</i> 50S subunits. Previously called YlqF. Not present in <i>E. coli</i>
RimM (21 K, YfjA)	Ribosome maturation factor M (RimM) binds to head of small ribosomal subunit to facilitate assembly. Previously called 21K or YfjA
RimN (YrdC)	Ribosome maturation factor N (RimN) has been suggested to bind the 16S rRNA to promote proper processing
RsgA (YjeQ/YloQ)	Ribosome small subunit-dependent GTPase A (RsgA) has a putative role in small subunit ribosomal assembly. Previously called YjeQ (<i>E. coli</i>). Homologues include YloQ/YqeH (<i>B. subtilis</i>) or YawG (yeast)
SrmB	Suppressor of temperature-sensitive mutation in ribosomal protein L24. SrmB is a DEAD box RNA helicase involved in ribosome biogenesis
YihA (YsxC)	See EngB

^a*E. coli* nomenclature given unless indicated.

the assembly process. These include factors that bind to the small 30S subunit, such as RimM, RbfA and Era, as well as to the large 50S ribosomal subunit, including Obg, Der and YlqF (Table 1). Since many of these factors appear to be highly conserved and in many cases specific for bacteria, they are considered as emerging targets for new antimicrobial drugs (Comartin and Brown, 2006). This article summarizes and updates the relevant sections on bacterial assembly from Wilson and Nierhaus (2007), and readers are directed to this article for background references. See also: [Bacterial Ribosomes](#); [Bacterial Ribosomes: Assembly](#); [Eukaryotic Ribosomes: Assembly](#)

Processing

In bacteria, the small and large rRNAs are transcribed together in a single transcript, which is processed by a number of endonucleases, in particular RNase III, which releases the pre-16S and pre-23S rRNAs from the transcript (see Deutscher and Li, 2001, for review of RNases). The

pre-23S rRNA contains 3–7 and 8 nucleotides (nts) at the 5' and 3' ends, respectively, while the pre-16S, termed 17S, contains 115 and 33 nts at the 5' and 3' ends, respectively. Although processing of the 5' end has been well characterized, consisting of the sequential action of RNase E and G, the RNase responsible for processing of the 3' end has not yet been identified (Figure 1). See also: [Ribonucleases](#)

Processing of rRNA

The 17S precursor containing 30S particles are inactive in translation, probably because they cannot associate with the 50S subunit. Since the 5' and 3' ends of the 16S rRNA in the mature 30S particle are located far apart, whereas in the precursor the extra nucleotides are base-paired, this additional secondary structure may either directly prohibit binding of the 50S subunit, or induce conformational changes in the 30S subunit that indirectly prohibit large subunit association. Additionally, the 3' end of the 16S rRNA contains the anti-Shine–Dalgarno (anti-SD)

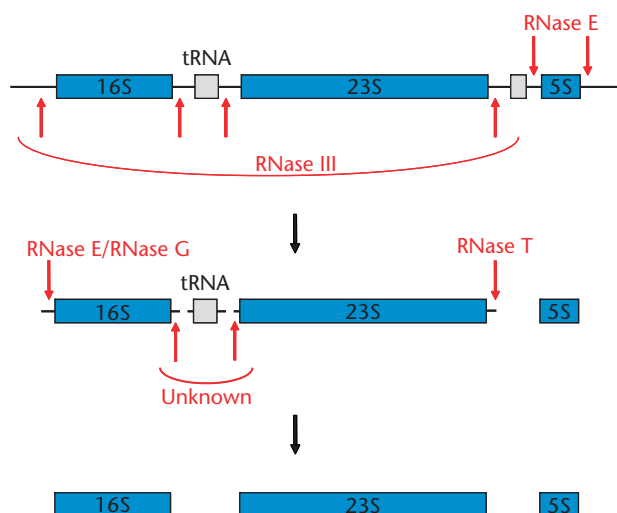


Figure 1 rRNA processing in bacteria. The rRNA operon in bacteria contains all three rRNAs, separated by noncoding sequences and tRNAs. Primary processing occurs at RNase III cleavage sites, formed by base pairing between sequences 5' and 3' to the rRNA sequence. In *E. coli* cleavage by RNase E (aided by RNase G) generates the mature 5' end of 16S and 5S rRNA and cleavage by RNase T generates the mature 3' end of 23S rRNA. The endonucleases for maturation of the 5' end of 23S rRNA and the 3' end of 16S and 5S rRNA remain unknown.

sequence that base pairs with the SD sequence present in many messenger RNAs (mRNAs). Blocking this interaction could also prevent mRNA recruitment and thus translation. In contrast, processing of the pre-23S rRNA does not appear to be as important since the pre-23S is found in polysomes. Structurally this can be rationalized, since in the mature 50S subunit, the 3' and 5' end remain base-paired, and are displaced relative to the active site (interface side) of the ribosome.

Modification

Modification of the rRNA occurs predominantly post-transcriptionally and consists of two main types, methylation and pseudouridylation. The *E. coli* ribosome contains 24 methylated nucleosides, 10 in the 16S and 14 in the 23S rRNA, and 11 pseudo-uridines (Ψ), 1 in the 16S and 10 in the 23S rRNA (Figure 2 and Table 2).

Although all of the pseudouridine synthase genes have been identified in *E. coli* (Del Campo *et al.*, 2001), a number of methylases responsible for rRNA modification have yet to be identified (Table 2). The largest question remaining unanswered, however, is the exact role of the modifications. Many of the modifications are dispensable for cell viability, with little observable effect on cell growth or ribosome function. There are some exceptions: One well-characterized methylase is KsgA that dimethylates highly conserved residues A1518/19 in h45 of the small subunit rRNA. Deletion of KsgA leads to a cold-sensitive phenotype, growth defects and in particular, alterations in 16S rRNA

processing, thus implicating KsgA in ribosome biogenesis (see Connolly *et al.*, 2008). Other exceptions include the loss of G2251 modification in yeast mitochondrial ribosomes, which leads to defects in subunit assembly, and the absence of 2'-O-methylation of U2552 affects subunit association. Of the 11 pseudouridine synthases in *E. coli*, only strains lacking RluD exhibit reduced growth rates and defects in ribosome biogenesis, such as accumulation of subunits. RluD is responsible for converting uridine to Ψ at the highly conserved positions 1911, 1915 and 1917 in 23S rRNA (Table 2). The location of these nucleotides in the loop of helix 69, which forms part of universally conserved intersubunit bridge B2a, is consistent with their influence on subunit association. Mapping all the methylations and pseudouridinylations onto the crystal structures of the 30S and 50S subunits reveals that they cluster around active sites of the ribosome, namely, the transfer RNA (tRNA)-transferase centre and intersubunit bridge areas on the 50S subunit (Decatur and Fournier, 2002; Figure 2a and b). Indeed, some of the modifications lead to resistance to antibiotics that bind at the active sites of the ribosome. **See also:** [Bacterial Antibiotic Resistance](#)

It should also be noted that a number of r-proteins are also modified, a classic example being the discovery that r-protein L7 is in fact just an acetylated version of L12. r-protein L11 is another example, which in *E. coli* is trimethylated at three positions (Met1, Lys3 and Lys29) by the methylase PrmA; however, the roles of these modifications have yet to be elucidated (see Cameron *et al.*, 2004, and references therein). **See also:** [Ribosomal Proteins: Role in Ribosomal Functions](#); [Ribosomal Proteins: Structure and Evolution](#)

Unwinding

E. coli cells have five DEAD-box genes, so-called because they contain nine conserved motifs, one of which is Asp-Glu-Ala-Asp (D-E-A-D). Of these five DEAD-box proteins, two have been shown to be involved in ribosome biogenesis, SrmB and CsdA, and a possible third is DbpA (reviewed by Iost and Dreyfus, 2006; Table 1). These families of proteins are adenosine triphosphate (ATP)-dependent RNA helicases, although the specificity of the reaction differs among the members. Unlike CsdA and SrmB, DbpA requires a specific sequence present in the 23S rRNA, namely helix 92, to stimulate its unwinding activity. The region responsible for this specificity appears to be located in the C-terminal region of the protein, since for the DbpA homologue in *Bacillus subtilis* YxiN, removal of the C-terminal domain removes all sequence specificity and appending this region to the catalytic core of the nonsequence-specific RNA helicase, SrmB, confers sequence specificity (Karginov *et al.*, 1995). This suggests that the C-terminal domain tethers the helicase to H92 in the pre-50S subunit, allowing the catalytic core to unwind neighbouring RNA duplexes to facilitate proper folding or

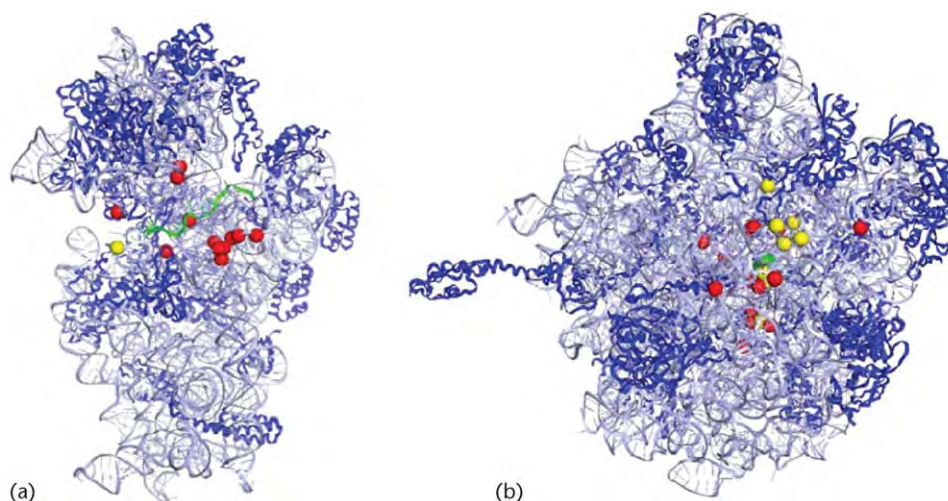


Figure 2 Sites of methylation (red) and pseudouridinylation (yellow) are shown as spheres on the (a) small and (b) large ribosomal subunits. rRNA and r-proteins are shown as ribbons in light and dark blue, respectively. In (a) a green ribbon indicates the path of the mRNA through the small subunit, whereas in (b) the antibiotic chloramphenicol (green) acts as a reference for peptidyltransferase centre on the large subunit. This figure was assembled from PDB accessions numbers 2AW4/7 (30S and 50S), 1YL3 (mRNA) and 1K01 (antibiotic) and is based on a figure from Decatur and Fournier (2002).

interaction with r-proteins. Indeed, deletion of either the *srnB* or *csdA* gene leads to accumulation of pre-50S particles, which in former case (Δ *srnB*) are lacking r-protein L13, an early assembly protein, whereas in the latter (Δ *csdA*) only late assembly proteins are absent. This suggests that SrmB acts earlier in the assembly pathway than CsdA (Charollais *et al.*, 2004). It should be noted that CsdA is induced by cold shock and therefore may be more important under these stress conditions (Jones *et al.*, 1996).

Chaperoning

Another set of protein factors that have been implicated in ribosome biogenesis are the chaperones DnaK/DnaJ/GrpE, GroEL/GroES. DnaK and GrpE have been shown to be stably associated with pre-30S assembly particles and their presence has been thought to overcome the need for a high temperature activation step required for *in vitro* reconstitution of 30S particles at 37°C or lower temperatures (Maki *et al.*, 2002). In contrast, it was recently shown that in *E. coli* strains carrying null mutations in either the *dnaK* or *dnaJ* genes, 30S and 50S ribosomal subunit biogenesis was slowed down in a temperature-dependent manner. At high temperature (44°C) precursor particles for both 30S (21S) and 50S (32S, 45S) subunits accumulated, whereas at normal temperature (30–37°C) ribosome assembly was significantly delayed (Al Refaii and Alix, 2009). Furthermore it was shown that assembly defects could partially be compensated by an overexpression of other heat-shock proteins (Al Refaii and Alix, 2009). This suggests that DnaK is in fact more important for ribosomal assembly at high temperatures as suggested earlier (Alix and Nierhaus, 2003). **See also:** [Chaperones, Chaperonin and Heat-Shock Proteins](#); [Protein Folding and Chaperones](#)

The hierarchy of small subunit assembly

In addition to modification, processing enzymes, helicases and chaperones, an increasing number of nonribosomal proteins have been found to be associated with the 30S (or pre-30S) subunit, and implicated in ribosomal assembly: RimM, RbfA, Era, RsgA and RimN ([Table 1](#)).

RimM binds the head of the small subunit

RimM (ribosome maturation factor *M*) is found associated with free 30S subunits, but not with 70S ribosomes (Bylund *et al.*, 1997). The first indication that RimM plays a role in assembly of the 30S subunit was the fact that deletion of the *rimM* gene (Δ *rimM*) affects translational efficiency (Bylund *et al.*, 1997) and leads to an accumulation of the precursor of 16S rRNA, termed 17S (Bylund *et al.*, 1998). RimM, previously termed 21K since it is a 21-kDa protein, has a two-domain structure, with the *N*- and *C*-terminal domains (NTD and CTD, respectively) exhibiting photosynthetic reaction center (PRC) β -barrel-like topologies ([Figure 3a](#)).

Conserved aromatic residues located at positions 106–108 (*E. coli* numbering) within the interdomain linker region ([Figure 3a](#)) have been proposed to be involved in protein binding. A double mutation, Y106A-Y107A, in RimM creates a strain with a phenotype similar to that seen for Δ *rimM* (Lövgren *et al.*, 2004). Suppressor mutations for the RimM mutant were identified as alterations in r-protein S13 (Δ 89–99), S19 (H83Y) or in helices 31 and 33b of the 16S rRNA (Lövgren *et al.*, 2004). In the mature 30S structure, these ribosomal elements cluster within the head region on the interface side ([Figure 3b and c](#)). A GST (glutathione-S-transferase)–RimM fusion protein has been shown to bind to S19 in the 30S

Table 2 Modifications in 16S and 23S rRNA of *E. coli*

Location	Enzyme	Modifies	Modification ^a
(A) 16S rRNA modifications			
516	RsuA (YejD)		Ψ
527	RsmG		m ⁷ G
966	RsmD (YhhF)	30S	m ² G
967	RsmB (RrmB)	16S	m ⁵ C
1207	RsmC (YjjT)	30S	m ² G
1402			m ⁴ Cm
1407	RsmF (YebU)	30S	m ⁵ C
1498	RsmE (YggJ)	30S	m ³ U
1516			m ² G
1518	RsmA (KsgA)	30S	m ⁶ ₂ A
1519	RsmA (KsgA)	30S	m ⁶ ₂ A
(B) 23S rRNA modifications			
745	RlmA(I) (RrmA and YebH)		m ¹ G
746	RluA (YabO)		Ψ
747	RumB (YbjF)		m ⁵ U (T)
748	RlmA(II) (TlrB)		m ¹ G
955	RluC (YccC)		Ψ
1618	RlmF (YbiN)		m ⁶ A
1835	RlmG (YgjO)		m ² G
1911	RluD (YfiL)		Ψ
1915	RluD (YfiL)		m ³ Ψ
1917	RluD (YfiL)		Ψ
1939	RumA (YgcA)		m ⁵ U (T)
1962	RlmI (YccW)		m ⁵ C
2030			m ⁶ A
2069			m ⁷ G
2251	RlmB (YjfH)		Gm
2445	RlmL (YcbY)		m ² G
2449			D
2457	RluE (YmfC)		Ψ
2498			Cm
2504	RluC (YccC)		Ψ
2552	RrmJ (FtsJ)		Um
2580	RluC (YccC)		Ψ
2604	RluF (YjbC)		Ψ
2605	RluB (YciL)		Ψ

^am_xN refers to methylation (m) of rRNA nucleotide N at the x position (with y number of methylation) of the base, whereas Nm indicates methylation of the sugar at the 2' position of nucleotide N.

subunit, whereas the RimM mutant did not (Lövgren *et al.*, 2004). The fact that most of the rRNA mutations, as well as S19 (H83Y) mutant, were more efficient suppressors of the rRNA deficiency in the RimM mutant, but not the Δ rimM strain, might be thought to indicate that the suppressor mutations restore binding of the mutant RimM to the ribosome. Surprisingly, this was not observed to be the case, at least for the S19 suppressor (Lövgren *et al.*, 2004), although this may only indicate that the interaction is very weak and/or transient. Certainly, it is easy to envisage how alterations in S13, which interacts directly with S19, or rRNA nucleotides neighbouring S19, could allow better binding of RimM by indirectly affecting the conformation of S19.

Alternatively, the suppressor mutations may mediate conformational changes within the 30S that promote more efficient rRNA processing or 30S maturation, in the absence of RimM or presence of the RimM mutant. Either way, the direct interaction with the head of the 30S subunit supports a role for RimM in the correct maturation of this region. An important step in understanding the action of RimM will be the identification of the substrate for RimM. Initial experiments using the GST–RimM fusion protein as a bait to pull out interaction partners in a cellular extract suggest that a number of r-proteins are absent in the complex and that mature 16S rRNA is present (Lövgren *et al.*, 2004); however, these results require further investigation.

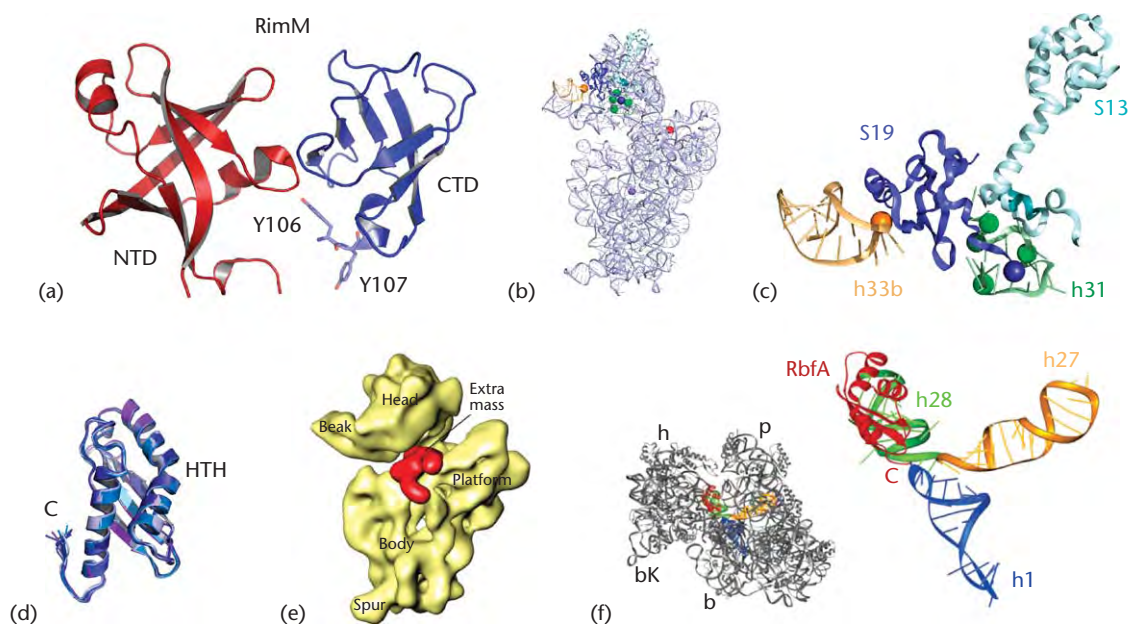


Figure 3 (a) Structure of RimM homologue from *Pseudomonas aeruginosa* (PDB2F1L), showing N- and C-terminal domains (NTD, red and CTD, blue) with Y106 and Y107 indicated as sticks. (b) and (c) Location of RimM suppressor mutations in the *E. coli* 30S subunit (PDB2AW4). G1015A in h33b (orange), D974A in h31 (green), $\Delta 89-99$ in S13 (cyan) and R81 in S19 (blue) are shown with spheres. On the 30S subunit, the 5' and 3' termini of the 16S rRNA are indicated with a blue and red sphere, respectively. (d) An ensemble of 10 NMR structures of RbfA (PDB1KKG), with the helix-turn-helix (HTH) motif indicated in the KH-domain, as well as the flexible C-terminus. Note the 24 C-terminal residues were not visualized, probably due to their flexible nature. (e) Cryo-EM reconstruction of RbfA-30S complex with 30S in yellow and extra density coloured red (Datta *et al.*, 2007). (f) Proximity of the C-terminus of RbfA (red) to helix 1 (h1, blue), central pseudoknot helix 27 (h27, orange) and helix 28 (h28, green) of 23S rRNA. (e) Reprinted from Datta *et al.* (2007) Structural aspects of RbfA action during small ribosomal subunit assembly. *Molecular Cell* **28**: 434–445. With permission from Elsevier.

RbfA induces conformational change in helices 44/45 of the 16S rRNA

Ribosome-binding factor A (RbfA) was first discovered as a multicopy suppressor for a dominant cold-sensitive C23U mutation located in the 5' end of the 16S rRNA (Dammel and Noller, 1995). Consistently, deletion of the *rbfA* gene results in a cold-sensitive phenotype for growth, a reduction in polysomes/70S ribosomes and a corresponding increase in 30S and 50S subunits (Dammel and Noller, 1995). Similar to the $\Delta rimM$ phenotype, $\Delta rbfA$ also displays an accumulation of the 17S rRNA (Bylund *et al.*, 1998; Inoue *et al.*, 2003). Interestingly, overexpression of RbfA complements, at least partially, the slow-growth phenotype of the $\Delta rimM$ strain, whereas the converse is not true, that is, RimM overexpression cannot complement a $\Delta rbfA$ phenotype (Bylund *et al.*, 1998). RbfA has been shown to associate specifically with the 30S subunits *in vivo*, and proposed to bind to the 5' terminal helix 1 of the 16S rRNA (Dammel and Noller, 1995). Nuclear magnetic resonance (NMR) and crystal structures reveal that RbfA has a single characteristic RNA-binding helix-turn-helix (HTH) containing KH-domain, with a flexible C-terminal extension that was not fully visualized in any of the available structures (Figure 3d; Huang *et al.*, 2003). Biochemically, the C-terminal extension has been shown to be important since *E. coli* RbfA lacking the C-terminal 25 amino acids cannot bind stably to the 30S, nor complement

the cold-sensitive $\Delta rbfA$ phenotype, although it can correct for the deficiency in rRNA processing (Xia *et al.*, 2003). Cryo-EM reconstruction of an RbfA-30S complex reveals that RbfA binds on the intersubunit side of the 30S subunit (Figure 3e) in an orientation such that the C-terminal tail extends through the body of the 30S and reaches towards the loop of h1 (Figure 3f; Datta *et al.*, 2007). This strategic location of RbfA on the 30S subunit, and interaction of RbfA with multiple rRNA helices and r-proteins, is suggestive of an important role in a late step in maturation of the 30S subunit. In addition, RbfA maintains the decoding region of the 30S subunit in a conformation unsuitable for the subunit's participation in protein synthesis. Specifically, RbfA appears to dramatically alter the position and conformation of helix 44, a functionally important segment of the 16S rRNA that is known to be directly involved in mRNA decoding and in the formation of two of the intersubunit bridges, B2a and B3 (Datta *et al.*, 2007). **See also:** Cold-shock Response in Microorganisms

Era overlaps in binding site with ribosomal protein S1

Era (*E. coli* ras-like protein) is a highly conserved guanine triphosphatase (GTPase), essential in *E. coli*, which binds to 30S subunits *in vitro* (Sayed *et al.*, 1999; Sharma *et al.*, 2005). Depletion of Era from the cell produces phenotypes reminiscent of the $\Delta rimM$ and $\Delta rbfA$ strains,

namely a reduction in 70S ribosomes and an accumulation of subunits and 17S precursor rRNA (Inoue *et al.*, 2003). The crystal structure of *E. coli* Era reveals a two-domain protein, with GTP-binding and KH RNA-binding domains located at the N- and C-terminus of the protein, respectively (Chen *et al.*, 1999). A recent cryo-electron microscopy reconstruction of *Thermus thermophilus* Era bound to the 30S subunit reveals that Era binds in a cavity formed by r-proteins S2, S7, S11 and S18, located between the head and the platform (Figure 4a and b) (Sharma *et al.*, 2005).

Docking of the crystal structures for Era and the 30S subunit into the cryo-EM density suggests that Era contacts four of the five rRNA domains, with the RNA-binding HTH motif located in the KH-domain in proximity to the 3' end of the 16S rRNA. This localization is also consistent with the fact that overexpression of KsgA, which dimethylates A1518 and A1519 located in the penultimate h45 of the 16S rRNA (Figure 4b), leads to suppression of a

cold-sensitive Era mutant (Lu and Inouye, 1998). Since the methylation state of A1518 and A1519 has been shown to affect the conformation of the 3' end of 16S rRNA, it seems likely that methylation promotes formation of an optimal RNA secondary structure for the Era mutant to function. Collectively, these data led to the suggestion that Era may act as an RNA chaperone, facilitating the correct positioning of the rRNA for processing by the maturation RNase (Sharma *et al.*, 2005).

The GTPase activity of Era appears to be essential for Era function, although it cannot be ruled out that this is related to the role of Era in many other cellular processes, such as cell division and carbon metabolism, rather than ribosome assembly. Certainly, the G-nucleotide appears to influence Era stability on the ribosome, since only the non-hydrolysable GTP form of Era could prevent association of 30S and 50S subunits *in vitro* (Sharma *et al.*, 2005). Thus, it is tempting to speculate that processing of the rRNA could trigger the GTPase activity of Era, but this remains to be

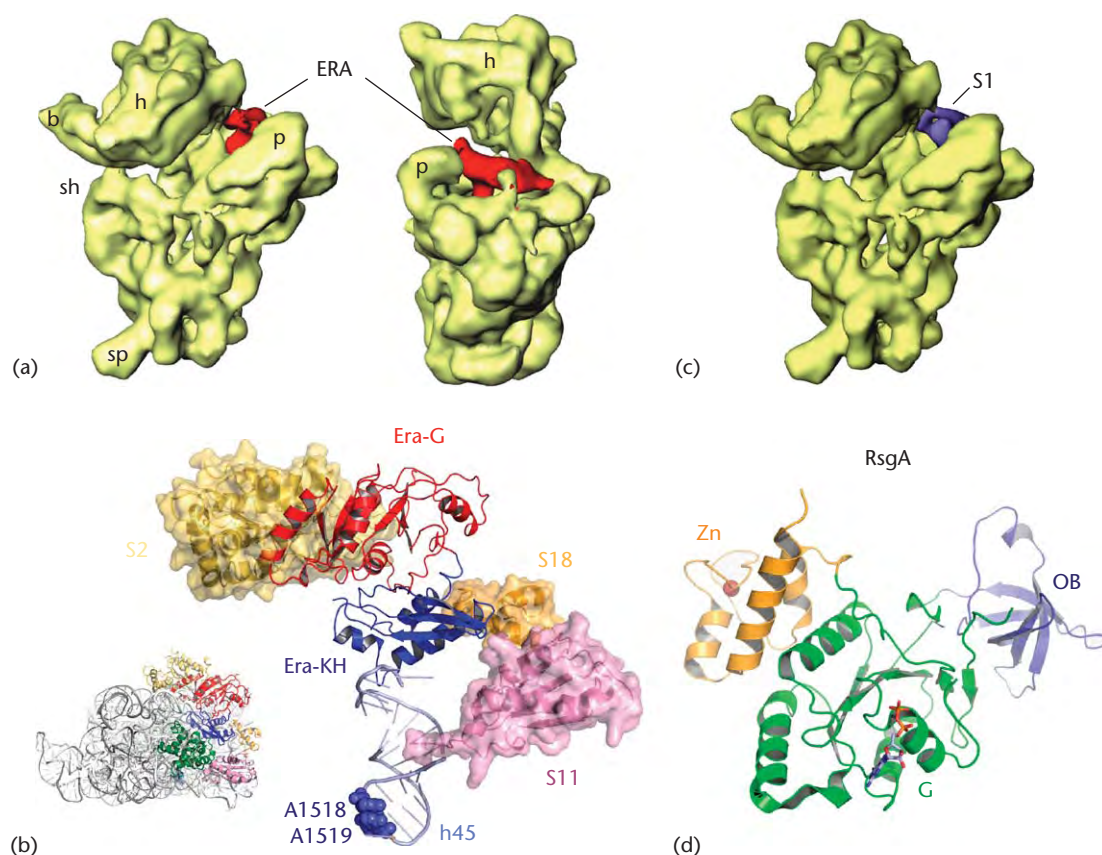


Figure 4 (a) 3D cryo-EM map showing the binding position of Era (red) on the 30S subunit (yellow). The 30S subunit is shown in an interface view and a platform-side view, respectively. (b) Model for the binding site of Era on the 30S subunit derived from cryo-EM reconstructions (Sharma *et al.*, 2005). The thumbnail shows birds-eye view onto 30S subunit for orientation. Enlargement shows that the G-domain of Era (red) interacts with r-protein S2 (yellow), whereas the KH-domain of Era (blue) contacts S11 (pink), S18 (orange) and S7 (not shown for clarity). In addition, the helix-turn-helix motif in the KH-domain approaches the 3' end of the 16S rRNA. The relative positions of A1518 and A1519 in helix 45 are also indicated. (c) Binding position of protein S1 (blue) in an interface view of the 30S subunit (yellow). In comparison with (a) Era and protein S1 show overlapping binding positions. (d) Structure of RsgA (YjeQ from *Thermotoga maritima*; Shin *et al.*, 2004) highlighting the N-terminal OB-fold domain (blue), G-domain (green) and C-terminal zinc finger domain (orange). The Zn ion is shown as a red sphere. (a) and (c) Reproduced from Sharma *et al.* (2005) Interaction of Era with the 30S ribosomal subunit: implications for 30S subunit assembly. *Molecular Cell* **18**(3): 319–329. With permission from Elsevier.

tested. The best fitting of the *E. coli* Era crystal structure into the cryo-EM density requires flexibility between the KH- (CTD) and G-domains (NTD). This is supported by a recent crystal structure of *T. thermophilus* Era in the GTP form (GDPNP, 5'-guanylylimidodiphosphate), which reveals an even more dramatic difference in the relative domain arrangement when compared to the nucleotide-free (apo) *E. coli* Era structure. Therefore, GTP hydrolysis could alter the conformation of Era to destabilize and release it from the ribosome. Alternatively (or additionally), r-protein S1 may play a role in recycling of Era from the 30S, since the binding position of Era on the 30S subunit overlaps significantly with that determined for S1 (Figure 4c; Sharma *et al.*, 2005). Since S1 is involved in mRNA recruitment to the 30S, Era may act as a control checkpoint, ensuring that only mature 30S subunits can enter into the translation initiation cycle, that is, Era would prevent binding of S1 to a precursor containing 30S subunits. This model would suggest that Era is involved in one of the last steps in 30S assembly. However, it should be noted that while Era can complement the $\Delta rbfA$ strain at high temperature, it cannot suppress $\Delta rimM$ or the cold-sensitive C23U strains (Inoue *et al.*, 2003). Determination of the binding sites of RbfA and RimM on (pre-)30S particles will go some way in providing further insight in the relationship between these factors.

RsgA (YloQ/YjeQ) is a GTPase that associates with the small subunit

Another GTPase that associates with the 30S subunit is *E. coli* YjeQ (Daigle and Brown, 2004) (YloQ in *B. subtilis*; Campbell *et al.*, 2005; recently renamed as RsgA, ribosome small subunit-dependent GTPase A; Himeno *et al.*, 2004). RsgA has a low intrinsic GTPase activity that is stimulated by 30S subunits and 70S ribosomes, but not 50S subunits (Daigle and Brown, 2004; Himeno *et al.*, 2004). RsgA is found associated with ribosomes at very low stoichiometry (1:200) *in vivo* (Daigle and Brown, 2004), and *in vitro* binds stably to 30S subunits in the presence of GDPNP, but not GTP or GDP (guanosine diphosphate) (Daigle and Brown, 2004; Himeno *et al.*, 2004). In the presence of GDPNP, all 70S ribosomes were dissociated into subunits by RsgA, suggesting an intersubunit localization of the factor (Himeno *et al.*, 2004). Indeed, aminoglycoside antibiotics such as neomycin, paromomycin and gentamycin, which bind in the decoding centre on the interface side of the 30S subunit, inhibit the ribosome-dependent GTPase of RsgA (Campbell *et al.*, 2005; Himeno *et al.*, 2004), possibly by preventing binding of RsgA to the ribosome (Himeno *et al.*, 2004). In contrast, chloramphenicol, which binds to the 50S subunit, as well as other 30S binding antibiotics, for example, tetracycline, kasugamycin and streptomycin, had no effect (Himeno *et al.*, 2004). Chemical footprinting experiments suggest that binding of RsgA induces conformational changes around the A site, P site and helix 44, and that GTP hydrolysis may lead to a partial conformational restoration in the head region that dissociates the GTPase

from the 30S subunit (Kimura *et al.*, 2008). The structure of RsgA is composed of three highly conserved domains, an *N*-terminal oligosaccharide/oligonucleotide-binding (OB)-fold, a central GTPase (G) domain that is circularly permuted (G4-G1-G2-G3 rather than G1-G2-G3-G4) and a *C*-terminal domain with a zinc (Zn)-binding motif (Shin *et al.*, 2004; Figure 4d). *N*-terminal truncations indicate that the OB domain is important for interaction of RsgA with the 30S (Daigle and Brown, 2004). Since the initiation factor IF1 consists of an OB-fold domain and binds in the A site of the 30S subunit, it will be interesting to investigate the interrelationship between these factors on the ribosome. Although RsgA is dispensable for viability of *E. coli* cells, loss of RsgA protein results in a slow-growth phenotype and an altered ribosome profile (Campbell *et al.*, 2005), which can be alleviated by overexpression of Era or initiation factor IF2, as well as further exacerbated by deletions in one of the seven genes (Δtgt , $\Delta ksgA$, $\Delta ssrA$, $\Delta rimM$, $\Delta rluD$, $\Delta trmE$ / $mmmE$ and $\Delta trmU$ / $mmmA$) (Campbell and Brown, 2008). Surprisingly, in the absence of RsgA most of the 70S ribosomes are present as subunits; the 30S subunits contained 17S precursor rRNA and stimulated RsgA GTPase less efficiently than wild-type 30S subunits (Himeno *et al.*, 2004). Collectively, these results clearly support the hypothesis that YjeQ has a role in late 30S subunit biogenesis.

YrdC (RimN), a putative 30S assembly factor

Selection of suppressors of a strain bearing a temperature-sensitive termination release factor 1 (RF1) mutation identified a 12 nucleotide deletion that removed the initiation codon from the *yrdC* gene. Characterization of the $\Delta yrdC$ strain revealed an accumulation of immature 30S subunits containing 17S rRNA. The structure of YrdC exhibits a large concave surface with positive electrostatic potential and the protein preferentially binds to double-stranded RNA (dsRNA) (Teplova *et al.*, 2000); however, no direct evidence for stable binding of YrdC to 30S particles has been forthcoming (Kaczanowska and Rydén-Aulin, 2005). Nevertheless, incubation of cell extracts from the $\Delta yrdC$ strain with YrdC protein led to maturation of the 16S rRNA, implicating YrdC in the assembly process and prompting the renaming of this protein to RimN (Kaczanowska and Rydén-Aulin, 2005). Other members of the same protein family as YrdC include yeast homologue Sua5, which has been suggested to be involved in translation re-initiation (Na *et al.*, 1992).

GTPases that affect large subunit assembly

In light of the large amount of fully sequenced genomes, database analysis has revealed that bacteria contain 11 universally conserved GTPases (Caldon *et al.*, 2001). While this list includes canonical translation factors such as EF-G, EF-Tu, IF2, the recently characterized elongation

factor LepA (EF4) and the signal sequence recognition pathway protein Ffh and FtsY, the list also identified new families of proteins, members of which, EngA (Der), EngB (YihA) and Obg (see **Table 2**), have been implicated in assembly of the 50S subunit (Brown, 2005). In addition, although the GTPase YlqF is not present in *E. coli*, it is widely distributed in Gram-positive bacteria and has been shown to be essential for growth in *B. subtilis* (Morimoto *et al.*, 2002). Two proteins implicated in 60S biogenesis in yeast, Nog2p and Nug1p, exhibit similarity to YlqF that extends beyond the G-domain. Furthermore, humans contain several homologues for YlqF, GTPBP7 and the nucleolar GTPases nucleostemin and GNL2 (Uicker *et al.*, 2006). Two recent publications addressing the role of YlqF nicely complement each other to reveal a role for this protein in a late assembly step of the large ribosomal subunit (Matsuo *et al.*, 2006; Uicker *et al.*, 2006), thus appearing to support the renaming of YlqF to RbgA (ribosome biogenesis GTPase A) (Uicker *et al.*, 2006). **See also: G Proteins**

Obg (CgtA/YhbZ), a possible link between stress and assembly

Homologues to the *obg* gene have been identified in all genomes sequenced so far, ranging from the smallest free-living bacteria to archaea (usually two genes, Nog1p and Rbg1p) and eukaryotes (usually four copies, including nucleolar Nog1p). The structure of the full-length Obg from *T. thermophilus* reveals three domains, a central G-domain flanked by N- and C-terminal domains, termed OBG and OCT (Obg-C-terminal), respectively, that are unique to Obg (**Figure 5a**; Kukimoto-Niino *et al.*, 2004). Obg has been implicated in many different cellular processes, ranging from deoxyribonucleic acid (DNA) replication, protein synthesis and cellular differentiation (reviewed by Brown, 2005). Indeed, the name Obg derives from SpoOB-associated GTP-binding protein, since the *B. subtilis* protein was shown to coexpress with SpoOB and be involved with sporulation.

RrmJ is a methyltransferase that modifies position U2552 of the 23S rRNA (see **Table 1**), and loss of this modification in a Δ *rrmJ* strain leads to a reduction in 70S ribosomes as well as an accumulation of both 30S and 50S subunits (Tan *et al.*, 2002). Overexpression of Obg (or EngA, but not Era) can rescue the slow-growth phenotype and restore the polysome profile resulting from an *rrmJ*-knockout, without leading to modification of U2552 (Tan *et al.*, 2002). Direct binding of Obg to 50S subunits has been observed for bacteria; *E. coli*, *Caulobacter crescentus* and *Vibrio harveyi*, as well as Obg homologues from yeast, namely, mitochondrial Mtg2p and nucleolar Nog1p (see Wilson and Nierhaus, 2007). Obg has a moderate affinity for G-nucleotides, exhibits slow GTP hydrolysis rates and exchanges G-nucleotides rapidly (Wout *et al.*, 2004). The nucleotide requirement of Obg for ribosome binding is unclear: *B. subtilis* Obg co-fractionates with ribosomes in a G-nucleotide-dependent fashion, exhibiting strongest interaction with GTP over GDP, whereas *E. coli* and

C. crescentus Obg seem to migrate with 50S subunits regardless of the presence or absence of G-nucleotide (Wout *et al.*, 2004). Interestingly, when subunits from purified 70S ribosomes were used instead of lysates, *E. coli* Obg bound both to 30S and 50S subunits, but only strongly in the presence of GDPNP (Jiang *et al.*, 2006). Similarly, *E. coli* Obg was found to interact with naked 16S and 23S rRNA in a nucleotide-specific manner, binding in the presence of GTP, but not GDP or absence of nucleotide (Sato *et al.*, 2005). Therefore, the G-domain does appear to play a role in the binding of Obg to the ribosome, and furthermore, that under some conditions binding to the 30S subunit is also possible. However the significance of this latter finding is unclear at present.

Depletion of Obg from the cell leads to a decrease in 70S ribosomes, an increase in both 30S and 50S subunits as well as the appearance of an intermediate pre-50S particle (Jiang *et al.*, 2006; Sato *et al.*, 2005). Furthermore, precursors to both the 16S and 23S rRNA are significantly increased, suggesting that RNA processing is impaired (Jiang *et al.*, 2006). It should be noted that defects in processing of the 16S rRNA can arise as secondary events due to defects in 23S rRNA maturation, which may well be the case here. Analysis of pre-50S particles reveal reduced levels of r-proteins L33, L34 and to a lesser extent L16 (Jiang *et al.*, 2006). These three proteins are late assembly proteins, suggesting that Obg is involved in a late step in 50S biogenesis, analogous to RrmJ, CsdA, EngA/B and RbgA. In addition, RrmJ and RluC (a pseudouridylase that modifies U955 of the 23S rRNA; **Table 1**) were also found in the pre-50S particle (Jiang *et al.*, 2006).

Pull-down assays using his-tagged *E. coli* Obg as bait, identified many interaction partners such as r-proteins from both 30S and 50S subunits, as well as CsdA, ClpA, hypothetical protein 274#5, and RNA polymerase β and β' subunits (Sato *et al.*, 2005). This latter finding is interesting since Obg interacts with RsbT, RsbW and RsbX, regulators that mediate stress activation of σ B, as well as SpoT (Wout *et al.*, 2004), a (p)ppGpp synthetase/hydrolase involved in the stringent response. Interestingly, in the crystal structure of *B. subtilis* Obg, one of the two molecules in the asymmetric unit was bound with ppGpp in the active site (Buglino *et al.*, 2002). Since ppGpp was not included in the crystallization conditions, the suggestion is that the molecule binds tightly to Obg and co-purifies with the protein. Comparing the conformations of nucleotide-free and GTP-bound forms of Obg reveals a dramatic rearrangement of the G-domain relative to the OBG domain (**Figure 5b** and **c**), supporting the suggestion that Obg senses and responds to the G-nucleotide state of the cell.

EngA (Der/YphC), the double Era-like GTPase

The EngA family of GTP-binding (G) proteins is unique in that it contains two consecutive G-domains (G1 and G2), located at the N-terminus of the protein, followed by a C-terminal RNA-binding KH-domain (Muench *et al.*, 2006;

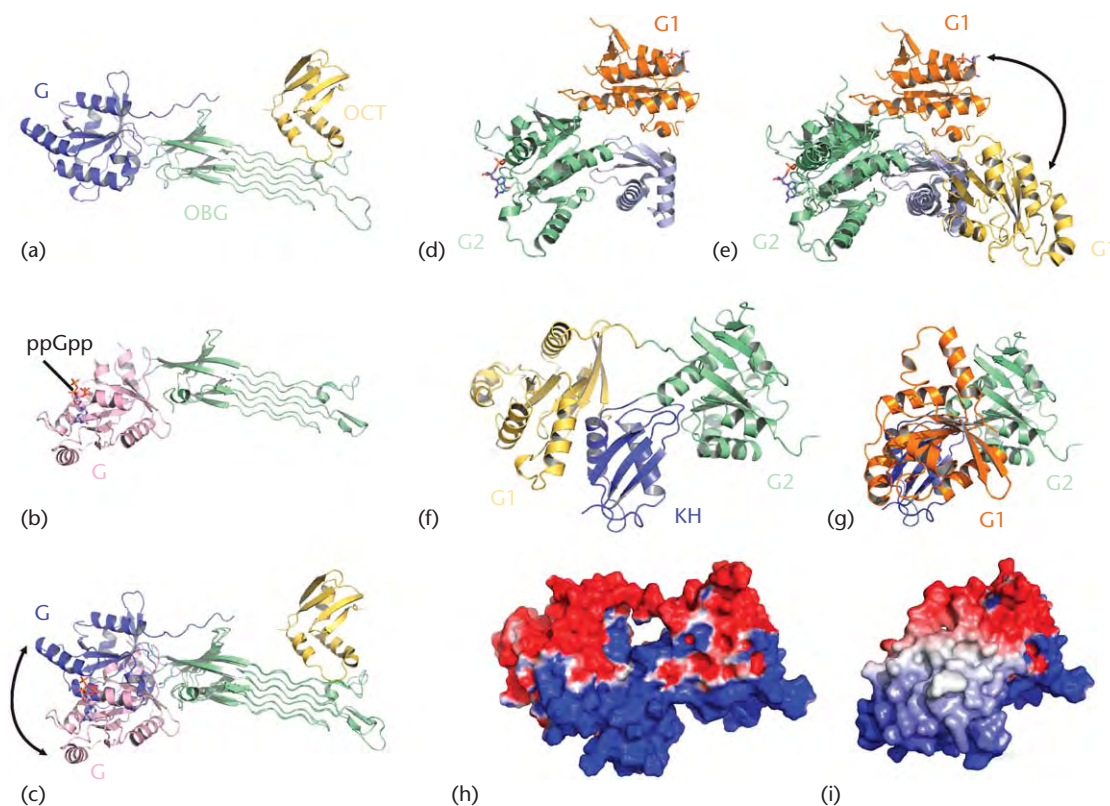


Figure 5 Structures of Obg from (a) *T. thermophilus* (PDB1UDX; Kukimoto-Niino *et al.*, 2004) and (b) *B. subtilis* (PDB1LNZ; Buglino *et al.*, 2002) with (c) a superposition of both structures aligned on the basis of the unique OBG domain (green). In (a) the OCT domain (yellow) was also visualized, whereas in (b) the signalling molecule ppGpp was found in the G-domain. The arrow in (c) indicates the different positions of the G-domains relative to the OBG domain in the two structures. (d) Structure of *T. maritima* Der (PDB1MKY; Robinson *et al.*, 2002) coloured to highlight the C-terminal KH-domain (blue) and the two G-domains (orange and green), which have GDP (blue) in the active sites. (e) Alignment of *T. maritima* Der with *B. subtilis* homologue (PDB2HJG; Muench *et al.*, 2006) on the basis of KH-domain, revealing the dramatically different position of the G1 domains (arrowed). (f) and (g) structure of Der in (f) 'open' and (g) 'closed' conformations, shown as ribbons (above) and (h) and (i) as surface representation highlighting regions of positive and negative electrostatic potential in blue and red, respectively (below). Note the rearrangement of the G1 domain in the closed conformation covers the highly basic KH-domain seen in the open conformation.

Robinson *et al.*, 2002; **Figure 5d**). *E. coli* EngA (also known as Der, double *Era*-like GTPase) as well as many homologues, such as *B. subtilis* YphC, have been shown to be essential for cell viability (Bharat *et al.*, 2006; Hwang and Inouye, 2006; Morimoto *et al.*, 2002). Consistently, EngA homologues are highly conserved in bacterial, but not archaeal or eukaryotic genomes (with the exception of *Arabidopsis thaliana*). Perhaps the first hint that EngA was involved in ribosome biogenesis was the report that overexpression of EngA, like that of Obg (see section on Obg (CgtA/YhbZ), a possible link between stress and assembly), could rescue the slow-growth phenotype of a *rrmJ*-knockout strain (Tan *et al.*, 2002). Indeed, similar phenotypes are observed when the EngA itself is depleted from the *E. coli* cell (Bharat *et al.*, 2006; Hwang and Inouye, 2006; Schaefer *et al.*, 2006), with the growth rate correlating with the amount of EngA present (Hwang and Inouye, 2006). Furthermore, the accumulating 50S subunits in the EngA-depleted strain are unstable at low Mg^{2+} concentrations, have reduced levels of r-proteins L9 and L18 (and to a lesser extent L2 and L6) and contain pre-23S rRNA

(with seven additional 5' nucleotides) (Hwang and Inouye, 2006). In contrast, the 30S subunit had the full complement of r-proteins, and while the precursor 17S rRNA was also present, this is likely to be a secondary effect due to the defect in 23S rRNA maturation (Hwang and Inouye, 2006). Surprisingly, an independent study analysing the content of the 45S peak from EngA-depleted cells found that r-proteins L16, L27 and L36 were absent, reminiscent of the particles accumulating in the YsxC- and RbgA-depleted strains (Schaefer *et al.*, 2006).

E. coli EngA has been shown to associate with 50S subunits, rather than with 70S ribosomes or 30S subunits (Bharat *et al.*, 2006; Hwang and Inouye, 2006; Schaefer *et al.*, 2006). Furthermore, the binding was dependent on the presence of nonhydrolysable GTPNP, whereas little or no binding was observed with GDP or GTP (Hwang and Inouye, 2006; Schaefer *et al.*, 2006). Both G-domains of EngA appear to be important for function and cell viability. EngA with either mutation S16A in GD1, or K216A (or S217A) in GD2, has reduced GTP-binding activity and is not able to rescue a $\Delta engA$ strain (Bharat *et al.*, 2006).

Similarly, mutations N118D in GD1, or N321D in GD2, cannot rescue a Δ engA strain at low temperature (30 °C). However, complementation is possible at higher temperatures (42 °C), but not with a double N118D/N321D EngA mutant (Hwang and Inouye, 2006). Consistently, binding of the double mutant to 50S subunits is significantly diminished compared to wild-type and N118D/N321D mutants (Hwang and Inouye, 2006). This suggests that at high temperature, a single G-domain is sufficient for EngA function. A recent study analysing the activities of the two G-domains of EngA independently suggests a distinct role for these domains with respect to ribosome binding: GTP binding to GD2 is necessary to observe an interaction between EngA and the ribosome, but this interaction can be stabilized by GTP binding to GD1. However, when GTP is exchanged to GDP for GD1, EngA appears to interact with 30S, 50S and 70S, suggesting that GD1 has a more regulatory function in ribosome binding (Tomar *et al.*, 2009).

Two structures for EngA are available, from *T. maritima* with GDP bound in G2 and two phosphate molecules bound to G1 (Robinson *et al.*, 2002), and *B. subtilis*, with GDP in both G1 and G2 active sites (Muench *et al.*, 2006). Aligning the two molecules on the basis of the C-terminal KH-domain, reveals that G2 is in the same relative orientation in the two structures, whereas G1 has undergone a dramatic conformational change (Figure 5e). The two phosphates in G1 of *T. maritima* EngA have been suggested to mimic the β and γ phosphates of GTP, inducing an 'on' state in the factor, whereas the GDP in *B. subtilis* EngA represents the 'off' state (Muench *et al.*, 2006). This is consistent with the open conformation representing the 'on' state, such that the highly basic surface of the KH-domain, which is responsible for RNA interaction, remaining exposed (Figure 5f and h), whereas in the closed 'off' state, G1 has shifted position to cover this region (Figure 5g and i; Muench *et al.*, 2006). This model is in agreement with the idea that EngA binds to the pre-50S in the GTP state, and that hydrolysis to the GDP state could provide a mechanism for dissociating

the factor from the mature subunit. Now it is important to determine whether EngA binds to the pre-50S particles and what the trigger for GTPase activation is.

EngB (YihA/YsxC), a probable late assembly factor for the large subunit

The genes encoding EngB family of proteins, *ysxC* in *B. subtilis* and *yihA* in *E. coli*, have been shown to be essential for cell viability. In *B. subtilis*, *ysxC* is located within a bicistronic operon, downstream of the *lonA* gene, which encodes a protease involved in protein degradation in response to environmental stress. YsxC has been shown to bind to 70S ribosomes and 50S, but not 30S subunits, with the strength of the interaction being increased by the presence of G-nucleotides (Schaefer *et al.*, 2006). The structure of YsxC in complex with GDPNP (Ruzheinikov *et al.*, 2004) reveals a single domain protein (Figure 6a), which lacks however any classic RNA-binding domains, such as the KH-domains seen in Era or EngA. The highly basic C-terminal α helix could potentially mediate interaction with rRNA (Figure 6a), but this has yet to be confirmed (Ruzheinikov *et al.*, 2004). Depletion of YsxC from the cell leads to a reduction in the level of 70S ribosomes as well as a concomitant accumulation of subunits. Interestingly, the migration of the large ribosomal subunit migrates at 44.5S, rather than the usual 50S position (Schaefer *et al.*, 2006). A comparative analysis of the 44.5S particle reveals the absence of r-proteins L16, L27 and L36, analogous to the 45S particles that accumulate in cells depleted of EngA or RbgA (Schaefer *et al.*, 2006). These proteins are clustered together adjacent to the peptidyltransferase centre of the mature 50S subunit, and are linked through common contacts with 23S rRNA: L16 and L36 both interact with H89, whereas L27 and L16 contact different regions of H38 (Figure 6b and c). Since these three proteins are late assembly proteins, the function of YsxC may be to convert the inactive 44.5S

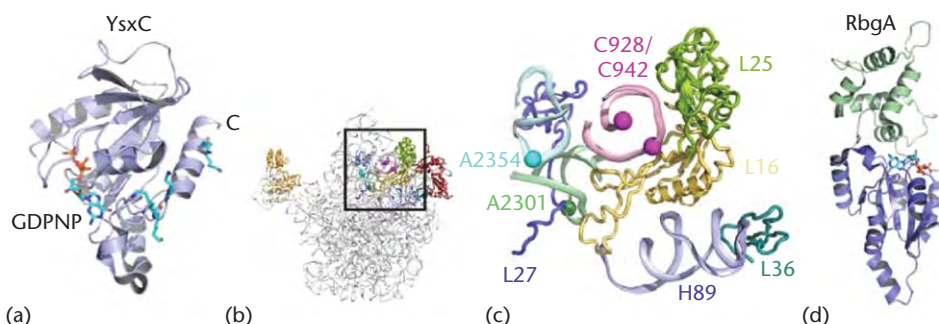


Figure 6 (a) Structure of YsxC in complex with GDPNP (magenta) (PDB1SVW; Ruzheinikov *et al.*, 2004). Note, the highly basic Lys and Arg residues located in the C-terminal (c) helix are also shown. (b) Binding site of RbgA (YlqF) on the large ribosomal subunit with enlargement of boxed area of inset subunit (with L1 (brown) and L11 (deep red) included for reference). (c) Ribosomal proteins L16 (orange), L25 (green) and L27 (blue) are highlighted, as are nucleotides C928 and C942 (magenta) in H38 (pink), A2301 (green) in H81 and A2354 (magenta) in H85. Figure uses *B. subtilis* numbering on *D. radiodurans* 50S structure as outlined by Matsuo *et al.* (2006). (d) Crystal structure of RbgA (PDB1PUJ) indicating two domain arrangement, with N-terminal G-domain (blue) with GTP molecule (magenta) and C-terminal acidic domain (green).

particle into an active 50S particle by recruiting these final groups of late assembly proteins.

RbgA (YlqF) may recruit L16 and L27 to the large subunit during assembly

Gradual depletion of RbgA from *B. subtilis* cells leads to a corresponding decrease in growth rate (Matsuo *et al.*, 2006; Uicker *et al.*, 2006), and is characterized by a change in gene expression, namely an upregulation of genes involved in protein synthesis and downregulation of metabolic genes (Uicker *et al.*, 2006). Similar responses are observed during conditions of nutrient starvation as well as when sublethal concentrations of translation inhibitors are given to cells. The ribosome profiles of RbgA-depleted cells show greatly reduced levels of 70S ribosomes and concomitant accumulation of subunits (Matsuo *et al.*, 2006; Uicker *et al.*, 2006). In addition the large ribosomal subunit migrates at 45S, rather than 50S, suggesting it is an assembly intermediate (pre-50S) (Matsuo *et al.*, 2006; Uicker *et al.*, 2006). The appearance of the 45S particle is directly related to growth rate and the level of RbgA expression, as well as being specific for RbgA depletion since no 45S peak is observed when EF-Tu and IF2 are depleted (Uicker *et al.*, 2006).

RbgA has been shown to bind stable to the precursor 45S particles (Uicker *et al.*, 2006); however, binding to the 50S subunit requires the presence of a nonhydrolysable GTP analogue (GDP γ S), since no binding is detected in the presence of GTP or GDP (Matsuo *et al.*, 2006). Consistently, the GTPase activity of RbgA is stimulated by the presence of the 50S subunit, however no comparison was made using 45S precursors. Analysis of the 45S particles reveals that r-protein L16, L27 and L36 are absent (Matsuo *et al.*, 2006; Schaefer *et al.*, 2006; Uicker *et al.*, 2006), and yeast two-hybrid and pull-down assays demonstrate that RbgA directly interacts with only one r-protein, namely L25 (Matsuo *et al.*, 2006). Binding of RbgA to the 50S subunit led to protection from DMS (dimethyl sulfate) of C928 and C942 (H38), A2301 (H81) and A2354 (H85) in the 23S rRNA. In the mature 50S subunit, L16, L25 and L27 interact with H38 and are in proximity to C928 (Figure 6b and c). In addition, an extension from L16 reaches towards A2301. The crystal structure of *B. subtilis* RbgA (PDB1PUJ) has two domains, an N-terminal G-domain connected through a conserved linker to an acidic C-terminal domain (CTD) (Figure 6d), which can adopt different relative orientations dependent on the GNP state (Kim *et al.*, 2008). Therefore it is tempting to speculate that it is the CTD of RbgA that interacts with the highly basic r-protein L25 and RbgA may even be involved in recruiting L16 and L27 to the ribosome. L16 and L27 are both late assembly proteins confirming that RbgA is involved in a late assembly step. The addition of L16 during assembly results in large conformational changes within the ribosome, which is consistent with the conversion of the 45S to 50S particle. The inability of 45S to interact with 30S subunits to form 70S ribosomes suggests that RbgA may act as

a control checkpoint, ensuring only mature 50S particles enter into the translation cycle (Uicker *et al.*, 2006).

References

- Alix JH and Nierhaus KH (2003) DnaK-facilitated ribosome assembly in *Escherichia coli* revisited. *RNA* **9**: 787–793.
- Al Refaii A and Alix JH (2009) Ribosome biogenesis is temperature-dependent and delayed in *E. coli* lacking the chaperones DnaK or DnaJ. *Molecular Microbiology* **71**: 748–762.
- Bharat A, Jiang M, Sullivan SM, Maddock JR and Brown ED (2006) Cooperative and critical roles for both G domains in the GTPase activity and cellular function of ribosome-associated *E. coli* EngA. *Journal of Bacteriology* **188**: 7992–7996.
- Brown ED (2005) Conserved P-loop GTPases of unknown function in bacteria: an emerging and vital ensemble in bacterial physiology. *Biochemistry and Cell Biology* **83**: 738–746.
- Buglino J, Shen V, Hakimian P and Lima CD (2002) Structural and biochemical analysis of the Obg GTP binding protein. *Structure* **10**: 1581–1592.
- Bylund G, Wipemo L, Lundberg L and Wikstrom P (1998) RimM and RbfA are essential for efficient processing of 16S rRNA in *E. coli*. *Journal of Bacteriology* **180**: 73–82.
- Bylund GO, Persson BC, Lundberg LAC and Wikstrom PM (1997) A novel ribosome-associated protein is important for efficient translation in *E. coli*. *Journal of Bacteriology* **179**: 4567–4574.
- Caldon CE, Yoong P and March PE (2001) Evolution of a molecular switch: universal bacterial GTPases regulate ribosome function. *Molecular Microbiology* **41**: 289–297.
- Cameron D, Gregory S, Thompson J *et al.* (2004) *Thermus thermophilus* L11 methyltransferase, PrmA, is dispensable for growth and preferentially modifies free ribosomal protein L11 prior to ribosome assembly. *Journal of Bacteriology* **186**: 5819–5825.
- Campbell TL and Brown ED (2008) Genetic interaction screens with ordered overexpression and deletion clone sets implicate the *E. coli* GTPase YjeQ in late ribosome biogenesis. *Journal of Bacteriology* **190**: 2537–2545.
- Campbell TL, Daigle DM and Brown ED (2005) Characterization of the *Bacillus subtilis* GTPase YloQ and its role in ribosome function. *Biochemical Journal* **389**: 843–852.
- Charollais J, Dreyfus M and Iost I (2004) CsdA, a cold-shock RNA helicase from *E. coli*, is involved in the biogenesis of 50S ribosomal subunit. *Nucleic Acids Research* **32**: 2751–2759.
- Chen X, Court D and Ji X (1999) Crystal structure of ERA: a GTPase-dependent cell cycle regulator containing an RNA binding motif. *Proceedings of the National Academy of Sciences of the USA* **96**: 8396–8401.
- Comartin DJ and Brown ED (2006) Non-ribosomal factors in ribosome subunit assembly are emerging targets for new antibacterial drugs. *Current Opinion in Pharmacology* **6**: 453–458.
- Connolly K, Rife JP and Culver G (2008) Mechanistic insight into the ribosome biogenesis functions of an ancient protein KsgA. *Molecular Microbiology* **70**: 1062–1075.
- Daigle DM and Brown ED (2004) Studies of the interaction of *E. coli* YjeQ with the ribosome *in vitro*. *Journal of Bacteriology* **186**: 1381–1387.
- Dammel CS and Noller HF (1995) Suppression of a cold-sensitive mutation in 16S rRNA by overexpression of a novel ribosome-binding factor, RbfA. *Genes & Development* **9**: 626–637.

- Datta PP, Wilson DN, Kawazoe M *et al.* (2007) Structural aspects of RbfA action during small ribosomal subunit assembly. *Molecular Cell* **28**: 434–445.
- Decatur W and Fournier M (2002) rRNA modifications and ribosome function. *TIBS* **27**: 344–351.
- Del Campo M, Kaya Y and Ofengand J (2001) Identification and site of action of the remaining four putative pseudouridine synthases in *E. coli*. *RNA* **7**: 1603–1615.
- Deutscher MP and Li Z (2001) Exoribonucleases and their multiple roles in RNA metabolism. *Progress in Nucleic Acid Research and Molecular Biology* **66**: 67–105.
- Dez C and Tollervey D (2004) Ribosome synthesis meets the cell cycle. *Current Opinion in Microbiology* **7**: 631–637.
- Himeno H, Hanawa-Suetsugu K, Kimura T *et al.* (2004) A novel GTPase activated by the small subunit of ribosome. *Nucleic Acids Research* **32**: 5303–5309.
- Huang Y, Swapna G, Rajan P *et al.* (2003) Solution NMR structure of ribosome-binding factor A (RbfA), a cold-shock adaptation protein from *E. coli*. *Journal of Molecular Biology* **327**: 521–536.
- Hwang J and Inouye M (2006) The tandem GTPase, Der, is essential for the biogenesis of 50S ribosomal subunits in *E. coli*. *Molecular Microbiology* **61**: 1660–1672.
- Inoue K, Alsina J, Chen J and Inouye M (2003) Suppression of defective ribosome assembly in a rbfA deletion mutant by overexpression of Era, an essential GTPase in *E. coli*. *Molecular Microbiology* **48**: 1005–1016.
- Iost I and Dreyfus M (2006) DEAD-box RNA helicases in *E. coli*. *Nucleic Acids Research* **34**: 4189–4197.
- Jiang M, Datta K, Walker A *et al.* (2006) The *E. coli* GTPase CgtA_E is involved in late steps of large ribosome assembly. *Journal of Bacteriology* **188**: 6757–6770.
- Jones PG, Mitta M, Kim Y, Jiang W and Inouye M (1996) Cold shock induces a major ribosomal-associated protein that unwinds double-stranded RNA in *E. coli*. *Proceedings of the National Academy of Sciences of the USA* **93**: 76–80.
- Kaczanowska M and Rydén-Aulin M (2005) The YrdC protein – a putative ribosome maturation factor. *Biochimica et Biophysica Acta* **1727**: 87–96.
- Karginov AV, Karginova OA, Spiridonova VA and Kopylov AM (1995) *In vivo* assembly of plasmid-expressed ribosomal protein S7 of *Thermus thermophilus* into *E. coli* ribosomes and conditions of its overexpression. *FEBS Letters* **369**: 158–160.
- Kim do J, Jang JY, Yoon HJ and Suh SW (2008) Crystal structure of YlqF, a circularly permuted GTPase: implications for its GTPase activation in 50S ribosomal subunit assembly. *Proteins* **72**: 1363–1370.
- Kimura T, Takagi K, Hirata Y *et al.* (2008) Ribosome-small-subunit-dependent GTPase interacts with tRNA-binding sites on the ribosome. *Journal of Molecular Biology* **381**: 467–477.
- Kukimoto-Niino M, Murayama K, Inoue M *et al.* (2004) Crystal structure of the GTP-binding protein Obg from *Thermus thermophilus* HB8. *Journal of Molecular Biology* **337**: 761–770.
- Lövgren J, Bylund G, Srivastava M *et al.* (2004) The PRC-barrel domain of the ribosome maturation protein RimM mediates binding to ribosomal protein S19 in the 30S ribosomal subunits. *RNA* **10**: 1798–1812.
- Lu Q and Inouye M (1998) The gene for 16S rRNA methyltransferase (ksgA) functions as a multicopy suppressor for a cold-sensitive mutant of era, an essential RAS-like GTP-binding protein in *E. coli*. *Journal of Bacteriology* **180**: 5243–5246.
- Maki JA, Schnobrich DJ and Culver GM (2002) The DnaK chaperone system facilitates 30S ribosomal subunit assembly. *Molecular Cell* **10**: 129–138.
- Matsuo Y, Morimoto T, Kuwano M *et al.* (2006) The GTP-binding protein YlqF participates in the late step of 50S ribosomal subunit assembly in *Bacillus subtilis*. *Journal of Biological Chemistry* **281**: 8110–8117.
- Morimoto T, Loh P, Hirai T *et al.* (2002) Six GTP-binding proteins of the Era/Obg family are essential for cell growth in *Bacillus subtilis*. *Microbiology* **148**: 3539–3552.
- Muench SP, Xu L, Sedelnikova SE and Rice DW (2006) The essential GTPase YphC displays a major domain rearrangement associated with nucleotide binding. *Proceedings of the National Academy of Sciences of the USA* **103**: 12359–12364.
- Na JG, Pinto I and Hampsey M (1992) Isolation and characterisation of SUA5, a novel gene required for normal growth in *Saccharomyces cerevisiae*. *Genetics* **131**: 791–801.
- Robinson V, Hwang J, Fox E, Inouye M and Stock A (2002) Domain arrangement of Der, a switch protein containing two GTPase domains. *Structure* **10**: 1649–1658.
- Ruzhenikov SN, Das SK, Sedelnikova SE *et al.* (2004) Analysis of the open and closed conformations of the GTP-binding protein YsxC from *Bacillus subtilis*. *Journal of Molecular Biology* **339**: 265–278.
- Sato A, Kobayashi G, Hayashi H *et al.* (2005) The GTP binding protein Obg homolog ObgE is involved in ribosome maturation. *Genes to Cells* **10**: 393–408.
- Sayed A, Matsuyama S and Inouye M (1999) Era, an essential *E. coli* small G-protein, binds to the 30S ribosomal subunit. *Biochemical and Biophysical Research Communications* **264**: 51–55.
- Schaefer L, Uicker WC, Wicker-Planquart C *et al.* (2006) Multiple GTPases participate in the assembly of the large ribosomal subunit in *Bacillus subtilis*. *Journal of Bacteriology* **188**: 8252–8258.
- Sharma MR, Barat C, Wilson DN *et al.* (2005) Interaction of Era with the 30S ribosomal subunit: implications for 30S subunit assembly. *Molecular Cell* **18**: 319–329.
- Shin DH, Lou Y, Jancarik J *et al.* (2004) Crystal structure of YjeQ from *Thermotoga maritima* contains a circularly permuted GTPase domain. *Proceedings of the National Academy of Sciences of the USA* **101**: 13198–13203.
- Tan J, Jakob U and Bardwell JC (2002) Overexpression of two different GTPases rescues a null mutation in a heat-induced rRNA methyltransferase. *Journal of Bacteriology* **184**: 2692–2698.
- Teplova M, Tereshko V, Sanishvili R *et al.* (2000) The structure of the yrdC gene product from *E. coli* reveals a new fold and suggests a role in RNA binding. *Protein Science* **9**: 2557–2566.
- Tomar SK, Dhimole N, Chatterjee M and Prakash B (2009) Distinct GDP/GTP bound states of the tandem G-domains of EngA regulate ribosome binding. *Nucleic Acids Research* **1–12**.
- Uicker WC, Schaefer L and Britton RA (2006) The essential GTPase RbgA (YlqF) is required for 50S ribosome assembly in *Bacillus subtilis*. *Molecular Microbiology* **59**: 528–540.
- Wilson DN and Nierhaus KH (2007) The weird and wonderful world of bacterial ribosome regulation. *Critical Reviews in Biochemistry and Molecular Biology* **42**: 187–219.

- Wout P, Pu K, Sullivan S *et al.* (2004) The *E. coli* GTPase CgtA_E cofractionates with the 50S ribosomal subunit and interacts with SpoT, a ppGpp synthetase/hydrolase. *Journal of Bacteriology* **186**: 5249–5257.
- Xia B, Ke H, Shinde U and Inouye M (2003) The role of RbfA in 16S rRNA processing and cell growth at low temperature in *E. coli*. *Journal of Molecular Biology* **332**: 575–584.
- ## Further Reading
- Bénédicte M (2005) Obg/CgtA, a signalling protein that controls replication, translation and morphological development. *Developmental Cell* **9**: 300–301.
- Kaczanowska M and Ryden-Aulin M (2007) Ribosome biogenesis and the translation process in *E. coli*. *Microbiology and Molecular Biology Reviews* **71**: 477–494.
- Maki JA and Culver GM (2005) Recent developments in factor-facilitated ribosome assembly. *Methods* **36**: 313–320.
- Nierhaus KH and Wilson DN (eds) (2004) *Protein Synthesis and Ribosome Structure: Translating the Genome*. Weinheim: WILEY-VCH Verlag GmbH&Co.
- Williamson JR (2008) Biophysical studies of bacterial ribosome assembly. *Current Opinion in Structural Biology* **18**: 299–304.
- Woodson SA (2008) RNA folding and ribosome assembly. *Current Opinion in Chemical Biology* **12**: 667–673.

Paper II

**Siibak T, Peil L, Dönhöfer A, Tats A,
Remm M, Wilson DN, Tenson T, Remme J.
*Antibiotic-induced ribosomal assembly defects result
from changes in the synthesis of ribosomal proteins.*
Mol Microbiol. 2011 Apr; 80(1): 54-67.**

Antibiotic-induced ribosomal assembly defects result from changes in the synthesis of ribosomal proteins

Triinu Siibak,¹ Lauri Peil,² Alexandra Dönhöfer,³
Age Tats,¹ Mado Remm,¹ Daniel N. Wilson,³
Tanel Tenson² and Jaanus Remme^{1*}

Institutes of ¹Molecular and Cell Biology and

²Technology, University of Tartu, Tartu, Estonia.

³Gene Center and Department for Biochemistry,
University of Munich, Munich, Germany.

Summary

Inhibitors of protein synthesis cause defects in the assembly of ribosomal subunits. In response to treatment with the antibiotics erythromycin or chloramphenicol, precursors of both large and small ribosomal subunits accumulate. We have used a pulse-labelling approach to demonstrate that the accumulating subribosomal particles mature into functional 70S ribosomes. The protein content of the precursor particles is heterogeneous and does not correspond with known assembly intermediates. Mass spectrometry indicates that production of ribosomal proteins in the presence of the antibiotics correlates with the amounts of the individual ribosomal proteins within the precursor particles. Thus, treatment of cells with chloramphenicol or erythromycin leads to an unbalanced synthesis of ribosomal proteins, providing the explanation for formation of assembly-defective particles. The operons for ribosomal proteins show a characteristic pattern of antibiotic inhibition where synthesis of the first proteins is inhibited weakly but gradually increases for the subsequent proteins in the operon. This phenomenon most likely reflects translational coupling and allows us to identify other putative coupled non-ribosomal operons in the *Escherichia coli* chromosome.

Introduction

Bacterial ribosomes are composed of three ribosomal RNAs (rRNAs) and over 50 ribosomal protein (r-proteins). The rRNA and r-proteins are organized into two unequal subunits, termed small (30S) and large (50S) subunits. In

addition to the transcription of the rRNA and translation of r-proteins, ribosome biogenesis also involves processing and modification of the constituent components and assembly of them into functional particles. The co-ordinated synthesis of the ~60 different molecules is achieved through a variety of regulatory mechanisms (Nomura *et al.*, 1984; Zengel and Lindahl, 1994; Condon *et al.*, 1995). Ribosome subunit assembly is fast and efficient, occurring within 2–3 min following the transcription of the rRNA (Lindahl, 1975). The high efficiency of ribosome assembly is evident from the negligible turnover of ribosomal components during exponential growth at moderate to fast rates in wild-type *Escherichia coli* (Bremer and Dennis, 1987). rRNA processing, modification and association with r-proteins is already initiated concomitant with transcription (reviewed by Kaczanowska and Ryden-Aulin, 2007). Short-lived intermediate particles of both subunits are formed during ribosome assembly (Lindahl, 1975). These particles have been extensively analysed using *in vitro* ribosome reconstitution approaches (reviewed by Nierhaus, 1991; Culver, 2003). One predominant precursor particle, the 21S particle, is observed during the small subunit, whereas two assembly intermediate particles, 34S and 43S, are seen during large subunit assembly. The protein composition of the subunit assembly intermediate particles has been used to define the order of the r-protein association with the rRNA, culminating in the ribosome subunit assembly maps (Held *et al.*, 1974; Herold and Nierhaus, 1987). Assembly maps depict the cooperativity between binding of individual proteins. More recent experiments have identified multiple parallel pathways for association of small ribosome subunit proteins with 16S rRNA during reconstitution of the 30S subunit (Talkington *et al.*, 2005; Mulder *et al.*, 2010).

Chloramphenicol and erythromycin are well-known inhibitors of protein synthesis (reviewed by Wilson, 2009). These antibiotics bind to the large ribosomal subunit (Schlünzen *et al.*, 2001; Bulkley *et al.*, 2010; Dunkle *et al.*, 2010), chloramphenicol inhibiting peptidyl transfer and release (Monro and Marcker, 1967; Tompkins *et al.*, 1970) and erythromycin entrance of the nascent peptide into the ribosome exit tunnel (Tenson *et al.*, 2003; Lovmar *et al.*, 2004). It was observed in the late 1950s that treatment of bacteria with chloramphenicol leads to the accumulation

Accepted 16 January, 2011. *For correspondence. E-mail jremme@ebc.ee; Tel. (+372) 7375031; Fax (+372) 7420286.

of defective ribosomal particles (Dagley and Sykes, 1959). After several years of studies it was concluded that the assembly inhibition is indirect, caused by inhibition of r-protein synthesis (Dodd *et al.*, 1991). In the 1990s it was recognized that erythromycin also causes accumulation of defective ribosomal particles (Chittum and Champney, 1995). In this case it was suggested that the drug binds to the ribosomal large subunit precursor particles and thereby directly inhibits the progression of subunit assembly (Usary and Champney, 2001). Our recent observation that both chloramphenicol and erythromycin inhibit assembly of both ribosomal subunits, in combination with the result that a ribosomal resistance mechanism that does not function on the precursor particles can rescue the erythromycin induced assembly defect, suggests that both drugs inhibit assembly indirectly (Siibak *et al.*, 2009). The indirect mechanism suggests that the composition of the assembly-defective particles reflects the amounts of r-proteins synthesized in the presence of the drugs, with production of different r-proteins being suppressed to different extents. Here we use quantitative mass spectrometry to determine the compositions of the precursor particles and measure the amounts of r-proteins produced in the presence of the antibiotics chloramphenicol and erythromycin.

Results

Time-course of ribosome subunit assembly

The assembly-defective ribosomal particles start to accumulate immediately after addition of chloramphenicol or erythromycin to the exponentially growing *E. coli* culture (Siibak *et al.*, 2009). We used a pulse-labelling approach to study whether or not the subribosomal particles are able to mature into 70S ribosomes. *E. coli* culture was grown at 25°C where ribosomal assembly is slower compared with the assembly at 37°C, thus allowing better resolution of the intermediate particles (Peil *et al.*, 2008; Al Refaii and Alix, 2009). The exponentially growing bacterial culture was incubated with either chloramphenicol or erythromycin for 5 min, which is sufficient for inhibition of translation and ribosome subunit assembly (Siibak *et al.*, 2009). RNA was labelled for 5 min with [³H]uridine, after which the transcription initiation was blocked with rifampicin. Cells collected at different time points (0, 5, 10, 20, 40 and 60 min), after rifampicin addition, were lysed and the ribosomes were analysed by sucrose density gradient centrifugation.

Figure 1A shows the time-course of ribosome assembly in the untreated cells. The optical curve shows the positions of the 70S ribosomes and the free 30S and 50S subunits. The radioactive diagram depicts the newly made ribosomal particles formed in the presence or absence of

drugs. In the first time point, collected at the time of rifampicin addition, the majority of radioactively labelled RNA was found in the 30S and 50S fractions, whereas 5 min later the radioactivity was distributed equally between the free subunits and the 70S fractions. After 10 min, most of the radioactive signal was found in the 70S fraction, indicating that the ribosome assembly was complete and that there was no significant degradation of rRNA. Further incubation did not change the distribution of radioactive RNA in sucrose gradients. Thus, the mean time for entering the newly transcribed rRNA into 70S pool is 5 min at 25°C, in agreement with previous observations (Peil *et al.*, 2008).

When erythromycin was added to the culture, most of the radioactivity was in the 30S and 25S fractions at the starting time point (Fig. 1B). After 40 min, approximately equal amounts of [³H]uridine were found in the 30S, 50S and 70S regions. Upon further incubation the proportion of radioactivity in the 70S fraction continued to grow leaving only a minor peak to the 35S region of the 60 min time point. Similar results were obtained with chloramphenicol, although assembly was a slightly faster in this case: already at 20 min after rifampicin addition, radioactivity is distributed equally in the 70S and free subunits (Fig. 1C). Nevertheless, 1 h after stopping RNA synthesis, most of the radioactivity was also found in the 70S ribosome fractions. In summary, the mean time of ribosome assembly was 40 min in the presence of erythromycin and 20 min in the presence of chloramphenicol. The results show that 70S ribosomes are assembled in the presence of chloramphenicol and erythromycin, but that the rate of ribosome assembly is significantly reduced. The latter finding is consistent with the slow maturation of rRNA observed in the presence of chloramphenicol or erythromycin (Siibak and Remme, 2010). Finally, it is important to note that majority of the rRNA is finally incorporated into 70S ribosomes without significant rRNA degradation being observed.

Protein content of the precursor particles

As a next step, chloramphenicol and erythromycin were added to the exponentially growing *E. coli* culture and the ribosomal particles accumulating in the presence of drugs were separated by two consecutive sucrose density gradient centrifugation steps (Fig. 2). The assembly intermediate particles were initially analysed by negative-stain electron microscopy (EM) (Fig. 2B and C) in comparison with mature 30S and 50S ribosomal subunits and 70S ribosomes (Fig. 2A). 35S and 45S particles are assembly intermediates of the large ribosomal subunit and 25S particles are precursors of the mature 30S ribosomal subunit. The results show that 25S and 35S intermediate particles isolated from chloramphenicol- and

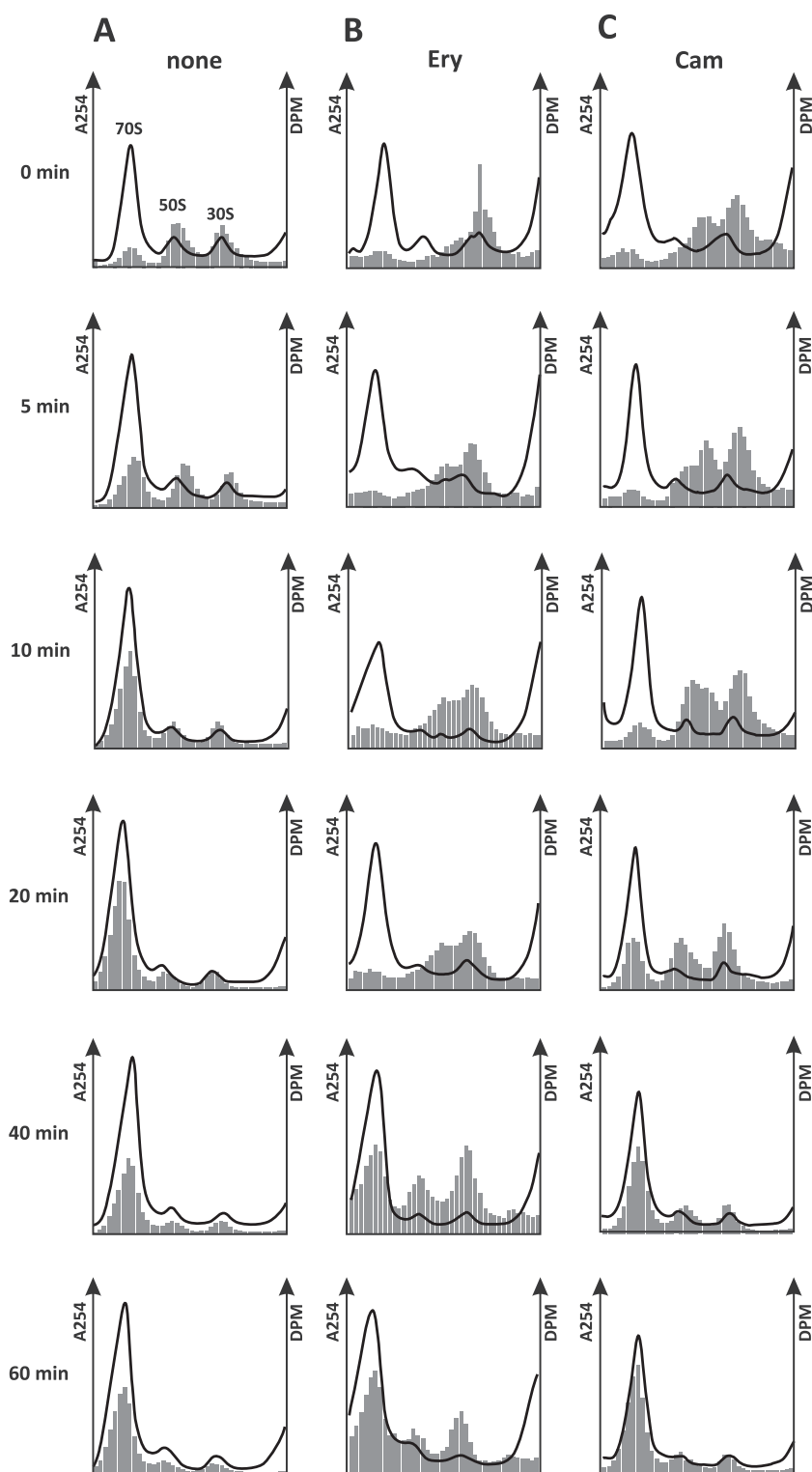


Fig. 1. Time-course of ribosome assembly shows that the drug-induced 25S, 35S and 45S particles are assembled into 70S ribosomes. (A) No antibiotics (none), (B) erythromycin (Ery, 100 $\mu\text{g ml}^{-1}$) or (C) chloramphenicol (Cam, 7 $\mu\text{g ml}^{-1}$) was added 5 min before labelling and RNA was labelled for 5 min with [^3H]uridine, after which the transcription initiation was blocked with rifampicin. Cells collected at different time points (0, 5, 10, 20, 40 and 60 min) were lysed, ribosomes were fractionated by centrifugation in sucrose density gradients, and the fractions were counted for radioactivity. The optical density profiles are shown by black lines and radioactivity profiles by grey bars.

erythromycin-treated cells are highly heterogeneous, with a tendency for aggregation. In contrast, 45S particles show higher homogeneity, with morphological similarity to mature 50S ribosomal subunits.

Subsequently, the levels of r-proteins in the assembly intermediate particles were determined using a quantitative mass-spectrometry approach. The collected particles were mixed with equimolar amount (according to the

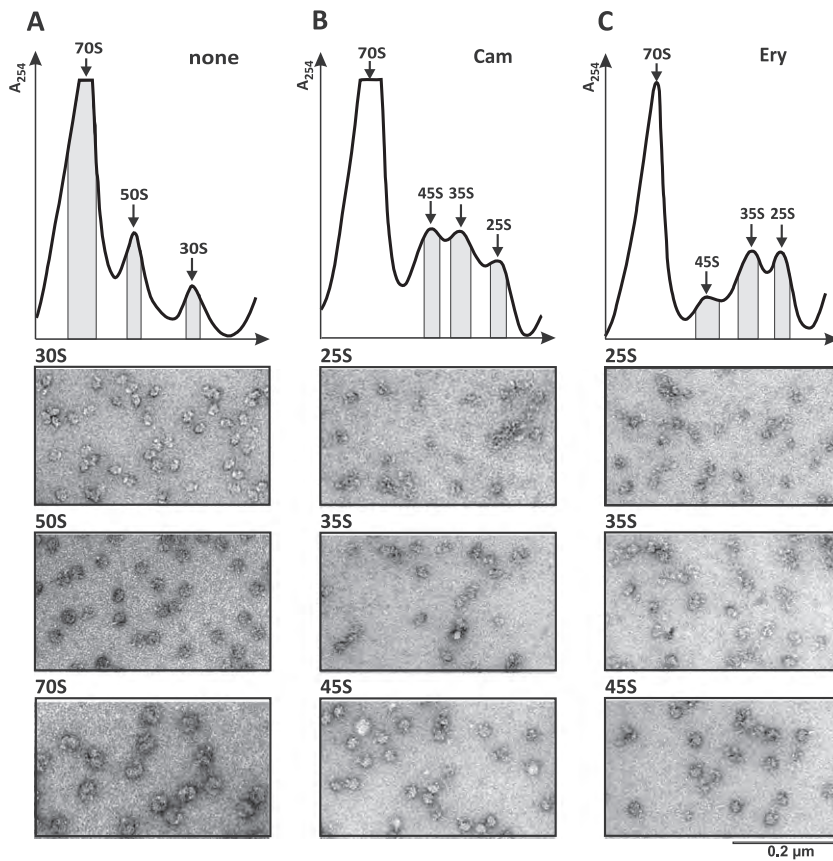


Fig. 2. Sucrose density gradient centrifugation profiles from (A) control with no antibiotic (none), (B) chloramphenicol (Cam)- and (C) erythromycin (Ery)-treated cells. Fractions from sucrose gradients were collected (grey shaded area) and negative-stain EM was performed on the (A) mature ribosomal subunits (30S and 50S) and 70S ribosomes, in comparison with intermediate particles from the small ribosomal subunit (25S) and the large ribosomal subunit (35S and 45S) from (B) Cam- and (C) Ery-treated cells.

absorbance at 260 nm) of the corresponding *E. coli* ribosomal subunit containing uniformly [^{15}N]-labelled r-proteins. R-proteins of the mixed particles were digested with trypsin and the [^{15}N]/[^{14}N] ratio in tryptic peptides was determined by mass spectrometry, as described previously (Pulk *et al.*, 2010). Relative amounts of r-proteins in the subribosomal particles were calculated by taking the [^{15}N]/[^{14}N] ratio of primary rRNA-binding proteins L3 and S15 as 100% for the large and small subunit proteins respectively (Fig. 3). The average occupancy of the reference proteins was 70% for S15 in the 25S, 90% for L3 in the 35S and 100% for L3 in the 45S particles (data not shown).

The 25S particles contain proteins S15, S16 and S18 in nearly equal high amounts. Other proteins are found in low or negligible levels, with the late assembly proteins S1, S2, S3 and S21 being present in the lowest amounts. Both chloramphenicol and erythromycin cause accumulation of particles with similar protein composition (Fig. 3A, correlation of protein composition between two particles is in Fig. S1). A difference is observed for proteins S4 and S11, which are more abundant in particles accumulating in response to chloramphenicol as compared with erythromycin (Fig. 3A). The protein composition of 25S particles suggests that the lack of primary 16S rRNA-binding

proteins is the reason for their accumulation in response to drug treatment.

In the 35S particles most proteins are present in low or negligible amounts relative to the level of L3. Only L11 is present at ~100% in the case of both antibiotics. In general, the two 35S fractions induced by either antibiotic are similar to each other (Fig. 3B, correlation in Fig. S2). The biggest difference concerns the large subunit assembly-initiator protein L24, which is present at ~100% in the 'chloramphenicol 35S particles', but four times less (~25%) in the 'erythromycin particles' (Fig. 3B). The other two proteins being present in erythromycin particles at considerably lower levels as compared with the chloramphenicol particles are L4 and L23. In contrast, L6 and L9 are present in erythromycin particles at considerably higher levels compared with the chloramphenicol particles. It is evident that the protein composition of 35S particles is different from the known early assembly particles (Herold and Nierhaus, 1987; Nierhaus, 1991). The 45S particle contains high levels of most of the large subunit proteins, with only L16, L35 and L36 being present at less than 30%. This is in line with the previous observation that L16 is required for the late events of large ribosome subunit assembly (Franceschi and Nierhaus, 1990). In the 25S and 35S particles most of the proteins

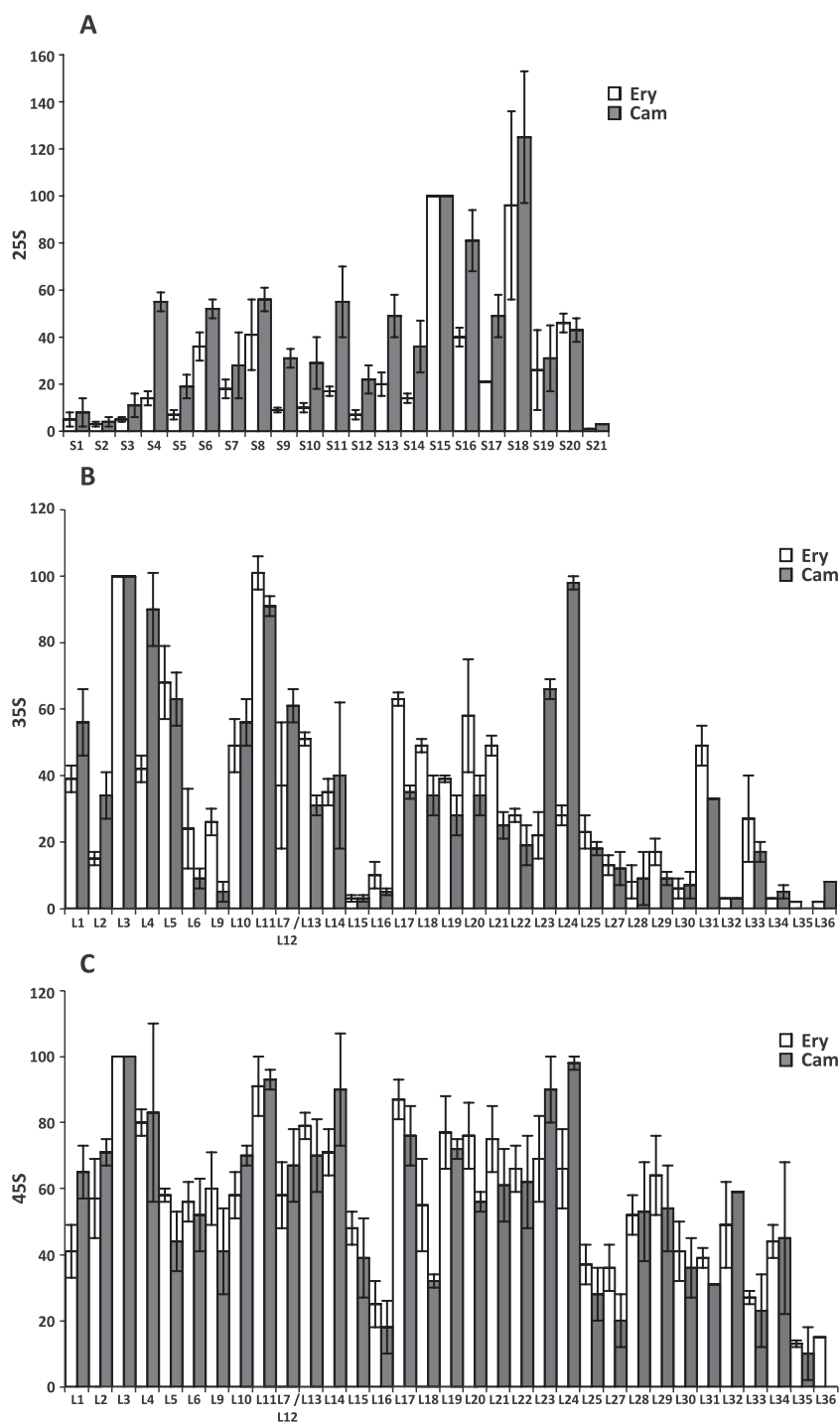


Fig. 3. Quantification of proteins from (A) 30S subunit precursor particles (25S) and (B and C) 50S subunit precursor particles (35S and 45S). 25S, 35S or 45S particles (^{14}N) were mixed with ^{15}N 30S or 50S subunits and r-proteins were isolated. The ratio of ^{14}N and ^{15}N r-proteins was determined by quantitative mass spectrometry and normalized against L3 (L3 = 100%). White bars indicate proteins from ribosomal particles in erythromycin (Ery)-treated cells, whereas grey bars indicate proteins from ribosomal particles in chloramphenicol (Cam)-treated cells. Standard error is indicated.

are present in substoichiometric amounts indicating that the particles are heterogeneous, in agreement with the EM images.

Proteins synthesized in the presence of the drugs

Ribosomal subunit assembly depends on the availability of the r-proteins. In particular, the primary binding assem-

bly initiator proteins have an important role during early stages of ribosome subunit assembly. Since the protein composition of 25S and 35S proteins does not coincide with that of the known early assembly intermediate particles (21S and 34S respectively) (Fig. 3), it might reflect instead the availability of r-proteins in the drug-treated cells. Additionally, an important point is whether the drugs inhibit production of r-proteins in a uniform manner or

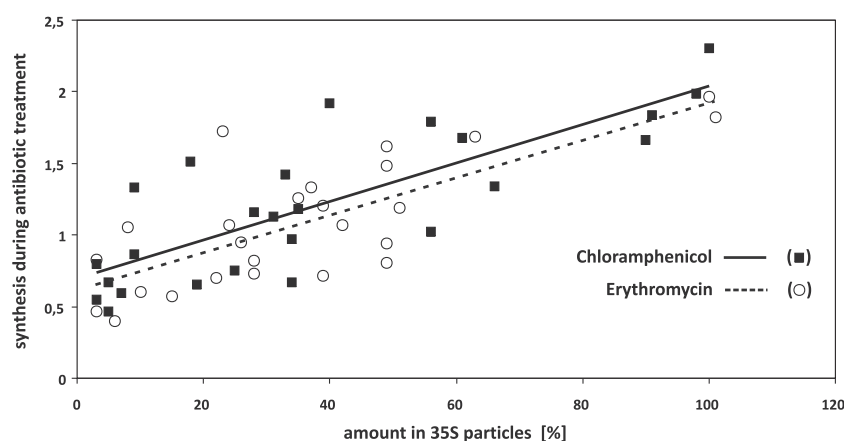


Fig. 4. Correlation of the protein content of the 35S particles with the synthesis of r-proteins in the presence of antibiotics erythromycin (Ery, white circles) and chloramphenicol (Cam, black squares). The protein content of the 35S was calculated as described for Fig. 3. The synthesis level is expressed as a ratio to the untreated control. The data for r-protein L4 are removed as synthesis of this protein is induced by both antibiotics at very high level.

whether the inhibition is more pronounced for some specific proteins. Therefore we used a pSILAC approach (Schwanhauser *et al.*, 2009) to measure the production of individual r-proteins in the presence of the antibiotics chloramphenicol and erythromycin. Exponentially growing cells were divided into two parts. In one sample 'light' medium (unlabelled amino acids, Arg0:Lys0) was changed against isotopically labelled 'heavy' medium (Arg10:Lys8) and antibiotic was added; cells were collected after 4 h. To obtain the control cells without antibiotic treatment, the other sample was diluted with equal amount of fresh unlabelled medium, after 2 h the medium was switched to 'medium' labelled (Arg6:Lys4) and the cells were collected after 2 h. The different labelling period in the presence (4 h) and absence of the antibiotics (2 h) was important to have similar label incorporation in both samples, as the antibiotics suppress protein synthesis and thereby label incorporation. Equal amounts of cells, as estimated by optical density, were mixed together, lysed and the proteins were protease digested and analysed by mass spectrometry. The measured heavy-to-medium ratio was used in calculations.

Inhibition of translation by chloramphenicol or erythromycin causes enhancement (for example, as seen for L5) or inhibition of r-protein synthesis as related to the level of average protein synthesis. However, production of individual r-proteins differs markedly (Table S1). To test for the possible correlations between synthesis of r-proteins and the compositions of the subribosomal particles, a linear regression analysis was used. The synthesis of large ribosomal subunit proteins correlates with their amounts in the 35S particles, the coefficient of determination, R^2 , was 0.38 for erythromycin measurements and 0.4 for the chloramphenicol case. In the case of both antibiotic treatments, the L5 level was unproportionally high. Therefore, after removal of the data for L5 the correlations become considerably stronger (R^2 around 0.6) (Fig. 4) indicating that the protein composition of 35S particles is largely determined by protein availability in the

cells. The correlation of 25S composition with ribosomal small subunit protein synthesis is weaker (R^2 being 0.28) in the case of erythromycin, or absent (R^2 being 0.08) in the case of chloramphenicol. We conclude that the composition of 35S particles, but not the 25S particles, reflects the protein levels produced in the cell in the presence of the drugs.

Detection of coupled cistrons using protein levels

The genes for r-proteins are organized in operons and certain r-proteins can act as a translational inhibitor within their own operon (Nomura *et al.*, 1984). In Fig. 5, the levels of synthesis of r-proteins are mapped onto the operon structures with examples of autogenous regulation (arrowed). Interestingly, in some operons, exemplified by the S10 operon, we observe a general trend where the first protein in the operon is synthesized at the highest level, followed by a gradual loss of production over the following cistrons. In the *spc* operon, L5 (encoded by the third cistron) is present in the highest amount, followed by a gradual decrease of proteins from the subsequent cistrons. There are some interesting exceptions to that rule, seen for L17, L7/L12 and L19 in the α , *rpoBC* and *trmD* operons respectively. The pattern of gradual decrease is consistent with the mechanism of translational coupling described previously for r-protein operons (Nomura *et al.*, 1984; Zengel and Lindahl, 1994). As the initiation of translation of a downstream gene depends on the number of ribosomes reaching the termination codon of the upstream gene the inhibition of translation would lead to gradual decrease of translation in the operon. Therefore we considered the gradually decreasing pattern in the operon as an indicator of translational coupling. We screened our data set for other, non-ribosomal operons exhibiting this pattern and found several potential candidates (Fig. 6). We note that while the gradual decrease is seen very clearly for ribosomal operons, only a limited number of other operons showed a similar pattern. This

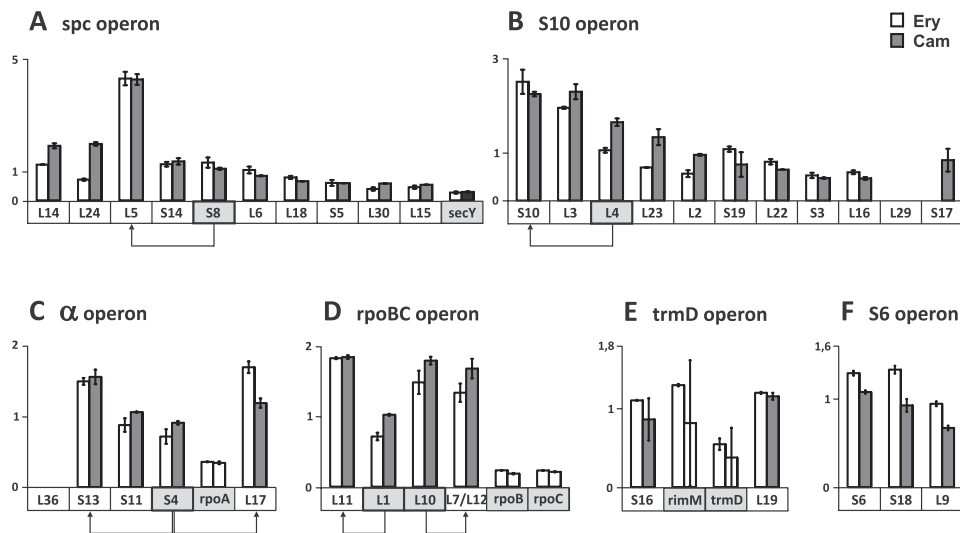


Fig. 5. Levels of r-protein synthesis in the presence of erythromycin (Ery, white bar) and chloramphenicol (Cam, grey bar) respectively. Feedback regulation of operons is shown with arrows, and regulatory r-proteins are highlighted with a grey box (Nomura *et al.*, 1984). Non-r-proteins are marked by white bars and grey-shaped boxes. Standard errors are indicated. (A) *spc* operon; (B) *S10* operon; (C) α operon; (D) *rpoBC* operon; (E) *trmD* operon; (F) *S6* operon.

may partly relate to the fact that while r-proteins are expressed at very high levels, other operons often code for proteins expressed at low to very low levels. This in turn hinders reliable mass-spectrometry measurements and creates 'holes' in the operon maps of the lower

expressed proteins. Nevertheless, a gradual decrease was observed in the *his* operon, although this was only in the presence of erythromycin. Another example of an operon showing a gradually decreasing pattern starts with *yceD*. In the *lptA* operon, the first three genes seem to be

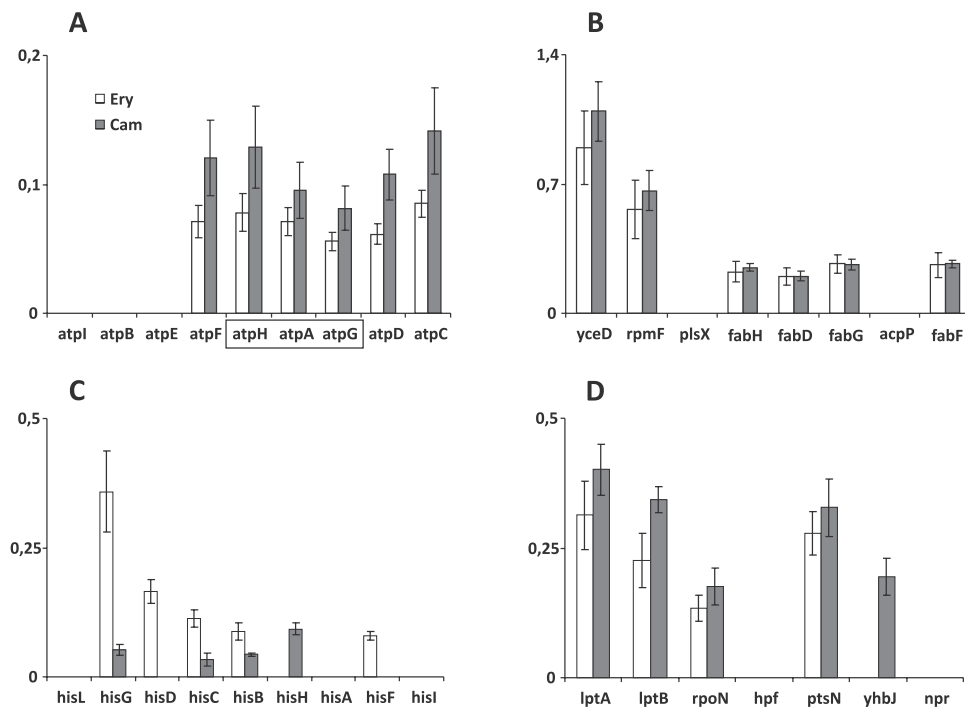


Fig. 6. Levels of protein synthesis in the presence of erythromycin (Ery, white bar) and chloramphenicol (Cam, grey bar) respectively. The data are presented on the operon structures. Standard errors are indicated. A. The well-documented case of translational coupling of *atpH*, *atpA* and *atpG* (boxed) (Hellmuth *et al.*, 1991; Rex *et al.*, 1994). B–D. Additional cases of translational coupling suggested by the current analysis.

coupled whereas the other genes in the operon do not. Translational coupling between *atpH*, *atpA* and *atpG* genes (Fig. 6A) has been described previously (Gerstel and McCarthy, 1989; Hellmuth *et al.*, 1991; Rex *et al.*, 1994) consistent with the gradual pattern observed in our data set.

Discussion

We have confirmed that assembly-defective particles accumulate in response to treatment of *E. coli* cells with either chloramphenicol or erythromycin (Fig. 2). Pulse-labelling experiments show (Fig. 1) that most of the particles can mature into functional ribosomes albeit with a reduced rate, which is qualitatively consistent with previous reports for chloramphenicol particles (Hosokawa and Nomura, 1965; Nomura and Hosokawa, 1965; Adesnik and Levinthal, 1969). The experiments indicate that the drug-induced subribosomal particles represent assembly intermediates. Why do chloramphenicol and erythromycin slow down ribosome subunit assembly? Binding to assembly intermediates causing direct inhibition has been proposed for erythromycin (Usary and Champney, 2001) and an indirect effect through inhibition of r-protein synthesis has been suggested for chloramphenicol (Dodd *et al.*, 1991).

Both erythromycin and chloramphenicol cause accumulation of 25S, 35S and 45S particles. The corresponding particles induced by both drugs have similar, although not identical, protein composition (Fig. 3), suggesting that the subribosomal particles of both antibiotics accumulate due to the similar defect in ribosome biogenesis. The 25S and 35S particles contain individual proteins at very different levels, with a continuum from only trace amounts (e.g. S1, S2 and L15, L16, L32) to apparent full occupancy (S15, S18 and L3, L4, L11). This shows that the particles are very heterogeneous, a finding we have confirmed by EM (Fig. 2). Furthermore, the heterogeneity of the subribosomal 25S and 35S particles indicates that the antibiotics do not block a specific state in the assembly, but rather act on a more general protein synthesis level. R-protein composition of the 45S particles is more complete as compared with that of the 35S (Fig. 3), although several proteins are still present in low amounts. Recently, Williamson and colleagues have analysed r-protein composition of the subribosomal particles formed in the presence of neomycin by using quantitative LC/MS approach (Sykes *et al.*, 2010). The protein composition of 21S particles formed in the presence of neomycin was very similar to that described here for 'chloramphenicol 25S particles'. Protein composition of the pre-50S subunits formed upon neomycin treatment described by Sykes *et al.* (2010) is similar to the protein content of the 'chloramphenicol-induced 35S subunits' (Fig. 3).

In *E. coli*, ribosomal assembly intermediates have been characterized using cell-free reconstitution systems. Assembly of the small subunit proceeds via one clearly separable precursor particle (21S) and the large subunit has two precursors (34S and 43S) (Lindahl, 1975). It is possible that the 25S, 35S and 45S subribosomal particles formed upon addition of antibiotics are related to the previously described precursor particles. Small subunit reconstitution experiments have revealed the proteins required for early assembly intermediate formation: S4, S7, S8, S15, S17 and S20 (Held *et al.*, 1974; Holmes and Culver, 2004). Large subunit reconstitution experiments identified L3, L4, L13, L20, L22 and L24 as essential proteins for the first assembly intermediate (34S) formation (Herold and Nierhaus, 1987). Proteins S4 and S7 of the small subunit and L3 and L24 of the large subunit were identified by reconstitution experiments as assembly initiator proteins (Nowotny and Nierhaus, 1982; 1988). Our data show that both erythromycin- and chloramphenicol-induced 25S particles contain the assembly essential proteins S4, S7, S8, S17 and S20 at levels < 60% of nominal amount. In the erythromycin-induced 35S particles, the early assembly essential proteins L4, L22 and L24 are present at levels < 50% (Fig. 3B), whereas in the chloramphenicol-induced 35S particles the proteins L13, L20 and L22 are also found at levels < 50%. This shows that several proteins identified previously as being essential for early assembly are present at low levels in the 35S and 25S particles. Since the particles are still formed and can mature into functional ribosomes, this suggests that under certain stress conditions, such as translation inhibition, assembly proceeds via alternative pathways. Precedents are documented; for example, in the absence of assembly initiator protein L24, protein L20 has been shown to take over its role in initiating large ribosome subunit assembly *in vitro* (Franceschi and Nierhaus, 1988). Similarly, multiple pathways of small subunit protein binding to 16S rRNA have been observed during 30S subunit reconstitution and a phenomenon termed the 'assembly landscape' explains incomplete cooperativity of small ribosome subunit assembly (Talkington *et al.*, 2005). Unlike the composition of 35S particles, the protein composition of 45S particles is in general agreement with that of the second assembly intermediate (43S particle) and thereby with the large ribosome subunit assembly map (Nierhaus, 1991).

The protein composition of the 35S and 45S particles might reflect direct inhibition of assembly by the drugs or be caused by unbalanced synthesis of r-proteins during antibiotic inhibition. To investigate this issue the proteins produced during antibiotic treatment were determined in relation to the proteins produced in the absence of the drugs. Inhibition of translation by chloramphenicol or erythromycin is expected to cause overexpression of

rRNA in relation to r-proteins. This in turn should lead to the derepression of r-protein operons (Dean *et al.*, 1981; Nomura *et al.*, 1984; Mattheakis and Nomura, 1988; Zengel and Lindahl, 1994). The protein composition of the subribosomal particles was compared with the relative levels of r-proteins produced in the presence of drugs. The synthesis of large subunit r-proteins correlates well with their amounts in the 35S particles (Fig. 4): All r-proteins present in 35S at levels near to 100% are produced at ratios above 1.5 when compared with the uninhibited control. Conversely, proteins produced at ratios around 0.5 are found in the 35S particles at levels < 10% (Table S1). The composition of the 25S particles does not however reflect the proteins produced in the presence of the drugs, but rather the assembly map, with the late assembly proteins being present in negligible amounts. The lack of correlation in the 25S may reflect the lower general exchangeability of small subunit r-proteins compared with large subunit r-proteins (Pulk *et al.*, 2010). Nevertheless, the observation that composition of the 35S particles reflects the amounts of r-proteins produced, in combination with the fact that the drugs inhibit assembly of both subunits, leads us to the conclusion that during treatment with either chloramphenicol or erythromycin, ribosomal assembly is inhibited through an indirect mechanism, i.e. via inhibition of r-protein synthesis.

In general, the levels of individual proteins produced in the cell are very similar in the presence of both chloramphenicol and erythromycin. The same is true for the protein compositions of the respective accumulating subribosomal particles. Still, there are some interesting differences between the two drugs: production of the proteins L23 and L24 is inhibited considerably stronger by erythromycin as compared with chloramphenicol, the difference being reflected in the composition of the corresponding 35S particles. The low level of the assembly initiator protein L24 can cause relative overrepresentation of 35S-like particles in the erythromycin-treated cells (Figs 1 and 2). Decreased level of L24 could also account for the apparently specific erythromycin inhibition of 50S subunit assembly, as observed by others (Usary and Champney, 2001). What might cause the erythromycin specific decrease in the L24 level? It has been observed previously that both antibiotics can have inhibitory effects depending on the nascent peptide sequence (Lovett and Rogers, 1996; Tenson and Ehrenberg, 2002; Ramu *et al.*, 2009; Starosta *et al.*, 2010), thus suggesting that this kind of sequence-dependent differences are operational also here. Alternatively, more indirect influences, through differential effects on cell physiology, are also possible.

We observed that the amounts of r-proteins synthesized in the presence of the drugs decrease in the operons, with the first proteins made in the highest

amounts followed by a gradual decrease (Fig. 5). Exceptions include the third cistron in the L5 *spc* operon, which is produced at higher levels than upstream genes encoding L14 and L24 (Fig. 5A). Interestingly, the regulator protein S8 binds to the mRNA in front of the L5 coding region (Cerretti *et al.*, 1988; Merianos *et al.*, 2004) suggesting that the cistrons under translationally coupled regulation start with the open reading frame for L5, whereas the upstream ones are regulated through the mRNA degradation-mediated retroregulation (Mattheakis *et al.*, 1989). Similarly, S4 and L10 act as regulator proteins for S13/L17 and L10/(L7/L12) in the α and *rpoBC* operons respectively (Fig. 5C and D) (Yates *et al.*, 1980; 1981). L19 in the *trmD* operon also appears to be independently regulated from S16-RimM-TrmD (Fig. 5F), although non-autogenous regulation has been suggested for this operon (Wikström *et al.*, 1988). It is also possible that the gradual decrease we describe is not caused by effects at the level of protein synthesis, but effects at the level of mRNA availability. Nevertheless, the data available for chloramphenicol inhibition (Cheung *et al.*, 2003) show that the gradual decrease in protein levels is not reflected in mRNA levels, leaving translational effects as the prime candidate to explain the current results. It is noteworthy that the results of r-protein expression upon chloramphenicol treatment obtained by Dennis (1976) are in agreement with the gradual decrease in operons at variety of drug concentrations.

We have collected the data for about 1400 members of the *E. coli* proteome, allowing us to ask if other operons respond in a similar manner to the r-protein operons. We note that one limitation was that many operons previously described to be translationally coupled (Schümperli *et al.*, 1982; Aksoy *et al.*, 1984; Harms *et al.*, 1988; Little *et al.*, 1989; Wilson and Macnab, 1990; Gan *et al.*, 1995; Lyngstadaas *et al.*, 1995) are expressed only in specific conditions and therefore not detectable in our analysis. Nevertheless, we could confirm some previously described cases, for example the translational coupling between *atpH*, *atpA* and *atpG* (Gerstel and McCarthy, 1989; Hellmuth *et al.*, 1991; Rex *et al.*, 1994) (Fig. 6). Furthermore, several new cases of translational coupling are suggested by our analysis (Fig. 6): a gradual decrease is observed in the histidine biosynthesis operon in the presence of erythromycin. It is interesting to note that the *his* operon is induced by erythromycin, but not by chloramphenicol. This induction can be caused by stalling ribosomes at the attenuator open reading frame *hisL* (Johnston *et al.*, 1980; Chan and Landick, 1993), consistent with the ability of erythromycin to allow synthesis of eight amino acids (Tenson *et al.*, 2003) causing ribosome stalling at the beginning of the histidine codon track required for functional attenuation. Both erythromycin and chloramphenicol cause gradual decreases in the *lptA* and

lptB genes required for lipopolysaccharide assembly (Sperandeo *et al.*, 2008), followed by *rpoN*, the sigma factor for nitrogen assimilation (Zhao *et al.*, 2010). A similar decrease is observed in the operon that combines the *rpmF* gene for r-protein L32 with genes for fatty acid biosynthesis (Podkovyrov and Larson, 1995; Zhang and Cronan, 1998). In general, the gradual decrease characteristic for r-protein genes was clearly seen for only a few non-ribosomal operons suggesting that translational coupling is not very common for the highly expressed genes in *E. coli*. For ribosomal biosynthesis the translational coupling is expected to lead for stoichiometric production of r-proteins. Similarly, translational coupling has been proposed to be involved in ensuring the stoichiometry of the ATP synthase complex (Rex *et al.*, 1994). The generally low level of translational coupling might indicate the lack of other complexes with such strict control of the stoichiometry of the components or the dominance of other mechanisms regulating protein production.

Experimental procedures

Strains

Escherichia coli strain MG1655 (Blattner *et al.*, 1997) was used in all experiments, except for SILAC labelling, where arginine and lysine auxotrophic strain AT713 was used instead (a generous gift from Dr Matthias Selbach, Max Delbrück Center for Molecular Medicine).

Isolation of *E. coli* ribosomal particles

Cells were grown at 25°C in 200 ml 2× YT medium (Sambrook and Russell, 2001) until the A_{600} reached 0.2. At this point, either erythromycin (final concentration, 100 µg ml⁻¹) or chloramphenicol (final concentration, 7 µg ml⁻¹) was added. The cultures were then incubated for a further 2 h. The cells were collected by centrifugation in a Sorvall GS-3 rotor at 4000 r.p.m. and 4°C for 10 min and were resuspended in 1 ml of lysis buffer [60 mM KCl, 60 mM NH₄Cl, 50 mM Tris-HCl (pH 8), 6 mM MgCl₂, 6 mM β-mercaptoethanol, 16% sucrose]; lysozyme and DNase I (Amresco, GE Healthcare) were added to final concentrations of 1 mg ml⁻¹ and 20 U ml⁻¹ respectively. The cells were incubated for 15 min at -70°C and then thawed in ice-cold water for 30 min. The freeze-thaw cycle was repeated twice, followed by centrifugation at 13 000 g and 4°C for 20 min. The supernatant was diluted twofold with buffer A [60 mM KCl, 60 mM NH₄Cl, 10 mM Tris-HCl (pH 8), 12 mM MgCl₂, 6 mM β-mercaptoethanol]. Lysate was first loaded onto a 30 ml, 10–25% (w/w) sucrose gradient prepared in buffer A and then centrifuged at 23 000 r.p.m. in an SW28 rotor (Beckman) at 4°C for 13.5 h. 45S, 35S and 25S particle fractions from antibiotic-treated cells were diluted twofold with buffer A and concentrated by ultrafiltration using Amicon Ultracel-100k filters. To ensure purity of the precursor particles, the collected fractions for each precursor were repurified using a second sucrose gradient centrifugation step.

Negative-stain electron microscopy

Ribosomal particles were diluted in Tico buffer [20 mM HEPES-HCl pH 7.6 (0°C), 6 mM MgCl₂, 30 mM NH₄Cl and 4 mM β-mercaptoethanol] to a final concentration of 1 A₂₆₀ ml⁻¹. One drop of each sample was deposited on a carbon-coated grid. After 30 s, grids were washed with distilled water and then stained with three drops of 2% aqueous uranyl acetate for 15 s. The remaining liquid was removed by touching the grid with filter paper. Micrographs were taken using a Morgagni transmission electron microscope (FEI), 40–100 kV, wide angle 1 K CCD at direct magnifications of 80–100 K.

Pulse labelling

Escherichia coli cells were grown at 25°C in 400 ml of tryptone (10 g l⁻¹)-yeast extract (1 g l⁻¹)-NaCl (10 g l⁻¹) until the A_{600} reached 0.2. Erythromycin (final concentration, 100 µg ml⁻¹) or chloramphenicol (final concentration, 7 µg ml⁻¹) was added, 5 min later 20 µCi of [³H]uridine (38 Ci mmol⁻¹; GE Healthcare) was added, and 5 min later incorporation of the label was stopped by adding rifampin (rifampicin) (final concentration, 500 µg ml⁻¹). Cells were collected at 0, 5, 10, 20, 20 and 60 min after the addition of rifampin by centrifugation and lysed, and ribosomes were analysed by sucrose gradient centrifugation as described above. Each sucrose gradient was fractionated into 40 fractions. High-molecular-weight material was precipitated by adding an equal volume of 20% trichloroacetic acid (TCA). The precipitates were collected on glass-fibre filters, and the radioactivity incorporated was measured by scintillation counting.

¹⁵N labelling and LC-MS/MS analysis

Escherichia coli strain MRE600 was uniformly labelled by growing the cells in the presence of ¹⁵NH₄Cl as the only nitrogen source (Kalju Vanatalu, Tallinn University of Technology). Cells were lysed and ribosomes extracted as described above.

For quantitative studies, one A₂₆₀ unit of [¹⁵N]-labelled 50S or 30S wild-type ribosome subunits was mixed either with one A₂₆₀ unit of 45S or 35S particles, or with one A₂₆₀ unit of 25S particles from antibiotics-treated cells respectively. Ribosomal particles were precipitated with 10% ice-cooled TCA and proteins dissolved in 7 M urea/2 M thiourea. For protease digestion, disulphide bridges were reduced with 1 mM DTT for 1 h at room temperature and cysteines blocked with 5 mM iodoacetamide (IAA) for 1.5 h at room temperature. The urea concentration was diluted by adding two volumes of 100 mM NH₃HCO₃, and proteins were digested with endoprotease LysC (1:50 enzyme/protein ratio, Wako, Japan) for 4 h at room temperature. Subsequently, two volumes of 100 mM NH₃HCO₃ were added, and peptides were further digested with trypsin (1:50 enzyme/protein ratio, Promega, USA) for 12 h at room temperature. Peptides corresponding to approximately 0.2 A₂₆₀ units of ribosomes were purified on C18 StageTips (Rappsilber *et al.*, 2007) and analysed using nano-LC-coupled mass spectrometry.

Peak lists for database searches were produced with raw2msm (Olsen *et al.*, 2005), and proteins were identified using the Mascot search engine 2.2 (Matrix Science, UK) run against a custom-made *E. coli* protein database (4978 entries) that included the most commonly observed contaminant sequences, such as proteases, keratins, etc. The search criteria were as follows: full tryptic specificity was required (Trypsin/P); two missed cleavages were allowed; carbamidomethylation was set as a fixed modification; oxidation (M), N-acetylation (protein) and N-formylation (protein) were set as variable modifications; [^{15}N] metabolic labelling was selected as quantification method; precursor ion mass tolerance was 5 p.p.m.; fragment ion mass tolerance was 0.8 Da; and the Mascot built-in decoy database option was used to estimate the false discovery rate (FDR) for peptides. The minimum ions score was set to 15 and the significance threshold was adjusted to keep FDR < 1% before saving the results for the subsequent quantitative analysis. Mascot result files were processed with MultiRawPrepare and N15 helper scripts before quantitative data analysis was performed with MSQuant v1.5 (<http://www.ncbi.nlm.nih.gov/pubmed/19888749>). Only bold red peptides were included in the analysis, classified by Mascot scores as Category A ≥ 33 , Category B ≥ 25 , Category C ≥ 15 ; protein was validated with a total ABC score of more than 40. N15 labelling was selected for quantification and only r-proteins were selected for quantifications, all quantified spectra were manually validated to remove borderline hits and erroneous quantifications; relative errors of protein quantifications were $\leq 20\%$ as determined by MSQuant.

pSILAC labelling

Escherichia coli strain AT713 was grown at 25°C in 75 ml of 'light' MOPS minimal medium supplemented with 0.1% glucose and 100 $\mu\text{g ml}^{-1}$ of each amino acid (including 'light' arginine and lysine, Arg0 and Lys0) until the A_{600} reached 0.2. Exponentially growing cells were divided into two parts and treated as described below.

Shortly, for antibiotic treatment one part of cells was pelleted and resuspended in pre-warmed MOPS 'heavy'-labelled medium (Arg10:Lys8, CNLM-539 and CNLM-291, Cambridge Isotope Laboratories) supplemented with either chloramphenicol or erythromycin (7 and 100 $\mu\text{g ml}^{-1}$ respectively). Treated cells were grown for further 4 h at 25°C and collected. Control cells not getting antibiotic treatment were initially diluted with equal amount of fresh pre-warmed 'light' medium, after 2 h of growth cells were pelleted and resuspended in pre-warmed MOPS minimal 'medium'-labelled medium (Arg6:Lys4, CLM-2265 and DLM-2640, Cambridge Isotope Laboratories). Control cells were grown for further 2 h at 25°C and collected. The different labelling period in the presence (4 h) or absence of the antibiotics (2 h) was important to have similar label incorporation in both samples, as the antibiotics suppress protein synthesis and thereby label incorporation. Equal amounts of cells, as estimated by optical density, were mixed together and processed as described below.

Cells were lysed in SDS/DTT/TRIS buffer according to FASP protocol (<http://www.ncbi.nlm.nih.gov/pubmed/19377485>) and total protein concentration was measured

using tryptophan fluorescence (excitation 295 nm, emission 350 nm, with an assumption that 1 μg of tryptophan equals to 91 μg of lysate). Next, 100 μg of lysate was LysC and trypsin double-digested according to FASP protocol (<http://www.ncbi.nlm.nih.gov/pubmed/19377485>), and resulting peptides were fractionated using SAX-C18 StageTip-based protocol (<http://www.ncbi.nlm.nih.gov/pubmed/19848406>) and analysed using nano-LC-coupled mass spectrometry.

Alternatively, 100 μg of lysate was methanol:chloroform precipitated (<http://www.ncbi.nlm.nih.gov/pubmed/6731838>) and subjected to in-solution digestion as described above. Digested peptides were fractionated into 12 fractions on an OFFGEL 3100 instrument (Agilent) according to manufacturer's instructions and modified protocol from <http://dx.doi.org/10.1002/pmic.200800351>, using 13-cm-long IPG 3-10 DryStrips (GE Healthcare). Peptide-containing fractions were acidified, purified on C18 StageTips (<http://www.ncbi.nlm.nih.gov/pubmed/17703201>) and analysed using nano-LC-coupled mass spectrometry.

Nano-LC-MS/MS

Peptides were separated by reversed-phase chromatography using an Agilent 1200 series nanoflow system (Agilent Technologies) connected to a LTQ Orbitrap classic mass spectrometer (Thermo Electron, Bremen, Germany) equipped with a nanoelectrospray ion source (Proxeon, Odense, Denmark). Purified peptides were dissolved in 0.5% formic acid and loaded on a fused silica emitter (75 $\mu\text{m} \times 150 \text{ mm}$, Proxeon) packed in-house with Repropur-Sil C18-AQ 3 μm particles (Dr Maisch, Germany) using a flow rate of 700 nl min $^{-1}$. SAX-fractionated SILAC-labelled peptides were separated with 240 min gradients as follows: pH 3–5 fraction – 8–36% B gradient, pH 6 fraction – 8–35% B gradient, pH 8 fraction – 5–33% B gradient, pH 11 fraction – 2–30% B gradient (A: 0.5% acetic acid, B: 0.5% acetic acid/80% acetonitrile) at a flow rate of 200 nl min $^{-1}$; IEF-fractionated SILAC-labelled peptides were separated with 120 min 3–40% B (A: 0.5% acetic acid, B: 0.5% acetic acid/80% acetonitrile) gradients at a flow rate of 200 nl min $^{-1}$. Eluted peptides were sprayed directly into LTQ Orbitrap mass spectrometer operated at 180°C capillary temperature and 2.4 kV spray voltage. The LTQ Orbitrap was operated in the data-dependent mode with up to five MS/MS scans being recorded for each precursor ion scan. Precursor ion spectra were recorded in profile in the Orbitrap (m/z 300–1900, $R = 60\,000$, max injection time 500 ms, max 1 000 000 charges); data-dependent MS/MS spectra were acquired in centroid in the LTQ (max injection time 150 ms, max 5 000 charges, normalized CE 35%, wideband activation enabled). Mono-isotopic precursor selection was enabled, singly charged ions and ions with an unassigned charge state were rejected, and each fragmented ion was dynamically excluded for 120 s. All measurements in the Orbitrap mass analyser were performed with lock-mass option enabled (lock masses were m/z 445.12003 and 519.13882).

Data analysis

Combined raw data files from SAX and IEF fractionations were analysed with the MaxQuant software package, version

1.0.13.13 (<http://www.ncbi.nlm.nih.gov/pubmed/19029910>, <http://www.ncbi.nlm.nih.gov/pubmed/19373234>). Generated peak lists were searched with the Mascot search engine 2.2 against an *E. coli* protein sequence database (downloaded from <http://www.ecogene.org> on 22 September 2009) supplemented with common contaminants (e.g. human keratins, trypsin) and reversed sequences of all entries in order to estimate false-positive rates. Mascot searches were performed with full tryptic specificity (Trypsin/P), a maximum of two missed cleavages and a mass tolerance of 0.5 Da for fragment ions. Carbamidomethylation of cysteine was set as fixed and methionine oxidation was set as variable modification. A maximum of three missed cleavages were allowed. In MaxQuant, FDR thresholds were set to 1% at both peptide and protein level, minimum required peptide length was set to six amino acids, maximum peptide PEP was set to 0.005 and at least three peptides and two ratio counts were required for protein identification and quantification.

Acknowledgements

We wish to thank Dr A. Liiv (University of Tartu) for help and advice and Dr K. Vanatalu (Tallinn University) for [¹⁵N]-labelled *E. coli* MRE600 biomass. This work was supported by the Human Frontiers of Science Organization (RGY0088/2008 to D.N.W.), by Estonian Science Foundation Grants No. 8197 (T.T.) and 7509 (J.R.), and by SF0180166s08 (T.T.) and SF0180164s08 (J.R.) from the Estonian Ministry of Education and Research. Mass-spectrometric analyses were in part supported by the European Regional Development Fund through the Center of Excellence in Chemical Biology (Institute of Technology, University of Tartu). Electronic data processing in Fig. 6 was supported by SF0180026s09 from the Estonian Ministry of Education and Research (M.R.) and by the EU through the European Regional Development Fund through the Estonian Centre of Excellence in Genomics.

References

- Adesnik, M., and Levinthal, C. (1969) Synthesis and maturation of ribosomal RNA in *Escherichia coli*. *J Mol Biol* **46**: 281–303.
- Aksoy, S., Squires, C., and Squires, C. (1984) Translational coupling of the *trpB* and *trpA* genes in the *Escherichia coli* tryptophan operon. *J Bacteriol* **157**: 363–367.
- Al Refaii, A., and Alix, J. (2009) Ribosome biogenesis is temperature-dependent and delayed in *Escherichia coli* lacking the chaperones DnaK or DnaJ. *Mol Microbiol* **71**: 748–762.
- Blattner, F., Plunkett, G.R., Bloch, C., Perna, N., Burland, V., Riley, M., et al. (1997) The complete genome sequence of *Escherichia coli* K-12. *Science* **277**: 1453–1462.
- Bremer, H., and Dennis, P.P. (1987) Modulation of chemical composition and other parameters of the cell by the growth rate. In *Escherichia coli and Salmonella typhimurium Cellular and Molecular Biology*. Neinhardt, F., Ingraham, J.L., Low, K.B., Magasanik, B., Schaechter, M., and Umberger, H.E. (eds). Washington, DC: American Society for Microbiology, pp. 1527–1542.
- Bulkley, D., Innis, C., Blaha, G., and Steitz, T. (2010) Revisiting the structures of several antibiotics bound to the bacterial ribosome. *Proc Natl Acad Sci USA* **107**: 17158–17163.
- Cerretti, D., Mattheakis, L., Kearney, K., Vu, L., and Nomura, M. (1988) Translational regulation of the *spc* operon in *Escherichia coli*. Identification and structural analysis of the target site for S8 repressor protein. *J Mol Biol* **204**: 309–329.
- Chan, C., and Landick, R. (1993) Dissection of the *his* leader pause site by base substitution reveals a multipartite signal that includes a pause RNA hairpin. *J Mol Biol* **233**: 25–42.
- Cheung, K., Badarinarayana, V., Selinger, D., Janse, D., and Church, G. (2003) A microarray-based antibiotic screen identifies a regulatory role for supercoiling in the osmotic stress response of *Escherichia coli*. *Genome Res* **13**: 206–215.
- Chittum, H., and Champney, W. (1995) Erythromycin inhibits the assembly of the large ribosomal subunit in growing *Escherichia coli* cells. *Curr Microbiol* **30**: 273–279.
- Condon, C., Squires, C., and Squires, C. (1995) Control of rRNA transcription in *Escherichia coli*. *Microbiol Rev* **59**: 623–645.
- Culver, G. (2003) Assembly of the 30S ribosomal subunit. *Biopolymers* **68**: 234–249.
- Dagley, S., and Sykes, J. (1959) Effect of drugs upon components of bacterial cytoplasm. *Nature* **183**: 1608–1609.
- Dean, D., Yates, J., and Nomura, M. (1981) Identification of ribosomal protein S7 as a repressor of translation within the *str* operon of *E. coli*. *Cell* **24**: 413–419.
- Dennis, P. (1976) Effects of chloramphenicol on the transcriptional activities of ribosomal RNA and ribosomal protein genes in *Escherichia coli*. *J Mol Biol* **108**: 535–546.
- Dodd, J., Kolb, J., and Nomura, M. (1991) Lack of complete cooperativity of ribosome assembly *in vitro* and its possible relevance to *in vivo* ribosome assembly and the regulation of ribosomal gene expression. *Biochimie* **73**: 757–767.
- Dunkle, J., Xiong, L., Mankin, A., and Cate, J. (2010) Structures of the *Escherichia coli* ribosome with antibiotics bound near the peptidyl transferase center explain spectra of drug action. *Proc Natl Acad Sci USA* **107**: 17152–17157.
- Franceschi, F., and Nierhaus, K. (1988) Ribosomal protein L20 can replace the assembly-initiator protein L24 at low temperatures. *Biochemistry* **27**: 7056–7059.
- Franceschi, F., and Nierhaus, K. (1990) Ribosomal proteins L15 and L16 are mere late assembly proteins of the large ribosomal subunit. Analysis of an *Escherichia coli* mutant lacking L15. *J Biol Chem* **265**: 16676–16682.
- Gan, K., Sankaran, K., Williams, M., Aldea, M., Rudd, K., Kushner, S., et al. (1995) The *umpA* gene of *Escherichia coli* encodes phosphatidylglycerol:prolipoprotein diacylglycerol transferase (Igt) and regulates thymidylate synthase levels through translational coupling. *J Bacteriol* **177**: 1879–1882.
- Gerstel, B., and McCarthy, J. (1989) Independent and coupled translational initiation of *atp* genes in *Escherichia coli*: experiments using chromosomal and plasmid-borne *lacZ* fusions. *Mol Microbiol* **3**: 851–859.
- Harms, E., Higgins, E., Chen, J., and Umberger, H. (1988) Translational coupling between the *ilvD* and *ilvA* genes of *Escherichia coli*. *J Bacteriol* **170**: 4798–4807.
- Held, W., Ballou, B., Mizushima, S., and Nomura, M. (1974)

- Assembly mapping of 30S ribosomal proteins from *Escherichia coli*. Further studies. *J Biol Chem* **249**: 3103–3111.
- Hellmuth, K., Rex, G., Surin, B., Zinck, R., and McCarthy, J. (1991) Translational coupling varying in efficiency between different pairs of genes in the central region of the *atp* operon of *Escherichia coli*. *Mol Microbiol* **5**: 813–824.
- Herold, M., and Nierhaus, K. (1987) Incorporation of six additional proteins to complete the assembly map of the 50S subunit from *Escherichia coli* ribosomes. *J Biol Chem* **262**: 8826–8833.
- Holmes, K., and Culver, G. (2004) Mapping structural differences between 30S ribosomal subunit assembly intermediates. *Nat Struct Mol Biol* **11**: 179–186.
- Hosokawa, K., and Nomura, M. (1965) Incomplete ribosomes produced in chloramphenicol- and puromycin-inhibited *Escherichia coli*. *J Mol Biol* **12**: 225–241.
- Johnston, H., Barnes, W., Chumley, F., Bossi, L., and Roth, J. (1980) Model for regulation of the histidine operon of *Salmonella*. *Proc Natl Acad Sci USA* **77**: 508–512.
- Kaczanowska, M., and Ryden-Aulin, M. (2007) Ribosome biogenesis and the translation process in *Escherichia coli*. *Microbiol Mol Biol Rev* **71**: 477–494.
- Lindahl, L. (1975) Intermediates and time kinetics of the *in vivo* assembly of *Escherichia coli* ribosomes. *J Mol Biol* **92**: 15–37.
- Little, S., Hyde, S., Campbell, C., Lilley, R., and Robinson, M. (1989) Translational coupling in the threonine operon of *Escherichia coli* K-12. *J Bacteriol* **171**: 3518–3522.
- Lovett, P., and Rogers, E. (1996) Ribosome regulation by the nascent peptide. *Microbiol Rev* **60**: 366–385.
- Lovmar, M., Tenson, T., and Ehrenberg, M. (2004) Kinetics of macrolide action: the josamycin and erythromycin cases. *J Biol Chem* **279**: 53506–53515.
- Lyngstadaas, A., Lbner-Olesen, A., and Boye, E. (1995) Characterization of three genes in the *dam*-containing operon of *Escherichia coli*. *Mol Gen Genet* **247**: 546–554.
- Mattheakis, L., and Nomura, M. (1988) Feedback regulation of the *spc* operon in *Escherichia coli*: translational coupling and mRNA processing. *J Bacteriol* **170**: 4484–4492.
- Mattheakis, L., Vu, L., Sor, F., and Nomura, M. (1989) Retro-regulation of the synthesis of ribosomal proteins L14 and L24 by feedback repressor S8 in *Escherichia coli*. *Proc Natl Acad Sci USA* **86**: 448–452.
- Merianos, H., Wang, J., and Moore, P. (2004) The structure of a ribosomal protein S8/*spc* operon mRNA complex. *RNA* **10**: 954–964.
- Monro, R., and Marcker, K. (1967) Ribosome-catalysed reaction of puromycin with a formylmethionine-containing oligonucleotide. *J Mol Biol* **25**: 347–350.
- Mulder, A., Yoshioka, C., Beck, A., Bunner, A., Milligan, R., Potter, C., et al. (2010) Visualizing ribosome biogenesis: parallel assembly pathways for the 30S subunit. *Science* **330**: 673–677.
- Nierhaus, K. (1991) The assembly of prokaryotic ribosomes. *Biochimie* **73**: 739–755.
- Nomura, M., and Hosokawa, K. (1965) Biosynthesis of ribosomes: fate of chloramphenicol particles and of pulse-labeled RNA in *Escherichia coli*. *J Mol Biol* **12**: 242–265.
- Nomura, M., Gourse, R., and Baughman, G. (1984) Regulation of the synthesis of ribosomes and ribosomal components. *Annu Rev Biochem* **53**: 75–117.
- Nowotny, V., and Nierhaus, K. (1982) Initiator proteins for the assembly of the 50S subunit from *Escherichia coli* ribosomes. *Proc Natl Acad Sci USA* **79**: 7238–7242.
- Nowotny, V., and Nierhaus, K. (1988) Assembly of the 30S subunit from *Escherichia coli* ribosomes occurs via two assembly domains which are initiated by S4 and S7. *Biochemistry* **27**: 7051–7055.
- Olsen, J., de Godoy, L., Li, G., Macek, B., Mortensen, P., Pesch, R., et al. (2005) Parts per million mass accuracy on an Orbitrap mass spectrometer via lock mass injection into a C-trap. *Mol Cell Proteomics* **4**: 2010–2021.
- Peil, L., Virumäe, K., and Remme, J. (2008) Ribosome assembly in *Escherichia coli* strains lacking the RNA helicase DeaD/CsdA or DbpA. *FEBS J* **275**: 3772–3782.
- Podkovyrov, S., and Larson, T. (1995) Lipid biosynthetic genes and a ribosomal protein gene are cotranscribed. *FEBS Lett* **368**: 429–431.
- Pulk, A., Liiv, A., Peil, L., Maiväli, Ü., Nierhaus, K., and Remme, J. (2010) Ribosome reactivation by replacement of damaged proteins. *Mol Microbiol* **75**: 801–814.
- Ramu, H., Mankin, A., and Vazquez-Laslop, N. (2009) Programmed drug-dependent ribosome stalling. *Mol Microbiol* **71**: 811–824.
- Rappsilber, J., Mann, M., and Ishihama, Y. (2007) Protocol for micro-purification, enrichment, pre-fractionation and storage of peptides for proteomics using StageTips. *Nat Protoc* **2**: 1896–1906.
- Rex, G., Surin, B., Besse, G., Schneppe, B., and McCarthy, J. (1994) The mechanism of translational coupling in *Escherichia coli*. Higher order structure in the *atpA* mRNA acts as a conformational switch regulating the access of *de novo* initiating ribosomes. *J Biol Chem* **269**: 18118–18127.
- Sambrook, J., and Russell, D. (2001) *Molecular Cloning: A Laboratory Manual*, 3rd edn. New York: Cold Spring Harbor Laboratory Press.
- Schlünzen, F., Zarivach, R., Harms, J., Bashan, A., Tocilj, A., Albrecht, R., et al. (2001) Structural basis for the interaction of antibiotics with the peptidyl transferase centre in eubacteria. *Nature* **413**: 814–821.
- Schümperli, D., McKenney, K., Sobieski, D., and Rosenberg, M. (1982) Translational coupling at an intercistronic boundary of the *Escherichia coli* galactose operon. *Cell* **30**: 865–871.
- Schwanhauser, B., Gossen, M., Dittmar, G., and Selbach, M. (2009) Global analysis of cellular protein translation by pulsed SILAC. *Proteomics* **9**: 205–209.
- Siibak, T., and Remme, J. (2010) Subribosomal particle analysis reveals the stages of bacterial ribosome assembly at which rRNA nucleotides are modified. *RNA* **16**: 2023–2032.
- Siibak, T., Peil, L., Xiong, L., Mankin, A., Remme, J., and Tenson, T. (2009) Erythromycin- and chloramphenicol-induced ribosomal assembly defects are secondary effects of protein synthesis inhibition. *Antimicrob Agents Chemother* **53**: 563–571.
- Sperandeo, P., Lau, F., Carpentieri, A., De Castro, C., Molinaro, A., Deho, G., et al. (2008) Functional analysis of the protein machinery required for transport of lipopolysaccharide to the outer membrane of *Escherichia coli*. *J Bacteriol* **190**: 4460–4469.
- Starosta, A., Karpenko, V., Shishkina, A., Mikolajka, A., Sum-

- batyan, N., Schlutzen, F., *et al.* (2010) Interplay between the ribosomal tunnel, nascent chain, and macrolides influences drug inhibition. *Chem Biol* **17**: 504–514.
- Sykes, M., Shajani, Z., Sperling, E., Beck, A., and Williamson, J. (2010) Quantitative proteomic analysis of ribosome assembly and turnover *in vivo*. *J Mol Biol* **403**: 331–345.
- Talkington, M., Siuzdak, G., and Williamson, J. (2005) An assembly landscape for the 30S ribosomal subunit. *Nature* **438**: 628–632.
- Tenson, T., and Ehrenberg, M. (2002) Regulatory nascent peptides in the ribosomal tunnel. *Cell* **108**: 591–594.
- Tenson, T., Lovmar, M., and Ehrenberg, M. (2003) The mechanism of action of macrolides, lincosamides and streptogramin B reveals the nascent peptide exit path in the ribosome. *J Mol Biol* **330**: 1005–1014.
- Tompkins, R., Scolnick, E., and Caskey, C. (1970) Peptide chain termination. VII. The ribosomal and release factor requirements for peptide release. *Proc Natl Acad Sci USA* **65**: 702–708.
- Usary, J., and Champney, W. (2001) Erythromycin inhibition of 50S ribosomal subunit formation in *Escherichia coli* cells. *Mol Microbiol* **40**: 951–962.
- Wikström, P., Byström, A., and Björk, G. (1988) Non-autogenous control of ribosomal protein synthesis from the *trmD* operon in *Escherichia coli*. *J Mol Biol* **203**: 141–152.
- Wilson, D. (2009) The A–Z of bacterial translation inhibitors. *Crit Rev Biochem Mol Biol* **44**: 393–433.
- Wilson, M., and Macnab, R. (1990) Co-overproduction and localization of the *Escherichia coli* motility proteins motA and motB. *J Bacteriol* **172**: 3932–3939.
- Yates, J., Arfsten, A., and Nomura, M. (1980) *In vitro* expression of *Escherichia coli* ribosomal protein genes: autogenous inhibition of translation. *Proc Natl Acad Sci USA* **77**: 1837–1841.
- Yates, J., Dean, D., Strycharz, W., and Nomura, M. (1981) *E. coli* ribosomal protein L10 inhibits translation of L10 and L7/L12 mRNAs by acting at a single site. *Nature* **294**: 190–192.
- Zengel, J., and Lindahl, L. (1994) Diverse mechanisms for regulating ribosomal protein synthesis in *Escherichia coli*. *Prog Nucleic Acid Res Mol Biol* **47**: 331–370.
- Zhang, Y., and Cronan, J.J. (1998) Transcriptional analysis of essential genes of the *Escherichia coli* fatty acid biosynthesis gene cluster by functional replacement with the analogous *Salmonella typhimurium* gene cluster. *J Bacteriol* **180**: 3295–3303.
- Zhao, K., Liu, M., and Burgess, R. (2010) Promoter and regulon analysis of nitrogen assimilation factor, sigma54, reveal alternative strategy for *E. coli* MG1655 flagellar biosynthesis. *Nucleic Acids Res* **38**: 1273–1283.

Supporting information

Additional supporting information may be found in the online version of this article.

Please note: Wiley-Blackwell are not responsible for the content or functionality of any supporting materials supplied by the authors. Any queries (other than missing material) should be directed to the corresponding author for the article.

**Márquez V, Fröhlich T, Armache JP, Sohmen D, Dönhöfer A, Mikolajka A,
Berninghausen O, Thomm M, Beckmann R, Arnold GJ, Wilson DN.
*Proteomic characterization of archaeal ribosomes reveals the
presence of novel archaeal specific ribosomal proteins.*
J Mol Biol. 2011 Feb 4; 405(5): 1215-32.**



Proteomic Characterization of Archaeal Ribosomes Reveals the Presence of Novel Archaeal-Specific Ribosomal Proteins

Viter Márquez^{1,2,†}, Thomas Fröhlich^{1,3,†}, Jean-Paul Armache^{1,2}, Daniel Sohmen^{1,2}, Alexandra Dönhöfer^{1,2}, Aleksandra Mikolajka^{1,2}, Otto Berninghausen^{1,2}, Michael Thomm⁴, Roland Beckmann^{1,2}, Georg J. Arnold^{1,3*} and Daniel N. Wilson^{1,2*}

¹Gene Center and Department of Biochemistry, Ludwig-Maximilians-Universität, Feodor Lynen Str. 25, 81377 Munich, Germany

²Center for Integrated Protein Science Munich, Ludwig-Maximilians-Universität, Munich, Germany

³Laboratory for Functional Genome Analysis, Gene Center and Department of Biochemistry, Ludwig-Maximilians-Universität, Feodor Lynen Str. 25, 81377 Munich, Germany

⁴Lehrstuhl für Mikrobiologie, Regensburg University, Universitätsstraße 32, 93053 Regensburg, Germany

Received 29 September 2010;
received in revised form
19 November 2010;
accepted 27 November 2010
Available online
4 December 2010

Edited by J. Doudna

Keywords:

archaea;
cryo electron microscopy;
Pyrobaculum aerophilum;
ribosomal protein;
Sulfolobus acidocaldarius;
mass spectrometry

Protein synthesis occurs in macromolecular particles called ribosomes. All ribosomes are composed of RNA and proteins. While the protein composition of bacterial and eukaryotic ribosomes has been well-characterized, a systematic analysis of archaeal ribosomes has been lacking. Here we report the first comprehensive two-dimensional PAGE and mass spectrometry analysis of archaeal ribosomes isolated from the thermophilic *Pyrobaculum aerophilum* and the thermoacidophilic *Sulfolobus acidocaldarius* Crenarchaeota. Our analysis identified all 66 ribosomal proteins (r-proteins) of the *P. aerophilum* small and large subunits, as well as all but two (62 of 64; 97%) r-proteins of the *S. acidocaldarius* small and large subunits that are predicted genomically. Some r-proteins were identified with one or two lysine methylations and N-terminal acetylations. In addition, we identify three hypothetical proteins that appear to be *bona fide* r-proteins of the *S. acidocaldarius* large subunit. Dissociation of r-proteins from the *S. acidocaldarius* large subunit indicates that the novel r-proteins establish tighter interactions with the large subunit than some integral r-proteins. Furthermore, cryo electron microscopy reconstructions of the *S. acidocaldarius* and *P. aerophilum* 50S subunits allow for a tentative localization of the binding site of the novel r-proteins. This study illustrates not only the potential diversity of the archaeal ribosomes but also the necessity to experimentally analyze the archaeal ribosomes to ascertain their protein

*Corresponding authors. D. N. Wilson is to be contacted at Gene Center, Feodor Lynen Str. 25, 81377 Munich, Germany. G. J. Arnold, Laboratory for Functional Genome Analysis, Gene Center and Department of Biochemistry, Ludwig-Maximilians-Universität, Feodor Lynen Str. 25, 81377 Munich, Germany. E-mail addresses: wilson@lmb.uni-muenchen.de; arnold@lmb.uni-muenchen.de.

† V.M. and T.F. contributed equally to this work.

Abbreviations used: r-protein, ribosomal protein; 2D, two-dimensional; MS/MS, tandem mass spectrometry; EM, electron microscopy; HSW, high-salt-washed; MS, mass spectrometry; EF-1 α , elongation factor 1 α ; CLP, chromatin-like protein; USP, universal stress protein; EF-G, elongation factor G; FA, formic acid; MALDI, matrix-assisted laser desorption/ionization; TFA, trifluoroacetic acid; PDB, Protein Data Bank.

composition. The discovery of novel archaeal r-proteins and factors may be the first step to understanding how archaeal ribosomes cope with extreme environmental conditions.

© 2010 Elsevier Ltd. All rights reserved.

Introduction

Protein synthesis occurs in large macromolecular particles called ribosomes (reviewed by Schmeing and Ramakrishnan¹). Ribosomes are composed of RNA and proteins. In bacteria, the 70S ribosome can be split into small (30S) and large (50S) ribosomal subunits. Although the active sites of small and large subunits responsible for decoding and peptide bond formation, respectively, are composed predominantly of RNA, the contribution of ribosomal proteins (r-proteins) is not to be overlooked.^{2,3} At the decoding site, r-protein S12 contributes to the fidelity of the codon–anticodon interaction of the mRNA–tRNA duplex,⁴ whereas at the peptidyltransferase center, the N-terminal extension of the r-protein L27 of bacterial ribosomes and the loop of L10e in eukaryotic ribosomes contacts the terminal CCA end of the P-site tRNA.^{5–8} R-proteins comprise the tRNA binding sites, stabilizing their interaction with and passage through the ribosome during translation.^{8–13} Moreover, many r-proteins play critical roles in facilitating various aspects of translation ranging from biogenesis to recruitment of translation factors and chaperones (reviewed by Wilson and Nierhaus² and Brodersen and Nissen³).

The *Escherichia coli* 70S ribosome contains 54 r-proteins: 21 in the small subunit (S1–S21) and 33 in the large subunit (L1–L36). R-proteins were originally numbered according to their position on two-dimensional (2D) PAGE; as a consequence, large acidic proteins have small numbers, and small basic proteins have large numbers.¹⁴ L7 is the N-acetylated version of L12; L8 was later found to be the pentameric complex of L10(L7/L12)₄; and L26 was later reassigned as S20. The genes for 48 of the 54 *E. coli* r-proteins are present in the genomes of all bacteria, whereas S1, S21, and S22 of the small subunit, as well as L25 and L30 of the large subunit, are missing in some bacteria. In fact, S22 associates with the ribosome during stationary phase and is therefore considered a ribosomal factor rather than a *bona fide* r-protein. Chloroplast ribosomes have homologues to all the *E. coli* r-proteins, except for L25 and L30, but in addition have six plastid-specific r-proteins,^{15,16} one of which (PSRP1) was subsequently shown to be a ribosomal factor rather than an r-protein.^{17,18} Mitochondrial ribosomes are even more diverse, with 81 r-proteins identified in the human mitochondrial 55S ribosome, 33 r-proteins identified in the small subunit, and 48 r-proteins identified in the large subunit.^{19–21}

Proteomic analysis of eukaryotic ribosomes ranging from yeast,^{22,23} fruit flies,²⁴ and plants²⁵ to

rodents^{26–28} and humans,^{29,30} together with genomic analysis,³¹ has identified ~78 r-proteins, 34 of which have homologues in bacteria. In contrast, no systematic study cataloguing the protein composition of archaeal ribosomes has been performed. Archaeal r-proteins have been characterized individually (e.g., see Kimura *et al.*³² and Auer *et al.*^{33,34}), leading to the identification of archaeal-specific r-protein LX,³⁵ or collectively, using 2D-PAGE.^{36–39} However, assignment of individual r-proteins by comparing 2D-PAGE profiles with data obtained from *E. coli* ribosomes is often ambiguous due to different buffer/running conditions, as well as the increased complexity of archaeal ribosomes. Genomic analysis indicates that archaeal ribosomes are intermediate in terms of composition between bacterial ribosomes and eukaryotic ribosomes, containing up to 68 r-protein families, of which 34 are common to bacteria and eukaryotes, 33 are present in eukaryotes only, and 1 (LX) is archaeal-specific.³¹ Ten of the r-protein families exhibit a heterogeneous distribution within archaea, with the ribosomes from Euryarchaeota predicted to have fewer r-proteins than their counterparts in Crenarchaeota (Fig. 1).³¹

Using 2D-PAGE and LC tandem mass spectrometry (MS/MS), we identified all 66 r-proteins of the small and large subunits of the thermophilic *Pyrobaculum aerophilum*. In addition to all but two (62 of 64; 97%) r-proteins of the *Sulfolobus acidocaldarius* small and large subunits, we identified three hypothetical proteins that are present in the thermoacidophilic *S. acidocaldarius* large subunit. These proteins interact more tightly with the large subunit than some integral r-proteins, suggesting that they are *bona fide* r-proteins. Cryo electron microscopy (EM) reconstructions of the *S. acidocaldarius* and *P. aerophilum* 50S subunits identified multiple potential binding sites for the novel r-proteins. In fact, in total, nine hypothetical proteins with pI values of >9 were identified within the small and large ribosomal subunits of these two Crenarchaeota, suggesting that the number of novel r-proteins in archaeal species may far exceed the predictions based on genomic analyses.

Results and Discussion

Near-complete proteomic characterization of Crenarchaeota r-proteins

Since genomic analyses indicate that, compared to Crenarchaeota, Euryarchaeota lineages appear to

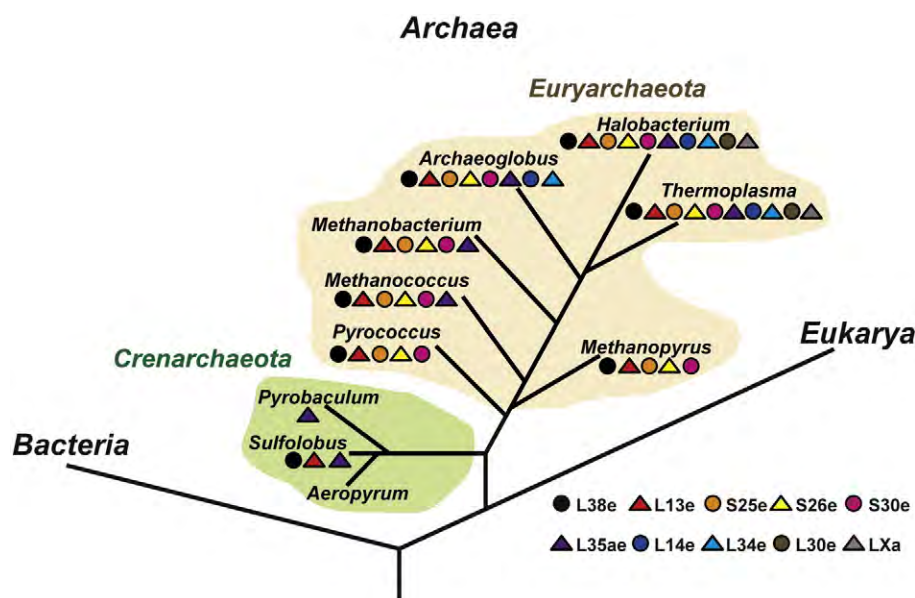


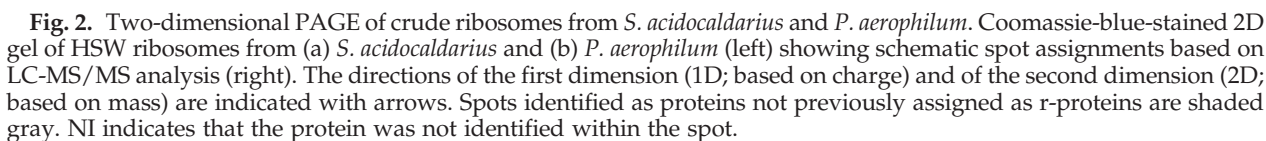
Fig. 1. Heterogeneous distribution of archaeal r-proteins (modified from Lecompte *et al.*³¹).

lack many r-protein families (Fig. 1),³¹ we selected two Crenarchaeota with completely sequenced genomes—*S. acidocaldarius* and *P. aerophilum*—from which ribosomes were isolated and their r-protein content was characterized. For example, the genome of the euryarchaeon *Haloarcula marismortui* predicts a total of 56 (25 small subunits/31 large subunits) r-proteins in the *H. marismortui* 70S ribosome, whereas the 70S ribosomes of the Crenarchaeota *S. acidocaldarius* and *P. aerophilum* are predicted to comprise 64 (28 and 36) and 66 (28 and 38) r-proteins, respectively. *S. acidocaldarius* is a thermoacidophilic crenarchaeon that grows optimally at 75–80 °C and pH 2–3, whereas *P. aerophilum* grows optimally at 100 °C and pH 7.0 (see [Materials and Methods](#)). Both Crenarchaeota can grow aerobically and, in fact, the species name *aerophilum* translates as “air-loving,” reflecting its ability to respire aerobically. Nevertheless, both archaea are slow-growing, and large-scale fermentation was required to obtain sufficient yields for the isolation and characterization of the ribosomes. Furthermore, ribosome yields were reduced by the necessity for repeated high-salt washing and centrifugation steps through sucrose cushions to obtain clarified ribosomal pellets.

The high-salt-washed (HSW) ribosomal fractions from *S. acidocaldarius* and *P. aerophilum* were analyzed by 2D-PAGE using the method of Kaltschmidt and Wittmann, and protein spots were identified by mass spectrometry (MS) (Fig. 2, [Tables 12](#)).¹⁴ From 2D-PAGE, it was possible to clearly identify spots corresponding to 51 of 64 (80%) r-proteins of the *S. acidocaldarius* 70S ribosome and 51 of 66 (78%) r-proteins of the *P. aerophilum* 70S ribosome. Missing r-proteins, such as S27ae, S27e, and S30e in the small subunit, as well as L24e, L39e, and L40e in the large

subunit, are between 6 kDa and 8 kDa and therefore are not resolved under these running conditions, which were optimized for the separation of higher-molecular-weight r-proteins. However, *S. acidocaldarius* and *P. aerophilum* ribosomal subunits were subsequently purified using sucrose gradients, and LC-MS/MS analysis of the purified fractions led to further identification of 26 of 28 (93%) and 36 of 36 (100%) r-proteins of the *S. acidocaldarius* 30S and 50S subunits, respectively, and 28 of 28 (100%) and 37 of 38 (97%) r-proteins of the *P. aerophilum* small and large subunits ([Tables 1](#) and [2](#)). Thus, in summary, only two r-proteins (S26e and S30e) from the *S. acidocaldarius* 30S subunit were not detected in any of the analyses.

Curiously, some r-proteins were assigned to multiple distinct spots on 2D-PAGE, such as L7ae, L29p, P0, and LX in *S. acidocaldarius* (Fig. 2a), and L7ae, L12p, and P0 in *P. aerophilum* (Fig. 2b). Consistently, we find that both LX and L29p are monomethylated on Lys residues 66 and 29, respectively (Fig. 3a and b). The stalk proteins P0 (L10 in bacteria) and L12p (P1–P2 in eukaryotes) are known to be modified in other organisms. In fact, L7 was originally mistakenly identified as a unique r-protein and was subsequently shown to be the N-terminally acetylated form of L12.⁴⁰ *E. coli* L12 is also methylated at K81 position.⁴¹ Likewise, in eukaryotes, P1 is acetylated⁴² and phosphorylated,^{42,43} and P2 is phosphorylated.⁴⁴ P0 is phosphorylated at the C-terminus in yeast;⁴⁵ in *E. coli*, the N-terminal Met of L10 is removed, and Lys residues 37 and 105 are acetylated.^{40,46} We also find that L12p is N-terminally acetylated; however, unlike in *E. coli*, the N-terminal methionine is not cleaved (Fig. S1). In addition, we could identify two distinct methylation



In addition to the expected r-proteins, a number of additional proteins were identified in the 2D gels of the HSW ribosomal fractions, as well as in the LC-

MS/MS of the purified 30S and 50S fractions from *S. acidocaldarius* and *P. aerophilum* (Fig. 2, Table 3). The presence of these proteins can reflect a stable interaction with the pelleted ribosomal particles or can reflect that the proteins pellet or migrate similarly to ribosomal particles, due to their being associated with membrane fragments [e.g., ABC transporter and nitrate reductase (NarGHI)] or their being part of a large macromolecular complex [e.g., the 19S proteasome or the α -subunit and the β -subunit of the thermosome (eukaryotic chaperonin CCT/TRiC), which forms a hexadecameric ($\alpha\beta$)₄ ($\alpha\beta$)₄ complex of ~1 MDa].⁴⁸ Consistent with their size, the thermosome subunits were detected in the HSW ribosomal fraction, as well as the purified 30S subunit but not in the purified 50S subunit fraction (Table 3). Moreover, the archaeal thermosome has been reported to be an RNA binding protein involved in rRNA processing.⁴⁹ Other proteins

Table 1. R-proteins of *S. acidocaldarius* identified by LC-MS and 2D-PAGE

Protein family	LC-MS	2D	Amino acids	gi ^a	Molecular mass (kDa)	pI
<i>Small subunit r-protein</i>						
S2p	✓	✓	225	70605938	25.7	5.8
S3ae	✓	—	197	70606435	22.6	10.2
S3p	✓	—	231	70606406	25.4	10.1
S4e	✓	✓	244	70606400	27.8	10.1
S4p	✓	✓	176	70605931	20.4	10.3
S5p	✓	✓	214	70606392	23.9	9.8
S6e	✓	✓	213	70606621	23.7	10.0
S7p	✓	✓	195	70606489	22.1	10.2
S8e	✓	✓	128	70606557	14.4	10.4
S8p	✓	✓	133	70606397	14.9	9.9
S9p	✓	✓	138	70605936	15.8	10.2
S10p	✓	—	102	70606487	11.9	10.5
S11p	✓	✓	132	70605932	14.1	11.5
S12p	✓	✓	147	70606491	16.1	11.3
S13p	✓	✓	170	70605930	19.4	10.5
S14p ^b	✓	—	63	68567046	7.6	10.2
S15p	✓	✓	153	70606619	17.8	10.5
S17e	✓	✓	82	70606477	9.6	5.3
S17p	✓	✓	108	162139951	12.3	9.9
S19e	✓	✓	154	70607213	18.0	10.6
S19p	✓	✓	140	70606408	16.4	10.6
S24e	✓	✓	118	70606643	13.3	10.3
S25e	✓	✓	109	70606631	12.3	10.5
S26e	—	—	95	68567938	10.8	9.9
S27ae	✓	—	67	70606642	7.8	9.9
S27e	✓	✓	66	70607041	7.3	10.4
S28e	✓	✓	84	70606501	9.5	10.5
S30e	—	—	54	68567754	6.2	11.8
<i>Large subunit r-protein</i>						
L1p	✓	✓	221	162139946	24.9	10.4
L2p	✓	✓	238	70606409	25.2	11.4
L3p	✓	✓	342	70606412	38.5	10.5
L4p	✓	✓	266	70606411	29.2	10.7
L5p	✓	✓	178	70606399	20.2	10.8
L6p	✓	✓	189	3914762	21.2	9.8
L7ae	✓	✓	126	70607262	13.7	8.2
L10e	✓	✓	176	70606018	19.9	10.4
L11p	✓	✓	170	70607203	18.2	9.5
L12p	✓	✓	105	70607200	11.1	4.8
L13p	✓	✓	148	70605935	16.7	10.9
L14e	✓	✓	96	70606603	10.7	9.9
L14p	✓	✓	138	70606402	15.2	10.9
L15e	✓	✓	217	70606432	26.0	11.7
L15p	✓	—	144	70606390	16.4	10.5
L18e	✓	✓	110	70605934	12.5	10.8
L18p	✓	✓	197	70606393	22.1	10.3
L19e	✓	✓	150	70606394	17.8	11.3
L21e	✓	✓	103	70606441	11.8	10.9
L22p	✓	✓	156	70606407	18.1	10.4
L23p	✓	✓	82	70606410	9.4	10.2
L24e	✓	—	62	70606500	7.1	10.4
L24p	✓	✓	134	70606401	15.5	10.6
L29p	✓	✓	69	70606405	8.1	10.5
L30e	✓	✓	104	70606493	11.5	9.8
L30p	✓	✓	156	70606391	17.9	10.2
L31e	✓	✓	129	70607210	15.2	10.8
L32e	✓	✓	131	70606395	15.2	11.1
L34e	✓	✓	87	70606386	10.1	10.5
L37e ^b	✓	✓	61	70606453	6.9	11.9
L37ae	✓	—	70	70606423	8.1	10.4
L39e ^b	✓	—	53	70607211	6.3	12.6
L40e	✓	✓	56	70606562	6.4	11.0
L44e	✓	✓	95	15921177	11.1	10.7

Table 1 (continued)

Protein family	LC-MS	2D	Amino acids	gi ^a	Molecular mass (kDa)	pI
LX	✓	✓	86	70607208	10.1	10.1
P0	✓	✓	335	70607201	36.5	9.1

^a gi refers to the GenInfo identifier for retrieval from NCBI.^b Identified with only a single peptide.

that are better known to be associated with the translational machinery, such as elongation factor 1 α (EF-1 α) and the translation initiation factors IF-6 and Sui1 (eIF1), were also identified (Table 3). In addition, the ribosome biogenesis factors CBF5 (pseudo-uridine synthetase) and fibrillar (rRNA 2'-O-methyltransferase), and rRNA processing proteins such as NOP56/58 were identified (Table 3). Fibrillar and NOP56/58, together with the archaeal r-protein L7ae, interact with C/D box sRNAs to form an RNP complex involved in 2'-OH ribose methylation, whereas CBF5, L7ae, NOP10, and Gar1 interact with H/ACA sRNAs to direct rRNA pseudo-uridylation.⁴⁷

Four proteins containing putative DNA/RNA-binding domains, which may be present due to interaction with nucleic acids [i.e., chromatin-like protein (CLP), TBP-interacting protein TIP49, transcription factor NusA-like protein, and zinc-ribbon RNA-binding domain protein], were identified (Table 3). Interestingly, we identified six and eight hypothetical proteins in the *S. acidocaldarius* and *P. aerophilum* ribosomal fractions, respectively, that have no known motifs and no sequence homology to any protein with a known function, yet many had pI values of >9.0, characteristic of r-proteins (Tables 1 and 2). While most of the spots for the additional proteins were significantly less intense than the r-protein spots (Fig. 2), there were a number of exceptions—particularly evident in the *S. acidocaldarius* 2D gel were the spots for hypothetical proteins Saci_1218, Saci_1337, and Saci_1586; CLP; and the universal stress protein (USP), all of which appeared to be stoichiometric with, or even more intense, than the majority of r-proteins (Fig. 2a). We thus considered the possibility that these proteins may be novel integral r-proteins of the *S. acidocaldarius* ribosome.

Identification and distribution of novel *S. acidocaldarius* large subunit r-proteins

In order to determine if the potential ribosome-associated proteins were *bona fide* r-proteins and whether they are integral to the small subunit or the large subunit, we applied the HSW ribosomal fractions onto 10–40% sucrose gradients. In contrast

Table 2. R-proteins of *P. aerophilum* identified by LC-MS and 2D-PAGE

Protein family	LC-MS	2D	Amino acids	gi ^a	Molecular mass (kDa)	pI
<i>Small subunit r-protein</i>						
S2p	✓	✓	208	18312202	23.9	9.0
S3ae	✓	✓	221	18314093	24.7	10.3
S3p	✓	✓	218	27734520	25.0	10.4
S4e	✓	✓	238	18313980	26.7	10.4
S4p	✓	✓	159	26399437	18.5	10.9
S5p	✓	✓	218	18312458	24.2	10.1
S6e	✓	✓	148	18312675	15.9	9.9
S7p	✓	✓	223	18312139	25.3	9.6
S8e	✓	✓	131	18313995	14.3	11.2
S8p	✓	✓	130	18313095	14.9	9.9
S9p	✓	✓	146	18312094	16.4	10.6
S10p	✓	✓	106	18313679	12.3	11.7
S11p	✓	✓	133	18313881	14.1	11.4
S12p	✓	✓	147	20140085	16.5	10.9
S13p	✓	—	152	18313810	16.7	10.6
S14p	✓	—	54	18313094	6.4	10.5
S15p	✓	✓	151	18314103	17.7	10.6
S17e	✓	✓	71	18312190	8.2	10.3
S17p	✓	✓	146	18160326	17.0	10.5
S19e	✓	✓	158	18313782	17.7	10.7
S19p	✓	✓	158	18312838	18.2	10.6
S24e	✓	✓	121	18313342	14.2	11.0
S25e	✓	✓	110	18313166	12.5	10.6
S26e	✓	—	98	18313151	11.3	10.7
S27ae	✓	—	65	18313341	7.6	10.3
S27e	✓	—	67	18313776	7.3	10.4
S28e	✓	✓	77	18314007	8.6	10.4
S30e	✓	—	55	18313356	6.2	12.4
<i>Large subunit r-protein</i>						
L1p	✓	✓	222	18313826	24.7	10.7
L2p	✓	✓	246	18312189	26.2	10.9
L3p	✓	✓	338	18313001	37.4	10.8
L4p	✓	✓	283	18313002	31.1	10.4
L5p	✓	✓	179	18314167	20.1	10.9
L6p	✓	✓	196	18313300	21.9	9.8
L7ae	✓	✓	151	18314009	16.1	9.4
L10e	✓	✓	180	18314160	20.2	10.5
L11p ^b	✓	—	167	18313825	18.6	9.6
L12p	✓	✓	110	18312824	11.5	4.5
L13e	✓	✓	159	18312773	18.1	11.6
L13p	✓	—	187	18312093	21.8	10.7
L14e	✓	✓	103	18312232	11.4	10.2
L14p	✓	✓	144	18313850	15.8	11.3
L15e	✓	✓	191	18312915	22.9	11.5
L15p	✓	✓	156	18314064	17.4	10.9
L18e	✓	✓	122	18312092	13.3	12.1
L18p	✓	✓	205	18313098	23.4	10.5
L19e	✓	✓	147	18313097	17.4	11.2
L21e	✓	—	100	18313998	11.5	10.7
L22p	✓	✓	168	18312876	19.6	11.1
L23p	—	✓	81	18313003	9.3	10.3
L24e	✓	—	58	18314008	6.7	10.6
L24p	✓	✓	123	18313979	14.2	11.8
L29p	✓	✓	75	18312872	9.0	11.6
L30e ^b	✓	✓	102	18312088	10.9	9.2
L30p	✓	—	178	18312459	20.3	10.3
L31e	✓	✓	91	18313818	10.6	10.9
L32e	✓	✓	152	18313096	18.0	11.7
L34e	✓	—	84	18313920	9.5	12.2
L37e	—	—	52	NA ^c	12.3	5.4
L37ae	✓	✓	105	18313176	11.8	10.8
L38e	✓	✓	67	18312825	7.9	9.8
L39e ^d	✓	—	51	29427908	6.0	13.4
L40e	✓	—	53	18313942	6.4	11.2

Table 2 (continued)

Protein family	LC-MS	2D	Amino acids	gi ^a	Molecular mass (kDa)	pI
L44e	✓	✓	91	18313777	10.6	10.9
LX	✓	✓	78	18313820	8.9	9.7
P0	✓	✓	345	18313827	38.0	9.9

^a gi refers to the GenInfo identifier for sequence retrieval from NCBI.

^b Identified with only a single peptide

^c Not annotated in NCBI, but reading frame identified by Lecompte *et al.*³¹

^d Inferred by sequence homology identity to *Pyrobaculum calidifontis* JCM 11548.

to *E. coli*, where a low level of magnesium was necessary to split the 70S ribosomes into the component subunits (Fig. 4a), 30S and 50S subunits and little or no 70S ribosomes were observed for *S. acidocaldarius* and *P. aerophilum* even with low-salt and high -magnesium (30 mM) concentrations (data not shown). Similar observations have been reported previously for a variety of *Desulfurococcus* ribosomes, with 70S particles only being observed when cross-linking agents, such as formaldehyde, were used on actively translating ribosomes.⁵⁰ The fractions corresponding to the *S. acidocaldarius* and *P. aerophilum* 30S and 50S subunits were collected, pooled, and pelleted (Fig. 4a–c). The purified subunits were analyzed by negative-stain EM, as performed previously for archaeal subunits.⁵¹ The images indicate that the purified subunits were homogeneous, although some contamination of the 30S subunits by chaperonins was evident, consistent with LC-MS/MS analysis (Fig. 4d). The purified *S. acidocaldarius* 30S and 50S subunits were then analyzed by 2D-PAGE, and the protein spots were identified by LC-MS/MS (Fig. 4e and f).

The r-protein assignments were consistent with those of the 2D gels of the high-salt ribosomal fraction and corresponded to the expected respective subunit composition (Fig. 2a). However, L7ae was also found at lower stoichiometry in the 30S fraction (Fig. 4e), which may reflect a promiscuous interaction with the 30S subunit, although we cannot exclude that it also results from the aforementioned involvement of L7ae in other biogenesis or processing complexes. Similarly, S24e is found at a surprisingly higher stoichiometry in the 50S subunit compared to the 30S subunit (Fig. 4e and f), possibly reflecting an as yet uncharacterized interaction of this protein with both ribosomal subunits. In contrast, it was immediately apparent that the spots for the CLP and the USP were absent. We also did not detect Rbp18 (Saci_1216), which has been proposed to interact with the *Sulfolobus solfataricus* 30S subunit,⁵² suggesting that CLP, USP, and Rbp18 are not integral r-proteins but may instead be only transiently associated with the

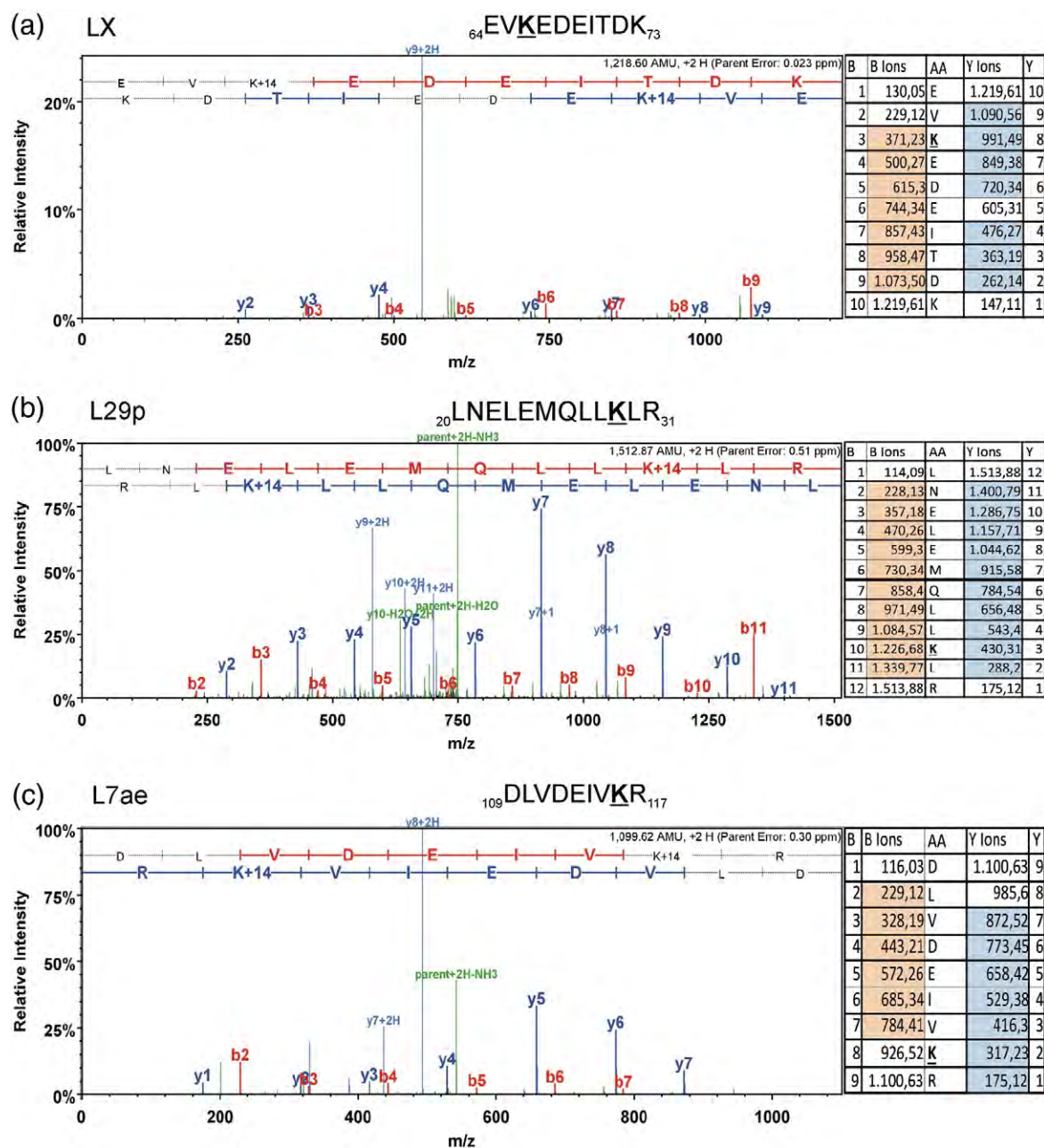


Fig. 3. MS identification of r-protein modifications. MS/MS spectra (left) and fragmentation tables (right) used for the identification of the monomethylation sites of r-proteins (a) LX, (b) L29p, and (c) L7ae. Monomethylated lysines within the peptide sequences are underlined and marked in boldface. Detected b-ions are highlighted in red, and y-ions are highlighted in blue.

ribosome. In contrast, the three hypothetical proteins Saci_1218, Saci_1337, and Saci_1586 were present in the 2D gel of the *S. acidocaldarius* 50S subunit (but not in the 30S subunit), with intensities paralleling those of *bona fide* r-proteins (Fig. 4f). Saci_1218, Saci_1337, and Saci_1586 are composed of 125 aa (14.6 kDa), 75 aa (8.8 kDa), and 80 aa (9.3 kDa), with pI values of 9.3, 9.9, and 8.0, respectively. We propose to rename Saci_1218,

Saci_1337, and Saci_1586 as L45a, L46a, and L47a, respectively, continuing the numerical nomenclature of known archaeal r-proteins.

At the time of writing, the genomes of 91 archaeal species had been completely sequenced. Homology searches against these genomes revealed that L45a (Saci_1218) has homologues present in all *Sulfolobus* species, with the exception of *Sulfolobus tokodaii* str. 7 (Fig. 5a). In contrast, L46a (Saci_1337) appears to be

Table 3. Potential ribosome-associated proteins identified by LC-MS/MS and 2D-PAGE

Protein group	Protein description	Species	gi ^a	LC-MS	2D
Translation-related factors	Elongation factor 1 α (EF-1 α)	PAE	18313751	30S	✓
		SAC	70606488	—	✓
	Translation initiation factor IF-6	PAE	18313819	30S/50S	—
		SAC	70607209	50S	—
	Translation initiation factor Sui1	PAE	18314004	30S	—
		SAC	70606655	30S	—
Ribosome biogenesis factors	Cbf5 (pseudo-uridine synthetase)	SAC	212373368	30S	—
	Fibrillarin (rRNA 2'-O-methyltransferase)	PAE	18313923	30S	—
		SAC	70607104	30S/50S	—
	NOP56 subunit (pre-rRNA processing protein)	PAE	18313924	30S/50S	✓
		SAC	70607105	50S	—
	Dim2p-like rRNA processing protein	PAE	18314094	30S/50S	—
RNA/DNA binding proteins	Chromatin-like protein (CLP)	SAC	70606751	30S	—
		PAE	18313194	30S/50S	—
	TBP-interacting protein TIP49	PAE	70607080	30S/50S	✓
	Transcription factor NusA-like protein	PAE	18312811	—	✓
		SAC	162139950	30S	—
	Zn-ribbon RNA binding protein (RBP)	PAE	18312108	30S	✓
Proteases, heat shock proteins, and chaperones	AAA ⁺ protease	PAE	70606567	30S	—
		SAC	18313875	30S	—
	FKBP-type PPIase	PAE	18312191	30S	✓
		PAE	18313227	30S	✓
	Hsp20	SAC	70607398	—	✓
		PAE	18313186	30S	—
	Proteasome, α -subunit	SAC	70606428	50S	—
		PAE	18313108	30S	✓
	Thermosome (chaperonin), α -subunit	PAE	18313954	30S	✓
		SAC	70606473	—	✓
	Thermosome (chaperonin), β -subunit	PAE	18313954	30S	✓
		SAC	70606473	—	✓
Other	Universal stress protein (USP)	SAC	70607374	—	✓
	ABC transporter	SAC	70606787	—	✓
	Acetyl-CoA acetyltransferase	PAE	18160913	30S	✓
	Acetyl-CoA acetyltransferase-associated protein	PAE	18313383	30S	—
	Nitrate reductase, α -subunit (narG)	PAE	18161785	30S/50S	—
	Nitrate reductase, β -subunit (narH)	PAE	18161786	30S/50S	—
Hypothetical proteins	Succinate dehydrogenase subunit	PAE	18159558	50S	—
	Sulfurtransferase	SAC	70607907	—	✓
	PAE0659 (pI=9.3)	PAE	18312079	50S	—
	PAE0944 (pI=6.1)	PAE	18312296	30S	—
	PAE1347 (pI=6.5)	PAE	18312573	30S/50S	—
	PAE1683 (pI=9.2)	PAE	18160290	30S/50S	✓
	PAE1820 (pI=8.1)	PAE	18160397	30S	—
	PAE2358 (pI=9.3)	PAE	18160809	50S	✓
	PAE3143 (pI=7.8)	PAE	18313855	30S/50S	—
	PAE3432 (pI=9.3)	PAE	18161642	30S/50S	—
	Saci_0899 (pI=6.2)	SAC	70606685	30S	—
	Saci_1218 (pI=9.3)	SAC	70606987	50S	✓
	Saci_1237 (pI=9.4)	SAC	70607006	30S	—
	Saci_1337 (pI=9.9)	SAC	70607095	50S	✓
	Saci_1435 (pI=9.5)	SAC	70607187	30S	—
	Saci_1586 (pI=8.0)	SAC	70607322	50S	✓

^a gi refers to the GenInfo identifier for sequence retrieval from NCBI.

more widely distributed, with homologues being found in all Thermoprotei genera (Fig. 5b) and with L47a (Saci_1586) being found in all Sulfolobaceae (Fig. 5c). Initial homology searches did not reveal a homologue of L47a within the genome of *S. tokodaii* str. 7; however, careful inspection of the genome context of the neighboring genes of L47a, namely *asnC* and *rpoM*, revealed the presence of an unannotated open reading frame, which encodes a protein with 64% identity to L47a (Fig. 5g). While most archaeal r-proteins are organized either within

the major conserved operons (α , *str*, *spc*, and *S10*) as in bacteria or in one of 10 archaeal-unique operons,⁵³ 11 archaeal r-proteins are not associated with any specific genomic context. Likewise, L45a and L46a do not appear to be within conserved operon structures, nor associated with any particular genes, although we note that the gene (Saci_1216) encoding the 30S subunit binding protein Rbp18,⁵² the ribosome biogenesis factor Gar1, and Ser-tRNA synthetase are in close proximity to L45a, L46a, and L47a (Fig. 5d–f), respectively.

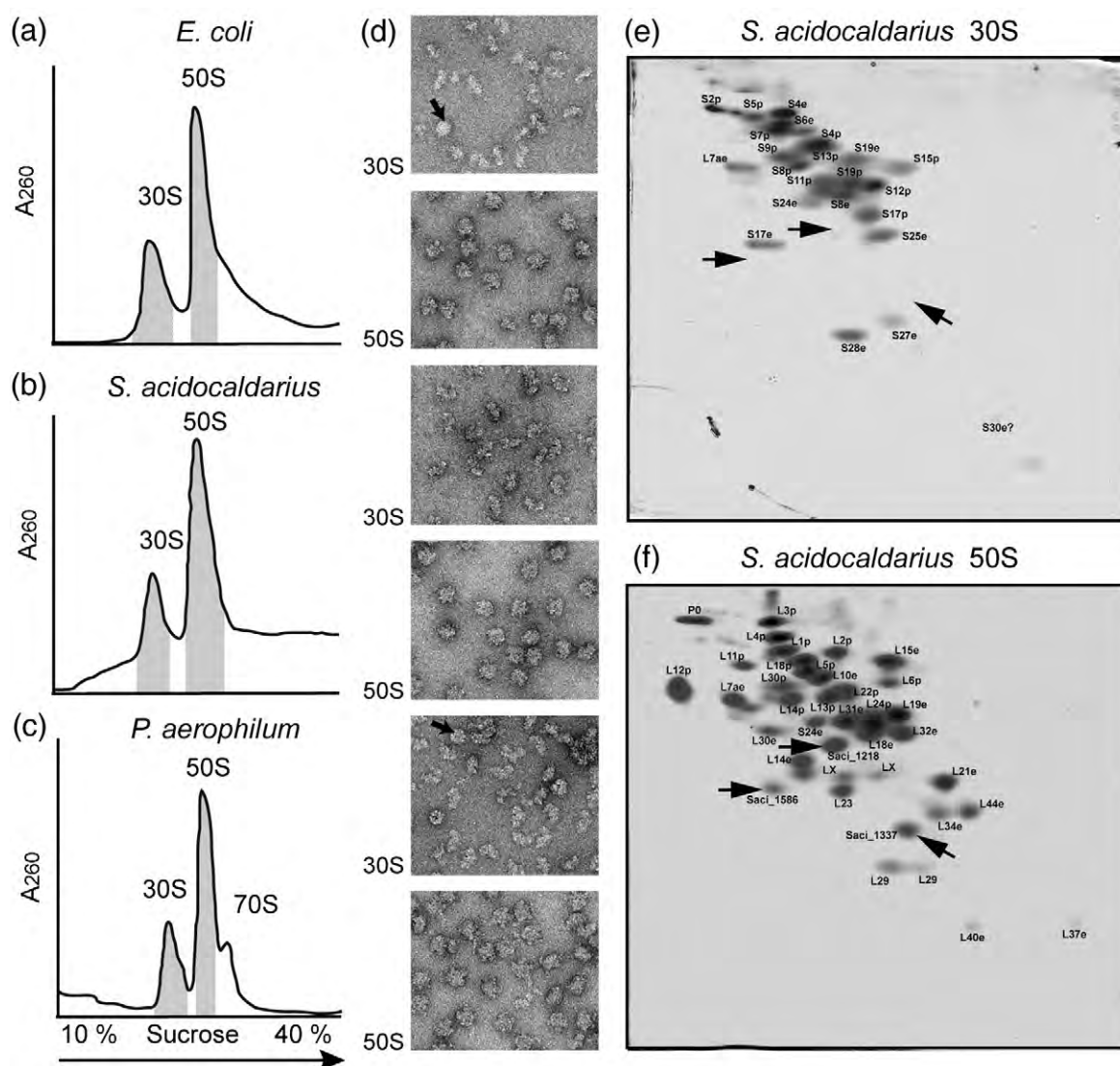


Fig. 4. Characterization of purified archaeal ribosomal subunits. Sucrose density gradient centrifugation profiles of HSW ribosomes from (a) *E. coli* as control, compared with (b) *S. acidocaldarius* and (c) *P. aerophilum* (left). (d) Negative-stain EM of 30S and 50S fractions isolated from (a)–(c) at a magnification of 90,000 \times . The arrow indicates chaperonin particles in ribosome preparations. Two-dimensional PAGE of *S. acidocaldarius* (e) 30S and (f) 50S subunits. The positions of the novel r-proteins Saci_1218, Saci_1337, and Saci_1586 are indicated by arrows in (e) and (f).

R-proteins identified in archaeal-unique operons are often found together with components of the transcriptional machinery (e.g., L30e is found together with genes encoding the transcription elongation factor NusA and the DNA-dependent RNA polymerase subunits RpoA, RpoB, and RpoH). This finding has been suggested to reflect the increasing coordination in the regulation of transcription and translation that has evolved in archaeal (and eukaryotic) lineages since the separation from bacterial phyla.⁵³ L45a neighbors the gene for a transcription regulator (Lrs14), whereas L46a is downstream of tflD, encoding the TATA binding protein of the transcription factor TFIID. Similarly,

L47a is often found downstream of genes encoding the transcriptional regulator AsnC and the DNA-directed RNA polymerase subunit M (RpoM).

NTPase activities of *S. acidocaldarius* small and large subunits

Ribosomes from higher eukaryotes, such as rat and bovine liver and rabbit reticulocytes, have been documented to harbor intrinsic ATPase activities.^{54,55} This prompted us to examine the purified archaeal ribosomes to assess whether any intrinsic ATP or GTP activities could be detected. As controls, the intrinsic ATPase/GTPase activities of

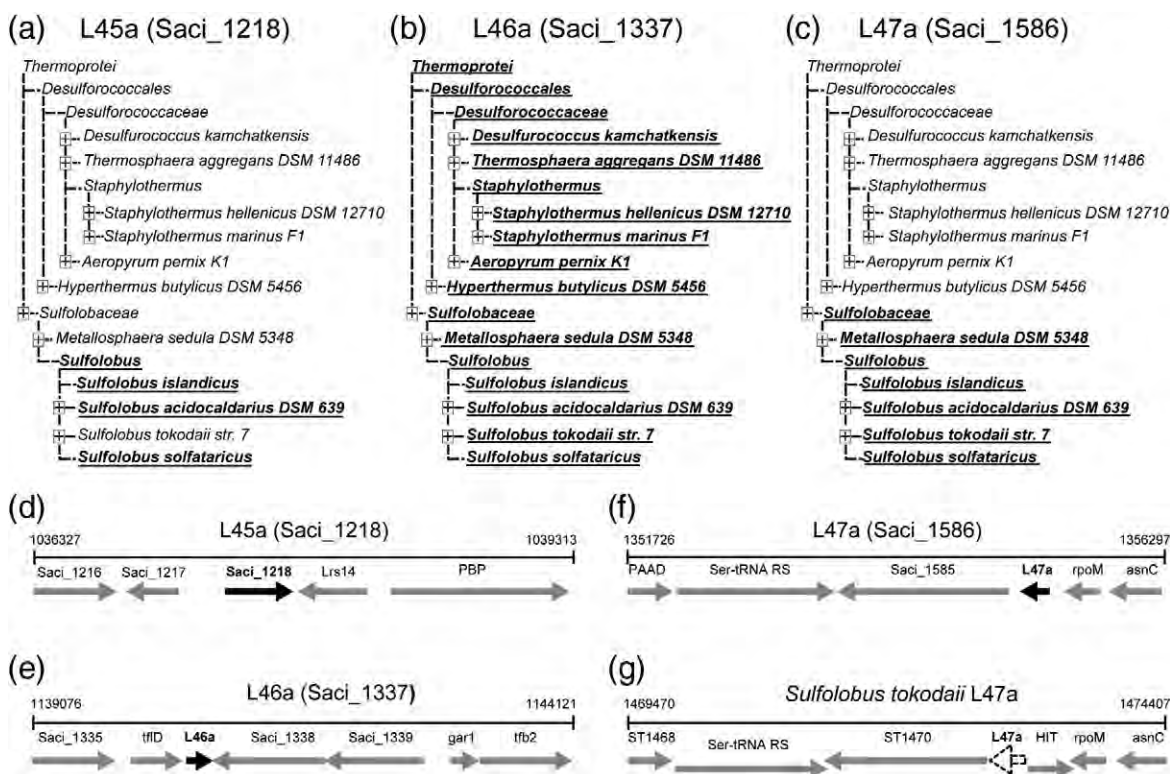
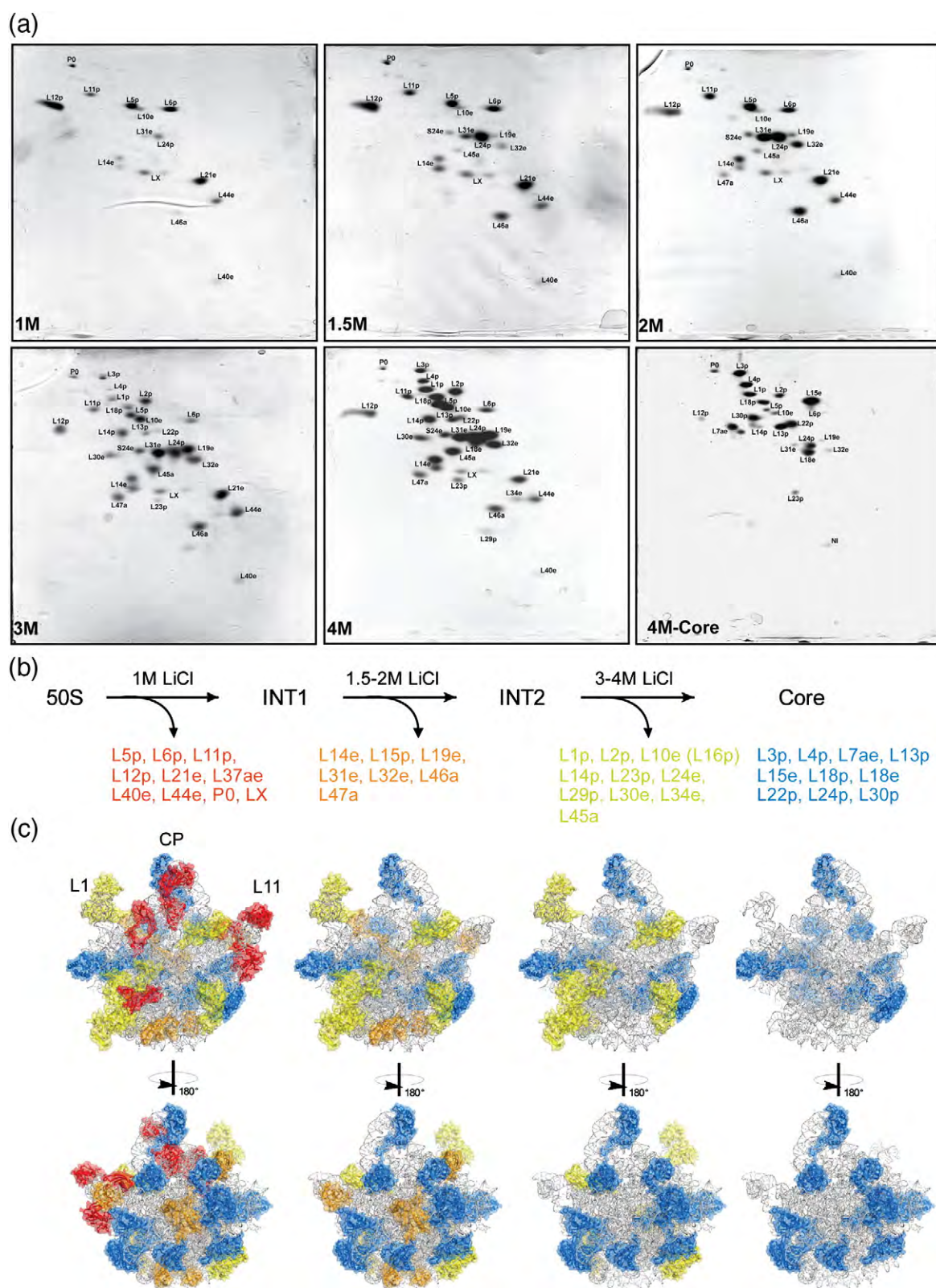


Fig. 5. Distribution and genomic organization of Saci r-proteins. Subsection of the archaeal taxonomic tree showing the relative distributions of (a) Saci_1218 (L45a), (b) Saci_1337 (L46a), and (c) Saci_1586 (L47a). Genomic organization of (d) Saci_1218 (L45a), (e) Saci_1337 (L46a), and (f) Saci_1586 (L47a). (g) Identification of a homologue of Saci_1586 in *S. tokodaii* str. 7 based on genomic context. Lrs14, transcription regulator Lrs14-like protein; PBP, periplasmic binding protein; tflD, TATA binding protein of the transcription factor TFIID; tbf2, transcription initiation factor 2; PAAD, phenylacetic acid degradation protein; Ser-tRNA RS, Ser-tRNA aminoacyl synthetase; RpoM, DNA-dependent RNA polymerase subunit M; Lrp, transcription regulator Lrp; HIT, histidine triad nucleotide binding protein.

E. coli 70S ribosomes, as well as those of the purified *E. coli* elongation factor G (EF-G), were tested in the presence and in the absence of *E. coli* 70S ribosomes. As seen in Fig. S3, no intrinsic ATPase or GTPase activity was detected for *E. coli* 70S ribosomes, nor for *S. acidocaldarius* 30S or 50S subunits, at 37 °C within 1 h. In comparison, high GTPase activity was detected within 1 h when *E. coli* EF-G was incubated together with *E. coli* 70S ribosomes. Similarly, after 24-h incubations, no intrinsic ATPase/GTPase activities were detected for *E. coli* 70S ribosomes. However, low ATPase and GTPase activities were detected for both *S. acidocaldarius* 30S or 50S subunits at levels similar to the intrinsic GTPase

activity of *E. coli* EF-G (Fig. S3). Similar experiments were performed with *Thermus thermophilus* 70S ribosomes and *S. acidocaldarius* 30S or 50S subunits at 60 °C, and no intrinsic ATPase or GTPase activity was detected after 1 h (data not shown). Longer incubations were not possible because of the elevated background signal due to a spontaneous cleavage of NTPs at 60 °C. Although we cannot completely rule out the presence of an intrinsic ATPase/GTPase activity of the archaeal subunits, we believe that the low activities detected are more consistent with the presence of residual contaminating factors, such as AAA⁺ proteases or EF-1 α , that were detected in the samples by MS (Table 3). Such a

Fig. 6. Two-dimensional gels for the incremental washing of *S. acidocaldarius* 50S subunits. (a) Coomassie-blue-stained 2D-PAGE of 1–4 M LiCl wash fractions from purified *S. acidocaldarius* 50S subunits, as well as the remaining r-proteins in the core 50S subunit after treatment with 4 M LiCl. (b) Scheme illustrating the subset of *S. acidocaldarius* 50S subunit r-proteins that are removed with increasing concentrations of LiCl (red, orange, and lime), as well as those remaining in the core after 4 M washing (blue). (c) Two views of a model for the *S. acidocaldarius* 50S subunits with r-proteins removed by 1.0 M, 1.5–2 M, and 3–4 M washing, as well as those remaining after 4 M washing, shown in red, orange, lime, and blue, respectively.



conclusion would be consistent with the lack of any highly conserved ATP and/or GTP binding motifs in any of the archaeal r-proteins.

Stepwise dissociation of archaeal 50S ribosomal subunits by LiCl

To investigate the interaction and stability of the novel archaeal r-proteins L45a, L46a, and L47a on the

50S subunit relative to other known r-proteins, we washed the *S. acidocaldarius* 50S subunit with increasing concentrations of LiCl (1 M, 1.5 M, 2 M, 3 M, or 4 M), precipitated the r-proteins that dissociated from the particles, and analyzed them by 2D-PAGE (Fig. 6a). In addition, 2D-PAGE was also performed on the core r-proteins that remain attached to the rRNA after washing with 4 M LiCl (Fig. 6a). A representation summarizing the order of

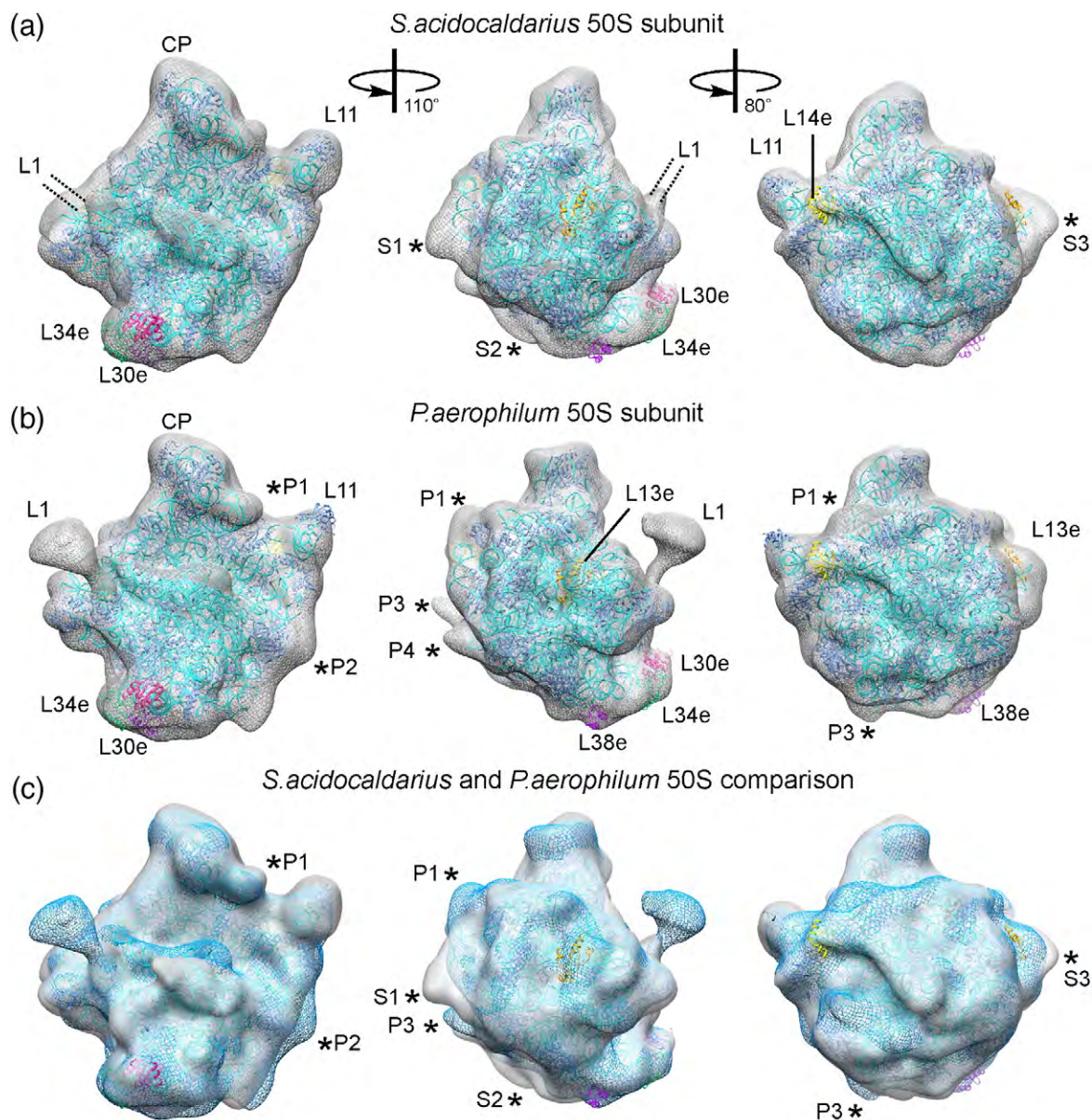


Fig. 7. Cryo-EM reconstructions of 50S subunits from *S. acidocaldarius* and *P. aerophilum*. Three different views of the cryo-EM maps (gray mesh) of 50S subunits from (a) *S. acidocaldarius* and (b) *P. aerophilum*, with a fitted crystal structure of the *H. marismortui* 50S subunit (PDB code 3CC2)⁶³ shown with RNA (cyan) and r-proteins (blue) as ribbons, with additional archaeal/eukaryotic-specific r-proteins included from Armache *et al.*⁸ (c) Comparison of the density maps of *S. acidocaldarius* (gray) and *P. aerophilum* (blue mesh). The density for r-proteins L30e and L34e is present in both *S. acidocaldarius* and *P. aerophilum* 50S subunits, whereas the density for L13e and L38e is present in only *P. aerophilum*. Potential locations for additional r-proteins in *S. acidocaldarius* and *P. aerophilum* are indicated with asterisks and labeled S1–S3 and P1–P4, respectively.

r-protein release by LiCl is shown schematically in Fig. 6b and graphically on a molecular model for the *S. acidocaldarius* 50S subunit in Fig. 6c. Surprisingly, although many integral r-proteins (L5p, L6p, L11p, L12p, L21e, L37ae, L44e, LX, and P0) were washed from the 50S subunit with 1 M LiCl, the r-proteins L45a, L46a, and L47a were not. L46a was removed with 1.5 M LiCl, whereas L45a and L47a only started to appear in the supernatant with 2–3 M LiCl washing, suggesting a tighter association with the 50S subunit (Fig. 6a). Generally, the trend is that the 3–4 M LiCl wash and core fractions contain predominantly universally conserved families [L1p, L2p, L3p, L4p, L13p, L14p, L16p (L10e), L18p, L22p, L24p, L29p, and L30p], with only a few archaeal/eukaryotic-specific families present (L7ae, L15e, L18e, L30e, L31e, and L34e). In contrast, the reverse trend is observed in the 1–2 M LiCl wash fractions, which contain more archaeal/eukaryotic-specific r-proteins than universal r-proteins. The dissociating universal r-proteins include L11p, L12p, and P0 (L10p) that form the stalk region, which is known to be easily removable from the ribosome.^{56,57} Studies using bacterial ribosomes have revealed that the susceptibility of r-proteins to removal by LiCl washing corresponds inversely to the order of assembly of r-proteins *in vivo* and from reconstitution studies.⁵⁸ Two-dimensional PAGE analysis of the *S. solfataricus* 50S core r-proteins following treatment with 3 M LiCl/6 M urea revealed a number of r-proteins; however, no direct identification of the r-proteins was performed.³⁹ Although the *in vitro* reconstitution of *S. solfataricus* and *Haloferax mediterranei* large ribosomal subunits was successfully performed, the order and dependency of r-proteins were not investigated.^{59,60} Nevertheless, the findings here are generally consistent with the LiCl treatment⁶¹ and *in vivo* analysis of the yeast 60S subunit assembly.⁶²

Cryo-EM reconstruction of archaeal large ribosomal subunits

Cryo-EM reconstructions of the *S. acidocaldarius* and *P. aerophilum* 50S subunits were determined to 27 Å and 25 Å (0.5 FSC) resolutions, respectively (Fig. 7). The resolution was limited by the need to use 50S subunits, rather than 70S ribosomes, in part due to an orientation bias of the 50S subunits on the cryogrids. Nevertheless, there was an excellent fit of the crystal structure of the archaeal *H. marismortui* 50S subunit⁶³ into both cryo-EM maps (Fig. 7a and b). The 23S rRNA sequences of *S. acidocaldarius* and *P. aerophilum* are very similar to that of *H. marismortui*; however, *S. acidocaldarius* and *P. aerophilum* 50S subunits contain additional r-proteins that are not present in *H. marismortui* (Fig. 1).³¹ Consistently, both maps had additional regions of density that were not occupied by the *H. marismortui*

50S subunit model (Fig. 7). Extra density is located on both maps on the interface side of the 50S subunit, just below the L1 stalk, consistent with the positions of L30e and L34e in eukaryotic 80S ribosomes^{8,64} (Fig. 7a and b). Similarly, additional density is located between the L11 stalk and the central protuberance on the solvent side of the large subunit where L14e is located.⁸ The *P. aerophilum* 50S subunit has two r-proteins (L13e and L38e) that are not found in *S. acidocaldarius* or *H. marismortui* 50S subunits (Fig. 1).³¹ Additional density (which is absent in the *S. acidocaldarius* 50S map) is observed in the *P. aerophilum* 50S map in the two positions where L13e and L38e are located in eukaryotic 80S ribosomes⁸ (Fig. 7c). The location of the archaeal-specific r-protein LX, which is present in both *S. acidocaldarius* and *P. aerophilum*, cannot be localized at this resolution. We could, however, identify at least three regions (S1–S3) with the remaining additional density in the *S. acidocaldarius* 50S map that are not present in the *P. aerophilum* 50S map, which could potentially be due to the additional *S. acidocaldarius* L45a, L46a, and L47a identified in this study; however, a higher resolution will be required to confirm this. Four regions (P1–P4) of additional density that are specific for the *P. aerophilum* 50S map were also observed (Fig. 7b and c), possibly reflecting the presence of additional as yet unknown *P. aerophilum* r-proteins, candidates for which were identified by LC-MS/MS in the 50S fraction (e.g. PAE0659 and PAE2358) (Table 3).

Materials and Methods

Growth of *S. acidocaldarius* and *P. aerophilum*

S. acidocaldarius (DSM 639^T) and *P. aerophilum* IM2^T (DSM 7523^T) were obtained from the culture collection of the Institute of Microbiology and Archaeal Center, University of Regensburg. *S. acidocaldarius* was grown under oxic conditions in modified ALLEN medium at 75 °C and pH 3.0,^{65,66} as described previously.⁶⁷ As substrate, 0.05% yeast extract, 0.2% saccharose, and 0.2% peptone were added. *P. aerophilum* was grown in BS medium at 97 °C, as previously described.⁶⁸ The medium was covered with a gas-phase H₂/CO₂ (80:20 vol/vol, 250 kPa), thereby using hydrogen as electron donor and nitrate (0.1%) as electron acceptor. Mass cultivation for both strains was carried out in 300 L of enamel-protected fermenters (HTE; BioEngineering, Wald, Switzerland). The cells were harvested by centrifugation (Padberg, Lahr, Germany), shock-frozen in liquid nitrogen, and stored at –80 °C until further use.

Preparation of ribosomal particles

Archaeal ribosomes were isolated and purified similarly as previously reported,^{50,69} but with some modifications. Briefly, cell pellets were dissolved in Tico buffer [20 mM

Hepes (pH 7.5), 10 mM Mg(OAc)₂, 30 mM NH₄OAc, and 4 mM β-mercaptoethanol] at 4 °C and subsequently disrupted with Microfluidizer (Microfluidics M-110L Pneumatic) at 18,000 psi. The crude homogenate was centrifuged twice at 30,000g at 4 °C for 30 min in order to obtain the S30 fraction. A crude ribosomal fraction was obtained by centrifugation at 100,000g for 5 h at 4 °C and by dissolution of the pellet in an equal volume of HSW buffer [20 mM Hepes, 10 mM Mg(OAc)₂, 500 mM NH₄OAc, and 4 mM β-mercaptoethanol (pH 7.5)]. Large debris was removed by centrifuging the crude ribosomes for 5 min at 18,000g at 4 °C. The clear supernatant was diluted 10-fold in HSW buffer and layered on top of 1.3 vol of 25% (wt/vol) sucrose cushion prepared in HSW buffer and centrifuged at 100,000g for 7 h at 4 °C. The pellet was resuspended in a minimal volume of Tico buffer and subsequently purified using sucrose density gradient centrifugation (10–40% sucrose in Tico buffer) at 46,000g for 17 h at 4 °C. Fractions corresponding to 50S and 30S subunits were separately pooled, pelleted at 140,000g for 12 h at 4 °C, and resuspended in a minimal volume of Tico buffer. *E. coli* ribosomes were prepared in accordance with Blaha *et al.*⁷⁰

Extraction of total r-proteins and 2D-PAGE

The total proteins from HSW ribosomes and purified ribosomal subunits were extracted by acetic acid in accordance with Nierhaus and Dohme⁷¹. Lyophilized proteins were further processed for LC-MS/MS analysis and 2D-PAGE. Around 2 μg of total proteins was necessary for LC-MS/MS, whereas 5–10 μg of total proteins was required for 2D-PAGE. Two-dimensional electrophoresis was performed as described by Kaltschmidt and Wittmann.¹⁴

Analysis of ribosomal particles by stepwise LiCl washing

Stepwise washing of purified 50S ribosomal subunits from *S. acidocaldarius* was performed in accordance with Homann and Nierhaus, with minor modifications.⁷² Briefly, five A₂₆₀ units of ribosomal particles were incubated in a total volume of 100 μl with 10 mM Tris-HCl (pH 7.8), 10 mM MgCl₂, 0.1 mM ethylenediaminetetraacetic acid, and appropriate concentrations of LiCl (0.6 M, 1 M, 1.5 M, 2 M, 3 M, and 4 M) for 4 h at 4 °C, with moderate shaking. The incubation reaction was further centrifuged at 160,000g for 12 h at 4 °C, and the dissociated proteins (supernatants) were precipitated with trichloroacetic acid. Lyophilized proteins were treated as described above for LC-MS/MS analysis and 2D-PAGE. In those cases where the core particle was analyzed (4 M LiCl core), the pellet obtained after ultracentrifugation was dissolved in Tico buffer, and the core proteins were extracted by acetic acid as described previously by Nierhaus and Dohme.⁷¹

Mass spectrometry

Excision and tryptic in-gel digestion of 2D gel spots

Spots of interest were automatically excised using a Proteiner robot (Bruker Daltonics, Leipzig, Germany) and transferred onto 96-well reaction plates (Intavis,

Köln, Germany). Digests were performed using a DigestPro MS digest robot (Intavis) using the following a protocol: (i) washing with 60 μl of 100% CH₃CN; (ii) rinsing with 45 μl of 50 mM NH₄HCO₃; (iii) washing with 60 μl of CH₃CN; (iv) 20-min incubation with 30 μl of 10 mM dithiothreitol in water at 65 °C; (v) 20-min incubation with 30 μl of 50 mM iodoacetamide in water; (vi) two 20-min washes with 60 μl of 50 mM NH₄HCO₃; (vii) one 20-min wash in 60 μl of CH₃CN; (viii) 15-min wash in 45 μl of CH₃CN; (ix) addition of 90 ng of modified porcine trypsin (Promega, Madison, WI, USA) in 15 μl of 50 mM NH₄HCO₃ and incubation at 37 °C for 6 h; (x) addition of 15 μl of 2.5% formic acid (FA); and (xi) collection of the supernatant peptide extracts on 96-well collection plates (Intavis).

Matrix-assisted laser desorption/ionization MS-based identification of 2D gel spots

Matrix-assisted laser desorption/ionization (MALDI) targets were prepared automatically using a DigestPro MS robot (Intavis) equipped with ZipTip C-18 reversed-phase tips (Millipore, Billerica, MA, USA) for desalting. The following protocol was used: (i) activation of ZipTips with 20 μl of 50% CH₃CN and 0.1% trifluoroacetic acid (TFA); (ii) washing with 20 μl of 0.1% TFA; (iii) loading of the tryptic digest; (iv) washing with 20 μl of 0.1% TFA; and (v) elution of peptides onto the MALDI target plate with 1–2 μl of matrix solution (8 mg/ml CHCA, 65% CH₃CN, and 0.1% TFA). MALDI TOF/TOF MS was performed on a 4800 MALDI TOF/TOF Analyzer (Applied Biosystems). For precursor ion scans, a mass range between 800 Da and 4000 Da was chosen, and a minimum signal-to-noise ratio of 20 was set for peak detection. The MS/MS spectra of the 20 most intense precursors within each spot were generated by 500 laser shots.

LC-MS/MS analysis of protein samples on the LTQ ion trap

Peptide samples were diluted in 40 μl of 0.1% FA and centrifuged for 15 min at 14,000 rpm at room temperature. A multidimensional liquid chromatography system (Ettan MDLC; GE Healthcare) connected upstream of the spectrometer was used for separation. Peptide samples were loaded onto a trap column (C18 PepMap100, 5 μm particle size, 100 Å, 300 μm × 5 mm column size; LC Packings Dionex) at a flow rate of 10 μl/min and subsequently separated by an RP column (C18 PepMap 100, 3 μm bead size, 75 μm i.d., 15 cm length; LC Packings) with an 80-min gradient from 0% solvent B to 30% solvent B (solvent A: 0.1% FA; solvent B: 84% CH₃CN/0.1% FA), followed by a 30-min gradient to 60% solvent B at a flow rate of 280 nl/min. Electrospray ionization was performed with a distal coated SilicaTip (FS-360-20-10-D-20; New Objective) at a needle voltage of 1.2 kV. MS/MS of peptide samples was performed on a linear ion-trap mass spectrometer (LTQ; Thermo Electron). MS and MS/MS analyses were performed using cycles of one MS scan (mass range *m/z* 300–1600) and three subsequent data-dependent MS/MS scans ("Dynamic Exclusion™ activated"; 35% collision energy).

LC-MS/MS analysis of protein samples on the Orbitrap XL instrument

Chromatographic separation of peptides was performed as described previously for LTQ ion-trap measurements, but using a Reprosil-Pur C18 separation column (Reprosil-Pur C18 AQ, 3 μ m, 150 nm \times 75 μ m; Dr. Maisch). Electrospray ionization was performed with a distal coated SilicaTip (FS-360-20-10-D-20; New Objective) and a needle voltage of 1.4 kV. In order to detect low-molecular-mass ammonium ions, we performed MS and MS/MS analyses using cycles of one MS scan (mass range m/z 300–2000) and three subsequent data-dependent CID MS/MS scans, followed by three HCD MS/MS scans ("Dynamic Exclusion™ activated"; 35% collision energy).

Database search and data analysis

MS/MS data were searched with Mascot version 2.1.03 (Matrix Science, Boston, MA, USA) using the NCBI nr 20091028 database and the following parameters: (i) enzyme: trypsin; (ii) fixed modification: carbamidomethyl (C); (iii) variable modifications: oxidation (M), methyl (K), and N-acetyl (protein); (iv) peptide mass tolerance: 2 Da for electrospray ionization measurements and 100 ppm for MALDI measurements; (v) MS/MS mass tolerance: 0.8 Da; (vi) peptide charges: 1+, 2+, and 3+; (vii) instrument: electrospray ionization trap; and (viii) allow up to one missed cleavage. Mascot results were further validated with the Scaffold software V 2.6 (Proteome Software, Inc., Portland, OR, USA). Protein identification was accepted if it could be established at >99.0% probability. In order to determine the number of false-positive identifications, we repeated MASCOT searches and Scaffold evaluations with a randomized version of the NCBI nr database. For the generation of this so-called "decoy database" consisting of random sequences with the same average amino acid composition, the decoy PerlScript (Matrix Science) was used.

Malachite Green GTPase activity assays

GTPase and ATPase activities were measured using the Malachite Green Phosphate Kit (BioAssay) that quantifies the green complex formed between Malachite Green, molybdate, and free orthophosphate, as described previously.⁷³ All reactions contained 30–90 nM *E. coli* 70S ribosomes, *S. acidocaldarius* 30S or 50S subunits, 20 μ M GTP or ATP, and/or 30–90 nM EF-G. Reactions were transferred onto 96-well microtiter plates and incubated at 37 °C or 60 °C for various lengths of time. Color formation was measured on Tecan-Infinite M1000 microplate reader at 650 nm. Reactions performed in the absence of ribosomes were used as background signal to account for the spontaneous hydrolysis of ATP or GTP.

Electron microscopy

Negative-stain EM

Ribosomal particles were resuspended in Tico buffer to a final concentration of 0.5–1 A_{260} /ml. One drop of each sample was deposited on carbon-coated grids. After 45 s, the grids were washed with distilled water. The grids were then stained with three drops of 2% aqueous uranyl

acetate for 15 s, and excess liquid was removed again by touching the grids with filter paper. Micrographs were taken with a Morgagni transmission electron microscope (FEI; 80 kV) equipped with a wide-angle 1000 CCD camera.

Cryo-EM and single-particle reconstruction

As described previously,⁷⁴ *S. acidocaldarius* and *P. aerophilum* 50S subunits were applied to carbon-coated holey grids. Images were collected on a Tecnai G2 Spirit TEM at 120 kV at a nominal magnification of 90,000 \times using an Eagle 4096 \times 4096-pixel CCD camera (FEI), resulting in a pixel size of 3.31 Å/pixel. The data were analyzed by determining the contrast transfer function with CTFFIND⁷⁵ and were further processed with the SPIDER software package,⁷⁶ using the *H. marismortui* 50S subunit [Protein Data Bank (PDB) code 3CC2]⁶³ filtered to between 20 Å and 25 Å as initial reference. For the final *S. acidocaldarius* and *P. aerophilum* 50S subunit reconstructions, 9301 and 9183 particles were used, respectively.

Modeling and figure preparation

The model for the *S. acidocaldarius* 50S subunit utilized the crystal structure of the archaeon *H. marismortui* 50S subunit (PDB code 3CC2),⁶³ with additional missing proteins added using the location of the homologues in the eukaryotic 80S ribosome.^{8,77} The models were fitted to the maps using Chimera,⁷⁸ and Figs. 5c and 6 were prepared using PyMOL (The PyMOL Molecular Graphics System, version 1.3, Schrödinger LLC) and Chimera, respectively.

Accession numbers

The cryo-EM maps of the *S. acidocaldarius* and *P. aerophilum* 50S subunits have been deposited in the three-dimensional EM database under accession numbers EMD-1797 and EMD-1797, respectively.

Supplementary materials related to this article can be found online at [doi:10.1016/j.jmb.2010.11.055](https://doi.org/10.1016/j.jmb.2010.11.055)

Acknowledgements

This research was supported by Deutsche Forschungsgemeinschaft grants SFB594 and SFB646 (to R.B.) and WI3285/1-1 (to D.N.W.).

References

- Schmeing, T. M. & Ramakrishnan, V. (2009). What recent ribosome structures have revealed about the mechanism of translation. *Nature*, **461**, 1234–1242.
- Wilson, D. N. & Nierhaus, K. H. (2005). Ribosomal proteins in the spotlight. *Crit. Rev. Biochem. Mol. Biol.* **40**, 243–267.
- Brodersen, D. & Nissen, P. (2005). The social life of ribosomal proteins. *FEBS J.* **272**, 2098–2108.

4. Ogle, J. M. & Ramakrishnan, V. (2005). Structural insights into translational fidelity. *Annu. Rev. Biochem.* **74**, 129–177.
5. Maguire, B. A., Beniaminov, A. D., Ramu, H., Mankin, A. S. & Zimmermann, R. A. (2005). A protein component at the heart of an RNA machine: the importance of protein l27 for the function of the bacterial ribosome. *Mol. Cell*, **20**, 427–435.
6. Voorhees, R. M., Weixlbaumer, A., Loakes, D., Kelley, A. C. & Ramakrishnan, V. (2009). Insights into substrate stabilization from snapshots of the peptidyl transferase center of the intact 70S ribosome. *Nat. Struct. Mol. Biol.* **16**, 528–533.
7. Bhushan, S., Meyer, H., Starosta, A., Becker, T., Mielke, T., Berninghausen, O. *et al.* (2010). Structural basis for translational stalling by human cytomegalovirus (hCMV) and fungal arginine attenuator peptide (AAP). *Mol. Cell*, **40**, 138–146.
8. Armache, J.-P., Jarasch, A., Anger, A. M., Villa, E., Becker, T., Blushan, S. *et al.* (2010). Localization of eukaryote-specific ribosomal proteins: implications for structure, function and evolution. *Proc. Natl Acad. Sci. USA*, **107**, 19754–19759.
9. Meskauskas, A. & Dinman, J. D. (2001). Ribosomal protein L5 helps anchor peptidyl-tRNA to the P-site in *Saccharomyces cerevisiae*. *RNA*, **7**, 1084–1096.
10. Yusupov, M. M., Yusupova, G. Z., Baucom, A., Lieberman, K., Earnest, T. N., Cate, J. H. & Noller, H. F. (2001). Crystal structure of the ribosome at 5.5 Å resolution. *Science*, **292**, 883–896.
11. Selmer, M., Dunham, C., Murphy, F. T., Weixlbaumer, A., Petry, S., Kelley, A. *et al.* (2006). Structure of the 70S ribosome complexed with mRNA and tRNA. *Science*, **313**, 1935–1942.
12. Jenner, L., Demeshkina, N., Yusupova, G. & Yusupov, M. (2010). Structural rearrangements of the ribosome at the tRNA proofreading step. *Nat. Struct. Mol. Biol.* **17**, 1072–1078.
13. Fischer, N., Konevega, A. L., Wintermeyer, W., Rodnina, M. V. & Stark, H. (2010). Ribosome dynamics and tRNA movement by time-resolved electron cryomicroscopy. *Nature*, **466**, 329–333.
14. Kaltschmidt, E. & Wittmann, H. G. (1970). Ribosomal proteins: VII. 2D polyacrylamide gel electrophoresis for fingerprinting of ribosomal proteins. *Anal. Biochem.* **36**, 401–412.
15. Yamaguchi, K. & Subramanian, A. R. (2000). The plastid ribosomal proteins. Identification of all the proteins in the 50S subunit of an organelle ribosome (chloroplast). *J. Biol. Chem.* **275**, 28466–28482.
16. Yamaguchi, K., von Knoblauch, K. & Subramanian, A. R. (2000). The plastid ribosomal proteins. Identification of all the proteins in the 30S subunit of an organelle ribosome (chloroplast). *J. Biol. Chem.* **275**, 28455–28465.
17. Sharma, M. R., Wilson, D. N., Datta, P. P., Barat, C., Schlutzen, F., Fucini, P. & Agrawal, R. K. (2007). Cryo-EM study of the spinach chloroplast ribosome reveals the structural and functional roles of plastid-specific ribosomal proteins. *Proc. Natl Acad. Sci. USA*, **104**, 19315–19320.
18. Sharma, M. R., Donhofer, A., Barat, C., Marquez, V., Datta, P. P., Fucini, P. *et al.* (2010). PSRP1 is not a ribosomal protein, but a ribosome-binding factor that is recycled by the ribosome-recycling factor (RRF) and elongation factor G (EF-G). *J. Biol. Chem.* **285**, 4006–4014.
19. Koc, E. C., Burkhart, W., Blackburn, K., Moseley, A. & Spremulli, L. L. (2001). The small subunit of the mammalian mitochondrial ribosome. Identification of the full complement of ribosomal proteins present. *J. Biol. Chem.* **276**, 19363–19374.
20. Koc, E. C., Burkhart, W., Blackburn, K., Moyer, M. B., Schlatzer, D. M., Moseley, A. & Spremulli, L. L. (2001). The large subunit of the mammalian mitochondrial ribosome. Analysis of the complement of ribosomal proteins present. *J. Biol. Chem.* **276**, 43958–43969.
21. Smits, P., Smeitink, J. A., van den Heuvel, L. P., Huynen, M. A. & Ettema, T. J. (2007). Reconstructing the evolution of the mitochondrial ribosomal proteome. *Nucleic Acids Res.* **35**, 4686–4703.
22. Lee, S., Berger, S., Martinovic, S., Pasa-Tolic, L., Anderson, G., Shen, Y. *et al.* (2002). Direct mass spectrometric analysis of intact proteins of the yeast large ribosomal subunit using capillary LC/FTICR. *Proc. Natl Acad. Sci. USA*, **99**, 5942–5947.
23. Link, A., Eng, J., Schieltz, D., Carmack, E., Mize, G., Morris, D. *et al.* (1999). Direct analysis of protein complexes using mass spectrometry. *Nat. Biotechnol.* **17**, 676–682.
24. Alonso, J. & Santaren, J. F. (2006). Characterization of the *Drosophila melanogaster* ribosomal proteome. *J. Proteome Res.* **5**, 2025–2032.
25. Giavalisco, P., Wilson, D., Kreidler, T., Lehrach, H., Klose, J., Gobom, J. & Fucini, P. (2005). High heterogeneity within the ribosomal proteins of the *Arabidopsis thaliana* 80S ribosome. *Plant Mol. Biol.* **57**, 577–591.
26. Louie, D. F., Resing, K. A., Lewis, T. S. & Ahn, N. G. (1996). Mass spectrometric analysis of 40S ribosomal proteins from rat-1 fibroblasts. *J. Biol. Chem.* **271**, 28189–28198.
27. Wool, I. G., Chan, Y. L. & Glück, A. (1995). Structure and evolution of mammalian ribosomal proteins. *Biochem. Cell Biol.* **73**, 933–947.
28. Sugihara, Y., Honda, H., Iida, T., Morinaga, T., Hino, S., Okajima, T. *et al.* (2010). Proteomic analysis of rodent ribosomes revealed heterogeneity including ribosomal proteins L10-like, L22-like 1, and L39-like. *J. Proteome Res.* **9**, 1351–1366.
29. Vladimirov, S. N., Ivanov, A. V., Karpova, G. G., Musolyamov, A. K., Egorov, T. A., Thiede, B. *et al.* (1996). Characterization of the human small-ribosomal-subunit proteins by N-terminal and internal sequencing, and mass spectrometry. *Eur. J. Biochem.* **239**, 144–149.
30. Odintsova, T. I., Muller, E. C., Ivanov, A. V., Egorov, T. A., Bienert, R., Vladimirov, S. N. *et al.* (2003). Characterization and analysis of posttranslational modifications of the human large cytoplasmic ribosomal subunit proteins by mass spectrometry and Edman sequencing. *J. Protein Chem.* **22**, 249–258.
31. Lecompte, O., Ripp, R., Thierry, J. C., Moras, D. & Poch, O. (2002). Comparative analysis of ribosomal proteins in complete genomes: an example of reductive evolution at the domain scale. *Nucleic Acids Res.* **30**, 5382–5390.
32. Kimura, M., Arndt, E., Hatakeyama, T. & Kimura, J. (1989). Ribosomal proteins in Halobacteria. *Can. J. Microbiol.* **35**, 195–199.

33. Auer, J., Lechner, K. & Bock, A. (1989). Gene organization and structure of two transcriptional units from *Methanococcus* coding for ribosomal proteins and elongation factors. *Can. J. Microbiol.* **35**, 200–204.
34. Auer, J., Spicker, G. & Bock, A. (1989). Organization and structure of the *Methanococcus* transcriptional unit homologous to the *Escherichia coli* "spectinomycin operon." Implications for the evolutionary relationship of 70S and 80S ribosomes. *J. Mol. Biol.* **209**, 21–36.
35. Ramirez, C., Louie, K. A. & Matheson, A. T. (1991). A small basic ribosomal protein from the extreme thermophilic archaeobacterium *Sulfolobus solfataricus* that has no equivalent in *Escherichia coli*. *FEBS Lett.* **284**, 39–41.
36. Strom, A. R. & Visentin, L. P. (1973). Acidic ribosomal proteins from the extreme halophile, *Halobacterium cutirubrum*. The simultaneous separation, identification and molecular weight determination. *FEBS Lett.* **37**, 274–280.
37. Londei, P., Teichner, A., Cammarano, P., De Rosa, M. & Gambacorta, A. (1983). Particle weights and protein composition of the ribosomal subunits of the extremely thermoacidophilic archaeobacterium *Caldariella acidophila*. *Biochem. J.* **209**, 461–470.
38. Teixido, J., Altamura, S., Londei, P. & Amils, R. (1989). Structural and functional exchangeability of 5S RNA species from the eubacterium *E. coli* and the thermoacidophilic archaeobacterium *Sulfolobus solfataricus*. *Nucleic Acids Res.* **17**, 845–851.
39. Altamura, S., Caprini, E., Sanchez, M. E. & Londei, P. (1991). Early assembly proteins of the large ribosomal subunit of the thermophilic archaeobacterium *Sulfolobus*. Identification and binding to heterologous rRNA species. *J. Biol. Chem.* **266**, 6195–6200.
40. Pettersson, I., Hardy, S. J. S. & Liljas, A. (1976). The ribosomal protein L8 is a complex of L7/L12 and L10. *FEBS Lett.* **6**, 135–138.
41. Arnold, R. J. & Reilly, J. P. (2002). Analysis of methylation and acetylation in *E. coli* ribosomal proteins. *Methods Mol. Biol.* **194**, 205–210.
42. Gauci, S., Helbig, A. O., Slijper, M., Krijgsveld, J., Heck, A. J. & Mohammed, S. (2009). Lys-N and trypsin cover complementary parts of the phosphoproteome in a refined SCX-based approach. *Anal. Chem.* **81**, 4493–4501.
43. Yu, L. R., Zhu, Z., Chan, K. C., Issaq, H. J., Dimitrov, D. S. & Veenstra, T. D. (2007). Improved titanium dioxide enrichment of phosphopeptides from HeLa cells and high confident phosphopeptide identification by cross-validation of MS/MS and MS/MS/MS spectra. *J. Proteome Res.* **6**, 4150–4162.
44. Moser, K. & White, F. M. (2006). Phosphoproteomic analysis of rat liver by high capacity IMAC and LC-MS/MS. *J. Proteome Res.* **5**, 98–104.
45. Rodriguez-Gabriel, M. A., Remacha, M. & Ballesta, J. P. (1998). Phosphorylation of ribosomal protein P0 is not essential for ribosome function but can affect translation. *Biochemistry*, **37**, 16620–16626.
46. Zhang, J., Sprung, R., Pei, J., Tan, X., Kim, S., Zhu, H. et al. (2009). Lysine acetylation is a highly abundant and evolutionarily conserved modification in *Escherichia coli*. *Mol. Cell. Proteomics*, **8**, 215–225.
47. Omer, A. D., Ziesche, S., Decatur, W. A., Fournier, M. J. & Dennis, P. P. (2003). RNA-modifying machines in archaea. *Mol. Microbiol.* **48**, 617–629.
48. Ditzel, L., Lowe, J., Stock, D., Stetter, K. O., Huber, H., Huber, R. & Steinbacher, S. (1998). Crystal structure of the thermosome, the archaeal chaperonin and homolog of CCT. *Cell*, **93**, 125–138.
49. Ruggero, D., Ciammaruconi, A. & Londei, P. (1998). The chaperonin of the archaeon *Sulfolobus solfataricus* is an RNA-binding protein that participates in ribosomal RNA processing. *EMBO J.* **17**, 3471–3477.
50. Londei, P., Altamura, S., Cammarano, P. & Petrucci, L. (1986). Differential features of ribosomes and of poly (U)-programmed cell-free systems derived from sulfur-dependent archaeobacterial species. *Eur. J. Biochem.* **157**, 455–462.
51. Henderson, E., Oakes, M., Clark, M. W., Lake, J. A., Matheson, A. T. & Zillig, W. (1984). A new ribosome structure. *Science*, **225**, 510–512.
52. Ciammaruconi, A., Gorini, S. & Londei, P. (2008). A bifunctional archaeal protein that is a component of 30S ribosomal subunits and interacts with C/D box small RNAs. *Archaea*, **2**, 151–158.
53. Wang, J., Dasgupta, I. & Fox, G. E. (2009). Many nonuniversal archaeal ribosomal proteins are found in conserved gene clusters. *Archaea*, **2**, 241–251.
54. Rodnina, M. V., Serebryanik, A. I., Ovcharenko, G. V. & Elskaya, V. (1994). ATPase strongly bound to higher eukaryotic ribosomes. *Eur. J. Biochem.* **225**, 305–310.
55. Ogata, K., Ohno, R., Terao, K., Iwasaki, K. & Endo, Y. (2000). Some properties and the possible role of intrinsic ATPase of rat liver 80S ribosomes in peptide bond elongation. *J. Biochem.* **127**, 221–231.
56. Hamel, E., Koka, M. & Nakamoto, T. (1972). Requirement of an *E. coli* 50S ribosomal protein component for effective interaction of the ribosome with T and G factors and with guanosine triphosphate. *J. Biol. Chem.* **247**, 805–814.
57. Uchiumi, T., Honma, S., Endo, Y. & Hachimori, A. (2002). Ribosomal proteins at the stalk region modulate functional rRNA structures in the GTPase center. *J. Biol. Chem.* **277**, 41401–41409.
58. Nierhaus, K. H. (1991). The assembly of prokaryotic ribosomes. *Biochimie*, **73**, 739–755.
59. Londei, P., Teixido, J., Acca, M., Cammarano, P. & Amils, R. (1986). Total reconstitution of active large ribosomal subunits of the thermoacidophilic archaeobacterium *Sulfolobus solfataricus*. *Nucleic Acids Res.* **14**, 2269–2285.
60. Sanchez, M. E., Urena, D., Amils, R. & Londei, P. (1990). *In vitro* reassembly of active large ribosomal subunits of the halophilic archaeobacterium *Haloferax mediterranei*. *Biochemistry*, **29**, 9256–9261.
61. El-Baradi, T. T., Raue, H. A., De Regt, C. H. & Planta, R. J. (1984). Stepwise dissociation of yeast 60S ribosomal subunits by LiCl and identification of L25 as a primary 26S rRNA binding protein. *Eur. J. Biochem.* **144**, 393–400.
62. Kruiswijk, T., Planta, R. J. & Krop, J. M. (1978). The course of the assembly of ribosomal subunits in yeast. *Biochim. Biophys. Acta*, **517**, 378–389.
63. Ban, N., Nissen, P., Hansen, J., Moore, P. B. & Steitz, T. A. (2000). The complete atomic structure of the large ribosomal subunit at 2.4 Å resolution. *Science*, **289**, 905–920.
64. Halic, M., Becker, T., Frank, J., Spahn, C. M. & Beckmann, R. (2005). Localization and dynamic

- behavior of ribosomal protein L30e. *Nat. Struct. Mol. Biol.* **12**, 467–468.
65. Allen, M. B. (1959). Studies with *Cyanidium caldarium*, an anomalously pigmented chlorophyte. *Arch. Mikrobiol.* **32**, 270–277.
66. Brock, T. D., Brock, K. M., Belly, R. T. & Weiss, R. L. (1972). *Sulfolobus*: a new genus of sulfur-oxidizing bacteria living at low pH and high temperature. *Arch. Mikrobiol.* **84**, 54–68.
67. Huber, G., Spinnler, C., Gambacorta, A. & Stetter, K. O. (1989). *Metallosphaera sedula* gen. and sp. nov. represents a new genus of aerobic, metal-mobilizing, thermoacidophilic archaebacteria. *Syst. Appl. Microbiol.* **12**, 38–47.
68. Volkl, P., Huber, R., Drobner, E., Rachel, R., Burggraf, S., Trincone, A. & Stetter, K. O. (1993). *Pyrobaculum aerophilum* sp. nov., a novel nitrate-reducing hyperthermophilic archaeum. *Appl. Environ. Microbiol.* **59**, 2918–2926.
69. Bommer, U., Burkhardt, N., Jünemann, R., Spahn, C. M. T., Triana-Alonso, F. J. & Nierhaus, K. H. (1996). Ribosomes and polysomes. In (Graham, J. & Rickwoods, D., eds), pp. 271–301, IRL Press at Oxford University Press, Oxford, UK.
70. Blaha, G., Stelzl, U., Spahn, C. M. T., Agrawal, R. K., Frank, J. & Nierhaus, K. H. (2000). Preparation of functional ribosomal complexes and the effect of buffer conditions on tRNA positions observed by cryoelectron microscopy. *Methods Enzymol.* **317**, 292–309.
71. Nierhaus, K. H. & Dohme, F. (1974). Total reconstitution of functionally active 50S ribosomal subunits from *E. coli*. *Proc. Natl Acad. Sci. USA*, **71**, 4713–4717.
72. Homann, H. E. & Nierhaus, K. H. (1971). Ribosomal proteins. Protein compositions of biosynthetic precursors and artificial subparticles from ribosomal subunits in *Escherichia coli* K 12. *Eur. J. Biochem.* **20**, 249–257.
73. Starosta, A. L., Qin, H., Mikolajka, A., Leung, G. Y., Schwinghammer, K., Nicolaou, K. C. *et al.* (2009). Identification of distinct thiopeptide–antibiotic precursor lead compounds using translation machinery assays. *Chem. Biol.* **16**, 1087–1096.
74. Wagenknecht, T., Frank, J., Boublik, M., Nurse, K. & Ofengand, J. (1988). Direct localization of the tRNA–anticodon interaction site on the *Escherichia coli* 30S ribosomal subunit by electron microscopy and computerized image averaging. *J. Mol. Biol.* **203**, 753–760.
75. Mindell, J. A. & Grigorieff, N. (2003). Accurate determination of local defocus and specimen tilt in electron microscopy. *J. Struct. Biol.* **142**, 334–347.
76. Frank, J., Radermacher, M., Penczek, P., Zhu, J., Li, Y., Ladjadj, M. & Leith, A. (1996). SPIDER and WEB: processing and visualization of images in 3D electron microscopy and related fields. *J. Struct. Biol.* **116**, 190–199.
77. Armache, J.-P., Jarasch, A., Anger, A. M., Villa, E., Becker, T., Bhushan, S. *et al.* (2010). Cryo-EM structure of a translating eukaryotic 80S ribosome at 5.5 Å resolution. *Proc. Natl Acad. Sci. USA*, **107**, 19748–19753.
78. Pettersen, E. F., Goddard, T. D., Huang, C. C., Couch, G. S., Greenblatt, D. M., Meng, E. C. & Ferrin, T. E. (2004). UCSF Chimera—a visualization system for exploratory research and analysis. *J. Comput. Chem.* **25**, 1605–1612.

Sharma MR*, Dönhöfer A*, Barat C, Marquez V,
Datta PP, Fucini P, Wilson DN, Agrawal RK.
*PSRP1 is not a ribosomal protein, but a ribosome binding
factor that is recycled by the ribosome-recycling
factor (RRF) and elongation factor G (EF-G).*
J Biol Chem. 2010 Feb 5; 285(6): 4006-14.

*Both authors contributed equally to this work.

PSRP1 Is Not a Ribosomal Protein, but a Ribosome-binding Factor That Is Recycled by the Ribosome-recycling Factor (RRF) and Elongation Factor G (EF-G)*^[5]

Received for publication, September 2, 2009, and in revised form, November 10, 2009. Published, JBC Papers in Press, December 4, 2009, DOI 10.1074/jbc.M109.062299

Manjuli R. Sharma^{‡1}, Alexandra Dönhöfer^{§¶1}, Chandana Barat^{‡2}, Viter Marquez^{§¶}, Partha P. Datta[‡], Paola Fucini^{||}, Daniel N. Wilson^{§¶3}, and Rajendra K. Agrawal^{‡**4}

From the [‡]Division of Translational Medicine, Wadsworth Center, New York State Department of Health, Empire State Plaza, Albany, New York 12201-0509, the [§]Center for Integrated Protein Science Munich (CiPSM) and [¶]Gene Center and Department of Chemistry and Biochemistry, Ludwig-Maximilians-Universität München, Feodor-Lynen-Strasse 25, D-81377 Munich, Germany, the ^{||}Cluster of Excellence for Macromolecular Complexes, Institut für Organische Chemie und Chemische Biologie, J. W. Goethe-Universität Frankfurt am Main, Max-von-Laue-Strasse 7, D-60438 Frankfurt am Main, Germany, and the ^{**}Department of Biomedical Sciences, School of Public Health, State University of New York at Albany, Albany, New York 12201

Plastid-specific ribosomal proteins (PSRPs) have been proposed to play roles in the light-dependent regulation of chloroplast translation. Here we demonstrate that PSRP1 is not a *bona fide* ribosomal protein, but rather a functional homologue of the *Escherichia coli* cold-shock protein pY. Three-dimensional Cryo-electron microscopic (Cryo-EM) reconstructions reveal that, like pY, PSRP1 binds within the intersubunit space of the 70S ribosome, at a site overlapping the positions of mRNA and A- and P-site tRNAs. PSRP1 induces conformational changes within ribosomal components that comprise several intersubunit bridges, including bridge B2a, thereby stabilizes the ribosome against dissociation. We find that the presence of PSRP1/pY lowers the binding of tRNA to the ribosome. Furthermore, similarly to tRNAs, PSRP1/pY is recycled from the ribosome by the concerted action of the ribosome-recycling factor (RRF) and elongation factor G (EF-G). These results suggest a novel function for EF-G and RRF in the post-stress return of PSRP1/pY-inactivated ribosomes to the actively translating pool.

Chloroplasts are intracellular organelles present in higher plants and algae; they contain the entire machinery with which the process of photosynthesis is conducted. According to the endosymbiotic theory of chloroplast evolution (1–3), this

organelle originated through engulfment of a photosynthetic unicellular prokaryote by a eukaryotic host cell, and the subsequent integration of the two genomes (that of the engulfed prokaryote, and the eukaryotic nucleus) through a process of gene transfers from the chloroplast to the nuclear genome. Thus, although the chloroplast carries its own transcriptional and translational machineries, the development and maintenance of the chloroplast are dependent on the coordinated expression of chloroplast- and nuclear-encoded gene products.

The light-dependent process of photosynthesis is the primary function of the chloroplast. Because the components that are crucial for the biogenesis of the photosynthetic apparatus are encoded by both the chloroplast and nuclear genomes, the plant cell has evolved several mechanisms to achieve concerted regulation of gene expression in the two cellular compartments, in response to changes in illumination (4–6). Regulation of gene expression is primarily post-transcriptional, and is achieved through altered mRNA processing and stability, and the control of the translational apparatus itself in response to environmental signals like light (7–9). It has been demonstrated that the redox state of the chloroplast achieved in response to photosynthetic electron transport can regulate protein synthesis within the chloroplast at the stages of initiation and elongation (10–12).

A detailed analysis of the chloroplast translational machinery, the chloroplast ribosome together with its trans-acting translational factors, will provide important clues as to how such gene regulation is achieved. Proteomic characterization of the chloroplast ribosomes (chlororibosomes) from spinach has revealed the presence of six plastid-specific ribosomal proteins (PSRPs),⁵ four of which are associated with the 30S subunit and two with the 50S subunit, in addition to the plastid orthologs of bacterial r-proteins (13–16). All six PSRPs are encoded by genes located in the nucleus and are synthesized in the cytoplasm as precursor polypeptides. However, the functional roles of these PSRPs have not yet been elucidated.

* This work was supported, in whole or in part, by National Institutes of Health Grant R01 GM61576 (to R. K. A.). This work was also supported by the Human Frontiers of Science Program (to D. N. W.) and the Deutsche Forschungsgemeinschaft Grant WI3285/1-1 (to D. N. W.).

The cryo-EM map of the *in vitro* and *in vivo* assembled *E. coli* 70S ribosome-PSRP1 complexes have been deposited in the EM Data Bank (<http://emdep.rutgers.edu>) with accession codes EMD-5125 and EMD-5126, respectively.

^[5] The on-line version of this article (available at <http://www.jbc.org>) contains supplemental Figs. S1–S5.

¹ Both authors contributed equally to this work.

² Present address: Dept. of Biotechnology, St. Xavier's College, 30 Park St., Kolkata-700016, West Bengal, India.

³ To whom correspondence may be addressed: Gene Center and Dept. of Chemistry and Biochemistry, Ludwig-Maximilians-Universität München, Feodor-Lynen-Strasse 25, D-81377 Munich, Germany. Fax: 49-89-474-7992; E-mail: wilson@lmb.uni-muenchen.de.

⁴ To whom correspondence may be addressed: Division of Translational Medicine, Wadsworth Center, New York State Dept. of Health, Empire State Plaza, Albany, New York 12201-0509. Fax: 518-474-7992; E-mail: agrawal@wadsworth.org.

⁵ The abbreviations used are: PSRP, plastid-specific ribosomal protein; cryo-EM, cryo-electron microscopy; RRF, ribosome-recycling factor; EF-G, elongation factor G; Trx, thioredoxin; LrtA, light-repressed transcript A; GDPNP, guanosine 5'-[β , γ -imido]diphosphate.

Here, we demonstrate that PSRP1 can interact with *Escherichia coli* 70S ribosomes, both *in vivo* and *in vitro*. Cryo-EM and three-dimensional image reconstruction reveal that PSRP1 binds within the intersubunit space of the ribosome, overlap-

ping the positions of the anticodon stem-loops of A- and P-site tRNAs. Binding of PSRP1 induces conformational changes within several ribosome intersubunit bridges and stabilizes the ribosome against dissociation. Additionally, we show that binding of PSRP1 to the 70S ribosome is stabilized by the presence of the ribosome-recycling factor (RRF), but unaffected by the presence of initiation factor 3 (IF3). However, in the presence of elongation factor G (EF-G-GTP) and RRF, PSRP1, and pY appear to be recycled from the ribosome analogously to tRNA. We propose a model describing how PSRP1/pY-inactivated ribosomes are returned to the translation cycle, once stress conditions have abated.

EXPERIMENTAL PROCEDURES

Expression of PSRPs in *E. coli* and Preparation of the *E. coli* 70S-PSRP1 Complexes—The gene encoding the mature PSRP1 was amplified from cDNA template and cloned into pET32b, thus introducing N-terminal thioredoxin (Trx) and 6× histidine (6×His) tags onto the mature PSRP1. *E. coli* pY and IF3 genes were amplified from *E. coli* gDNA and cloned into pET-14b. All plasmids were transformed into BL21(DE3), protein expression was induced at mid-log phase with 1 mM isopropyl-1-thio-β-D-galactopyranoside, and the cells were harvested at late log-phase. Cells were lysed by freeze thawing and were resuspended on ice in Buffer A (20 mM Hepes-KOH, pH 7.8, 10 mM MgCl₂, 60 mM NH₄Cl, 4 mM β-mercaptoethanol), in the presence of lysozyme (1 μg/ml) and phenylmethylsulfonyl fluoride (0.2 mM). Lysates were clarified by centrifugation at 30,000 × g for 30 min, and the supernatant (S30) was then applied to 10–30% sucrose gradients in Buffer A. Fractions corresponding to the 70S ribosome peak were pooled, and the ribosomes were pelleted at 80,000 × g for 20 h. Pellets were resuspended in Buffer A, aliquoted, snap-frozen in liquid nitrogen, and stored at –80 °C. PSRP1, IF3, RRF, EF-G, and pY protein were purified using Ni-nitrilotriacetic acid-agarose (Qiagen) per the manufacturer's instructions. The eluted PSRP1 protein was dialyzed into 20 mM Tris-HCl, pH 7.8, 150 mM NaCl, 2 mM CaCl₂, and stored at –80 °C, whereas IF3 was dialyzed into 20 mM Tris-HCl, pH 7.1, 0.2 M NH₄Cl, 1 mM EDTA, 5 mM β-mercaptoethanol, 10% glycerol, and stored at –30 °C. *E. coli* pY was purified as described previously (17). Binding assays and sucrose gradients were performed as previously described (18). Dissociation assays were performed using tight-couple *E. coli* 70S ribosomes that were incubated in the presence or absence of protein factors in Buffer B (20 mM Hepes-KOH pH 7.8, 2.5 mM MgCl₂ or 5 mM MgCl₂, 200 mM NH₄Cl, 4 mM β-mercaptoethanol), before being applied to a 10–30% sucrose gradient in Buffer B.

Binding Assays—Binding assays were performed as described previously (18) with some modifications. *E. coli* ribosomes (0.4 μM) were

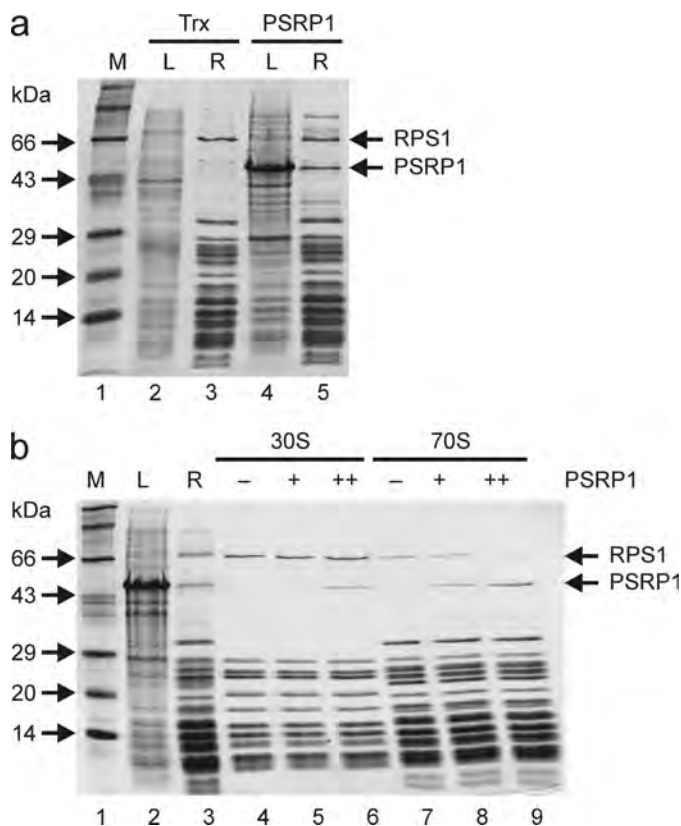


FIGURE 1. Binding of spinach PSRP1 to *E. coli* ribosomes. *a*, Coomassie Blue-stained SDS-PAGE with lysate (L) and purified 70S ribosomes (R) from *E. coli* cells overexpressing PSRP1 (lanes 4 and 5) or Trx control (lanes 2 and 3). *b*, 30S subunits (lanes 4–6) or 70S ribosomes (lanes 7–9) were incubated in the absence (–) or presence of a 2.5× (+) or 5× (++) excess of PSRP1 protein, before being centrifuged through a 10% sucrose cushion, with the pellet then subjected to SDS-PAGE and Coomassie Blue staining. Lysate (lane 2) and 70S ribosomes (lane 3) from *a* are included for reference. Arrows in *a* and *b* indicate ribosomal protein S1 (RPS1), PSRP1 positions in 70S ribosome (lanes 3 and 5 in panel *a*), and relevant protein marker sizes (lane 1).

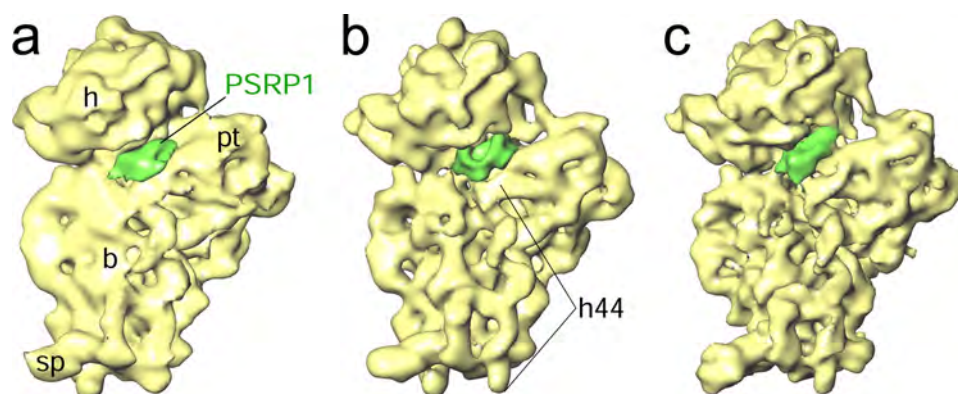


FIGURE 2. Binding position of PSRP1 on the *E. coli* 30S ribosomal subunit. Both the 30S subunit (yellow) and PSRP1 (green) masses were derived from the cryo-EM maps of 70S-PSRP1 complexes (see supplemental Fig. S2) that were obtained under *a* (*in vivo*) and *b* (*in vitro*) conditions; *c*, the 30S subunit portion of the chloroplast 70S map (26), with density corresponding to PSRP1 shown in green. The 50S ribosomal subunit has been computationally removed from all three maps, to reveal the PSRP1-binding position. The 30S subunit maps are shown from their subunit-subunit interface side. Landmarks of the 30S subunit: *b*, body; *h*, head; *pt*, platform; *sp*, spur; and *h44*, 16S rRNA helix 44.

Function of Plastid-specific Ribosomal Protein 1

incubated with varying amounts of protein factors (5× PSRP1 and 10× molar excess of RRF over 70S ribosomes; 5× molar excess of PSRP1 and IF3 over 30S ribosomes; 10× molar excess of PSRP1, RRF and EF-G over 70S ribosomes in the presence of 0.5 mM GTP and GDPNP) for 20 min at 37 °C in binding buffer (20 mM Hepes-KOH, pH 7.6, 10 mM MgCl₂, 30 mM NH₄Cl) before being loaded on a 10% sucrose cushion in binding buffer and centrifuged for 30 min at 75,000 rpm in a TLN 100 rotor at 4 °C. For each condition, aliquots of the initial reaction (R), supernatant (S) and pellet (P) after centrifugation were analyzed by 15% SDS-PAGE and stained with Coomassie Blue. In all cases, controls were performed with protein factors alone (no ribosomes present), and no pelleting of the factors was observed. At least three independent binding assays were performed per experiment, and the binding stoichiometries of the relevant factors were quantified using ImageQuant TL (GE Healthcare).

tRNA Binding Assays—tRNA binding assays were performed as described previously (19). Briefly, in a total volume of 25 μl, *E. coli* ribosomes (0.4 μM) were incubated separately with 12 μM of PSRP1, pY, and/or RRF in the presence of 0.4 μM [³²P]tRNA^{Met} (and the presence or absence of 5 μM MF-mRNA (19)). The binding of [³²P]tRNA^{Met} to ribosomes was monitored by filtration on Millipore filters (0.45 μm HA) and subsequent scintillation counting. The adjusted final ionic conditions for the binding assays were 20 mM Hepes-KOH, pH 7.5, 6 mM MgOAc, 150 mM NH₄Cl, 4 mM β-mercaptoethanol.

Ribosome-recycling Assays—Recycling assays were performed as previously described (20) with the following modifications. Briefly, *E. coli* 70S ribosomes (0.4 μM) were incubated with 10× molar excess of protein factors indicated for each reaction in binding buffer (20 mM Hepes-KOH, pH 7.6, 8.2 mM MgCl₂, 80 mM NH₄Cl, 4 mM β-mercaptoethanol) for 20 min at 37 °C in a total volume of 150 μl, before being loaded on a 5–30% sucrose gradient in the same buffer and centrifuged in a SW40 rotor at 19,000 rpm for 16.5 h at 4 °C. Gradients were monitored at 254 nm, from top to bottom.

Cryo-electron Microscopy and Three-dimensional Image Reconstruction—All EM data were collected on a Tecnai F20 field emission gun electron microscope (FEI, Eindhoven, The Netherlands), equipped with low-dose kit, and an Oxford cryo-transfer holder, at a magnification of ×50,760. For the *in vitro* and *in vivo* assembled *E. coli* 70S·PSRP1 complexes, 53 and 37 micrographs, respectively, were scanned on a Zeiss flatbed scanner (Z/I Imaging Corporation, Huntsville, AL), with a step size of 14 μm, corresponding to 2.76 Å on the object scale. The projection-matching procedure within the SPIDER software (21) was employed to obtain three-dimensional maps. We used a 11.5 Å resolution *E. coli* 70S ribosome map (22) as the initial reference. For the *in vitro* complex, 32,611 images sorted into 18 groups (according to defocus values, ranging from 1.2 to 4.2 μm), were selected, after visual and cross-correlation-based screening and removal of images from over-represented groups among the initial set of 83 representative views of the ribosome, and were used in the final reconstruction. For the *in vivo* complex, 18,317 images were sorted into 15 defocus groups ranging from 1.6 μm to 4.3 μm. The resolution of the final CTF-corrected three-dimensional map, estimated using the Fourier

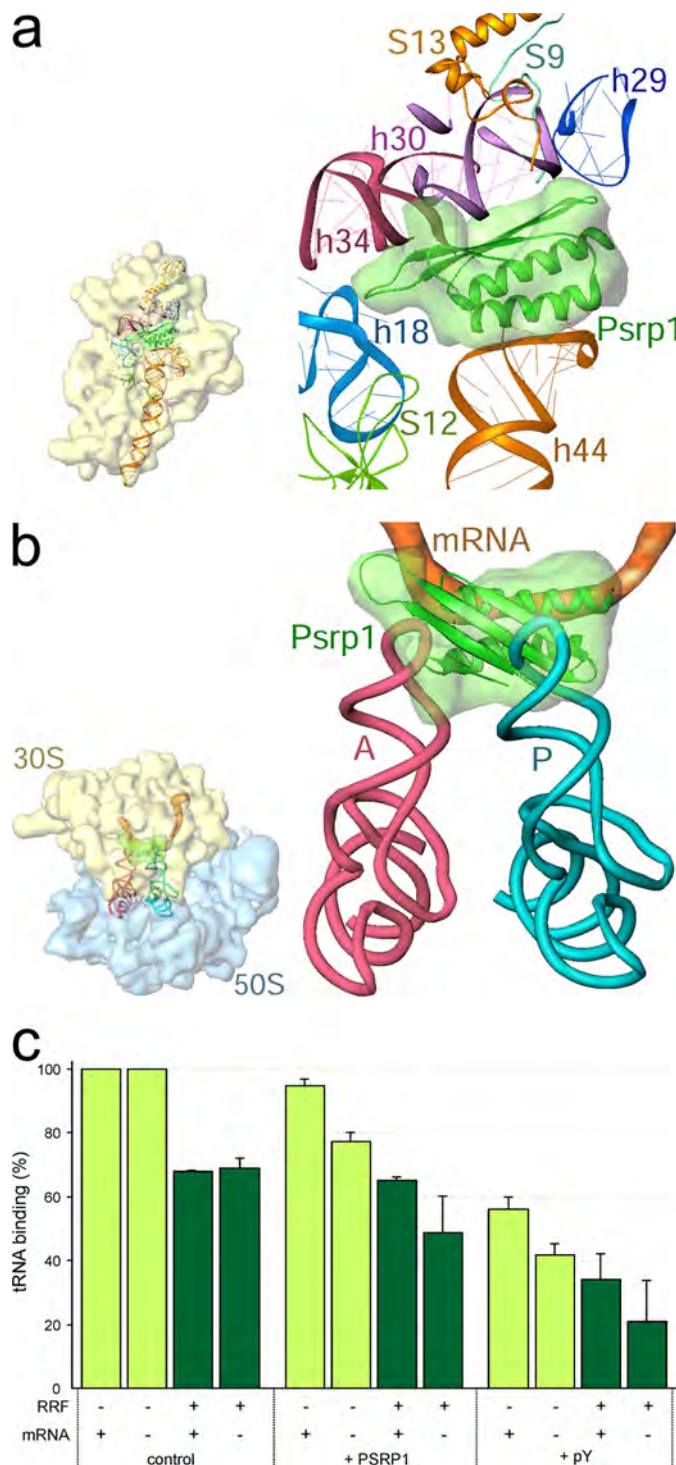


FIGURE 3. Sites of interaction between PSRP1 and the 30S ribosomal subunit and binding position of PSRP1 relative to the mRNA and tRNAs on the ribosome. *a*, x-ray crystallographic structures of the *E. coli* 30S ribosomal subunit (47) and homology model of the PSRP1 (green) were fitted into the cryo-EM map of the 70S·PSRP1 complex. The orientation of the 30S ribosome is shown in a thumbnail on the lower left. Numbers following S and h identify ribosomal proteins and 16S rRNA helices, respectively, within the 30S subunit. *b*, binding position of PSRP1 with respect to the binding sites of mRNA (orange, Ref. 48), and A- (pink) and P- (navy blue) site tRNAs (31, 32). A and P labels indicate A- and P- site tRNAs, respectively. The orientation of the 70S ribosome is depicted in the thumbnail at the lower left. *c*, binding of [³²P]tRNA^{Met} to *E. coli* 70S ribosomes in the presence and absence of MF-mRNA, PSRP1, and pY, with and without RRF. Binding of tRNA in the absence of factors was arbitrarily assigned as 100%. Error bars represent the S.E. of the mean.

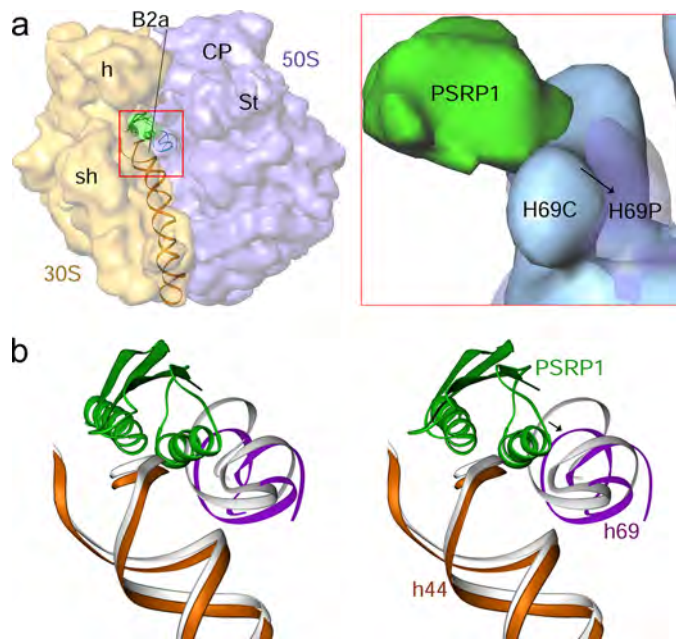


FIGURE 4. Conformational change in bridge B2a upon PSRP1 binding. *a*, 30S (semitransparent orange) and 50S (semitransparent indigo) subunits are shown side-by-side, with bridge B2a region boxed. The right panel shows the enlarged boxed area, with control 50S subunit map (solid blue) superimposed to show the proximity of PSRP1 (green) to density corresponding to 23S rRNA helix 69 (H69C) and shift in H69 position in the PSRP1-bound map (H69P, semitransparent indigo). In the inset, the ribosome masses from the far and near planes have been computationally removed for visual clarity. *b*, stereo-representation of h44 (orange), h69 (indigo), and PSRP1 (green) shown in ribbons, as derived by fitting of coordinates of those components into the *in vivo* PSRP1-bound 70S ribosome map. The control h44 and h69 are shown in gray. The arrow indicates the direction of movement of H69 upon PSRP1 binding. Landmarks of the 30S subunit: sh, shoulder; the rest of the landmarks are the same as in the legend to Fig. 2. Landmarks of the 50S subunit: CP, central protuberance; St, L7/L12 stalk.

shell correlation with a cut-off value of 0.5 (22), was 9.8 Å (or ~7.6 Å by the 3σ criterion) and 14.1 Å (or ~10.1 Å by the 3σ criterion), respectively, for the *in vitro* and *in vivo* complexes.

The fall-off of the Fourier amplitudes toward higher spatial frequencies was corrected for the map of *in vitro* complex as described previously (22). Mass corresponding to PSRP1 was isolated through comparison with the cryo-EM map of the ligand-free *E. coli* 70S ribosome. The homology model of PSRP1 was generated using Swiss-Model (23). Visualization and interpretation of the map, and docking of crystallographic structures, were performed using SPIDER, IRIS Explorer (Numerical Algorithms Group, Inc., Downers Grove, IL), O (24), and Ribbons (25).

RESULTS

Binding of Spinach PSRP1 to the *E. coli* Ribosome—The mature form of spinach PSRP1 was cloned into pET32b; the construct introduces an N-terminal Trx fusion linked to the protein via a six-histidine (6×His) affinity tag. Trx-PSRP1 was overexpressed in *E. coli*, and the ribosomes isolated from log-phase cells were subjected to sucrose-density gradient centrifugation. SDS-PAGE and Western blotting against the 6×His tag indicated that Trx-PSRP1 migrated with 70S ribosomes. PSRP1 remained bound at near-stoichiometric levels to 70S ribosomes purified from the sucrose gradients, consistent

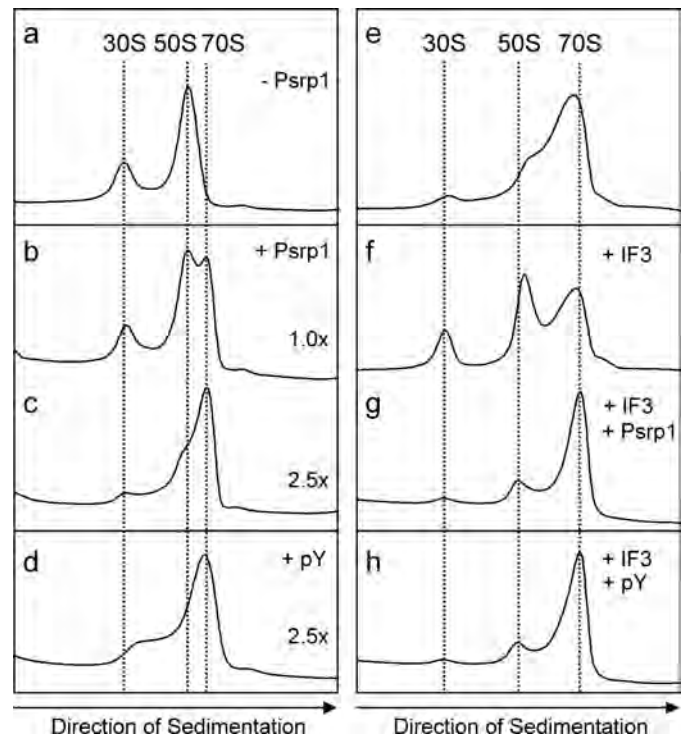


FIGURE 5. Binding of spinach PSRP1 stabilizes *E. coli* 70S ribosomes. *a–d*, 70S ribosomes were incubated in low magnesium buffer, and the subunit dissociation was monitored by sucrose density gradient (10–30%) centrifugation in the absence of PSRP1 (*a*), or in the presence of equimolar (1×) (*b*), 2.5-fold excess of PSRP1 protein (*c*), or 2.5-fold excess of *E. coli* pY protein (*d*). *e–h*, 70S ribosomes were incubated in a buffer that induces minimal dissociation, in the absence of IF3 (*e*), or in the presence of 10-fold excess of IF3 protein (*f*), 10-fold excess of IF3 and 2.5-fold excess of PSRP1 protein (*g*), or 10-fold excess of IF3 and 2.5-fold excess of *E. coli* pY protein (*h*). In *a–h*, the migration positions of 70S ribosomes, 30S and 50S subunits are indicated by dotted vertical lines, and the direction of sedimentation is indicated by an arrow.

with a tight association (Fig. 1*a*, lane 5), whereas no equivalent band was observed for the Trx control (Fig. 1*a*, lane 3).

To complement the *in vivo* results, we performed *in vitro* ribosome binding assays using purified Trx-PSRP1 protein. The use of Trx fusion enables the binding of PSRP1 to be monitored directly by Coomassie Blue-stained SDS-PAGE gels, because the Trx (17 kDa) fusion increases the molecular mass of PSRP1 (27 kDa) to 44 kDa, such that it migrates above the majority of the *E. coli* ribosomal proteins (<30 kDa). Consistent with the *in vivo* results, Trx-PSRP1 binds to *E. coli* 70S ribosomes (Fig. 1*b*, lanes 8 and 9), as well as to 30S subunits (Fig. 1*b*, lanes 5 and 6), and binding increases with increasing excess of PSRP1 protein, saturating at 10:1 factor/ribosome ratio (supplemental Fig. S1*a*). Furthermore, the binding is specific; Trx-PSRP1 does not bind to *E. coli* 50S subunits (supplemental Fig. S1*b*). The *in vivo* purified 70S·Trx-PSRP1 complex, and the *in vitro* 70S·Trx-PSRP1 complex prepared with 20-fold excess of PSRP1 protein, were then analyzed by cryo-EM and single particle image reconstruction, to determine the binding site of PSRP1.

Site of Binding of PSRP1 on the *E. coli* 70S Ribosome—Comparison of the cryo-EM maps of the *in vivo* and *in vitro* assembled *E. coli* 70S-PSRP1 complexes with the map of empty *E. coli* 70S ribosome (control) shows extra mass-density in the inter-subunit space on the 30S subunit; this mass-density could be

Function of Plastid-specific Ribosomal Protein 1

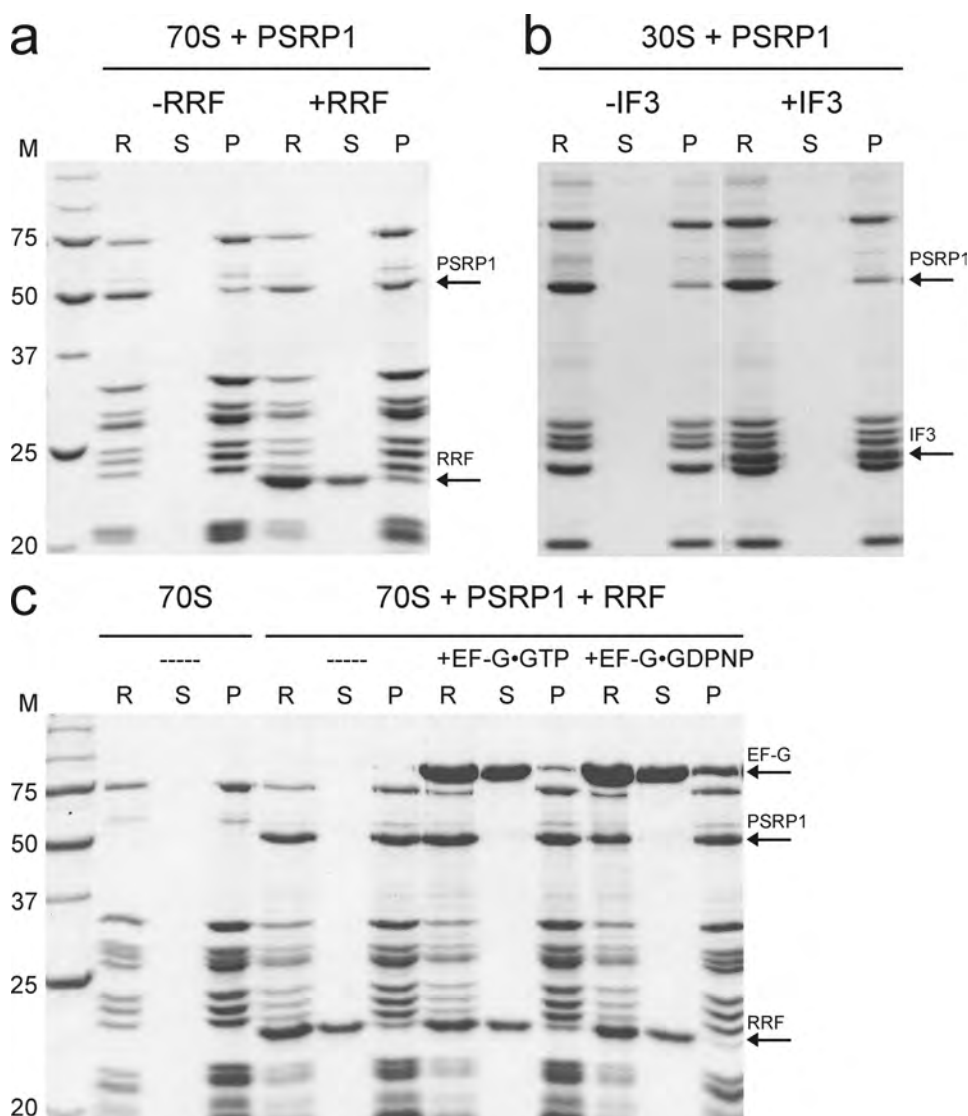


FIGURE 6. Binding of PSRP1 to the ribosome in the presence of different factors. *a*, binding of PSRP1 to 70S ribosomes in the absence or presence of RRF (–RRF or +RRF, respectively). The binding of PSRP1 increases 1.6 ± 0.2 -fold in the presence of RRF. *b*, SDS-PAGE result showing the binding of PSRP1, in the absence or presence of IF3 (–IF3 and +IF3, respectively), to the small ribosomal subunit (30S). The presence of IF3 does not influence the binding of PSRP1 (IF3/PSRP1 binding stoichiometry is 1.1 ± 0.2). *c*, binding of PSRP1 and RRF to 70S ribosomes, and the effect of binding upon addition of different nucleotides together with EF-G. In the reaction with EF-G•GDPNP in comparison to EF-G•GTP, the binding of EF-G increases 3.0 ± 0.3 -fold, the binding of PSRP1 remains unaffected (PSRP1(GDPNP)/PSRP1(GTP) binding stoichiometry is 0.9 ± 0.1), and the binding of RRF decreases about 0.6 ± 0.2 -fold, respectively. In all cases, at least three independent experiments were performed, and the errors represent the S.D. from the mean. For each condition, aliquots of the initial reaction (R), supernatant (S), and pellet (P) were loaded on 15% gel and stained with Coomassie Blue. M denotes marker lanes. Protein bands are marked on the right.

readily assigned to PSRP1 (Fig. 2, *a* and *b*, supplemental Fig. S2). The shape and location of the density feature representing PSRP1 is very similar, between the *in vitro* and *in vivo* complexes. However, the *in vitro* map shows finer details because of its higher resolution (9.8 Å), relative to the *in vivo* map (14 Å). The density, when viewed from the subunit-interface side, spans across the neck region of the 30S subunit, making contacts with the tip of helix 44 (h44) as well as components of the 30S head. The region of the 50S subunit closest to the PSRP1 density is helix 69 (H69) of the 23S rRNA. The binding position of PSRP1 seen in the present eubacterial 70S ribosome•PSRP1 complex maps closely match with that observed in the spinach

chloroplast 70S ribosome (26, Fig. 2c). This comparison strongly supports our assignment of PSRP1 within the eubacterial 70S ribosome•PSRP1 complexes, given that the N-terminal Trx domain was not present in the chloroplast map. However, density corresponding to the Trx domain is visible only in the difference maps, suggesting that this domain is highly flexible on the ribosome.

PSRP1 Is a Ribosome-binding Factor Rather Than a Ribosomal Protein—Genes homologous to spinach PSRP1 can be found in all completely sequenced plant (nuclear) genomes, where they also encode signal sequences targeting the PSRP1 protein into the chloroplast. PSRP1 homologues are also found in cyanobacteria, green algae, and plasmodium species, as well as in several eubacterial lineages. However, the chloroplast PSRP1 proteins are generally larger than the eubacterial homologues, especially the γ -proteobacteria. For example, the mature spinach PSRP1 protein is 236 amino acids in length (27), whereas the *E. coli* homologue is less than half that length, with a sequence of only 113 amino acids homologous to the N-terminal region of PSRP1 (supplemental Fig. S3). The solution structures of the *E. coli* (28, 29) and *Haemophilus influenzae* (30) PSRP1 homologues reveal a single globular domain comprising two α -helices and a four-stranded β -sheet. We used these structures as templates to generate a homology model for the N-terminal domain (NTD) of spinach PSRP1, which we subsequently docked into the PSRP1 density from

the cryo-EM map of the *in vitro* assembled 70S•PSRP1 complex (Fig. 3a). We find that one side of PSRP1, consisting of the two α -helices, is oriented toward the top of 16S rRNA helix 44 (h44), whereas the surface formed by the four-stranded β -sheet of PSRP1 forms extensive contacts with h30; the loop between two of the β -sheets, β 2 and β 3, appears to be sandwiched between helices h34 and h18. Our placement of the NTD of PSRP1 is in excellent agreement with the location of the *E. coli* homologue of PSRP1, protein Y (pY), bound to the *E. coli* 70S ribosome (17). PSRP1 binds in the region corresponding to the path of mRNA on the interface side of the 30S subunit, overlapping the positions of the anticodon stem-loops of A- and P-site

tRNAs (Fig. 3*b*) (31, 32). Consistently, we show that PSRP1 and pY inhibit the binding of tRNA to 70S ribosomes (light green bars in Fig. 3*c*), as has been reported previously for pY (17, 33). pY was much more effective than PSRP1, and the presence of mRNA appeared to increase the stability of the tRNA on the ribosome (Fig. 3*c*). Indeed, the binding position of PSRP1 reported here on an *E. coli* ribosome, as well as in the homologous chloroplast ribosome (26), is incompatible with translation. Furthermore, the similarity in binding sites of PSRP1 and pY (17) on the ribosome, together with their high sequence homology suggests a functional similarity between the two proteins, leading us to suggest that PSRP1 is a pY-like stress response factor, rather than a ribosomal protein.

The weaker density for the CTD of PSRP1 region suggests that this segment is flexible and does not contribute significantly to ribosome binding. This observation is consistent with the fact that overexpression of the CTD alone does not lead to significant binding of PSRP1 to 70S ribosomes. Additionally, a PSRP1 mutant, in which a 56-amino acid "acidic region" (supplemental Fig. S3) was deleted from the CTD, still binds to 70S ribosomes (34).

PSRP1 Contacts Intersubunit Bridge Elements and Stabilizes the 70S Ribosome—The binding of PSRP1 induces conformational changes in various regions of both the 30S and 50S subunits. Several of these changes involve ribosomal components that form intersubunit bridges, including the 16S rRNA helix 44 (h44) and 23S rRNA helix 69 (H69) that interact with one another to form bridge B2a (Fig. 4*a*), one of the largest and most conserved intersubunit bridges in the ribosome (32). Apparent reorganization of regions involved in the formation of this and other bridges (supplemental Fig. S4) suggested to us that PSRP1 binding significantly alters the strength of association of the two ribosomal subunits. Binding of the PSRP1 shifts H69 slightly toward the 50S subunit, such that α -helix 1 of the PSRP1 is situated at the junction of H69 and h44 (Fig. 4*b*). The observed shift in H69 might have been facilitated by the electronegative surface potential of the PSRP1 α -helix 1 facing the H69 (supplemental Fig. S5). Whereas the direction of H69 shift would imply a weakened bridge B2a, direct interactions of PSRP1 with both h44 and H69 appear somehow to further strengthen the bridge (see below).

To further investigate the effect of PSRP1 on the association of two ribosomal subunits, two different types of dissociation assays were performed in the presence and absence of PSRP1/pY and/or initiation factor 3 (IF3) (Fig. 5). IF3 is known as an anti-association factor, which can split weakly associated 70S ribosomes (17, 35). First, *E. coli* 70S ribosomes were incubated in a buffer containing low magnesium, in the absence (Fig. 5*a*) or presence of PSRP1 (Fig. 5, *b* and *c*) or *E. coli* pY (Fig. 5*d*). In the absence of PSRP1 (or pY), the low magnesium leads to dissociation of the 70S ribosomes into 30S and 50S subunits. However, the presence of increasing concentrations of PSRP1 leads to stabilization of the 70S ribosomes (Fig. 5, *b* and *c*), analogous to what is observed in the presence of *E. coli* pY (Fig. 5*d*) (17). Second, 70S ribosomes were incubated in a buffer that induces minimal dissociation of 70S ribosomes into subunits, in the absence of *E. coli* IF3 (Fig. 5*e*), but clear dissociation in the presence of IF3 (Fig. 5*f*). In contrast, the addition of PSRP1 (Fig. 5*g*) or *E. coli* pY (Fig. 5*h*) counteracts the effects of IF3 to stabilize the 70S ribosomes to a greater extent than that observed in the presence (Fig. 5*f*) or absence of IF3 (Fig. 5*e*). Collectively, these observations suggest that PSRP1 is functionally analogous to *E. coli* pY (17), at least in terms of stabilizing the 70S ribosome against dissociation. This observation further supports our assignment of PSRP1 as a stress response factor rather than an innate ribosomal protein.

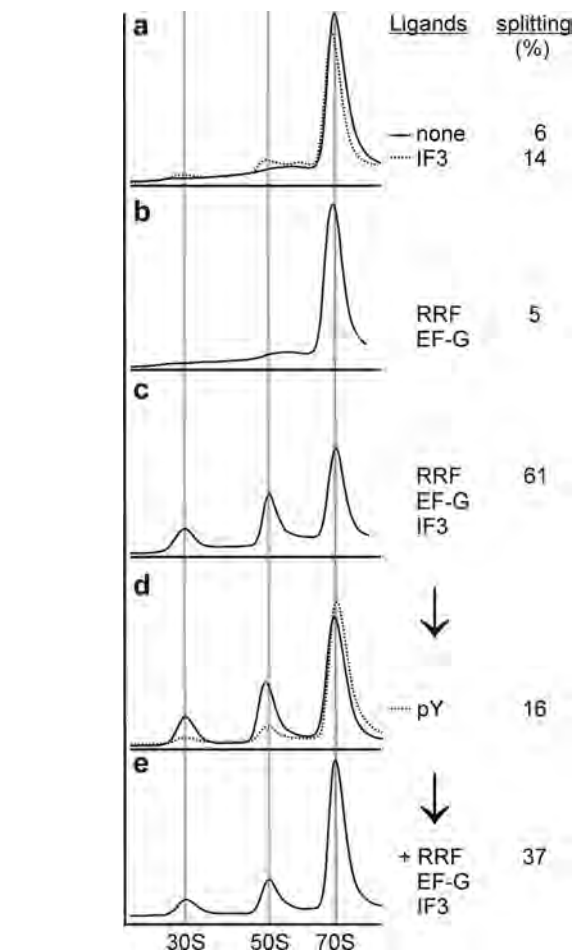


FIGURE 7. Ribosomal subunit association and dissociation under various conditions. *E. coli* 70S ribosomes (0.4 μ M) were incubated alone (none, solid line) or with 10 \times IF3 (IF3, dotted line) (a), with 10 \times RRF and EF-G (b), or with 10 \times RRF, EF-G, and IF3 (c). In addition with 10 \times pY (dotted line), 70S splitting is reduced (d). By increasing the amounts of RRF, EF-G, and IF3 (20 \times), more splitting of 70S ribosomes occurs (e). Peaks of 30S and 50S subunits and 70S ribosomes, are indicated.

lize the 70S ribosomes to a greater extent than that observed in the presence (Fig. 5*f*) or absence of IF3 (Fig. 5*e*). Collectively, these observations suggest that PSRP1 is functionally analogous to *E. coli* pY (17), at least in terms of stabilizing the 70S ribosome against dissociation. This observation further supports our assignment of PSRP1 as a stress response factor rather than an innate ribosomal protein.

PSRP1 Is Recycled from the Ribosome, Analogous to tRNA, by the Tandem Actions of RRF and EF-G—The RRF works in conjunction with a GTPase, EF-G, and initiation factor 3 (IF3), to split post-termination complexes (PoTC) in a GTP-dependent manner, and to recycle the component ribosomal subunits for the next round of translation (36). In the chloroplast ribosome, RRF has been found to directly contact PSRP1 (26). This led us to hypothesize that perhaps RRF, EF-G, and IF3 play a role in recycling PSRP1 from the ribosome after the stress conditions are relieved. To investigate the interplay between these factors, we first performed a series of binding assays. We found that the presence of RRF significantly promotes the binding of PSRP1 to 70S ribosomes (Fig. 6*a*). Consistently, in our tRNA binding assays, we observe that the competitive effects of RRF and

Function of Plastid-specific Ribosomal Protein 1

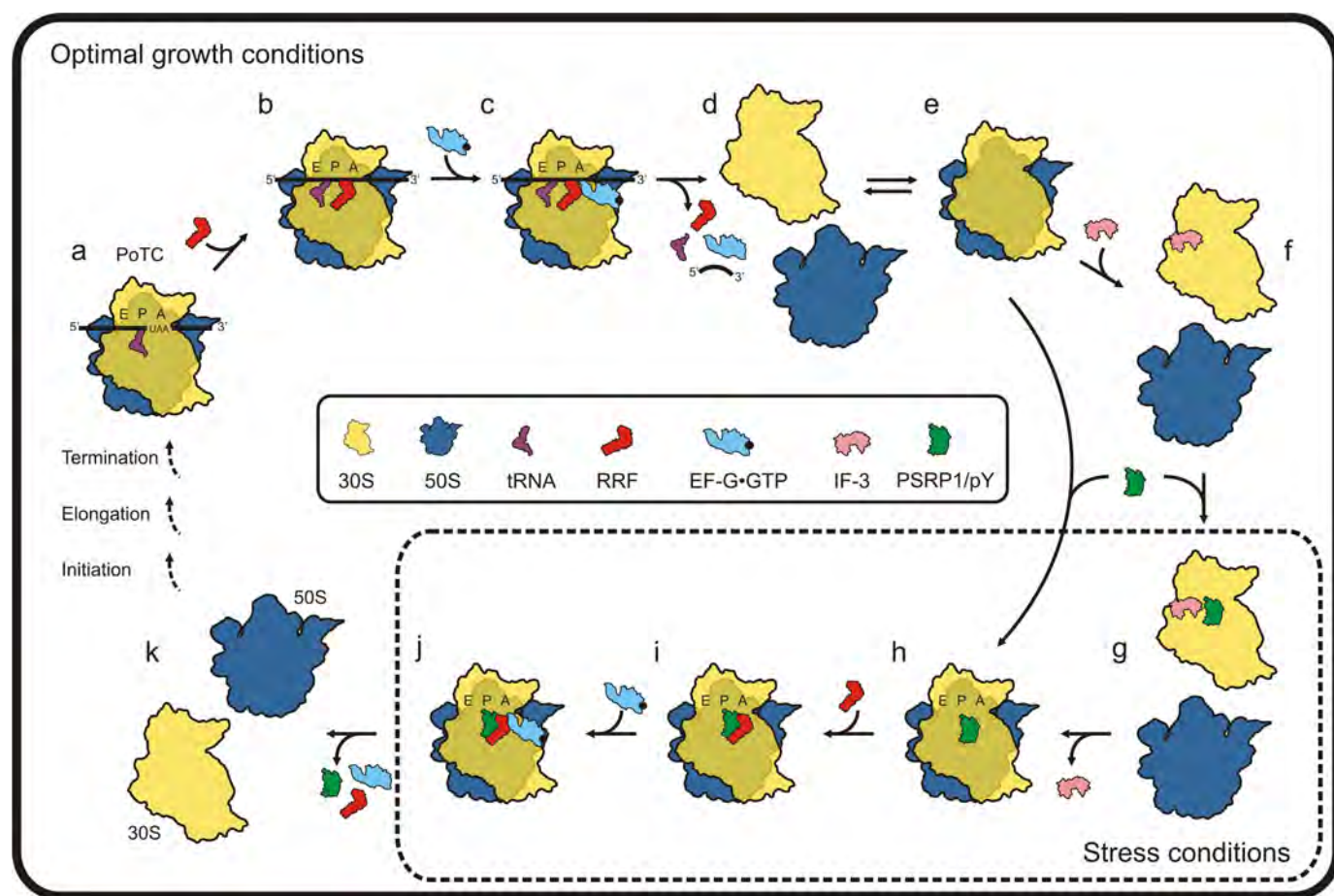


FIGURE 8. The proposed model for the action of pY/PSRP1 under conditions of stress, and the return of stored ribosomes to the actively translating pool under optimal growth conditions. Components of the model are described within the figure; for the specific steps (a–k) of the cycle, see the text.

PSRP1/pY with tRNA binding to 70S ribosomes are additive (dark green bars in Fig. 3c). In contrast, binding of PSRP1 to the 30S subunit is not influenced by the presence of IF3 (Fig. 6b). In the next experiment, we pre-bound PSRP1 and RRF to the ribosome (as in Fig. 6a) and then monitored the binding of EF-G in the presence of either GTP or a non-hydrolyzable analog, GDPNP (Fig. 6c). In the presence of GDPNP, very strong binding of EF-G was observed; binding of PSRP1 remained unaffected, whereas binding of RRF was decreased (Fig. 6c), suggesting that PSRP1, RRF, and EF-G•GDPNP cannot co-occupy a given ribosome. In contrast, in the presence of GTP, low-level binding of EF-G is observed, whereas PSRP1 and RRF binding remains unaffected. One possible explanation for the low stoichiometry of EF-G on the ribosome is that EF-G is cycling on and off the ribosome; however, it is unclear whether subunit dissociation is taking place under these conditions. To test this, we monitored the splitting of 70S ribosomes into subunits, on sucrose gradients (Fig. 7). As previously reported (20, 37, 38), this reaction is dependent on the presence of RRF and EF-G•GTP (Fig. 7, a–c). In these experiments, the concentration of IF3 used exerts no dissociative effect alone (Fig. 7a), but is instead needed to prevent the dissociated subunits from reassociating during centrifugation through the sucrose gradients (Fig. 7c) (20). When 70S ribosomes were prebound with pY (or PSRP1), the dissociative effects of RRF, EF-G, and IF3 were significantly reduced (Fig. 7d). The pY-mediated reassociation and

the EF-G/RRF-mediated dissociation appeared to be competitive events, because further increasing the concentrations of RRF and EF-G shifted the equilibrium toward dissociation (Fig. 7e).

DISCUSSION

The PSRPs from higher plants show extensive sequence similarity with cyanobacterial PSRP1 homologues (supplemental Fig. S3). In the photosynthetic cyanobacterium *Synechococcus* PCC 7002, the PSRP1 homologue is termed *LrtA* (Light-repressed transcript A), because the transcript encoding the protein has been shown to be light-regulated (39). The *LrtA* transcript was not detectable upon continuous illumination, but after a transfer to dark the transcript level became very high. Upon re-illumination (20 min), the transcript level was reduced to 20% and after 40 min *LrtA* was not detectable any longer (39). Therefore, we suggest that expression of PSRP1 may also be light-regulated, and that PSRP1 has a function analogous to that of *E. coli* pY, in stabilizing 70S ribosomes under conditions unfavorable for translation. Whereas *E. coli* pY performs this function under cold-shock conditions, PSRP1 may function in dark conditions; however, further work will be required to verify this.

Based on our results, we propose a model for the role of pY and PSRP1 during conditions of stress, in particular, how the stored ribosomes are returned to the actively translating pool once growth conditions are restored (Fig. 8). Under optimal growth conditions, post-termination complexes are split into

the component subunits through the action of RRF and EF-G (Fig. 8, *a–d*) (36). IF3 prevents reassociation of the subunits by direct binding to the 30S subunit (Fig. 8, *e* and *f*) (20, 37, 38). Under stress conditions, such as cold shock for *E. coli* or darkness for plants, the stress response factors, pY and PSRP1, are up-regulated (39, 40), leading to binding of stress factor to empty 70S ribosomes or 30S subunits (Fig. 8, *g* and *h*). Binding of the stress protein to 30S subunits can occur independently of the presence of IF3 (Figs. 5*b* and 7*g*); stress factor promotes binding of the 50S subunits to form 70S ribosomes (Fig. 7*d*), and thus leads to a loss of IF3 binding (Fig. 8*h*) (41). Protein Y-stabilized ribosomes have been shown to be translationally inactive (33), consistent with the mapping of pY and PSRP1 to the site overlapping the mRNA and A- and P-tRNA binding sites (Fig. 3*b*). The pY/PSRP1-bound ribosomes thus evidently represent a storage state, such that a pool of mature ribosomes is present and ready to participate in translation once the stress conditions are alleviated. The shift to optimal growth conditions switches off the stringent response leading to an up-regulation of components involved in translation, including translation factors such as RRF and EF-G (reviewed in Ref. 42). Because RRF, EF-G, and PSRP1/pY cannot occupy a given ribosome simultaneously (Fig. 6*c*), and because the presence of RRF and EF-G-GTP leads to splitting of PSRP1-70S complexes (Fig. 7*d*), we propose a novel shared role for RRF and EF-G during the post-stress response. This role is the recycling of the stress factor from the ribosome (Fig. 8, *i* and *j*), so that the 30S and 50S subunits can be returned to the translation cycle (Fig. 8*k*). Mechanistically, we envisage the process as operating in a fashion similar to the recycling of the PoTC by RRF and EF-G, in that the RRF progresses through the ribosome from the A-site toward the E-site, and in doing so it disrupts the interaction between h44 and H69. Intersubunit bridge B2a is thereby broken, leading to dissociation of the 70S ribosome into subunits (43, 44). Along this pathway, RRF would also be expected to dislodge the stress protein; however, we have not thus far been able to distinguish between the possibility that the factor remains bound to the 30S subunit and the possibility that it re-binds following dissociation. Whereas our study allows us to propose a functional role of PSRP1 in plastid translation, the possibility of involvement of this protein in other physiological events of the plastids cannot be ruled out.

In addition to cold-shock conditions, pY is found bound to 70S ribosomes in stationary-phase *E. coli* cells, suggesting that the pY family of proteins play a more general role in the stress response. In the stationary-phase, 70S ribosomes also dimerize to form 100S particles, a process that is mediated by the ribosome modulation factor (RMF) and hibernation promotion factor (HPF) (45). Interestingly, HPF shows 40% sequence homology with pY (46), perhaps hinting that HPF also binds within the intersubunit space, and be similarly subject to RRF- and EF-G-mediated post-stress recycling.

Acknowledgments—We thank Dr. Kenichi Yamaguchi for kindly providing the cDNA clones of the spinach chloroplast PSRPs, Timothy Booth for cryo-EM data collection, and Prof. Knud Nierhaus and Dr. Oliver Vesper for providing the pRRF expression plasmid.

REFERENCES

- Daniell, H., and Parkinson, C. L. (2003) *Nat. Biotechnol.* **21**, 374–375
- Huang, C. Y., Ayliffe, M. A., and Timmis, J. N. (2003) *Nature* **422**, 72–76
- Timmis, J. N., Ayliffe, M. A., Huang, C. Y., and Martin, W. (2004) *Nat. Rev. Genet.* **5**, 123–135
- Barkan, A., and Goldschmidt-Clermont, M. (2000) *Biochimie* **82**, 559–572
- Somanchi, A., and Mayfield, S. P. (1999) *Curr. Opin. Plant Biol.* **2**, 404–409
- Bruick, R. K., and Mayfield, S. P. (1999) *Trends Plant Sci.* **4**, 190–195
- Gray, J. C., Sullivan, J. A., Wang, J. H., Jerome, C. A., and MacLean, D. (2003) *Philos. Trans. R. Soc. Lond. B Biol. Sci.* **358**, 135–144; discussion 144–145
- Manuell, A., Beligni, M. V., Yamaguchi, K., and Mayfield, S. P. (2004) *Biochem. Soc. Trans.* **32**, 601–605
- Zerges, W. (2000) *Biochimie* **82**, 583–601
- Dai, S., Schwendtmayer, C., Schürmann, P., Ramaswamy, S., and Eklund, H. (2000) *Science* **287**, 655–658
- Barnes, D., and Mayfield, S. P. (2003) *Antioxid. Redox Signal.* **5**, 89–94
- Kim, J., and Mayfield, S. P. (1997) *Science* **278**, 1954–1957
- Yamaguchi, K., and Subramanian, A. R. (2000) *J. Biol. Chem.* **275**, 28466–28482
- Yamaguchi, K., and Subramanian, A. R. (2003) *Eur. J. Biochem.* **270**, 190–205
- Yamaguchi, K., von Knoblauch, K., and Subramanian, A. R. (2000) *J. Biol. Chem.* **275**, 28455–28465
- Yamaguchi, K., Prieto, S., Beligni, M. V., Haynes, P. A., McDonald, W. H., Yates, J. R., 3rd, and Mayfield, S. P. (2002) *Plant Cell* **14**, 2957–2974
- Vila-Sanjurjo, A., Schuwirth, B. S., Hau, C. W., and Cate, J. H. (2004) *Nat. Struct. Mol. Biol.* **11**, 1054–1059
- Sharma, M. R., Barat, C., Wilson, D. N., Booth, T. M., Kawazoe, M., Hori-Takemoto, C., Shirouzu, M., Yokoyama, S., Fucini, P., and Agrawal, R. K. (2005) *Mol. Cell* **18**, 319–329
- Gnirke, A., Geigenmüller, U., Rheinberger, H. J., and Nierhaus, L. H. (1989) *J. Biol. Chem.* **264**, 7291–7301
- Hirokawa, G., Nijman, R. M., Raj, V. S., Kaji, H., Igarashi, K., and Kaji, A. (2005) *RNA* **11**, 1317–1328
- Frank, J., Penczek, P., Agrawal, R. K., Grassucci, R. A., and Heagle, A. B. (2000) *Methods Enzymol.* **317**, 276–291
- Gabashvili, I. S., Agrawal, R. K., Spahn, C. M., Grassucci, R. A., Svergun, D. I., Frank, J., and Penczek, P. (2000) *Cell* **100**, 537–549
- Schwede, T., Kopp, J., Guex, N., and Peitsch, M. C. (2003) *Nucleic Acids Res.* **31**, 3381–3385
- Jones, T. A., Zou, J. Y., Cowan, S. W., and Kjeldgaard, M. (1991) *Acta Crystallogr. A* **47**, 110–119
- Carson, M. (1991) *Appl. Crystallogr.* **24**, 103–106
- Sharma, M. R., Wilson, D. N., Datta, P. P., Barat, C., Schlutzen, F., Fucini, P., and Agrawal, R. K. (2007) *Proc. Natl. Acad. Sci. U.S.A.* **104**, 19315–19320
- Johnson, C. H., Kruft, V., and Subramanian, A. R. (1990) *J. Biol. Chem.* **265**, 12790–12795
- Ye, K., Serganov, A., Hu, W., Garber, M., and Patel, D. J. (2002) *Eur. J. Biochem.* **269**, 5182–5191
- Rak, A., Kalinin, A., Shcherbakov, D., and Bayer, P. (2002) *Biochem. Biophys. Res. Comm.* **299**, 710–714
- Parsons, L., Eisenstein, E., and Orban, J. (2001) *Biochemistry* **40**, 10979–10986
- Agrawal, R. K., Spahn, C. M., Penczek, P., Grassucci, R. A., Nierhaus, K. H., and Frank, J. (2000) *J. Cell Biol.* **150**, 447–460
- Yusupov, M. M., Yusupova, G. Z., Baucorn, A., Lieberman, K., Earnest, T. N., Cate, J. H., and Noller, H. F. (2001) *Science* **292**, 883–896
- Agafonov, D. E., Kolb, V. A., and Spirin, A. S. (2001) *EMBO Rep.* **2**, 399–402
- Bubunencko, M. G., and Subramanian, A. R. (1994) *J. Biol. Chem.* **269**, 18223–18231
- Brock, S., Szkaradkiewicz, K., and Sprinzl, M. (1998) *Mol. Microbiol.* **29**, 409–417
- Hirokawa, G., Demeshkina, N., Iwakura, N., Kaji, H., and Kaji, A. (2006)

Function of Plastid-specific Ribosomal Protein 1

- Trends Biochem. Sci.* **31**, 143–149
37. Peske, F., Rodnina, M. V., and Wintermeyer, W. (2005) *Mol. Cell* **18**, 403–412
38. Zavialov, A. V., Hauryliuk, V. V., and Ehrenberg, M. (2005) *Mol. Cell* **18**, 675–686
39. Tan, X., Varughese, M., and Widger, W. R. (1994) *J. Biol. Chem.* **269**, 20905–20912
40. Maki, Y., Yoshida, H., and Wada, A. (2000) *Genes Cells* **5**, 965–974
41. Firpo, M. A., Connelly, M. B., Goss, D. J., and Dahlberg, A. E. (1996) *J. Biol. Chem.* **271**, 4693–4698
42. Condon, C., Squires, C., and Squires, C. L. (1995) *Microbiol. Rev.* **59**, 623–645
43. Agrawal, R. K., Sharma, M. R., Kiel, M. C., Hirokawa, G., Booth, T. M., Spahn, C. M., Grassucci, R. A., Kaji, A., and Frank, J. (2004) *Proc. Natl. Acad. Sci. U.S.A.* **101**, 8900–8905
44. Barat, C., Datta, P. P., Raj, V. S., Sharma, M. R., Kaji, H., Kaji, A., and Agrawal, R. K. (2007) *Mol. Cell* **27**, 250–261
45. Ueta, M., Ohniwa, R. L., Yoshida, H., Maki, Y., Wada, C., and Wada, A. (2008) *J. Biochem.* **143**, 425–433
46. Ueta, M., Yoshida, H., Wada, C., Baba, T., Mori, H., and Wada, A. (2005) *Genes Cells* **10**, 1103–1112
47. Schuwirth, B. S., Borovinskaya, M. A., Hau, C. W., Zhang, W., Vila-Sanjurjo, A., Holton, J. M., and Cate, J. H. (2005) *Science* **310**, 827–834
48. Yusupova, G., Jenner, L., Rees, B., Moras, D., and Yusupov, M. (2006) *Nature* **444**, 391–394

Ratje AH, Loerke J, Mikolajka A, Brünner M, Hildebrand PW,
Starosta AL, Dönhöfer A, Connell SR, Fucini P, Mielke T,
Whitford PC, Onuchic JN, Yu Y, Sanbonmatsu KY,
Hartmann RK, Penczek PA, Wilson DN, Spahn CM.
*Head swivel on the ribosome facilitates translocation
by means of intra-subunit tRNA hybrid sites.*
Nature. 2010 Dec 2; 468(7324): 713-6.

Head swivel on the ribosome facilitates translocation by means of intra-subunit tRNA hybrid sites

Andreas H. Ratje^{1,2}, Justus Loerke¹, Aleksandra Mikolajka^{3,4}, Matthias Br  nner¹, Peter W. Hildebrand¹, Agata L. Starosta³, Alexandra D  nh  fer³, Sean R. Connell⁵, Paola Fucini⁵, Thorsten Mielke^{1,6}, Paul C. Whitford⁷, Jos   N. Onuchic⁸, Yanan Yu⁹, Karissa Y. Sanbonmatsu⁷, Roland K. Hartmann², Pawel A. Penczek¹⁰, Daniel N. Wilson^{3,4} & Christian M. T. Spahn¹

The elongation cycle of protein synthesis involves the delivery of aminoacyl-transfer RNAs to the aminoacyl-tRNA-binding site (A site) of the ribosome, followed by peptide-bond formation and translocation of the tRNAs through the ribosome to reopen the A site^{1,2}. The translocation reaction is catalysed by elongation factor G (EF-G) in a GTP-dependent manner³. Despite the availability of structures of various EF-G-ribosome complexes, the precise mechanism by which tRNAs move through the ribosome still remains unclear. Here we use multiparticle cryoelectron microscopy analysis to resolve two previously unseen subpopulations within *Thermus thermophilus* EF-G-ribosome complexes at subnanometre resolution, one of them with a partly translocated tRNA. Comparison of these substates reveals that translocation of tRNA on the 30S subunit parallels the swivelling of the 30S head and is coupled to unratcheting of the 30S body. Because the tRNA maintains contact with the peptidyl-tRNA-binding site (P site) on the 30S head and simultaneously establishes interaction with the exit site (E site) on the 30S platform, a novel intra-subunit 'pe/E' hybrid state is formed. This state is stabilized by domain IV of EF-G, which interacts with the swivelled 30S-head conformation. These findings provide direct structural and mechanistic insight into the 'missing link' in terms of tRNA intermediates involved in the universally conserved translocation process.

After peptide-bond formation, pre-translocational (PRE) ribosomes carry a peptidyl-tRNA at the A site and a deacylated tRNA at the P site^{1,3,4}. This is a highly dynamic state of the ribosome, which fluctuates between classical states with A tRNA and P tRNA and hybrid states with A/P tRNAs (A/P denotes that the tRNA is in the A site on the 30S subunit and the P site on the 50S subunit) and P/E tRNAs⁵⁻⁸. Hybrid state formation is coupled to spontaneous rotation of the 30S subunit relative to the 50S subunit⁹⁻¹¹ and is stabilized by the binding of EF-G¹²⁻¹⁴. The ratchet-like subunit rearrangement induced by EF-G and eukaryotic elongation factor 2 (eEF2) also includes a swivel movement of the head that is roughly orthogonal to the inter-subunit rotation of the ribosomal subunits¹⁴⁻¹⁶. EF-G catalyses translocation of the hybrid-state tRNAs on the 30S subunit to form a post-translocational (POST) state ribosome with tRNAs located at classical P and E sites. The translocation process is accelerated by the GTPase activity of EF-G stimulated by the ribosome^{17,18}. However, it is still not known how tRNAs are translocated with respect to the 30S subunit and how the messenger RNA is advanced by one codon.

Structural snapshots of the translocation process come from cryoelectron microscopy and X-ray analysis of EF-G bound to ribosome complexes^{12-14,19}. Despite considerable effort^{12,20-22}, no direct structural information is available for ribosomal PRE complexes simultaneously

containing EF-G and an A tRNA. It seems that this state is too dynamic and transient to be captured, resulting in either a POST state containing EF-G or a PRE state without EF-G bound^{20,22}. Indeed, the stable EF-G-bound POST state determined by X-ray crystallography reveals a non-ratcheted ribosome with tRNAs in classical P/P and E/E sites¹⁹. Therefore, structural insights into intermediate states of translocation—that is, ratcheted ribosomal EF-G complexes—have used complexes without an A-site peptidyl-tRNA¹²⁻¹⁴.

In this study we used the antibiotic fusidic acid (FA) to stall EF-G on the 70S ribosome. FA permits the hydrolysis of GTP by EF-G but prevents the associated changes in EF-G that normally accompany hydrolysis¹⁹. After complex formation and the collection of cryoelectron microscopy data, we employed multiparticle refinement to resolve the heterogeneity of the data (Supplementary Fig. 1). In the first phase of multiparticle refinement a large population of particle images of ribosomes containing EF-G was obtained that yielded a structure in a ratcheted conformation. As refinement progressed to higher resolution, the presence of intrinsic conformational heterogeneity necessitated a second phase of multiparticle refinement, resulting in two final reconstructions of the 70S-EF-G-GDP-FA complex (Fig. 1), at resolutions of 7.6 Å and 7.8 Å (using a 0.5 Fourier shell correlation cut-off criterion), respectively (Supplementary Fig. 2). Both maps have density attributed to EF-G, but they show significant conformational differences (Supplementary Movies 1 and 2): specifically, the substates are distinguished by different degrees of subunit ratcheting and positioning of the L1 protuberance, and also by the swivel movement of the head of the 30S subunit relative to the body/platform (Fig. 1e, f, Supplementary Figs 3 and 4, and Supplementary Table 1). Unlike previous cryoelectron microscopy and X-ray structures of ribosome-EF-G complexes, movement of the head and body/platform of the 30S subunit is uncoupled: in substate I, the 30S subunit is ratcheted by about 7° relative to the 50S subunit, but there is only a modest (roughly 5°) swivelling of the 30S head. In contrast, the 30S in substate II is only ratcheted by about 4°, but there is a very large (roughly 18°) swivel of the head (Supplementary Table 1).

The identification of two different ratcheted substates within the 70S-EF-G-GDP-FA complex prompted us to investigate whether such intrinsic heterogeneity also exists in our previous 70S-EF-G-GMPPNP cryoelectron microscopy data set¹⁴. Additional multiparticle refinement did indeed reveal that the 70S-EF-G-GMPPNP complex could be subdivided into two substates that seemed to be equivalent to those identified in the 70S-EF-G-GDP-FA complex (Supplementary Fig. 5 and Supplementary Table 1). Our findings here provide evidence supporting the emerging energy-landscape model that allows the sampling of several metastable conformations for a defined ribosomal

¹Institut f  r Medizinische Physik und Biophysik, Charit   – Universit  tsmedizin Berlin, Ziegelstrasse 5–9, 10117-Berlin, Germany. ²Institut f  r Pharmazeutische Chemie, Philipps-Universit  t Marburg, 35037 Marburg, Germany. ³Gene Center and Department of Biochemistry, Ludwig-Maximilians-Universit  t, Feodor-Lynenstrasse 25, 81377 M  nchen, Germany. ⁴Center for Integrated Protein Science, Ludwig-Maximilians-Universit  t M  nchen, 81377 M  nchen, Germany. ⁵Frankfurt Institute for Molecular Life Sciences, Institute of Organic Chemistry and Chemical Biology, Goethe University Frankfurt, Max-von-Laue-Strasse 7, D-60438 Frankfurt am Main, Germany. ⁶UltraStrukturNetzwerk, Max Planck Institute for Molecular Genetics, 14195 Berlin, Germany. ⁷Theoretical Biology and Biophysics Group, Theoretical Division, Los Alamos National Laboratory, Los Alamos, New Mexico 87545, USA. ⁸Center for Theoretical Biological Physics and Department of Physics, University of California, San Diego, La Jolla, California 92093, USA. ⁹Florida State University, Department of Computer Science, Tallahassee, Florida 32306, USA. ¹⁰The University of Texas – Houston Medical School, 6431 Fannin, Houston, Texas 77030, USA.

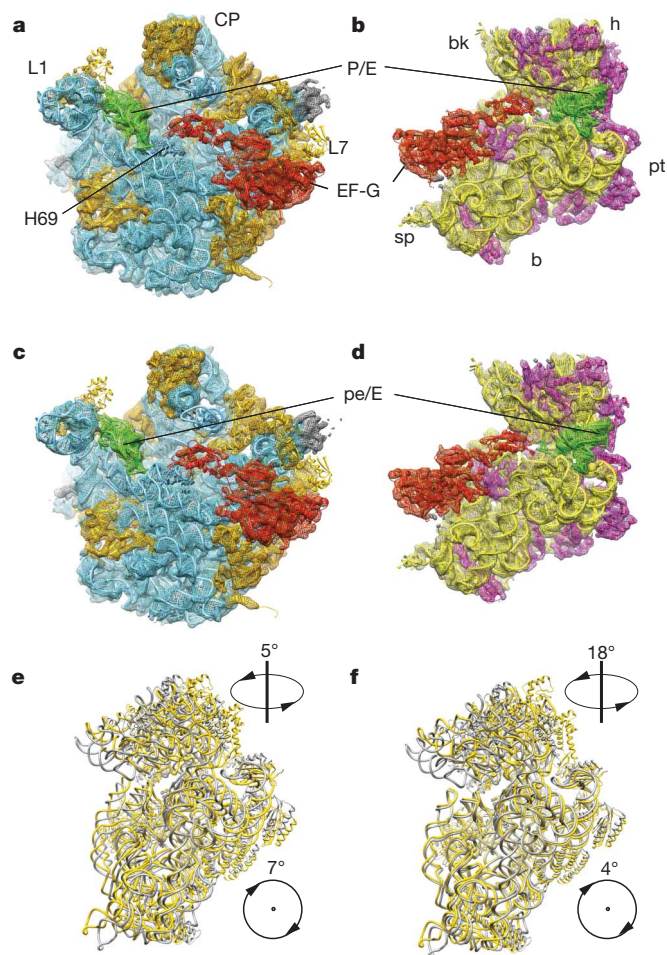


Figure 1 | Substates I (TI^{PRE}) and II (TI^{POST}) of the 70S-EF-G-GDP-FA complex. **a–d**, Cryoelectron microscopy maps of TI^{PRE} (**a**, **b**) and TI^{POST} (**c**, **d**) of the 70S-EF-G-GDP-FA complex are shown in mesh form with docked models in ribbon representation: EF-G (red), tRNA (green), 23S/5S rRNA (blue), 50S ribosomal proteins (orange), 16S rRNA (yellow) and the 30S ribosomal proteins (magenta). The maps are shown from the 30S side with the 30S subunit computationally removed (**a**, **c**) and from the 50S side with the 50S subunit computationally removed (**b**, **d**). CP, central protuberance; bk, beak; sp, spur; pt, platform; h, head; b, back; L1 and L7, ribosomal proteins L1 and L7, respectively; H69, helix 69 of 23S rRNA. **e**, **f**, The 30S subunit of TI^{PRE} (**e**) and TI^{POST} (**f**) (yellow) is compared with the 30S subunit of the POST state¹⁹ (grey) by aligning the respective 50S subunits. Arrows with numbers indicate the direction and magnitude (Supplementary Table 1) of the inter-subunit rotation and the head-swivel from the unrotated state to TI^{PRE} or TI^{POST} , respectively.

complex⁸. The subnanometre resolution of the 70S-EF-G-GDP-FA subpopulations enabled the visualization of secondary structure and thus the generation of molecular models (Fig. 1) by applying our newly developed MDFIT algorithm (see Methods). Comparison with available structures reveals that substate I is similar in conformation to the ratcheted substate of the PRE complex^{9,10} (Supplementary Table 1) and also that the tRNA is bound in a hybrid P/E site (Fig. 2a). We therefore consider substate I to be related to a pre-translocational intermediate (TI^{PRE}).

In contrast, substate II of the 70S-EF-G-GDP-FA complex represents a novel conformational state of the 70S ribosome. The anticodon stem-loop (ASL) of the tRNA has moved by 8–10 Å compared with the P/E position of TI^{PRE} as it maintains strong association with the P-site components of the head and follows the large 18° swivel movement of the head (Fig. 2b and Supplementary Movie 3). Because the tRNA interacts simultaneously with P-site components of the head as well as E-site components of the platform, it can be thought of as a 30S

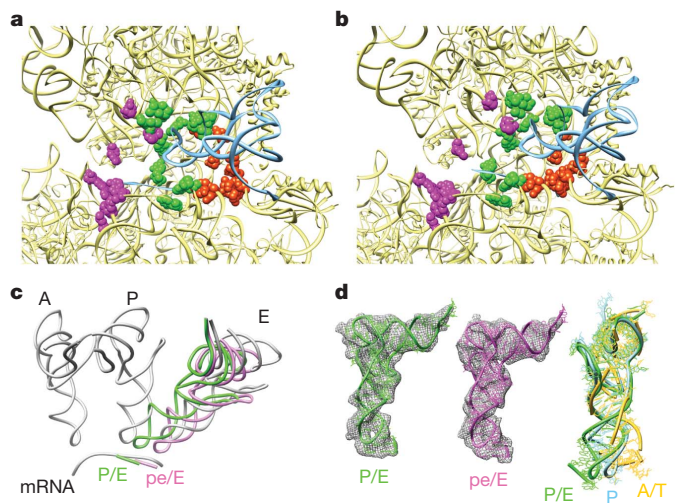


Figure 2 | Localization and conformation of the tRNA of substates I (TI^{PRE}) and II (TI^{POST}). **a**, **b**, Close-up of the tRNA-binding regions of the 30S subunit of TI^{PRE} (**a**) and TI^{POST} (**b**). The 30S subunit and tRNAs are shown as yellow and blue ribbons, respectively; ribosomal residues that contact A, P and E tRNA (magenta, green and orange) are shown as spheres. **c**, In a common 50S alignment, the P/E tRNA (green) of TI^{PRE} and the pe/E tRNA (magenta) of TI^{POST} together with their respective mRNA codons are compared with mRNA and classical A, P and E tRNA positions (grey). **d**, Density for the tRNAs (wire mesh) with molecular models for the P/E tRNA of TI^{PRE} (left, green) and the pe/E tRNA of TI^{POST} (middle, magenta). On the right, the model for P/E tRNA (green), which is essentially the same as that for pe/E-tRNA (root mean squared deviation 1.5 Å), is compared with a classical P tRNA (blue) and an A/T tRNA (yellow) by alignment of the acceptor-stem, D-stem and T-stem loops.

intra-subunit hybrid site (Fig. 2b). Moreover, because the contacts of the CCA end of the tRNA with the E site on the 50S subunit remain unaffected, we extend the previous nomenclature of hybrid sites⁵ and refer to this newly identified state as a pe/E hybrid state (P site on head and E site on platform of the 30S subunit, and E site on the 50S subunit).

The ASL of the pe/E tRNA together with the bound mRNA codon is very close to the position of a fully translocated E/E tRNA (Fig. 2c and Supplementary Movie 4). Apparently, head-swivelling coupled with partial unratcheting of the body/platform of the 30S subunit leads to tRNA translocation, suggesting that substate II of the 70S-EF-G-GDP-FA complex is related to a post-translocational intermediate state (TI^{POST}). We note that although the intermediate states visualized here contain only one tRNA, a second tRNA (ap/P) can be superimposed on the TI^{POST} state without steric interference with the binding position of EF-G (Supplementary Fig. 6). Thus, the structures presented here seem to be valid models for translocation intermediates (see also Supplementary Information for further discussion), but structures of translocation intermediates with two tRNAs will be necessary for the validation of these predictions. The presence of the ratchet-like subunit rearrangement in the yeast 80S-eEF2-sordarin complex¹⁵ hints that translocation in prokaryotes and eukaryotes may use related intermediate conformations. This structure showed a strong head swivel comparable to that of bacterial TI^{POST} combined with a strong inter-subunit rotation of bacterial TI^{PRE} . Thus, the conformation of the 80S-eEF2-sordarin complex¹⁵, although obtained by classical single-particle methods, may present a further intermediate between TI^{PRE} and TI^{POST} .

Whereas the P/E and pe/E tRNAs are in a twisted conformation (Fig. 2d), the overall conformations of EF-G in TI^{PRE} and TI^{POST} are remarkably similar to each other (Fig. 1) and to that observed in the cryoelectron microscopy reconstruction of the 70S-EF-G-GMPPNP¹⁴ as well as in the recent X-ray structure of EF-G-GDP-FA bound to a POST-state ribosome¹⁹ (Fig. 3a). However, one difference between the two EF-G-GDP-FA substates relates to the interaction patterns of domain IV of EF-G: in the TI^{PRE} state, domain IV does not seem to

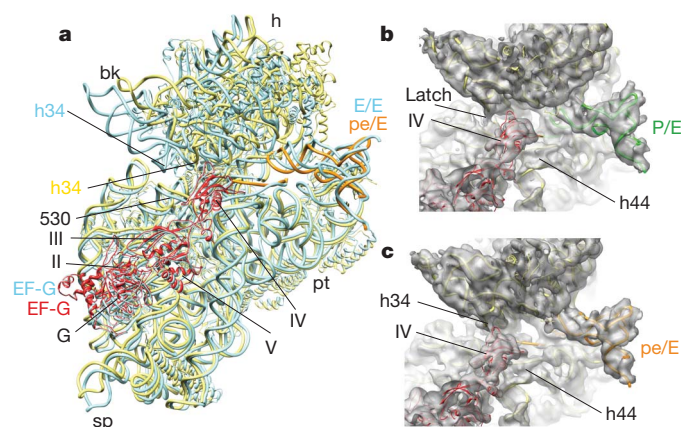


Figure 3 | EF-G stabilizes the swivelled head movement in the TI^{POST} state. **a**, Comparison of the position of FA-stalled EF-G and the 30S subunit between TI^{POST} and the POST-state 70S-EF-G-GDP-FA complex¹⁹. All shown components of the POST-state 70S-EF-G-GDP-FA complex¹⁹ are depicted as blue ribbons. The 30S, EF-G and pe/E tRNA of TI^{POST} are represented by yellow, red and orange ribbons, respectively. **b**, **c**, Close-up of the decoding region and domain IV of EF-G in the same orientation as in **a**. The surfaces of TI^{PRE} (**b**) and TI^{POST} (**c**) are transparent with molecular models in ribbon representation (30S subunit, yellow; EF-G, red; P/E tRNA, green; pe/E tRNA, orange). The arrows mark the closed latch between helix h34 and the 530 region of TI^{PRE} (**b**) and the interaction between h34 and domain IV of EF-G within TI^{POST} .

interact significantly with the ribosome (Fig. 3b), whereas a small shift in the binding position of EF-G and the large swivel of the head facilitate a more extensive interaction of domain IV of EF-G with helix h34 of the 16S rRNA in the TI^{POST} state (Fig. 3c). Together, h34 and the nucleotide 530 region of 16S rRNA form the so-called latch of the mRNA entry channel. Because of the head-swivel in the TI^{POST} state, h34 has moved about 12 Å away from the 530 region, leading to an opening of the latch (Fig. 3c) similar to that observed previously when eEF2 was trapped on the yeast 80S ribosome with sordarin¹⁵. This may facilitate the movement of the mRNA-tRNA₂ complex. Consistent

with this observation, transient protection of h34 by EF-G against chemical modification during the translocation reaction has been reported previously²³. The direct interaction of domain IV of EF-G with h34 may therefore bias the energy landscape of the ribosome towards TI^{POST} .

Until now, intermediate states of inter-subunit rotation have been considered to be intermediates on the pathway to the fully rotated state¹⁶. The present findings implicate unratcheting (in combination with the large swivel of the 30S head), rather than ratcheting, as being coupled to the translocation movement of the tRNAs and the mRNA with respect to the 30S subunit. Collectively, the insights gained from the structures of the TI^{PRE} and TI^{POST} states enable us to provide a structural explanation for the process of translocation in a model in which tRNA movements are facilitated by head-swivel, ratcheting and unratcheting motions of the ribosome (Fig. 4). These motions may be influenced by the GTPase reaction on EF-G; a network of interactions involving domain III and the ordered switch I region of EF-G and the γ -phosphate of GTP was proposed to stabilize the rotated state of the 30S subunit¹⁴. Accordingly, fast GTP hydrolysis by EF-G¹⁷ could destabilize the direct and indirect interactions of switch I of EF-G with the maximally rotated 30S subunit^{14,24}, therefore increasing the propensity of the 30S subunit to rotate backwards. The unratcheting motion produces a counter-movement of the body/platform with respect to the head, thereby reducing the distance that the tRNAs have to travel during translocation. Intra-subunit hybrid states allow the 30S subunit to maintain partial contacts with the tRNAs at any time of the translocation reaction. In the context of the ribosome's functioning during translocation as a Brownian ratchet machine²⁵, our model suggests that EF-G acts as a dynamic pawl, decoupling the unratcheting motions of the ribosome from the transition of hybrid-state tRNAs back into classical states. EF-G thereby provides directionality and accelerates translocation of the tRNAs by means of several intermediate inter-subunit and intra-subunit hybrid states into the classical P/P and E/E sites of the POST state.

METHODS SUMMARY

Tight-coupled 70S ribosomes from *Thermus thermophilus* were isolated by sucrose-gradient centrifugation and incubated with EF-G in the presence of GTP and FA. The resulting complexes were flash-frozen and imaged under low-dose conditions

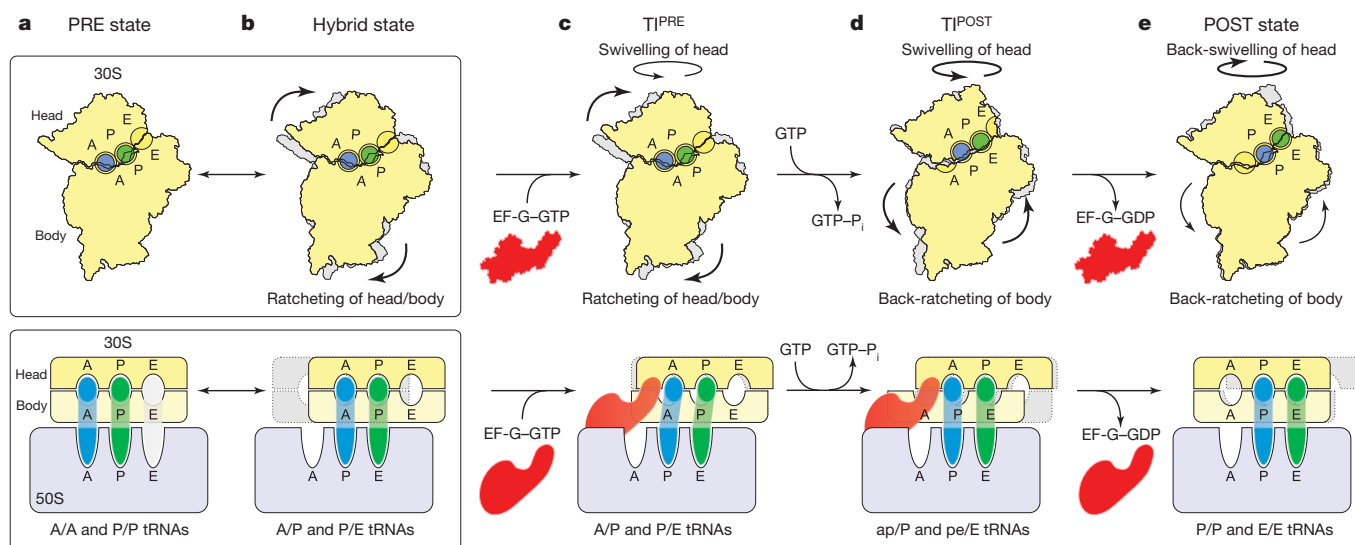


Figure 4 | Model for translocation. **a**, **b**, The PRE ribosome exists in a dynamic equilibrium between base states with classical A/A and P/P tRNAs (**a**) and rotated states with hybrid A/P and P/E tRNAs^{6,7,9–11} (**b**). **c**, Binding of EF-G-GTP to PRE state (**a**) or hybrid state (**b**) stabilizes the ratcheted state¹² as observed in TI^{PRE} . **d**, Fast GTP hydrolysis by EF-G¹⁷ accelerates translocation by means of an unlocking step on the 30S subunit¹⁸. Domain IV of EF-G uncouples unratcheting from the reverse movement of the A/P and P/E tRNAs

back into classical states; that is, a doorstop function. Through a head-swivelling and unratcheting motion, the tRNAs move from aa/P and pp/E into the 30S intra-subunit ap/P and pe/E hybrid states. **e**, Complete unratcheting of the 30S subunit leads to the POST-state 70S-EF-G complex¹⁹. Back-swivelling of the 30S head re-establishes tRNAs in the classical (pp/P) P and E (ee/E) states. Translocation is completed by the dissociation of EF-G-GDP.

with the use of an FEI Polara G2 electron microscope. The collected data were digitized and processed with multiparticle refinement protocols implemented in SPIDER²⁶. To interpret the resulting cryoelectron microscopy maps in molecular terms, a newly developed algorithm (MDFIT)²⁷ that integrates molecular simulation with experimental maps was employed.

Full Methods and any associated references are available in the online version of the paper at www.nature.com/nature.

Received 5 February; accepted 30 September 2010.

- Frank, J. & Spahn, C. M. The ribosome and the mechanism of protein synthesis. *Rep. Prog. Phys.* **69**, 1383–1417 (2006).
- Schmeing, T. M. & Ramakrishnan, V. What recent ribosome structures have revealed about the mechanism of translation. *Nature* **461**, 1234–1242 (2009).
- Shoji, S., Walker, S. E. & Fredrick, K. Ribosomal translocation: one step closer to the molecular mechanism. *ACS Chem. Biol.* **4**, 93–107 (2009).
- Ramakrishnan, V. Ribosome structure and the mechanism of translation. *Cell* **108**, 557–572 (2002).
- Moazed, D. & Noller, H. F. Intermediate states in the movement of transfer RNA in the ribosome. *Nature* **342**, 142–148 (1989).
- Munro, J. B., Altman, R. B., O'Connor, N. & Blanchard, S. C. Identification of two distinct hybrid state intermediates on the ribosome. *Mol. Cell* **25**, 505–517 (2007).
- Blanchard, S. C. *et al.* tRNA dynamics on the ribosome during translation. *Proc. Natl Acad. Sci. USA* **101**, 12893–12898 (2004).
- Munro, J. B., Sanbonmatsu, K. Y., Spahn, C. M. & Blanchard, S. C. Navigating the ribosome's metastable energy landscape. *Trends Biochem. Sci.* **34**, 390–400 (2009).
- Agirrezabala, X. *et al.* Visualization of the hybrid state of tRNA binding promoted by spontaneous ratcheting of the ribosome. *Mol. Cell* **32**, 190–197 (2008).
- Julian, P. *et al.* Structure of ratcheted ribosomes with tRNAs in hybrid states. *Proc. Natl Acad. Sci. USA* **105**, 16924–16927 (2008).
- Fischer, N. *et al.* Ribosome dynamics and tRNA movement by time-resolved electron cryomicroscopy. *Nature* **466**, 329–333 (2010).
- Valle, M. *et al.* Locking and unlocking of ribosomal motions. *Cell* **114**, 123–134 (2003).
- Frank, J. & Agrawal, R. K. A ratchet-like inter-subunit reorganization of the ribosome during translocation. *Nature* **406**, 318–322 (2000).
- Connell, S. R. *et al.* Structural basis for interaction of the ribosome with the switch regions of GTP-bound elongation factors. *Mol. Cell* **25**, 751–764 (2007).
- Spahn, C. M. *et al.* Domain movements of elongation factor eEF2 and the eukaryotic 80S ribosome facilitate tRNA translocation. *EMBO J.* **23**, 1008–1019 (2004).
- Zhang, W., Dunkle, J. A. & Cate, J. H. Structures of the ribosome in intermediate states of ratcheting. *Science* **325**, 1014–1017 (2009).
- Rodnina, M., Savelsbergh, A., Katunin, V. I. & Wintermeyer, W. Hydrolysis of GTP by elongation factor G drives tRNA movement on the ribosome. *Nature* **385**, 37–41 (1997).
- Savelsbergh, A. *et al.* An elongation factor G-induced ribosome rearrangement precedes tRNA-mRNA translocation. *Mol. Cell* **11**, 1517–1523 (2003).
- Gao, Y. G. *et al.* The structure of the ribosome with elongation factor G trapped in the posttranslocational state. *Science* **326**, 694–699 (2009).
- Penczek, P. A., Frank, J. & Spahn, C. M. A method of focused classification, based on the bootstrap 3D variance analysis, and its application to EF-G-dependent translocation. *J. Struct. Biol.* **154**, 184–194 (2006).
- Agrawal, R. K. *et al.* EF-G-dependent GTP hydrolysis induces translocation accompanied by large conformational changes in the 70S ribosome. *Nature Struct. Biol.* **6**, 643–647 (1999).
- Scheres, S. H. *et al.* Disentangling conformational states of macromolecules in 3D-EM through likelihood optimization. *Nature Methods* **4**, 27–29 (2007).
- Matassova, A. B., Rodnina, M. V. & Wintermeyer, W. Elongation factor G-induced structural change in helix 34 of 16S rRNA related to translocation on the ribosome. *RNA* **7**, 1879–1885 (2001).
- Ticu, C. *et al.* Conformational changes in switch I of EF-G drive its directional cycling on and off the ribosome. *EMBO J.* **28**, 2053–2065 (2009).
- Spirin, A. S. The ribosome as a conveying thermal ratchet machine. *J. Biol. Chem.* **284**, 21103–21119 (2009).
- Schuetz, J. C. *et al.* GTPase activation of elongation factor EF-Tu by the ribosome during decoding. *EMBO J.* **28**, 755–765 (2009).
- Whitford, P. C. *et al.* Accommodation of aminoacyl-tRNA into the ribosome involves reversible excursions along multiple pathways. *RNA* **16**, 1196–1204 (2010).

Supplementary Information is linked to the online version of the paper at www.nature.com/nature.

Acknowledgements The present work was supported by grants from the Deutsche Forschungsgemeinschaft (DFG; SFB 740 TP A3 and TP Z1, SP 1130/2-1 to C.M.T.S., FU579 1-3 to P.F., HA 1672/7-5 to R.K.H. and WI3285/1-1 to D.N.W.), the European Union 3D-EM Network of Excellence (to C.M.T.S.), the European Union and Senatsverwaltung für Wissenschaft, Forschung und Kultur Berlin (UltraStructureNetwork, Anwenderzentrum) and US National Institutes of Health (NIH; grant GM 60635 to P.A.P.), the Cluster of Excellence 'Macromolecular complexes' at the Goethe University Frankfurt (DFG Project EXC 115 to P.F. and S.C.), and the Human Frontiers of Science Program Young Investigators Award HFSP67/07 (to P.F.). We thank the New Mexico Computing Application Center for generous time on the Encanto Supercomputer. P.C.W. is currently funded by a LANL Director's Fellowship. This work was also supported by the Center for Theoretical Biological Physics sponsored by the National Science Foundation (NSF; grant PHY-0822283) with additional support from NSF-MCB-0543906, the LANL LDRD program and NIH grant R01-GM072686.

Author Contributions A.M., A.L.S. and A.D. prepared the complexes. A.H.R. and T.M. collected the cryoelectron microscopy data. A.H.R., J.L., M.B., S.R.C. and C.M.T.S. did the image processing. P.C.W., Y.Y., J.O. and K.Y.S. developed and employed the MDFIT method. P.W.H. participated in docking and analysed the FA-binding site. A.H.R., R.K.H., S.R.C., P.F., P.A.P., D.N.W. and C.M.T.S. discussed the results and wrote the paper.

Author Information The electron density maps and models of the T1^{PRE} and the T1^{POST} complexes have been deposited in the 3D-EM database with accession numbers EMD-1798 and EMD-1799, and in the Protein Data Bank database with PDB IDs 2xxy, 2xtg, 2xux and 2xuy. Reprints and permissions information is available at www.nature.com/reprints. The authors declare no competing financial interests. Readers are welcome to comment on the online version of this article at www.nature.com/nature. Correspondence and requests for materials should be addressed to C.M.T.S. (christian.spahn@charite.de) or D.N.W. (wilson@lmb.uni-muenchen.de).

METHODS

Formation of the EF-G-70S-GDP-FA complex. The *fusA* gene, encoding EF-G, was cloned from *Thermus thermophilus* HB8 genomic DNA into pET-46 Ek/LIC vector using primers (TthEFG_for, 5'-GCC CGC CCG GTG GTG ATG CAG CTC TTC CTG GGC TCC GCC CTG AAG AAC-3'; TthEFG_rev, 5'-GTT CTT CAG GGC GGA GCC CAG GAA GAG CTG CAT CAC CAC CGG GCG CGC-3') in accordance with the manufacturer's instructions (Novagen) and expressed in BL21 (DE3) cells. Recombinant EF-G protein was then purified with a Ni²⁺-nitrilotriacetate affinity column, followed by gel filtration in a buffer containing 10 mM Tris pH 7.8, 100 mM NaCl and 10 mM 2-mercaptoethanol. Tight-coupled 70S ribosomes were purified from exponential-phase *T. thermophilus* cells by using sucrose-density-gradient centrifugation, as described previously for 30S subunits²⁸. As observed previously, the ribosomes contained a co-purified tRNA^{14,29}. Binding of EF-G to 70S ribosomes was done by incubating 20 μ M purified EF-G protein for 15 min with 5 μ M *T. thermophilus* 70S ribosomes, 500 μ M GTP and 500 μ M FA at 65 °C, in a buffer containing 10 mM HEPES-KOH pH 7.8, 30 mM MgCl₂ and 75 mM NH₄Cl. The occupancy of EF-G in the complexes was about 60–70%, as judged by centrifugal binding assay²⁸.

Cryoelectron microscopy and image processing. Ribosomal complexes were diluted to a concentration of 30 nM and subsequently frozen onto Quantifoil grids using a Vitrobot (FEI) device. Micrographs were collected on a Tecnai G2 Polara (FEI) at 300 kV and a magnification of $\times 39,000$ under low-dose conditions ($19\text{ e}^- \text{Å}^{-2}$) and scanned on a D8200 Primscan drum scanner (Heidelberger Druckmaschinen) with a step size of 4.758 μ m, corresponding to 1.26 Å on the specimen scale.

The Contrast Transfer Function defocus values for the micrographs were determined with CTFind³⁰. Ribosomal projection images were automatically identified with the program Signature³¹ and were subsequently screened visually or automatically. From the selected projections, a reconstruction was generated by projection matching procedures and refined with the SPIDER software package³². The complete data set comprised 586,848 projection images collected from 677 micrographs at a defocus range of 1.3–4.8 μ m. During the later refinement rounds, positivity of the reference volumes was enforced, the power spectrum of the cryoelectron microscopy map was scaled to the power spectrum of a model density derived from the atomic coordinates of the X-ray structure of the 70S ribosome³³, and the map was subsequently low-pass filtered according to the current resolution estimate.

After a first phase of multiparticle refinement^{20,26,34,35}, performed with three-times or two-times decimated pictures, we obtained a major subpopulation (52%; 303,665 particle images) that had strong EF-G density (Supplementary Fig. 1). However, as refinement progressed and the resolution reached the subnanometre range the data set was deemed heterogeneous. Parts of the 30S subunit, especially the head domain, became partly disordered. A second phase of multiparticle refinement was therefore employed, leading to the subdivision of the data into two further substates having EF-G (Supplementary Fig. 1). Both data subsets were further refined individually at full image size. The final reconstructions of substate I (113,214 particle images) and substate II (156,332 particle images) reached resolutions of 7.8 Å and 7.6 Å, respectively (Supplementary Fig. 2).

Using a similar strategy we revisited the previous data set (362,361 particle images; 371 micrographs) of the 70S-EF-G-GMPPNP complex¹⁴. In a first phase of multiparticle refinement a major population (118,991 particle images) was further sorted by a second phase of multiparticle refinement resulting in substate I (58,911 particle images) and substate II (38,055 particle images). The resolutions of the maps were 9.6 Å and 10.5 Å, respectively. As the resolution for the reconstructions of the 70S-EF-G-GMPPNP complex was significantly lower (as a result of the smaller size data set) than the resolutions obtained for the 70S-EF-G-GDP-FA complex, we restricted the comparison to a dissection of only the global conformational changes, such as ratcheting and head swivelling.

Nevertheless, this analysis suggests that the 70S-EF-G-GMPPNP complex coexists in two substates that resemble TI^{PRE} and TI^{POST} of the 70S-EF-G-GDP-FA complex (Supplementary Fig. 5 and Supplementary Table 1). The ratio of particles within each of the two substates of the 70S-EF-G-GMPPNP complex is inverted with respect to the 70S-EF-G-GDP-FA complex: in the 70S-EF-G-GMPPNP complex the particle ratio of TI^{PRE} and TI^{POST} is about 3:2 (58,911:38,055), whereas in the 70S-EF-G-GDP-FA complex the ratio is about 2:3 (113,214:156,332). This means that most of the ribosomes in the 70S-EF-G complex stalled with a non-hydrolysable GTP analogue are in TI^{PRE} (substate I), having a fully ratcheted 30S subunit but only a modest head swivel. However, in the 70S-EF-G complex stalled with GTP and FA, TI^{POST} dominates and here an intermediate inter-subunit rotation is coupled with a large head swivel instead (Supplementary Figs 4 and 5 and Supplementary Table 1).

Structure-based simulation fitting (MDFIT). To determine atomic models consistent with the cryoelectron microscopy densities, we employed structure-based

molecular simulation^{27,36,37} together with an energetic term developed in ref. 38, which incorporates the correlation between the simulated and experimental electron density throughout the simulation. Tama and co-workers³⁸ developed a similar method, which used a standard explicit solvent force field, as opposed to the structure-based force field. The advantage of the structure-based force field is that, because the potential energy function is defined by the X-ray structure, MDFIT retains tertiary contacts present in the X-ray structure without special constraints. Furthermore, because MDFIT explicitly includes all non-hydrogen atoms, there are no atomic clashes and proper stereochemistry is maintained in all fits.

We began the MDFIT procedure with a structure-based potential energy function defined by the classical unratcheted conformation. To induce hybrid-state formation and subunit pivoting we introduced the energetic term based on the correlation between the simulated cryoelectron microscopy map and the experimentally determined cryoelectron microscopy map. Specifically, the potential energy function is

$$V = V^{\text{SB}} + V^{\text{map}} = V^{\text{SB}} - W \sum_{ijk} \rho_{ijk}^{\text{sim}} \rho_{ijk}^{\text{exp}} \quad (1)$$

where W is the energetic weight of the map and ρ_{ijk}^{exp} and ρ_{ijk}^{sim} are the normalized experimental and simulated electron densities at voxel (i,j,k) , respectively. The quantity V^{SB} is the structure-based potential energy function. To calculate the simulated map, each atom is described by a Gaussian function of width 5 Å with the tail truncated at 1% of the peak value. Here, because the structure-based forcefield has 1 unit (all calculations were in reduced units) of stabilizing energy per atom (by construction), we set W to a comparable value of 150,000. The contributions to the force due to V^{map} were updated every 200 time steps. Fitting simulations employed Langevin dynamics. All simulations were performed with code based on Gromacs version 4.0.5 (refs 39, 40). Calculations were performed on the Encanto Supercomputer. The structure-based force field is freely available online (<http://smog.ucsd.edu>).

Structural models. The crystallographic structure of the 70S ribosome in complex with EF-G¹⁹ (PDB IDs 2WRI and 2WRJ) was used as an initial structure for MDFIT. Proteins without side chains in the X-ray structure were removed. The carboxy-terminal domain of ribosomal protein L7 from PDB entry 1RQU⁴¹ was inserted by hand, before fitting. The E-site tRNA was also removed from the initial X-ray structure in accordance with the cryoelectron microscopy map. The P-site tRNA was included in the fitting process. To facilitate fitting of the tRNA molecule into a P/E conformation, stabilizing interactions between the tRNA and the ribosome were removed. Stabilizing interactions between EF-G and the ribosome (due to their proximity in the crystal structure) were also excluded from the calculations, as were stabilizing interactions between L7 and all other components in the system. Further, crystallographic interactions found between the 3'-CCA end of the E-site tRNA with the E site of the 50S subunit were reintroduced as short-range (of the type 6-12; see refs 27, 36, 37) attractive interactions between the 3'-CCA end of the fitted tRNA and the E site of the 50S subunit. Introducing these interactions ensured that the 3'-CCA end of the P/E tRNA was in a conformation identical to that of a classically bound E-site tRNA, although because these interactions were short-range they only affected the process once the major rearrangements in the tRNA had already been achieved. Codon-anti-codon interactions were restrained by harmonic interactions with minima corresponding to the classical configuration.

The tRNA-ribosome-EF-G crystal structure was first manually aligned in VMD⁴², as a single rigid unit, to the map of TI^{PRE}. The first round of fitting was performed with the TI^{PRE} map after subjecting it to a 4-Å Gaussian low-pass filter. This filter decreased noise, effectively smoothing the energetic profile associated with V^{map} , which permitted more rapid fits. After 10^6 integration steps, the fit was continued for an additional 10^6 steps with V^{map} based on the TI^{PRE} map filtered at 2 Å. The TI^{POST} map, filtered at 2 Å, was then fitted, using the TI^{PRE} 4-Å fitted structure as the initial structure.

28. Sharma, M. R. *et al.* Interaction of Era with the 30S ribosomal subunit implications for 30S subunit assembly. *Mol. Cell* **18**, 319–329 (2005).
29. Yusupov, M. M. *et al.* Crystal structure of the ribosome at 5.5 Å resolution. *Science* **292**, 883–896 (2001).
30. Mindell, J. A. & Grigorieff, N. Accurate determination of local defocus and specimen tilt in electron microscopy. *J. Struct. Biol.* **142**, 334–347 (2003).
31. Chen, J. Z. & Grigorieff, N. SIGNATURE: a single-particle selection system for molecular electron microscopy. *J. Struct. Biol.* **157**, 168–173 (2006).
32. Frank, J. *et al.* SPIDER and WEB: processing and visualization of images in 3D electron microscopy and related fields. *J. Struct. Biol.* **116**, 190–199 (1996).
33. Selmer, M. *et al.* Structure of the 70S ribosome complexed with mRNA and tRNA. *Science* **313**, 1935–1942 (2006).
34. Spahn, C. M. & Penczek, P. A. Exploring conformational modes of macromolecular assemblies by multiparticle cryo-EM. *Curr. Opin. Struct. Biol.* **19**, 623–631 (2009).

35. Connell, S. R. *et al.* A new tRNA intermediate revealed on the ribosome during EF4-mediated back-translocation. *Nature Struct. Mol. Biol.* **15**, 910–915 (2008).
36. Whitford, P. C. *et al.* An all-atom structure-based potential for proteins: bridging minimal models with all-atom empirical forcefields. *Proteins* **75**, 430–441 (2009).
37. Whitford, P. C. *et al.* Nonlocal helix formation is key to understanding S-adenosylmethionine-1 riboswitch function. *Biophys. J.* **96**, L7–L9 (2009).
38. Orzechowski, M. & Tama, F. Flexible fitting of high-resolution x-ray structures into cryoelectron microscopy maps using biased molecular dynamics simulations. *Biophys. J.* **95**, 5692–5705 (2008).
39. Lindahl, E., Hess, B. & van der Spoel, D. J. GROMACS 3.0: a package for molecular simulation and trajectory analysis. *J. Mol. Model.* **7**, 306–317 (2001).
40. Berendsen, H. J. C., van der Spoel, D. & van Drunen, R. GROMACS: a message-passing parallel molecular dynamics implementation. *Comput. Phys. Commun.* **91**, 43–56 (1995).
41. Bocharov, E. V. *et al.* From structure and dynamics of protein L7/L12 to molecular switching in ribosome. *J. Biol. Chem.* **279**, 17697–17706 (2004).
42. Humphrey, W., Dalke, A. & Schulten, K. VMD: visual molecular dynamics. *J. Mol. Graph.* **14**, 33–38 (1996).

Curriculum Vitae Alexandra Dönhöfer

Geburtsdatum/-ort: 04.05.1982, München
Staatsangehörigkeit: Deutsch

AUSBILDUNG UND PROMOTION

09/2007 – 03/2012 Promotion am Genzentrum der LMU München
AG Dr. Daniel N. Wilson, Prof. Dr. Roland Beckmann
Thema: „*Auxiliary factors regulating ribosome function: Roles in biogenesis, antibiotic resistance and ribosome recycling*”

09/2006 – 05/2007 Diplomarbeit, LMU München, Institut für Mikrobiologie
AG Prof. Dr. Kirsten Jung
Thema: „Einfluss der Cysteinreste auf die Aktivität des membran- gebundenen Transkriptionsaktivators CadC in *Escherichia coli*“

10/2001 – 05/2007 Studium der Biologie an der Ludwig-Maximilians-Universität München mit Hauptfach Mikrobiologie und den Nebenfächern Genetik, Biochemie und Pharmakologie/ Toxikologie

09/1992 – 05/2001 Allgemeine Hochschulreife am Gymnasium Gröbenzell
Leistungskurse Biologie und Englisch

BERUFSAUSBILDUNG

07/2001 – 09/2005 Ausbildung zur Rettungssanitäterin
Malteser Hilfsdienst e.V., München

KONFERENZEN

08/2009 8th International Conference on Ribosome Synthesis (Poster)
EMBO Conference Series, Regensburg, Deutschland

05/2010 Ribosomes 2010 (Poster)
Orvieto, Italien

PRÄSENTATIONEN

05/2008 “*Factor-mediated assembly of ribosomal particles*”
Poster, Genzentrum, Retreat

06/2009 “*PSRP1 is not a ribosomal protein but a stress response factor*”
Vortrag, Genzentrum, Doktoranden-Seminar

08/2009 “*PSRP1 is a stress response factor rather than a ribosomal protein*”
Poster, EMBO Konferenz, Regensburg

- 05/2010 ***“PSRP1 is not a ribosomal protein, but a ribosome binding factor that is recycled by RRF and EF-G”*** Poster, Ribosomes 2010
- 06/2011 ***“Antibiotic-induced ribosomal assembly defects result from changes in the synthesis of ribosomal proteins”***
Poster, Genzentrum, Retreat
-

PUBLIKATIONEN

- (1) Siibak T, Peil L, Dönhöfer A, Tats A, Remm M, Wilson DN, Tenson T, Remme J: Antibiotic-induced ribosomal assembly defects result from changes in the synthesis of ribosomal proteins. *Mol. Microbiol.* 2011 Apr; 80(1): 54-67.
- (2) Tetsch L, Koller C, Dönhöfer A, Jung K: Detection and function of an intramolecular disulfide bond in the pH-responsive CadC of *Escherichia coli*. *BMC Microbiol.* 2011 Apr 12, 11(1): 74.
- (3) Márquez V, Fröhlich T, Armache JP, Sohmen D, Dönhöfer A, Mikolajka A, Berninghausen O, Thomm M, Beckmann R, Arnold GJ, Wilson DN: Proteomic characterization of archaeal ribosomes reveals the presence of novel archaeal-specific ribosomal proteins. *J. Mol. Biol.* 2011 Feb 4; 405(5): 1215-32.
- (4) Ratje AH, Loerke J, Mikolajka A, Brünner M, Hildebrand PW, Starosta AL, Dönhöfer A, Connell SR, Fucini P, Mielke T, Whitford PC, Onuchic JN, Yu Y, Sanbonmatsu KY, Hartmann RK, Penczek PA, Wilson DN, Spahn CM: Head swivel on the ribosome facilitates translocation by means of intra-subunit tRNA hybrid sites. *Nature.* 2010 Dec 2; 468(7324): 713-6.
- (5) Sharma MR*, Dönhöfer A*, Barat C, Marquez V, Datta PP, Fucini P, Wilson DN, Agrawal RK: PSRP1 Is Not a Ribosomal Protein, but a Ribosome-binding Factor That Is Recycled by the Ribosome-recycling Factor (RRF) and Elongation Factor G (EF-G). *J. Biol. Chem.* 2010, 285: 4006-4014.
- * Diese Autoren haben zu gleichen Teilen zu dieser Arbeit beigetragen.
- (6) Dönhöfer A, Sharma MR, Datta PP, Nierhaus KH, Agrawal RK, Wilson DN: Factor-Mediated Ribosome Assembly in Bacteria. *Encyclopedia of Life Sciences (ELS)*, September 15, 2009.